## *Aspects of structure and bonding in carbocations and plasma polymers, with particular emphasis on the use of ESCA*

Johnson, Stephen Arthur

A thesis entitled

# "Aspects of Structure and Bonding in Carbocations and Plasma Polymers, with particular emphasis on the use of ESCA"

submitted by

Stephen Arthur Johnson, B.Sc. Hons (Dunelm)

a Candidate for the Degree of Doctor of Philosophy



St. Cuthbert's Society,
University of Durham.

March 1985

to my mother

*"Where there is no vision,*

*the people perish".*

Proverbs, XXIX, v.18.

MEMORANDUM

The work described in this thesis was carried out at the University of Durham between October 1981 and August 1984. Apart from the exception noted below, and except where acknowledged by reference, this is the original work of the author and has not been submitted for any other degree.

The MNDO SCF MO investigation described in Chapter Six is the joint work of W.J. Brennan and the present author, and as such has already been submitted as part of Dr. Brennan's Ph.D. thesis (Durham 1984). This work has formed the subject of the following publication:

"An MNDO SCF MO Investigation of some Structural Isomers of the Perfluoro Diazines (Pyrimidine, Pyrazine and Pyridazine) of Relevance to their Plasma Polymerisation".

D.T. Clark, S.A. Johnson, W.J. Brennan

J. Polym.Sci.,Polym.Chem.Ed. (1984), 22, 2145.

ACKNOWLEDGEMENTS

I wish to thank my supervisors, Professor David Clark and Dr. Hugh Munro for the opportunity to carry out this research, for their help and enthusiasm, and for their patience. I am also indebted to the SERC for the provision of a research grant.

The carrying out of this work would certainly have been far more difficult were it not for the skill and expertise of George Rowe and, Jim Hodgson and the "lads" in the workshop, who have played an important role in the preservation of the ageing species *"Electronicus Spectromicus 200B"*! In a different sphere, the effort of Lascelles Williams at UMRCC in implementing the MNDO program on the CDC 7600 was obviously of great importance. I gratefully acknowledge these contributions.

I owe a great deal to many people within the Chemistry Department and especially to my colleagues in the ESCA lab., for their helpful discussions, comments and criticisms; in particular I am very pleased to have had the opportunity of working with Bill Brennan and Jeff Eaves, whose support and friendship I have valued greatly.

I am grateful to Rob Allaker for preparing the norbornyl chloride used in Chapter 2 and I wish to thank Mrs. Marion Wilson for typing my "tatolly logible monuscrapt"!

# ASPECTS OF STRUCTURE AND BONDING IN CARBOCATIONS AND PLASMA POLYMERS, WITH PARTICULAR EMPHASIS ON THE USE OF ESCA

by
STEPHEN ARTHUR JOHNSON

## ABSTRACT

Since photoionisation occurs on a timescale which is rapid compared with that of nuclear motion, X-ray Photoelectron Spectroscopy (XPS or ESCA) is an ideal technique to study (controversial) carbocations in which potentially rapid rearrangement may be occurring. Previous attempts at (parts of) this work have not produced totally accepted results. In this work a method is presented for the preparation of carbocations *in situ* in the source of an ESCA spectrometer, by the use of molecular beams. Preparation of the t-butyl cation by ionisation of the chloride using antimony pentafluoride was concluded to be a gas-phase reaction. This was contrasted with the probable gas-surface nature of the protonation of alkenes using fluorosulphuric acid, which has led to the successful ESCA observation of both the 2-norbornyl and sec-butyl cations. The experimental $C_{1s}$ core-hole spectra of the solid-state species are close to those predicted theoretically for the nonclassical 2-norbornyl cation and the partially methyl-bridged sec-butyl cation.

The ability to study amorphous thin films is another important facet of the ESCA technique which has been exploited in the study of plasma polymers produced in an inductively-coupled RF glow-discharge flow reactor. The study was specifically aimed at the incorporation of metals into a perfluorobenzene plasma polymer by attempting to evaporate the metal from a resistively heated molybdenum coil. This was unsuccessful and the major metal incorporation was of molybdenum oxides, though these were present in amounts comparable with those in samples previously produced by an etching mechanism.

Since theoretical calculations are one method of "probing" reactive media, semi-empirical molecular-orbital calculations (MNDO) have been performed on an extensive series of species which are potential intermediates in perfluorodiaza-benzene plasmas (in particular the valence isomers) to gain some insight into these systems in an attempt to rationalise experimentally determined (ESCA) data.

CONTENTS


| | Page No. |
|---|---|
| Memorandum | i |
| Acknowledgements | ii |
| ABSTRACT | iii |
| CHAPTER ONE - AN INTRODUCTION TO THE INVESTIGATION OF CARBOCATION STRUCTURE | 1 |
| 1.1 Introduction - The Great Debate | 2 |
| 1.2 Probes of Carbocation structure | 3 |
| 1.2.1 NMR Methods | 3 |
| 1.2.2 The potential of ESCA | 7 |
| 1.2.3 Theoretical Investigations | 9 |
| 1.3 The Effect of Solvation | 10 |
| 1.4 Methods of Carbocation formation | 12 |
| 1.4.1 Antimony pentafluoride and organic halides | 13 |
| 1.4.2 Protonation of alkenes | 16 |
| CHAPTER TWO - THE IONISATION OF ALKYL HALIDES | 19 |
| 2.1 Preliminary experiments | 20 |
| 2.1.1 The Olah method | 20 |
| 2.1.2 The Insertion Lock Method | 24 |
| 2.1.3 Molecular Beams | 25 |
| 2.2 Experimental | 36 |
| 2.2.1 Apparatus and methods | 36 |
| 2.2.2 Analysis of precursors | 43 |
| (i) Antimony pentafluoride | 43 |
| (ii) Exo-2-norbornyl chloride | 46 |
| 2.3 Results and Discussion | 48 |
| 2.3.1 Codeposition of antimony pentafluoride and t-butyl halides | 48 |
| 2.3.2 The Multilayer Method | 58 |
| 2.3.3 Bilayer (Norbornyl chloride and antimony pentafluoride) | 61 |
| 2.4 Summary | 72 |

Page No.

CHAPTER THREE - THE PROTONATION OF ALKENES 74

3.1 Experimental 75

3.1.1 Apparatus and Methods 75

(i) Norbornene 75
(ii) Cis-but-2-ene 75

3.1.2 Analysis of precursors 77

(i) "Magic" Acid 77
(ii) Fluorosulphuric acid 79
(iii) Norbornene 86
(iv) Cis-but-2-ene 87

3.2 The 2-Norbornyl Cation 89

3.2.1 Earlier work 89

(i) Experimental 89
(ii) Theoretical 92

3.2.2 Results and Discussion 98

3.3 The sec-butyl cation 114

3.3.1 Earlier work 114

(i) Experimental 114
(ii) Theoretical 117

3.3.2 Results and Discussion 119

3.4 Summary 125

CHAPTER FOUR - AN INTRODUCTION TO "GLOW-DISCHARGE" PLASMAS AND THEIR CHEMICAL APPLICATIONS 127

4.1 Plasmas- definition, classification and production 128

4.2 Plasma applications 131

4.2.1 Organic Plasma Chemistry 131
4.2.2 Plasma etching 133
4.2.3 Plasma Polymerization 134
4.2.4 Surface Modification 139

4.3 Two contemporary lines of research 140

4.3.1 Plasma Diagnostics 140
4.3.2 Metal Incorporation into Plasma Polymers 142

(i) Methods 142

(a) The use of organometallics 143
(b) The Etching-Polymerisation incorporation of metal 145
(c) Metal Evaporation 148

(ii) Applications of metal incorporated plasma polymers 150

Page No.

CHAPTER FIVE - THE INCORPORATION OF MOLYBDENUM INTO A PERFLUOROBENZENE PLASMA POLYMER 151

5.1 Introduction 152

5.2 Experimental 152

5.3 Results and Discussion 156

5.3.1 Variation of Atomiser Voltage 159
5.3.2 Variation of Plasma Parameters 165

(i) Time 165
(ii) Variation with pressure 167
(iii) Variation with power 170

5.3.3 Variation of the atomiser-coil separation 172
5.3.4 The molybdenum/oxygen ratio and molybdenum chemical state 179
5.3.5 Summary of the results 183

5.4 The Nature of the Metal Incorporation 184

5.4.1 The evaporation of molybdenum 184
5.4.2 Plasma Etching 185
5.4.3 The formation of Molybdenum Trioxide 187

5.5 The Importance of the Work 190

5.6 Summary 193

CHAPTER SIX - AN MNDO SCF MO INVESTIGATION OF SOME STRUCTURAL ISOMERS OF THE PERFLUORO DIAZINES (PYRIMIDINE, PYRAZINE AND PYRIDAZINE) OF RELEVANCE TO THEIR PLASMA POLYMERIZATION 195

6.1 Introduction 196

6.2 Computational Details 198

6.3 Results and Discussion 198

6.3.1 Ground States 198

(i) Parent perfluoro heteroaromatics 198
(ii) Diazafulvenes 200
(iii) Diazadienynes 201
(iv) Diaza Dewar Benzenes 203
(v) Diazabenzvalenes 204
(vi) Diazaprismanes 205
(vii) Summary of Ground State Results 205

6.3.2 Excited States 206

(i) Cations 206
(ii) Singlet and triplet states 207

CHAPTER SIX (contd.) Page No.

6.3.3 Application to Plasma Polymerisation of these Compounds 210

(i) Interconversion of parent isomers 210
(ii) Polymerisation 214
(iii) Elimination 215

6.4 Summary 216

APPENDIX A - ELECTRON SPECTROSCOPY FOR CHEMICAL APPLICATIONS 218

A.1 Introduction 219

A.2 Instrumentation 220

A.2.1 The X-ray Source 220
A.2.2 The Sample Chamber 222
A.2.3 The Electron Energy Analysis System 224
A.2.4 Electron detection and display 228

A.3 Processes involved in ESCA 230

A.3.1 Photoionisation 230
A.3.2 Relaxation 230
A.3.3 Shake-up and Shake-off processes 232
A.3.4 The Fate of Core-Holes 233

A.4 Features of ESCA Spectra 233

A.4.1 Binding Energies and Energy Referencing 233
A.4.2 Chemical Shifts 237

(i) Origin of Chemical Shifts 237
(ii) Methods of calculating chemical shifts 239
(iii) The Auger Parameter and Two-dimensional chemical state plots 239

A.4.3 Other Fine Structure 241

(i) Spin-Orbit Splitting 241
(ii) Multiplet Splitting 242
(iii) Electrostatic Splitting 244

A.4.4 Signal Intensities 244

(i) Homogeneous Samples 245
(ii) Substrate-Overlayer Model and Non-destructive Depth Profiling 248

APPENDIX B - COLLOQUIA AND CONFERENCES 252

REFERENCES 262

# CHAPTER ONE

# AN INTRODUCTION TO THE INVESTIGATION OF CARBOCATION STRUCTURE

## 1.1 Introduction - The Great Debate

One of the most controversial areas of modern chemistry has been the question of bridging in carbocations.[1-6] The problem is difficult to define precisely, but concerns whether a positive charge can be delocalised by interaction with σ-electron density, in an analogous fashion to the well established delocalisation by π-electron density, and, if this can occur, when does it and how important is it. The largest debate has centred around the norbornyl cation since this system is considered to be ideally structured for possible σ-interaction. Put in another way the question is whether the classical ion (I) is an intermediate, with the nonclassical ion (II) being a transition state, or *vice versa*.

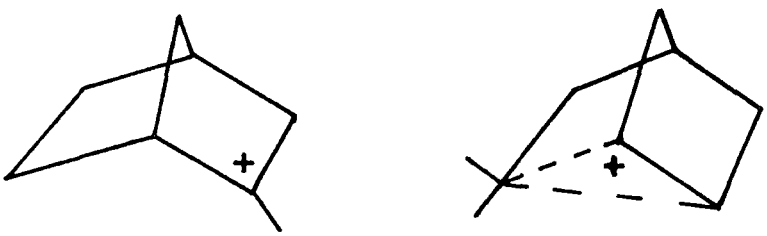

I II

Many techniques and methods have been applied to this problem, studying the cation in solid, liquid and gaseous phases. One major line of investigation has been the study of rates of solvolysis reactions, but it is important to realise that rates of reaction depend upon the difference in energy between the ground and transition states, and therefore information about the structure of an intermediate is only

obtained by assuming its similarity with the transition state; however, in some of the controversial cases discussed, the energy difference between potential intermediates is sufficiently small, that such an assumption could lead to error. Thus following the discovery that carboations could have more than a transitory existence, in so-called stable-ion media,[7] a second major line of investigation has been the spectroscopic structural investigation of the ion. To some extent these different approaches lie at the very heart of the problem since results considered conclusive in one phase may not be readily extrapolated to another.

The discussion presented here concentrates mainly on the methods designed to give information on the intrinsic electronic structure of species under stable-ion conditions since clearly this is the area in which the ESCA data belong. This is followed by a short discussion of the relevance of information from such studies to those in the solvolysis field. Theoretical calculations are included in this work partly because lack of solvation in the gas phase means that the results may be comparable to those from studies under stable-ion conditions, but more importantly because geometry optimisation of the possible carbocation isomers forms the basis for calculating expected chemical shifts in the ESCA spectrum.

## 1.2 Probes of Carbocation structure

### 1.2.1 NMR Methods

Nuclear magnetic resonance (NMR) has been the most extensively used technique for structural investigation,

but suffers from the serious drawback that the timescale of the technique is comparatively slow leaving ambiguity as to whether a single resonance observed is just one resonance or the time-averaged result of two or more. An early attempt to distinguish between these possibilities was based on comparison between the observed shift and that expected on the basis of model systems.[8] For example, in the case of the 2,3-dimethyl-2-butyl cation (III) the $^{13}C$ shift observed for the two central carbons is -3.4 ppm.* On the basis that the cation centre and methyl group shifts of tertiary

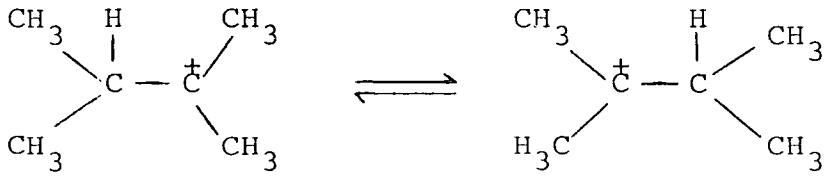

(III)

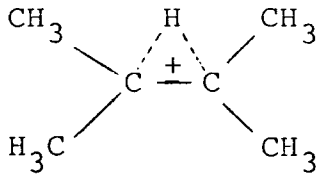

butyl cation (-135.4, +141.6 ppm. respectively) are a good model for the two carbon environments, the resonance absorption of these in an equilibrating ion is predicted to occur at 6.2 ppm. Since this value is in good agreement with that experimentally observed, the system is concluded to be equilibrating classical ions. The result obtained though, must depend on the model systems chosen. The method has been criticised[9] since its basis is that NMR shifts are determined by charge density, whilst it is known that other factors are involved.[10] Indeed whilst this model suggests that certain

* In ppm. from $^{13}CS_2$.

shifts are not consistent with equilibrating classical ions, the converse, that they are consistent with nonclassical ions, has not been shown.

More recently a method involving the additivity of $^{13}C$ NMR chemical shifts has been applied.[11] In this the sum of the chemical shifts of the carbon atoms of a carbocation are compared with the same sum for the parent hydrocarbon. Whilst ions considered to have classical structures show differences in the total shifts of these species, which are generally between 350 and 390 ppm., ions considered to have nonclassical structures show shift differences from the parent hydrocarbon which are substantially less (<200 ppm.). The number of cations, with very varying structures, for which this correlation is found, suggests the validity of the method.

In between these extremes, a third class is found. Whereas classical ions, by definition, involve no bridging, nonclassical ions have generally been considered to be symmetrical structures, where the bridging group is equally shared between two atoms. In between these classes there is expected to be a graduation of bridging, and thus some, at least, of the intermediate class of cations identified, are considered to be unsymmetrically bridged ions.

Another approach to the problem outlined above (the possibility of a single NMR peak being the time-averaged result of resonances from more than one environment) is to continually cool down the system in order to reach the temperature at which the process causing the averaging, is frozen out. Formerly such a method was limited to a temperature

of ∿-160°C (using the best available mixture of the solvents $SO_2F_2$ and $SO_2ClF$),[12] but the *naissance* of solid-state NMR has removed this limitation and spectra can now be obtained at a temperature as low as 5K,[13] leaving little room for the possibility of processes not being frozen out.

Probably the most elegant method applied to the problem of whether carbocations are bridged or equilibrating is the Isotopic Perturbation of Resonance,[14] which has been shown to be able to determine whether a potential energy surface has a single or double minimum, even when the barrier in the latter case may be below ∿3kcal/mole. For example the 1,2-dimethylcyclopentyl cation (IV)[15] undergoes rapid degenerate rearrangement, so that C1 and C2 give a single, time-averaged NMR peak. The introduction of deuterium, in

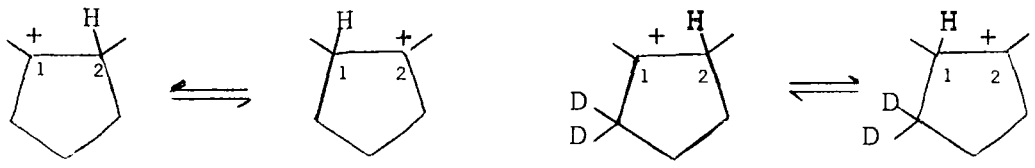


(IV)

a symmetry-breaking position, leads to a slight energy preference of one of the ions; consequently the system spends slightly longer in one isomeric form than the other, so that C1 and C2 are no longer averaged to give a single resonance, but give separate lines with a splitting of as much as 100 ppm (in the $^{13}C$ NMR spectrum). Splitting is also observed in the case of nonequilibrating, single-minimum potential energy

surfaces. In the cyclohexenyl cation (V),[16] C1 and C3


(V)

are equivalent and give rise to a single resonance. Substitution by deuterium at, for example, C1, leads to a non-symmetrical ion, so that C1 and C3 have different environments; consequently splitting is observed, but in this case it is only ∿0.5 ppm. This difference, of about two orders of magnitude, in the splittings observed in the $^{13}C$ NMR spectrum upon the introduction of (symmetry-breaking) deuterium, enables the distinction between rapidly equilibrating (classical) and static (nonclassical) ions.

### 1.2.2 The potential of ESCA

It is generally agreed that ESCA has the potential to resolve unambiguously the problem about the structure of the norbornyl cation under stable ion conditions[1,3,17] since the timescale of the photoionization event central to the technique is $\sim 10^{-16}$ $s^{-1}$ enabling distinction between rapidly equilibrating and static ions.

Initially the ESCA spectra of the t-butyl, trityl and tropylium carbocations were reported.[18] The t-butyl cation, an example of a carbocation with a substantially localised charge, yielded a $C_{1s}$ spectrum which clearly showed

two peaks that were separated in binding energy by 3.4eV (this is the internal shift). Furthermore the intensity ratio was 3:1, and the spectrum was easily interpretable in terms of a single charged carbon, which consequently exhibited an increased $C_{1s}$ binding energy. Conversely the $C_{1s}$ core-hole spectra of the trityl and tropylium cations showed only a single peak, and this was interpreted as being consistent with the extensive charge delocalisation of these ions. These results were an early demonstration of the use of ESCA in studying carbocations.

The unity about the potential of ESCA falls short, however, of agreement over the data available for the norbornyl cation[19-21] (discussed in Section 3.2.1) and it has been stated that it is regrettable that an independent confirmation has never been published.[3,17] Thus, the aim of the present work is to try to establish an experiment which can repeatedly produce carbocations in a form amenable to study by ESCA, thus enabling confirmation, or otherwise, of the earlier results.

It is instructive to compare the NMR and ESCA experiments. The relatively fast time-scale of the latter has already been pointed out. Low temperatures are required for both experiments, but for different reasons; in both cases, provided the formation of carbocations occurs below a moderately low temperature, with no localised heating, rearrangement to more stable cations will not occur. For example, the sec-butyl cation does not rearrange to the tertiary cation below $\sim -30^{o}C$.[22] Whereas the low temperatures ($\sim -160^{o}C$) involved in NMR experiments[12] are an attempt to "freeze-out" fast re-

arrangements, the temperature required for ESCA experiments needs only to be sufficient to initially condense reagents and subsequently to avoid them pumping off. Within these constraints though, the ESCA experiment should be carried out at as high a temperature as possible, since the problems of surface contamination increase as the temperature decreases. Thus, for example, most of the experiments described in this work, were carried out using a substrate temperature of $\sim$-120$^{o}$C.

Another important difference between NMR and ESCA is that the shifts involved in the latter can be readily interpreted. In early work it was shown that ESCA binding energy shifts correlated well with atomic charges derived from relatively simple theoretical models whilst *ab initio* calculations permit more rigorous correlations.[23] This is to be contrasted with the situation found for $^{13}$C NMR shifts, even of closely related compounds.[24] It is partly for this reason that sections are included on the theoretical calculations of the carbocations of interest, since these provide the basis for predicting core-hole spectra.

### 1.2.3 Theoretical Investigations

One of the main uses of theoretical chemistry lies in its ability to predict results which are difficult to observe experimentally; this explains the abundant literature on theoretical studies of reactive intermediates. Carbocations are particularly amenable to this type of investigation[25,26] since they are closed-shell systems, and since the overall positive charge of the system leads to contraction of electron clouds which consequently are more easily represented, in

contrast to the more diffuse clouds of carbanions. "Generation" of carbocations in a computer is therefore inherently attractive, particularly since rearrangements can be precisely controlled, and quenching totally avoided!

One of the problems, however, with any theoretical approach, is in assessing the accuracy of the result obtained, and indeed different levels of theory can lead to different conclusions. A second cautionary note is that calculations on carbocations attempt to probe the inherent electronic structure of the isolated ion; thus the results obtained are generally most directly comparable with those from gas-phase studies. In solution (and maybe, to a much smaller extent, even under stable-ion conditions) solvation effects are inevitably present, and from the few theoretical studies of this aspect (see Section 1.3), differential solvation may be important and lead to a different order of ion stabilities from that obtained for the gas phase.

## 1.3 The Effect of Solvation

Early theoretical results[27-30] suggested that solvation of carbocations with a localised charge would be greater than for a delocalised charge. This conclusion was mainly based on the study of solvation of the ethyl[30] and homocubyl cations[28] by a single molecule of hydrogen chloride, which showed an energetic preference for ion-pairs based around classical cation structures. Inclusion of a further four solvent molecules in the case of the ethyl cation did not change the relative ordering.

More recently experimental results have been used to show that differential solvation of carbocations is not of large magnitude.[31] For example, the rate of the methyl scrambling process in the t-amyl cation (VI) was found to be the same within experimental error, in different super-acid

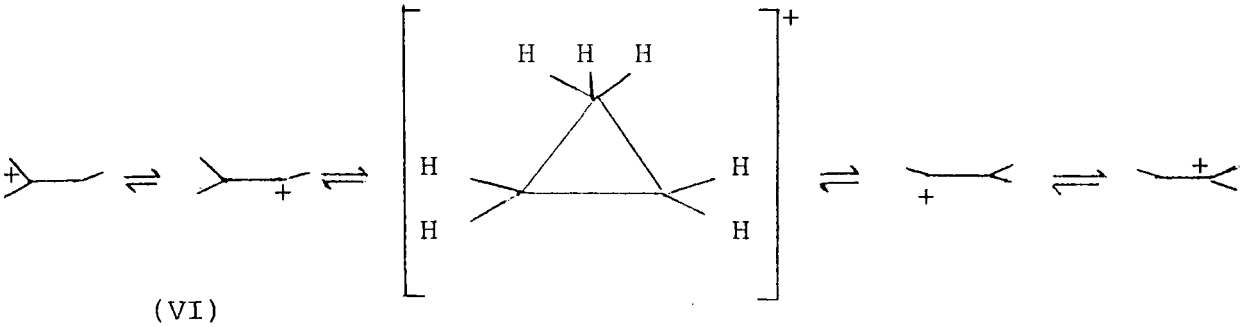

(VI)

solvent systems, and from this it was concluded that solvation of the ion and transition state was similar. If this were not the case then solvents of varying solvating abilities would be expected to differentially solvate the ion and transition state to different extents, thus changing the activation barrier for the process and consequently its rate would vary in different solvents.

One piece of experimental evidence though, which does not fit this general conclusion is the rotational barrier of the allyl cation (VII).

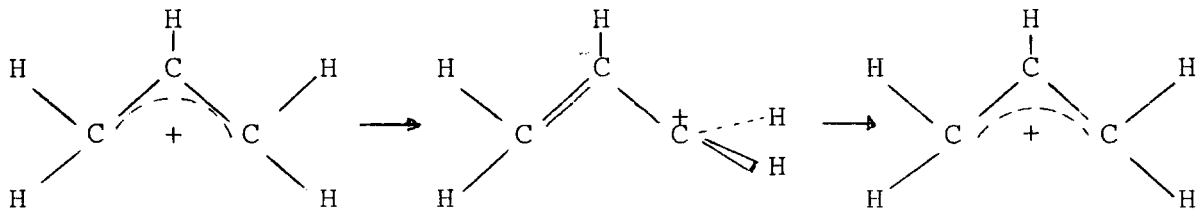

(VII)

The gas phase barrier of 34kcal/mol decreases to ∿24kcal/mol in superacid solution[32] and this is consistent with greater solvation of the perpendicular, transition state, form of the ion, where the charge is more localised.

Since the experimental results generally showed that differential solvation was not an important factor, it was suggested[31] that the different result obtained from theoretical calculations derived from the relatively poor representation of a solvent by, at best, five molecules of hydrogen chloride. Very recently, however, calculations on the allyl cation in liquid hydrogen fluoride, involving a much larger number of solvent molecules were reported,[33] and these showed differential solvation for localised and delocalised cations; but this is the one system for which differential solvation is found experimentally!

## 1.4 Methods of Carbocation formation

There are two basic methods for the formation of carbocations from molecules:[34,35]

(1) Ionisation of a compound in which a group adjacent to a carbon atom leaves with a pair of electrons (*i.e.* heterolytic fission)

$$R - X \longrightarrow R^+ + X^-$$

(2) The addition of a positive species (frequently a proton) to one atom of an unsaturated species, leaving the other (carbon) atom with a positive charge.

$$\diagup\!\!\diagdown C = Z + P^+ \longrightarrow \diagup\!\!\diagdown \overset{+}{C} - Z - P$$

Both these methods have been used in this work and are discussed in more detail below. A third method involves electron removal from an electrically neutral species, *e.g.* a radical.

### 1.4.1 Antimony pentafluoride and organic halides

Perhaps the most frequently encountered example of heterolytic fission of a precursor is the ionisation of organic halides which can be conveniently achieved using the strong Lewis acid, antimony pentafluoride. Preparation by this route has been used by several groups, and the reaction extensively studied.

The first reported carbocation, prepared by this method, was the t-butyl cation,[36] generated by dissolving t-BuF in excess $SbF_5$ as solvent. The presence of a carbocation was suggested from the proton NMR (run at $\sim 40^{\circ}C$) where a single, substantially deshielded peak, free from $^{1}H$-$^{19}F$ coupling was observed. The general utility of the method was demonstrated by also preparing $C_3$ and $C_5$ cations from the corresponding alkyl fluorides;[7] excess $SbF_5$ was always required and it was assumed that it was capable of solvating the cations. To enable lower temperature spectroscopic observation, solvents were introduced, sulphur dioxide in particular, and later sulphuryl-chlorofluoride and -fluoride ($SO_2ClF$, $SO_2F_2$). The ionisation was also shown to proceed using alkyl chlorides. The effect of solvents on carbocation has been extensively studied more recently.[37]

However, the presence of solvents can complicate the basic ionisation process; for example a side reaction is known to occur between sulphur dioxide and excess antimony pentafluoride. Also from solution studies of carbocations, the process from neutral to ionised molecule involves several stages.[38] Initial ionisation leads only to a tightly bound

ion-pair contained in a solvent cage, from which a solvent separated ion-pair is formed, which separates to give (solvated) "free" ions. Thus the exact state of the reagent molecules is complex.

The main reason for introducing solvents is to enable low temperature spectroscopic studies. For example in the molecular beam method (see below) a two component ion mix is prepared from the organic halide and Lewis acid, solvent only being added at a later stage to enable transfer of the sample into a tube for NMR observation. That the solvent is not necessary for the ionisation process is clear, not only from the original work,[7] but also from results of spectroscopic studies of carbocation salts in the solid state;[13,39-41] (but see Section 2.4).

The original preparation of alkyl hexafluoroantimonates by means of slowly adding the alkyl halide to liquid antimony pentafluoride (at $\sim$5-7$^{o}$C)[7] was only suitable for the most stable isomeric cation; for example, all butyl fluorides yield the t-butyl cation. Early attempts to prepare less stable cations centred on lowering the temperature at which the reagents were brought together, but rearranged products were observed;[22] a solvent was needed because of the high melting point of the Lewis acid. Since then, a much improved method has been reported,[42-43] which was designed to prepare cations from unsaturated precursors (where polymerisation can easily occur) and those prone to rearrange to thermodynamically more stable cations; in essence, molecular beams of reagents are co-condensed onto a liquid-nitrogen cooled surface, within

a chamber evacuated to $<1x10^{-5}$T before the deposition is begun. In this way an intimate ion mix is prepared in which the precursor is matrix isolated in excess antimony pentafluoride close to liquid nitrogen temperature. Similar procedures have been used to prepare samples for solid-state NMR study.[39]

It should be noted that the equation

$$R - X \longrightarrow R^+ + X^-$$

is a simplified expression of the reaction which occurs. Antimony pentafluoride is known to associate in all three phases.[44] Whilst the solid is a cyclic tetramer, the liquid phase consists of $SbF_6$ octahedra, where two corner fluorine atoms bridge between the units; at ambient temperature antimony pentafluoride vapour exists mainly as monomer, dimer and trimer, with small concentrations of higher oligomers, and even at $>100^{o}C$ the vapour exists as both monomer and dimer.

Studies of the t-BuF/$SbF_5$/$SO_2$ system using $^{19}F$ NMR established, by comparison with $CsSb_2F_{11}$, that the anion present is $Sb_2F_{11}^-$.[45] In the absence of the solvent, higher polyanions were thought to be present. This work is also important since, because anions are found to be present in these systems, it follows that cations are also present and thus adds more weight to the conclusion that the product is an ion-pair as opposed to a highly polar donor-acceptor complex.

One other basic problem which has been identified in this route to carbocations is the potential for the formation of halonium ions.[46]

The production of gas phase carbocations by this route has been carefully studied.[47,48] In

these experiments reaction was performed by allowing the two beams of reagents to meet at 90° to one another. Pressures in the reactor were not given, but if they are similar to those used in earlier work they are >100T.[49] Product ions are detected by a mass spectrometer. It was found that by adjusting the nozzle temperature of the antimony pentafluoride beam, the amount of monomer, dimer, *etc.* could be varied, and thus reactions of various organic halides with the different oligomers could be deduced. For example, it was concluded that t-butyl bromide reacted with the dimer, whilst t-butyl chloride does not react with either the monomer or dimer.

### 1.4.2 Protonation of alkenes

Protonation of norbornene appears to be an ideal way of generating the norbornyl cation. Indeed, this method has been tried. The product of the reaction of fluoroantimonic acid with norbornene at low temperature, was shown by NMR to be the same as that obtained by ionisation of exo-2-norbornyl chloride.[50] However protonation by fluoroantimonic ($HF-SbF_5$) or "Magic" acid ($HSO_3F-SbF_5$) involves essentially three reagents, which increases the problems in preparing samples for ESCA analysis. Superacids are needed though, in order to have the best chance of forming an ion pair, as opposed to a polarised donor-acceptor complex; consequently fluorosulphuric acid was chosen since this is one of the strongest simple protonic acids known.[51]

The conductivity of fluorosulphuric acid occurs largely from its autoprotolysis,

$$2HSO_3F \rightleftharpoons H_2SO_3F^+ + SO_3F^-$$

which gives rise to proton transfer conduction and this is used to explain the considerably greater ionic mobilities found for this solvent.[52]

The mechanism of hydrolysis of the acid is complicated and incompletely understood.[53] Part of the acid hydrolyses rapidly to hydrogen fluoride and sulphuric acid, whilst the remainder forms the hydroxonium salt, $H_3O^+ SO_3F^-$. The fluorosulphate anion then slowly hydrolyses[54] through decomposition of the S-F bond.

$$HSO_3F + H_2O \longrightarrow \begin{cases} HF + H_2SO_4 \\ H_3O^+ SO_3F^- \end{cases}$$

$$SO_3F^- + H_2O \longrightarrow HSO_4^- + HF.$$

The chemistry of superacids, particularly with alkenes and alkanes, is complex,[55] and protonation is not the only mechanism of carbocation formation in such systems. For example, although the norbornyl cation has been prepared by protonation of norbornene using $HFSbF_5$, the same cation is reported to be formed from norbornane using either $HF\text{-}SbF_5$ or $FSO_3H\text{-}SbF_5$ [56] where these superacids act as hydride abstractors. Similarly when cycloheptatriene is slowly added to fluorosulphuric acid at room temperature the tropylium cation is formed.[57] However this latter mechanism of cation formation, hydride abstraction from an unsaturated precursor, is suggested to be limited to the formation of stable cations; indeed, the particular reaction of fluorosulphuric acid with norbornene is reported, in solvent ($SO_2ClF$) at $-130^oC$ to give exo-2-norbornyl fluorosulphate.[58]

It has been suggested that one problem with the preparation of carbocations from olefins is polymerisation[43] because the addition of a cation to an alkene is extremely facile. Indeed this seems to have been a problem in the reaction of cycloheptatriene with fluorosulphuric acid where the yield of the tropylium ion was ∿30%;[57] but under suitable conditions, such as vigorous shaking of reagents,[58] or the molecular beam method,[42,43] this appears to be avoidable. However the possibility of this type of side-reaction should be borne in mind.

# CHAPTER TWO

# THE IONISATION OF ALKYL HALIDES

## 2.1 Preliminary experiments

*A priori* there are perhaps several ways of bringing together the carbocation precursors in relation to the spectrometer. Each method has its own intrinsic advantages and disadvantages.

### 2.1.1 The Olah method

In this method the carbocation is formed external to the spectrometer and the sample is then introduced onto a pre-cooled substrate in a nitrogen atmosphere.[18] The basic problem encountered in this work was in the use of the probe cooling system which, designed for cooling samples in High Vacuum, was inappropriate for cooling a sample exposed to the atmosphere; generally this limited cooling of the probe to $\sim -30^{\circ}C$. This is only adequate for comparatively stable carbocations. A second problem of this approach is the condensation inherent with cold probes; thus the lower the desired probe temperature, the better the quality of the surrounding atmosphere must be. It is relevant to note that whereas Olah states that the observed carbocation spectra were recorded at liquid nitrogen temperature, the probe is only described as "precooled" before entry into high vacuum.[18]

Thus, the method is at its best for samples which require minimal, or no cooling. For example, spectra of the triphenyl hexachloroantimonate cation can readily be recorded using this method (Figure 2.1).

Distinction between a localised and delocalised system should follow directly from observation of the $C_{1s}$

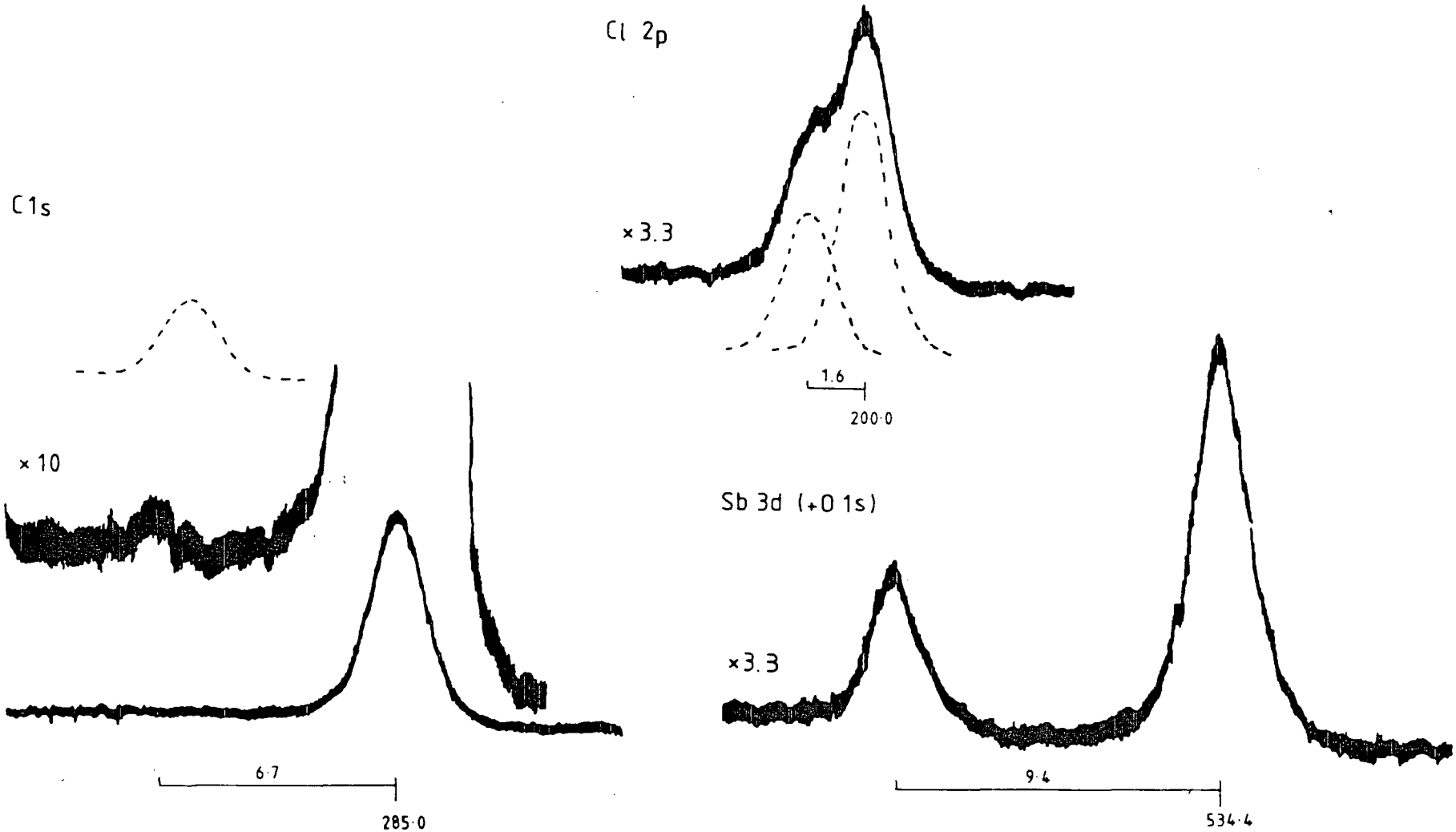


Figure 2.1 CORE-HOLE SPECTRA OF TRIPHENYL HEXACHLOROANTIMONATE CATION (Ambient temperature)

The inset on the $C_{1s}$ spectrum shows the theoretical intensity, on the expanded scale, of a carbon bearing a localised positive charge. Binding energies (referenced to $C_{1s}$ at 285.0) are shown in eV.

core-hole spectrum, but it is important to realise that it is the inter-relationship between the spectra of all the elements present that throws light on whether the observed $C_{1s}$ spectrum is actually that of the pure carbocation. Thus the intensity ratio of 2.9 determined for the peaks at binding energies of ∿534 and 543eV suggests that a fair amount of oxygen is present (subsequently this ratio is referred to as the "purity" ratio); the higher binding energy peak arises from the $Sb_{3d^3/_2}$ core-hole, whilst the other is not only the $Sb_{3d^5/_2}$ , but also the $O_{1s}$ core-hole state, these latter two being accidentally coincident. In the absence of oxygen the expected intensity ratio for the antimony doublet is 3:2 ($Sb_{3d^5/_2}$ : $Sb_{3d^3/_2}$) or 1.5; thus a value of 2.9 suggests the presence of a fair amount of oxygen in the surface. However, in the present case there is no evidence of a shoulder on either peak, nor significant peak broadening, nor is there evidence for C-O functionality in the $C_{1s}$ spectrum; such features would arise in the event of hydrolysis of the system, from an increase in the number of oxidation states of antimony present and quenching of the cation salt. Similarly the relatively clear $Cl_{2p}$ doublet peak suggests the integrity of the counter-ion is maintained, and from this the integrity of the carbocation is inferred.

A second contamination problem inherent in the use of diffusion pumped spectrometers is that of hydrocarbon build up. All samples in such systems gradually develop an overlayer of adventitious hydrocarbon and this problem becomes accentuated in the case of a cooled probe, where in the limit of liquid nitrogen cooling, the probe tip would become com-

petitive with the trap pumping. Core level intensity ratios of compounds of known stoichiometry are therefore important because they can give information about the thickness of this overlayer. In the present example the C/Cl stoichiometric ratio, derived from the intensity ratio using a pre-determined sensitivity factor, is 4.9 which compares unfavourably with that determined from the compound formula of 3.2, and suggests that up to 35% of the $C_{1s}$ spectra arises from surface contamination. (Surface orientational effects can confuse calculations of this nature; however in the present case, the calculated oxygen signal supports the conclusion that this particular sample does appear to have acquired a fair amount of surface contamination).

The triphenyl ("trityl") carbocation is well known to be delocalised and this is borne out by the $C_{1s}$ spectrum. The inset (Fig.2.1) shows the approximate intensity of the high binding energy peak which would occur in the case of a localised carbocation (assuming 35% contamination of the main $C_{1s}$ peak); from earlier results[18] this peak would be 3-4eV from the main $C_{1s}$ peak. The much smaller intensity peak which does occur at 6.7eV higher binding energy is attributable to shake-up events of the benzene rings.

In view of the limitations of the probe cooling system whilst the probe is outside the spectrometer, a more direct method of cooling the probe tip was tried, in which the probe tip prior to insertion into the insertion lock rests on a copper block, immersed in a liquid nitrogen bath. However this represented only a marginal improvement and did not lead to any positive results.

### 2.1.2 The Insertion Lock Method

The basic idea behind this method is to use the insertion lock as a reaction chamber. The probe was introduced to the first O-ring in the insertion lock, before cooling was commenced. The advantage is that in the low vacuum the probe tip could be cooled to $\sim -50^{\circ}C$. Even at this moderately low temperature problems were encountered with Omni-seals "sticking" to the cooled probe, presenting problems in probe movement in and out of the spectrometer.

Generally a thin film of antimony pentafluoride was introduced onto a gold substrate inside a glove-box. The probe was cooled in the insertion lock and then the Lewis acid was exposed to an atmosphere of alkyl halide (normally t-Butyl chloride) injected through a septum entry port. After a given time (varied from 1 to 30 minutes) the excess alkyl halide was pumped away and the probe pushed through to the spectrometer source.

Initially it was hoped that this method would lead to a lower degree of contamination, since the carbocation would be formed in low vacuum, and would never need to be exposed to atmospheric pressure as in the previous method. However the presence of two distinct peaks in the $F_{1s}$ spectrum of antimony pentafluoride, separated by $\sim$3eV, coupled with a $^{C}/_{Cl}$ ratio often greater than 15:1 was clearly diagnostic of heavy contamination and an unsuccessful deposition of the t-butyl chloride. Presumably in the time inherent in cooling the probe to $-50^{\circ}C$ ($\sim$20-30 minutes), the antimony pentafluoride surface was rendered inert, partly by hydrolysis and

partly by deposition of extraneous hydrocarbon, so that reaction with the alkyl halide could not proceed.

### 2.1.3 Molecular Beams

Saunders *et al* pioneered a vacuum line molecular beam preparation of carbocations suitable for unstable species such as the sec-butyl cation.[42,43] Ideally then, this would be adapted to enable the preparation of carbocations *in situ* in the source of the spectrometer. The main difficulty with the method lies in the possibility of contamination of the spectrometer source, through the use of molecular beams of chemicals such as antimony pentafluoride. Indeed this problem was encountered and consequently a dedicated spectrometer was required for the work. However it was found that the extent of sample contamination could be greatly reduced by using a diffuse argon discharge, at low vacuum, within the source (see Section 2.2.1); this was followed by a conventional bake-out.

The biggest advantage of the method is that a probe can be inserted into high vacuum before cooling and that, other than being rotated to alternately present the sample to molecular beams or the X-ray source, no movement of the cold probe is necessary. Also since the probe was cooled in high vacuum it was possible to routinely attain temperatures of -120$^{o}$C for several hours, and sometimes even below this for a more limited time. Thus this method has the potential to prepare unstable carbocations.

Reservoir shafts are conventionally used to introduce liquids into the spectrometer. The use of a hypodermic syringe to inject samples through the septum entry is inappropriate for a viscous air sensitive sample such as antimony pentafluoride, and thus a reservoir shaft was adapted to take a glass sample tube (Fig. 2.2). The

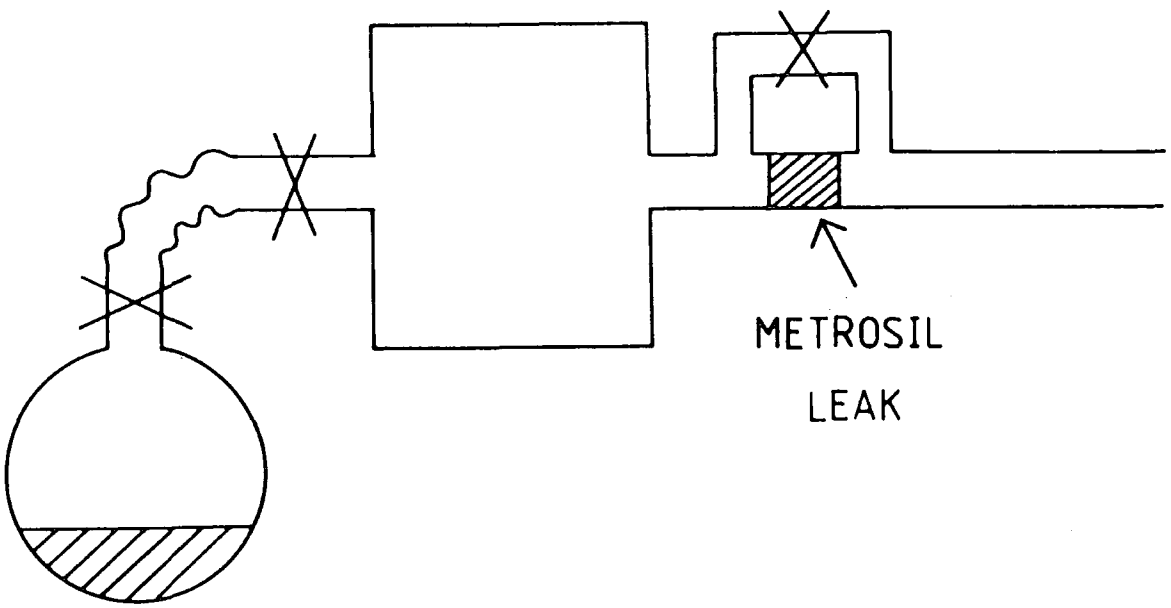


Figure 2.2 SCHEMATIC OF ADAPTED RESERVOIR SHAFT

antimony pentafluoride could be purified and degassed on a vacuum line and easily connected up for the molecular beam preparation. By using a hairdryer to warm the sample tube, the Lewis acid could be deposited onto a gold substrate

cooled to -120°C. The intense spectra obtained (Fig.2.3) show that a fairly thick layer of the reagent was deposited,

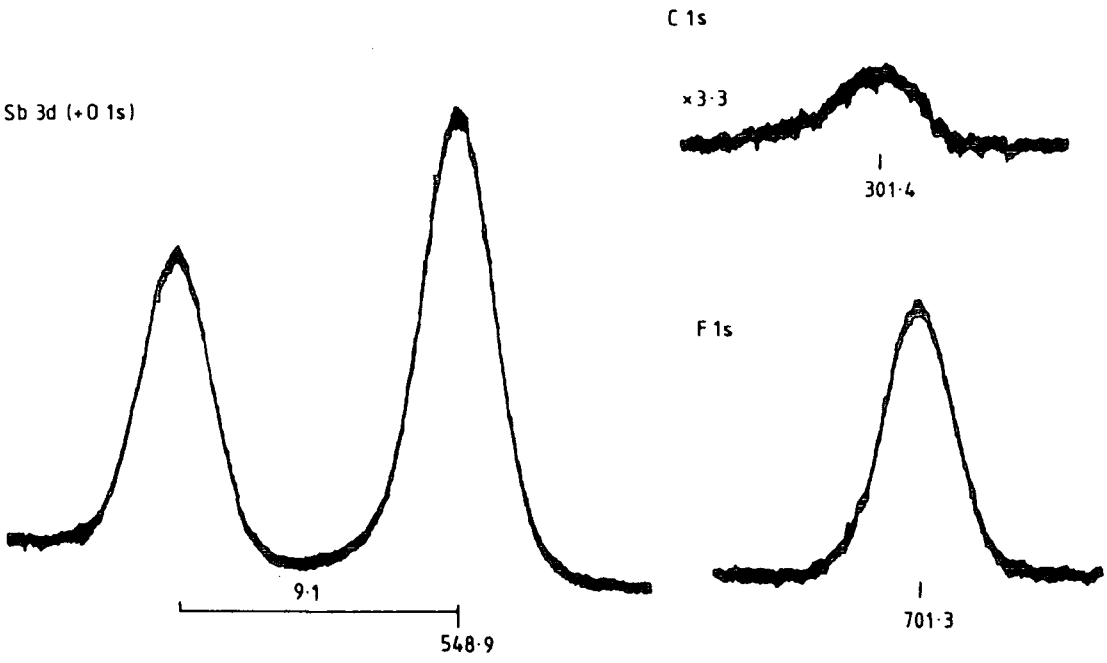


Figure 2.3 ANTIMONY PENTAFLUORIDE DEPOSITED ONTO A GOLD SUBSTRATE FROM THE ADAPTED RESERVOIR SHAFT (Substrate temperature -120°C)

and this was confirmed by the absence of the $Au_{4f}$ signal in a wide-scan spectrum and the fact that the film was visible on the substrate.

The $C_{1s}$ peak appears at high binding energy (∿301eV) and this is attributable to a combination of charging and the fact that in the presence of the antimony pentafluoride the organic material will almost certainly have been fluorinated

to some extent. Using a $C_{1s}/F_{1s}$ sensitivity factor of 0.52, the relative intensities of the two core level peaks suggests a maximum contamination level of one carbon for every five fluorines, though if the carbon signal arises only from an overlayer, the contamination could be less. For comparison with later results the $Sb_{3d^3/2}/C_{1s}$ intensity ratio was determined as ∿12. By using the method outlined in Section 2.1.1, and the "purity" ratio of 1.64, the peak at binding energy ∿549eV is assigned as ∿92% intensity from $Sb_{3d^5/2}$ and 8% from $O_{1s}$. To enable a determination of the stoichiometric formula of the deposited layer, an experimental sensitivity factor for the $Sb_{3d^5/2}$ level, relative to the $C_{1s}$ level, can be calculated as follows. The sensitivity factor determined by experiment depends on two quantities, the photoionisation cross-section of the core-level (which can be calculated[59]), and an instrumental sensitivity factor. This latter quantity depends largely on the kinetic energy of the electron being detected. In the present case the instrumental factor for the electron arising from the $Sb_{3d^5/2}$ level will be the same as that for an electron from the $O_{1s}$ level (since the two have the same kinetic energy). The photoionisation cross-section of the $O_{1s}$ level is 2.85, and relative to $C_{1s}$, the experimentally determined sensitivity factor is 1.67.[60] This leads to an instrument sensitivity factor of ∿0.59 for electrons of kinetic energy ∿700eV. Using this value, together with the photoionisation cross-section of the $Sb_{3d\ 5/2}$ core level of 16.13 leads to an expected experimental sensitivity factor of ∿9.5. (Similarly, 6.3 for $Sb_{3d^3/2}$). These figures are summarised in Table 2.1,

TABLE 2.1

| | Core-hole state | | | |
|---|---|---|---|---|
| | $C_{1s}$ | $F_{1s}$ | $O_{1s}$ | $Sb_{3d^{5}/_{2}}$ |
| Experimental S.F. | 1 | 2 | 1.67 | 9.5 |
| Core-level X section | 1 | 4.26 | 2.85 | 16.13 |
| Instrumental S.F. | 1 | 0.47 | 0.59 | 0.59 |

along with those for the $F_{1s}$ level for comparison. Note that all figures have been related to the $C_{1s}$ level as standard. This semi-empirical value of 9.5 compares favourably with an approximate value of 9 determined from the spectra of the (contaminated) triphenyl hexachloroantimonate carbocation discussed in Section 2.1.1.

The stoichiometry of the deposited material can now be derived as $SbO_{0.5}F_{2.8}$. The first hydrolysis product of antimony pentafluoride is $SbOF_3$ and thus the observed $^{Sb}/_{F}$ stoichiometry of 2.8 suggests almost total first-stage hydrolysis; the $^{Sb}/_{O}$ ratio however, is consistent with the presence of only 50% $SbOF_3$. To some extent this inconsistency could be explained by the presence of moisture at the very surface, causing differential attenuation of the $Sb_{3d}$ and $F_{1s}$ core level signals. It should also be borne in mind though, that the stoichiometry determined rests heavily on the sensitivity factors used and these were established mainly from polymer systems; it is conceivable that they are not totally applicable to all systems. Another potential source of error, particularly in determining the Sb/O ratio, is the method of

using a single straight base-line in defining the peak areas, *i.e.* a problem of data manipulation; in this context it should be noted that the "purity" ratio, determined for all antimony pentafluoride samples deposited by molecular beams, was consistently ∿1.6-1.7 and never as low as the theoretical value for a pure antimony doublet of 1.5; of course it could be that the higher value represents the level of contamination inherent in the present experiments. It is shown later (Section 2.2.2) that the "purity" ratio turns out to be an insensitive test of the extent of hydrolysis.

Although the deposited layer may be relatively impure, the use of reservoir shaft molecular beams does represent a significant improvement over the insertion lock method, in forming a potentially reactive surface for the preparation of carbocations.

Deposition of tertiary butyl chloride was attempted on top of a layer of antimony pentafluoride (Fig.2.4). It was possible to deposit a sufficiently thin film of the alkyl halide that the Lewis acid could still be spectroscopically observed through it. Whilst the approximate shape of the $C_{1s}$ spectrum obtained suggests that this was successful, the relatively low intensity of the $Cl_{2p}$ signal leads to a $^{C}/_{Cl}$ stoichiometry of 8:1. Initially from this it might be concluded that contamination is still a problem. Deconvolution of the $C_{1s}$ spectrum suggests that it contains at least three components at relative binding energies, 0, 1.7 and 3.0eV, from the most intense component, and this cannot be explained simply by adventitious hydrocarbon. It is possible

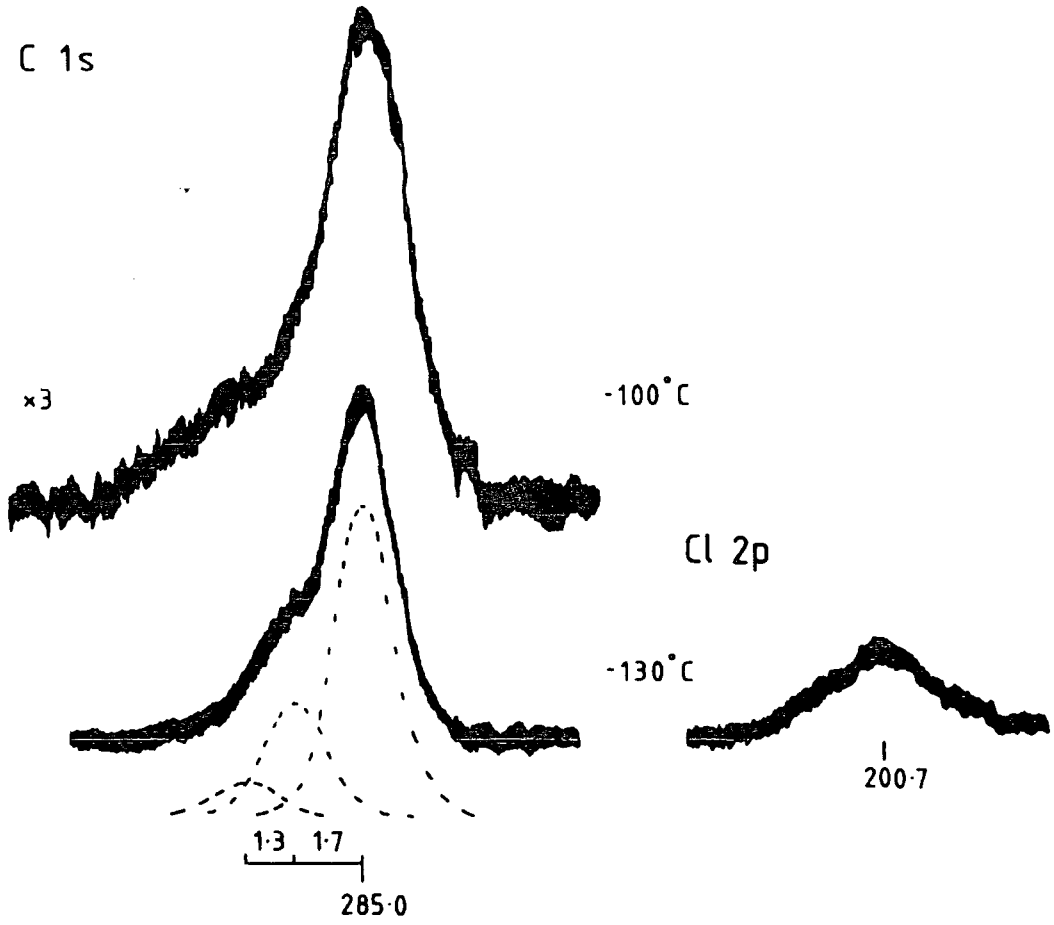


Figure 2.4 T-BUTYL CHLORIDE DEPOSITED ON TOP OF A LAYER OF ANTIMONY PENTAFLUORIDE
Effect of varying temperature (All Binding energies and internal shifts in eV).

that there is a small amount of carbocation present contributing to the high binding energy tail, but the spectrum cannot be simply a mixture of ionised and unionised alkyl chloride since this would still have a $^{C}/_{Cl}$ ratio of 4. It is far more probable that the tail is attributable to partial fluorination of the system. Indeed in another attempt at this experiment, where a very similar $C_{1s}$ spectrum was recorded, a low intensity peak was observed, to higher binding energy (∿3eV) of the main $F_{1s}$ peak (Fig.2.5); this is consistent with the presence of organic fluorine in these systems and helps to explain the large $^{C}/_{Cl}$ ratio.

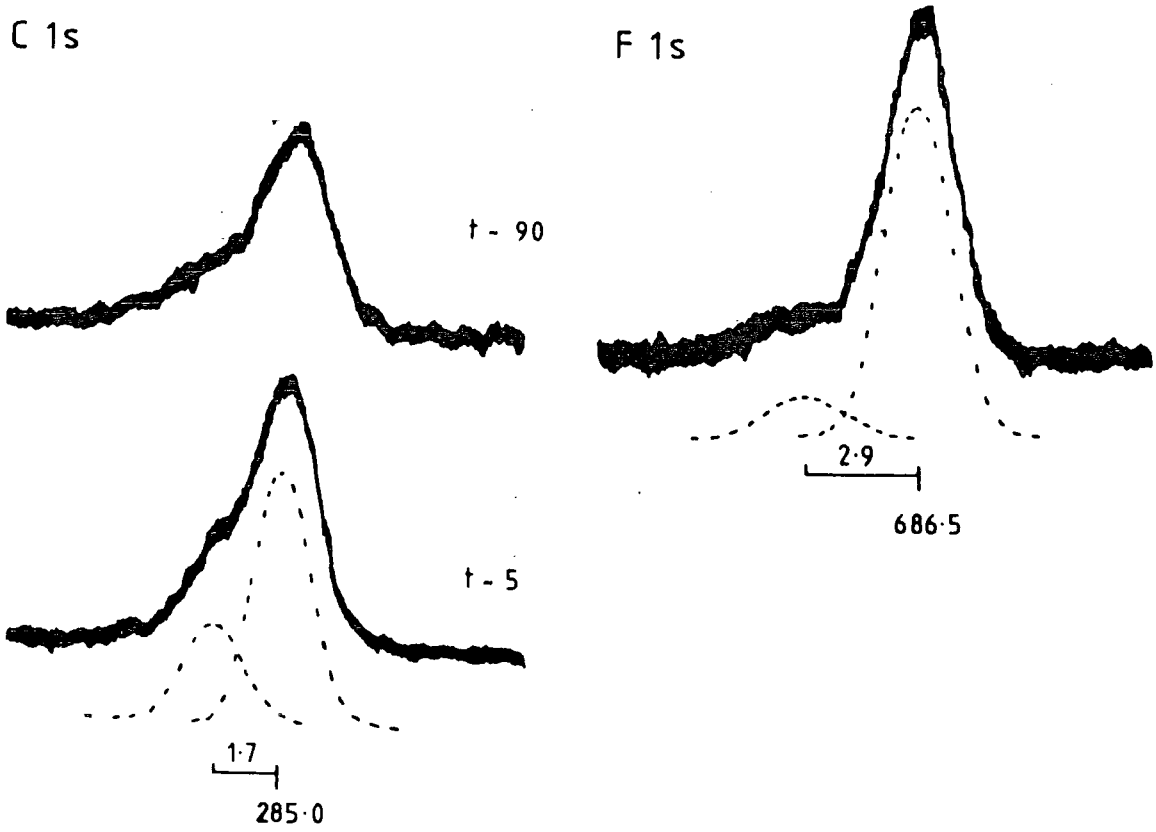


Figure 2.5 T-BUTYL CHLORIDE DEPOSITED ON TOP OF A LAYER OF ANTIMONY PENTAFLUORIDE
Effect of time; times (mins.) are from deposition of the alkyl halide. (All binding energies and internal shifts in eV).

It has been suggested that ionisation of an alkyl halide by antimony pentafluoride, might not occur immediately at low temperatures but that the reaction mix needs to be warmed.[42] Thus conceivably the two deposited layers had not reacted, simply because at -120°C the molecules do not have enough energy to do so. If this were the case, then upon warming, complete ionisation might occur, giving rise to a carbocation spectrum. On allowing the system to warm to -100°C, broadening of the high binding energy side of the peak was observed, but the resolution of peaks, expected in

an ionised system did not occur. One problem with this warming-up technique is that the speed of other side reactions (*e.g.* hydrolysis and fluorination) will also be increased. In the present instance further warming to -90°C led, over a twenty minute period, to almost total loss of $C_{1s}$ signal intensity, suggesting that the organic species were still very volatile, and this is consistent with ionisation not having occurred.

It seems improbable that halogen exchange between antimony pentafluoride and t-butyl chloride occurs and that ionisation does not (though such behaviour is known for the methyl system);[61] therefore it is assumed that the organic fluorine most likely arises as an impurity in the deposition of the antimony pentafluoride. If contamination of this type and intensity was consistently present, it would immediately put a severe limitation on the quality of carbocation spectra which could be obtained from this method; in other experiments though contamination of this type was not always apparent, but its presence in one experiment suggests its possible presence in all experiments. Ideally then the deposited Lewis acid would be fully characterised before deposition of the alkyl halide. Inevitably though, this delay might lead to slight hydrolysis of the surface and thus prejudice the possibility of carbocation formation.

Warming up the bilayer of reagents to induce ionisation had been unsuccessful since at -100°C and above this the volatile alkyl halide was lost. The same type of method was used to attempt the ionisation of cyclopentyl

chloride, but although the probe tip was allowed to warm to $-80^{o}C$, ionisation was not apparent and at this temperature the $C_{1s}$ signal intensity began to decrease and there was a concomitant pressure rise in the source.

Since it appeared that ionisation of the alkyl halide layer had not occurred at $-120^{o}C$, an attempt was made to prepare the t-butyl cation by using a single reservoir shaft and injecting the alkyl halide into the antimony pentafluoride-containing reservoir. This method might be suitable for the t-butyl cation itself, because of its relative stability, but less stable cations would of course rapidly rearrange. It should be noted too that this is not a type of molecular beam preparation as such; here the reagents were brought together at comparatively high pressure (perhaps $\sim 10^{-1}$T) inside the reservoir, and the only molecular beam is that issuing from the reservoir shaft AFTER reaction. Initially the pressure in the source remained comparatively high ($\sim 2 \times 10^{-6}$T). Though the overall $^{C}/_{Cl}$ stoichiometry of 5.2 suggests low contamination, the $C_{1s}$ spectrum shows only one carbon environment (Fig.2.6); not only was there no peak at 3-4eV from the main one (expected for a positive-charge bearing carbon) there was also no peak at $\sim$1.6eV higher binding energy, expected for a chlorine-substituted carbon. Spectra recorded $\sim$45 minutes later, when the pressure had dropped back to $\sim 2 \times 10^{-7}$T, yielded a $^{C}/_{Cl}$ stoichiometry of 1.3. These facts can be interpreted by supposing that a side reaction occurs in which the alkyl halide eliminates hydrogen chloride, giving rise to an independence of the carbon and chlorine species (see Section 2.3.1).

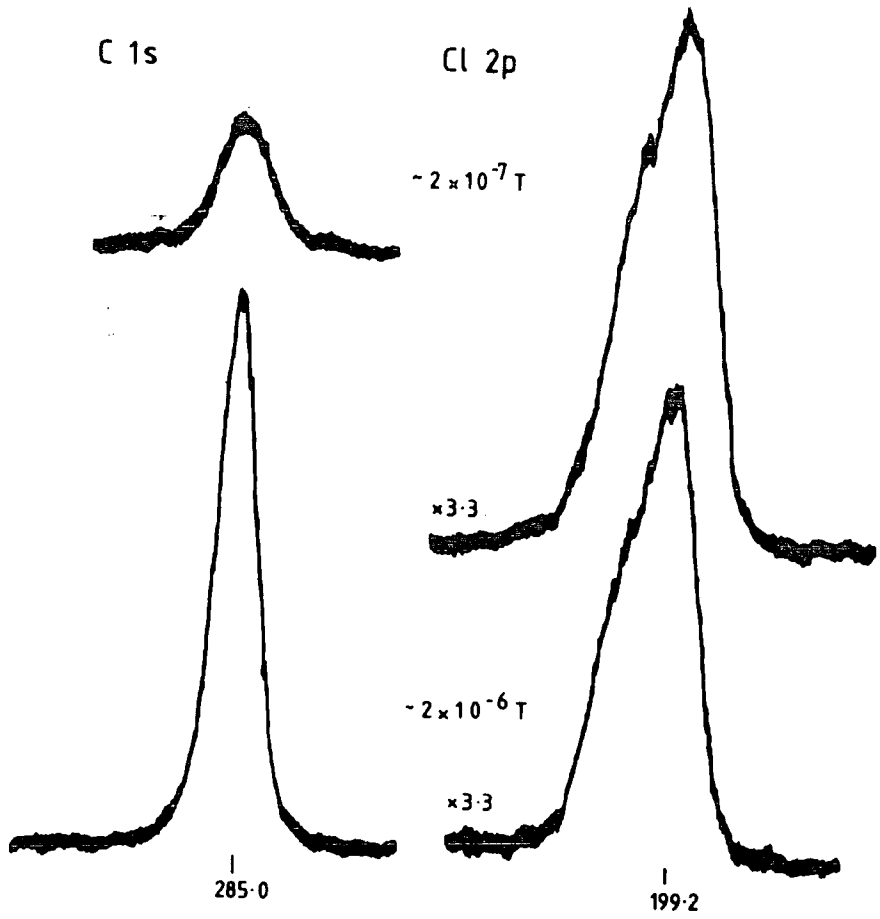


Figure 2.6 CO-DEPOSITION OF ANTIMONY PENTAFLUORIDE AND T-BUTYL CHLORIDE FROM A SINGLE RESERVOIR SHAFT (Source pressures given).

In view of the failure of the bilayer-deposited material to react, it was considered desirable to attempt the preparation of a more intimate ion mix. This would ideally be done by a codeposition (*i.e.* simultaneous deposition) of the two reagents onto a cooled substrate. Such an experiment can be envisaged using two reservoir shafts, but the insertion lock configuration on the ES 200 does not permit two shafts to be aimed at a cooled probe from geometrically equivalent positions. More importantly though, an on-off capability is difficult to achieve because of the metrosil leak which continues to allow the passage of chemicals remaining in the reservoir, and thus the only effective way

of shutting off a beam is to withdraw the shaft and close the ball valve of the insertion lock. Also the reservoir shaft contributes a fairly large "dead-space" and increased path-length, and this must seriously increase the chance of contamination. For these reasons, a system was envisaged in which short pipes with a valve control, led directly into the source. This method is described and discussed extensively in the following sections.

## 2.2 Experimental

### 2.2.1 Apparatus and methods

The molecular beam method[42,43] was instigated by interfacing a grease-free glass vacuum line to the ES 200 (Fig.2.7; Plate 2.1). Two 70mm copper gasket conflat ports on the front of the spectrometer were used to mount ¼" O.D. stainless steel pipes with an internal length of 3¼"; from instrument drawings it was calculated that these would carry the molecular beams to within ∿¾" of the probe-tip. Externally the pipes were terminated by metal valves - a standard stainless-steel bellows-seal valve (SS-4H) on the alkyl halide "arm", and a more corrosion resistant Inconel valve on the antimony pentafluoride "arm". The latter was a conventional screw thread metering valve, which on its own allowed a fair degree of control of this beam. Control of the organic halide was originally by a capillary (40x0.5mm)[42] but was very soon replaced by a Needle valve to permit accurate and reproducible beam conditions. Thus the relatively insensitive SS-4H valve was only needed as an on-off control.

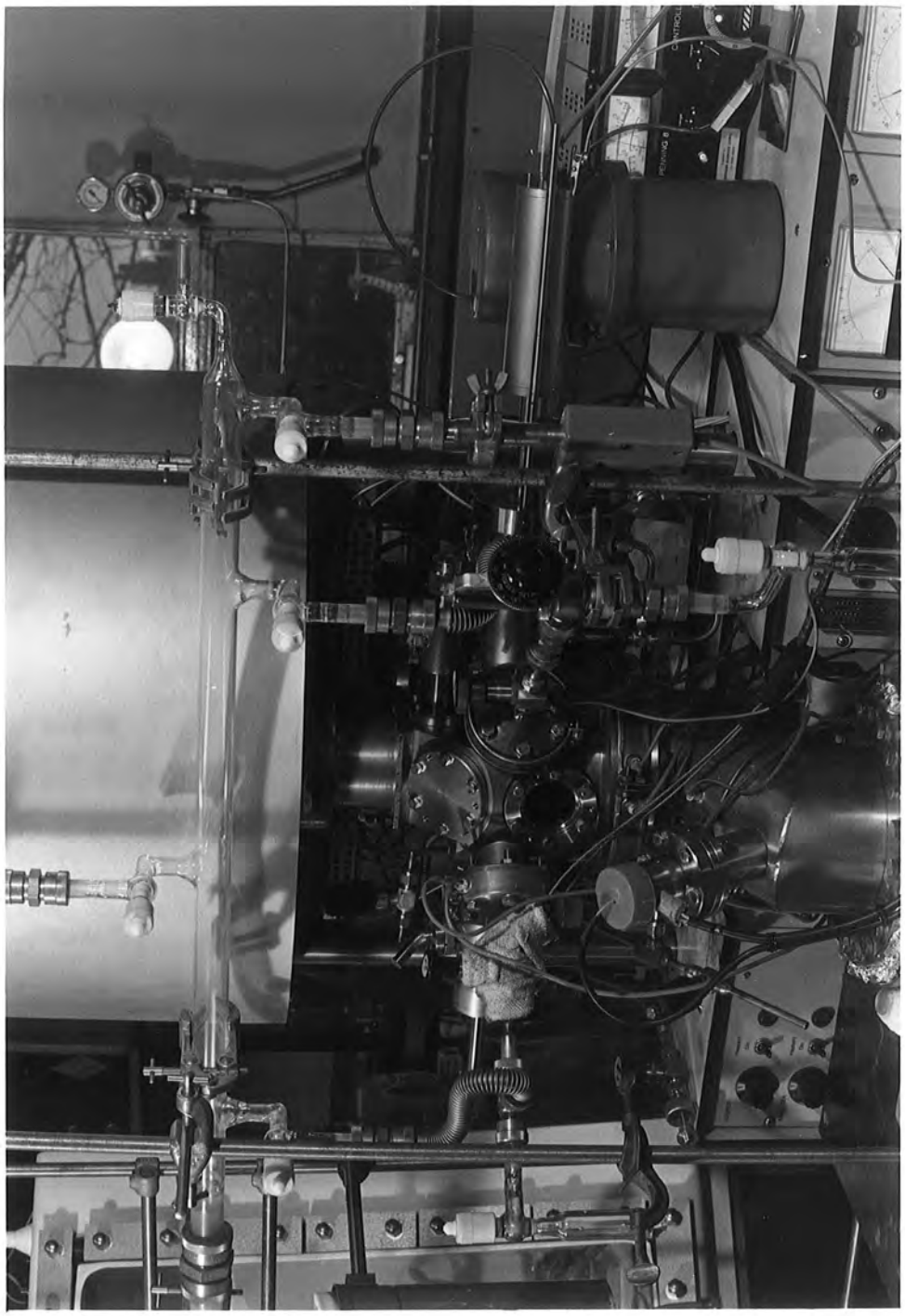

Plate 2.1

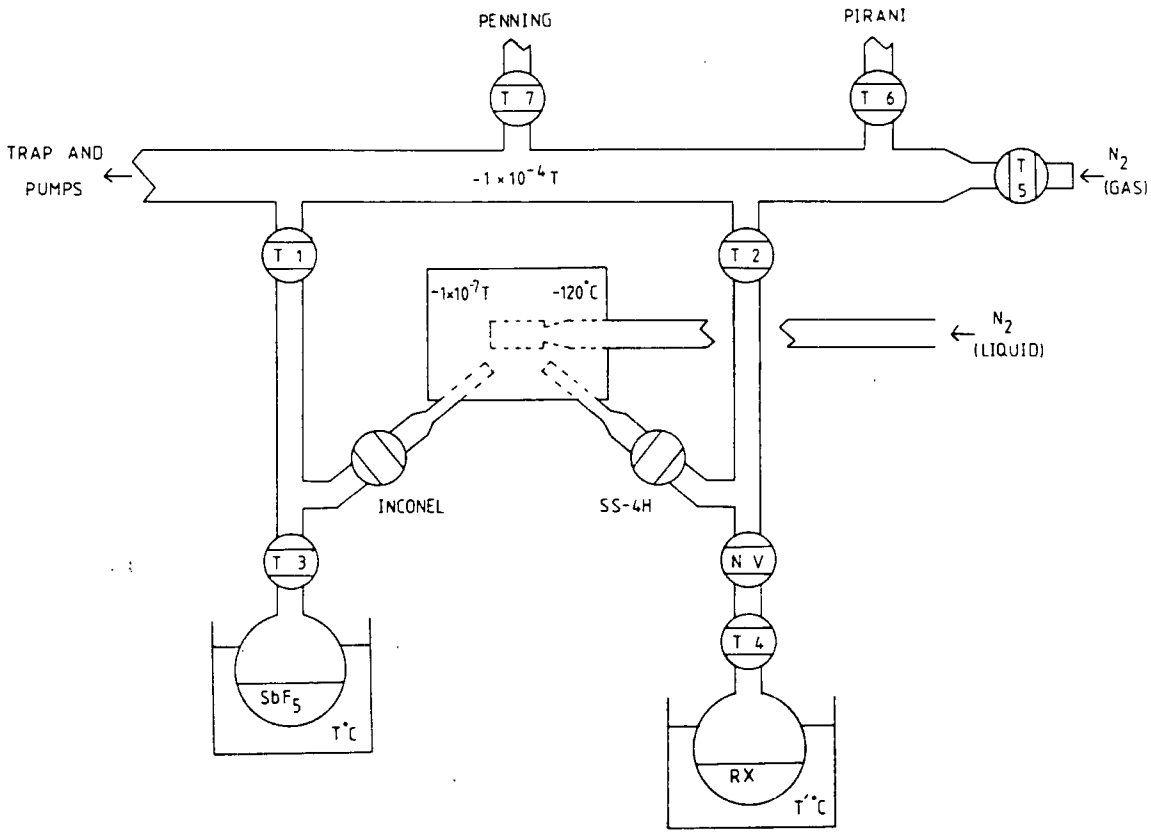


Figure 2.7 SCHEMATIC OF THE MOLECULAR BEAM EXPERIMENT

The vacuum line was pumped by an ED50 two-stage rotary backing pump, and an 80 $ls^{-1}$ E203D oil diffusion pump backed by an E2M2 two-stage rotary, this combination giving relatively rapid cleaning-out of reagent filled arms. A conventional liquid nitrogen trap was included. All taps on the line were teflon, and connections were made by means of Cajon ultra-torr couplings. The molecular beam pipes into the spectrometer were connected to the line by means of flexible stainless steel tubing. Pressure measurements were made using Penning and corrosion resistant Pirani gauges.

A standard procedure was routinely used for the deposition experiments. The two reagents were degassed using rotary and diffusion pumps to $\sim 6 \times 10^{-4}$T, and then connected to the vacuum line. (The metal valves into the spectrometer are of course initially closed). The arms are pumped down to $\sim 1 \times 10^{-4}$ (T1, T2, Needle valve, open; T3, T4, closed). At this stage the metal valves can be slowly opened. The Ion 7 gauge, monitoring the spectrometer source pressure, initially registers $\sim 8 \times 10^{-7}$ but this quickly pumps down to $\sim 3 \times 10^{-7}$T; with both T1 and T2 closed the pressure drops to $\sim 2 \times 10^{-7}$T. (Spectrometer base-pressure is $\sim 1 \times 10^{-7}$T). In the event of a leak in either arm, then closing off T1 or T2 leads to a pressure rise in the source, since the leak would then be pumped solely through the spectrometer, and not through the vacuum line as well. Leak testing using the source gauge was found to be more sensitive than using the Penning.

Prior to the deposition of all reagents, the X-rays, Ion pump and analyser were turned off, and the analyser valve closed. This was simply a protective measure.

To deposit the antimony pentafluoride, after pumping out the arm with T1 and the metal valve open, T1 was closed, then the metal valve; T3 was opened to allow vapour into the arm, and the metal valve was used to control the flow. For the organic halide, having pumped out the arm with T2, the metal valve and the needle valve open, T2 and the NV were closed, T4 was opened, and the beam controlled by the NV. Obviously extreme care must be exercised in allowing reagents into the source in this fashion. Additional control of the beams was sometimes obtained by varying the temperature of the reagent reservoirs.

The Ion 7 source gauge was used to determine the extent of reagent flow; thus for example, having cooled the probe to $-120^{o}C$, the first beam was let in to a source pressure of (for example) $\sim 1 \times 10^{-4}$T, and steadied at this, before letting in the second beam, to bring the total pressure up to $\sim 2 \times 10^{-4}$T. The beams could be quickly stopped by operating the metal valves ; in an ideal experiment the source pressure would rapidly return to the base pressure, however when using inlet pressures of $6 \times 10^{-4}$T it normally took at least 10-15 minutes for the pressure to return to $\sim 4 \times 10^{-7}$. Spectral observation normally commenced when the source pressure was $\sim 1 \times 10^{-6}$T, which was generally within a few minutes of closing the valves.

The arms were cleaned out, in succession, by allowing the reagents to condense in the vacuum line trap; the organic reagent arm was usually cleaned out first, and then that of the antimony pentafluoride; this avoided involatile product formation in the vacuum line. To avoid contamination and corrosion, the Penning head was closed off from the line, as much as possible, during such clean-out cycles. The vacuum line was routinely let up to nitrogen when emptying the trap.

Some problems were encountered with small air-leaks in the Inconel valve body, assumed to be associated with wear of the screw-thread barrel mechanism; initially this could be solved by keeping the valve warm, but eventually the valve had to be replaced. These problems were also associated with a loss of valve control, due to tightening of the body assembly, and in later experiments (butene + $FSO_3H$) the Inconel valve was used simply as an on-off control for the alkene flow, modulated by a needle valve, whilst the SS-4H was found to be suitable for the acid beam.

A gold substrate was used, mounted on a copper probe-tip. The cleanliness of the substrate and source were routinely monitored by recording carbon and oxygen/antimony spectra upon first insertion of the probe and again $\sim$45 minutes later when the probe had been cooled to $-120^{o}C$.

Analysis of all materials was normally conducted at a substrate angle of $30^{o}$; thus the probe had simply to be rotated through $120^{o}$ to change from the analysis to the deposition position, the orientation of the substrate being normal to the molecular beams in the latter case.

Early experiments suggested that antimony contamination of the spectrometer would be a problem; thus a fairly crude, but high current, Argon ion gun (of CEGB design) was fitted. Prior to baking the machine it was let-up, using argon, to a pressure of ∿0.1T. A diffuse discharge (as opposed to a discrete ion beam) was initiated using a voltage of ∿2.3kV, and subsequent increase of the power supply to a maximum, gave a discharge current of ∿9mA. The discharge was usually operated for 6-8 hrs., and the machine baked the following day. The analyser valve was closed prior to initiating the discharge, since its possible effect on the electron-multiplier was unknown; contamination was anyway expected to be greatest in the source where the molecular beams were being used. The sputtering action of the discharge appears to have been successful, since significant antimony contamination was not subsequently observed.

Antimony pentafluoride, fluorosulphuric acid, or "Magic" Acid ($SbF_5$-$FSO_3H$) were transferred from their storage bottles to a standard sample degassing tube, with a teflon stopper, using a glass pipette. The operation was carried out under an inert atmosphere produced by nitrogen flowing through an inverted funnel. Normally no purification was considered necessary other than degassing.

The commercial alkyl halides (t-BuCl, t-BuBr, cyclopentyl chloride) were vacuum distilled from a tube containing phosphorous pentoxide to ensure that they were as dry as possible. Exo-2-norbornyl chloride was prepared by the hydrochlorination of norbornene in pentane at -78°C,[62]

and GLC and GC-MS used to show that the product was ∿95% pure; the main impurity was some unreacted norbornene, which proved difficult to separate.

Norbornene was transferred by warming it, and then pouring into a sample tube, followed by degassing; cis-but-2-ene and t-butyl fluoride were used directly from their cylinders.

### 2.2.2 Analysis of precursors

#### (i) Antimony pentafluoride

Antimony pentafluoride was allowed into the source to a pressure of $1 \times 10^{-5}$T for 30 seconds, and condensed onto a substrate cooled to -120°C (Fig.2.8). Signals arising from the gold substrate were not observed. The "purity" ratio was ∿1.7, comparable to that from use of the reservoir shafts and suggests that some oxygen may be present, but as noted earlier this ratio was fairly typical and a theoretical ratio of 1.5 was never observed. The $Sb_{3d^{3}/_{2}}$ /$C_{1s}$ intensity ratio is ∿92, and suggests a Sb/C stoichiometry of ∿15:1. Comparison of these results with those obtained using a reservoir shaft suggest that the organic contamination is almost an order of magnitude less when using a valved beam (*c.f.* $Sb_{3d^{3}/_{2}}$ /$C_{1s}$ intensity ratio ∿12). The $Sb_{3d^{3}/_{2}}$ /$F_{1s}$ intensity ratio is initially 0.95, equivalent (using bulk sensitivity factors) to a stoichiometry of $SbF_{3.5}$, and this suggests that a large part of the surface may actually be species such as $SbOF_3$.

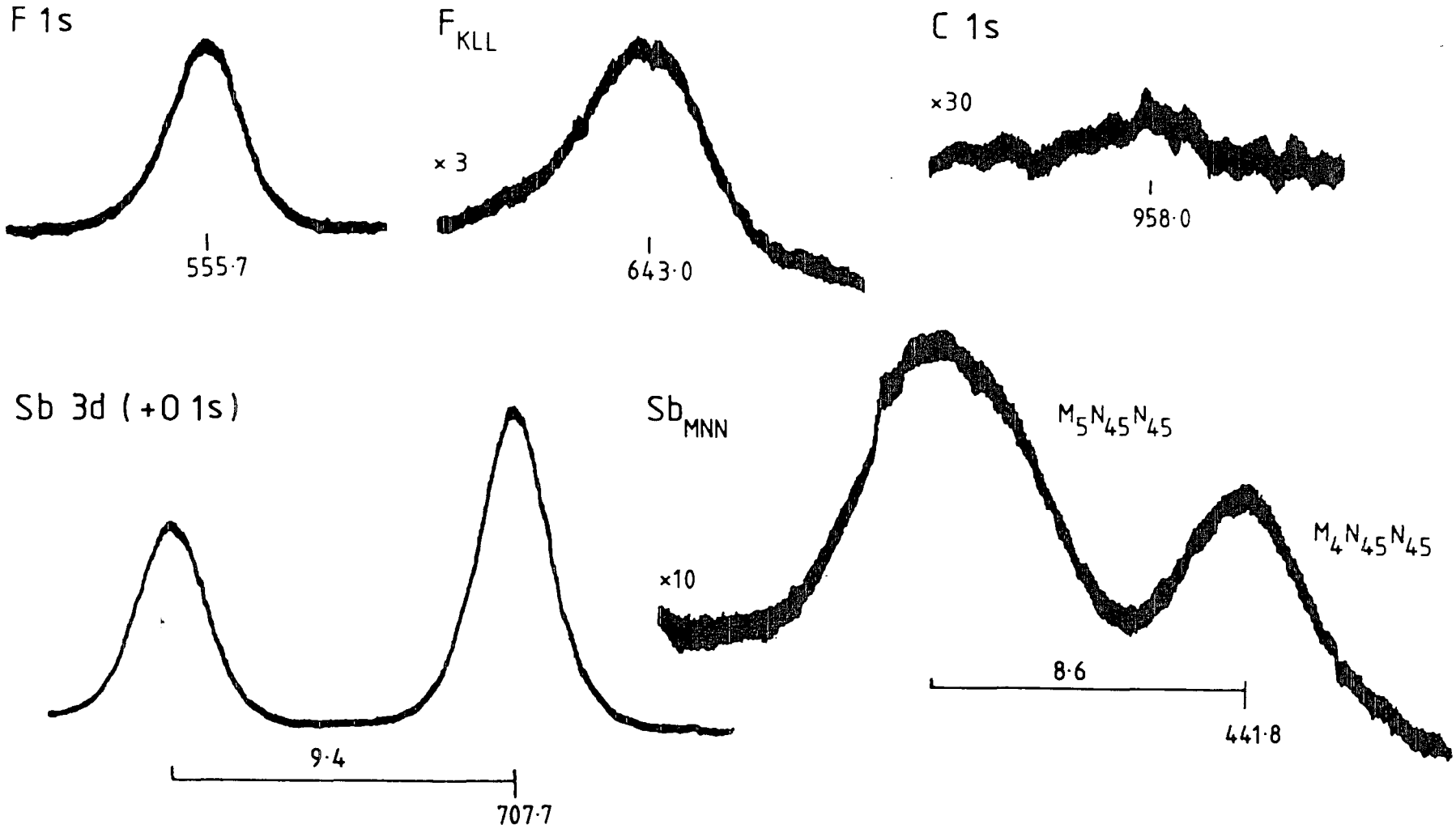


Figure 2.8 ANTIMONY PENTAFLUORIDE DEPOSITED ON A GOLD SUBSTRATE. (Kinetic energies and peak separations in eV).

The small $C_{1s}$ peak occurs at a kinetic energy of 958eV, but as indicated previously it is impossible to charge reference from this peak since its environment is unknown and the intensity of the tail from the inorganic fluorine in the $F_{1s}$ peak precludes the possibility of determining from that core-level, whether a small amount of organic fluorine is present. However, though binding energies, corrected for charging, cannot be calculated, the surface can be further characterised by the determination of Auger parameters. This is particularly suitable for the present case since the parameter is independent of sample-charging, and because suitable peaks are present in the $MgK_{\alpha_{1,2}}$ excited spectrum, for both antimony and fluorine. Conventionally the most intense Auger and photoelectron lines are used; for example in the case of antimony this would be the $M_5N_{45}N_{45}$ and $Sb_{3d^5/_2}$ . However the $M_5N_{45}N_{45}$ transition is particularly broad and therefore in this work it was considered preferable to use the adjacent $M_4N_{45}N_{45}$ peak, where the kinetic energy is more precisely de fined; similarly since the peaks at kinetic energy ∿700eV suggest that oxygen may contribute significantly to the higher kinetic energy peak along with the $Sb_{3d^5/_2}$ level, the $Sb_{3d^3/_2}$ kinetic energy was used in the calculation of a modified Auger parameter type value for the system ($\alpha'_T$). In the present example $\alpha'_T$ is 997.1 and the modified Auger parameter for fluorine $\alpha'$ is 1340.9. In general though, Auger parameters appropriate to ionised systems could not be determined. Not only was the amount of haloantimonate counter-ion small compared with the excess Lewis acid, but also the system was rarely stable enough to enable complete characterisation corres-

ponding to a single $C_{1s}$ spectrum.

After about three hours the "purity" ratio was still ∿1.7, whilst the $Sb_{3d\,3/2}$ /$C_{1s}$ ratio had decreased by a factor of two, suggesting only minimal build-up of adventitious hydrocarbon. The $Sb_{3d\,3/2}$ /$F_{1s}$ ratio however had increased to 1.2; about 1½ hours after deposition an intermediate value of ∿1.1 had been observed. These figures are consistent with slight hydrolysis of the Lewis acid on standing in the spectrometer, and they suggest that it is the $Sb_{3d\,3/2}$ /$F_{1s}$ intensity ratio which is most sensitive to this occurring, since loss of hydrogen fluoride, consequent upon hydrolysis, causes an increase in this ratio, whilst any changes in oxygen signal are apparently lost within the high intensity $Sb_{3d\,5/2}$ signal.

It is regrettable that the "purity" ratio is not sensitive to changes caused by hydrolysis; since the ratio depends on electrons with the same kinetic energy, its value will be largely independent of overlayer effects. Generally attenuation of the electrons giving rise to one peak involved in a ratio, is greater than for the other, due to differences in mean free paths of electrons of different kinetic energies. A ratio which was independent of overlayer effects would have been extremely useful in determining the extent of hydrolysis of a substrate, beneath an overlayer (see Section 2.3.3).

(ii) Exo-2-norbornyl chloride

The source was let up to a pressure of ∿$1\times10^{-5}$T for 1 minute, in order to condense norbornyl chloride onto a substrate pre-cooled to -120°C (Fig.2.9). The initial wide

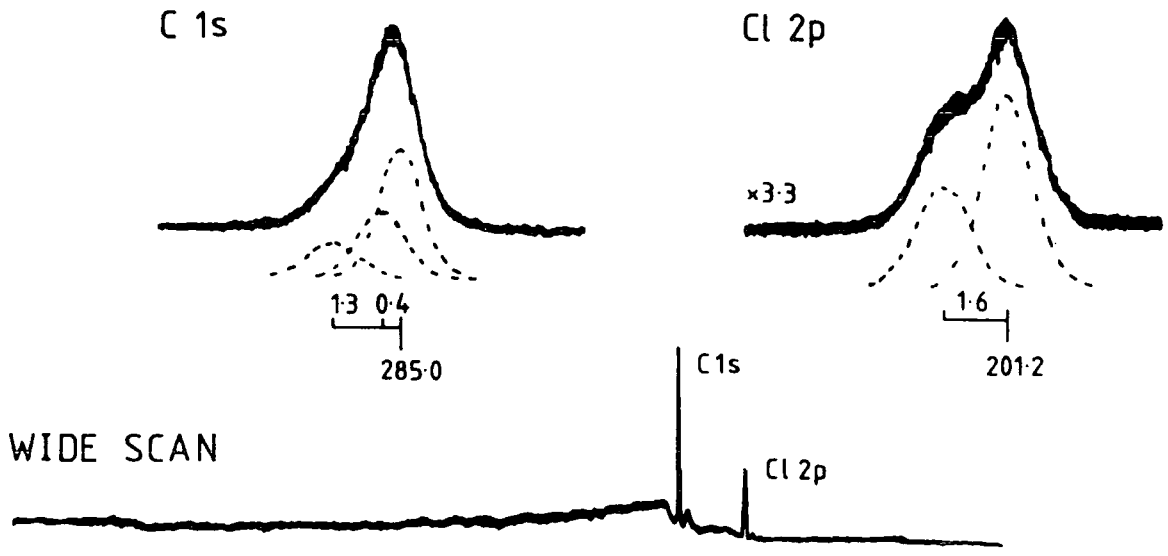


Figure 2.9 EXO-2-NORBORNYL CHLORIDE DEPOSITED ON A GOLD SUBSTRATE (Binding energies, referenced to $C_{1s}$ at 285.0, and internal shifts in eV).

scan spectrum shows that not only does the deposited film obscure the gold substrate, but that the only elements present are carbon and chlorine. The high resolution $C_{1s}$ core-level spectra can be resolved as three peaks with an intensity ratio of 1:2:4. The most intense component is assigned a binding energy of 285.0eV; the smallest intensity component is shifted to 1.7eV higher binding energy, and this is consistent with a C-Cl functionality. The intermediate peak, with a shift of 0.4eV from, and an intensity of 50% of, the main component arises from the two carbons with a β-chlorine substituent. The $Cl_{2p}$ core-level shows typical (unresolved)

doublet structure and can be resolved as two components, with an internal shift of ∿1.6eV and where the high binding energy component is ∿35% of the total peak intensity. With reference to the $C_{1s}$ (hydrocarbon) component at 285.0eV, the $Cl_{2p^{3}/_{2}}$ level has a binding energy of 201.2eV, consistent with its organic nature. The overall $^{C}/_{Cl}$ stoichiometry is 6.5, in tolerable agreement with the theoretical value of 7.

## 2.3 Results and Discussion

### 2.3.1 Codeposition of antimony pentafluoride and t-butyl halides

The first experiment attempted using both arms of the experimental configuration described was a codeposition of antimony pentafluoride and tertiary-butyl chloride onto a gold substrate cooled to -120°C. The Lewis acid (bath temperature ∿0°C) was allowed in till the source pressure was $\sim 2 \times 10^{-5}$T and then the chloride (bath temperature ∿-30°C) was introduced; a total pressure of $\sim 4 \times 10^{-5}$T was intended, but lack of control of the beam (at this stage the capillary was in use) led to a total pressure of $\sim 6 \times 10^{-4}$T. The beams were left for ∿3 minutes and then closed off. The very encouraging $C_{1s}$ spectrum (Fig.2.10) displaying a clearly resolved high binding energy peak, and the $Cl_{2p}$ peak were recorded.

From these spectra the $^{C}/_{Cl}$ stoichiometry of the deposited surface layer was ∿3. The high pressure of alkyl halide used for the deposition meant that the source pressure did not return quickly to $\sim 1 \times 10^{-6}$T, and thus conceivably

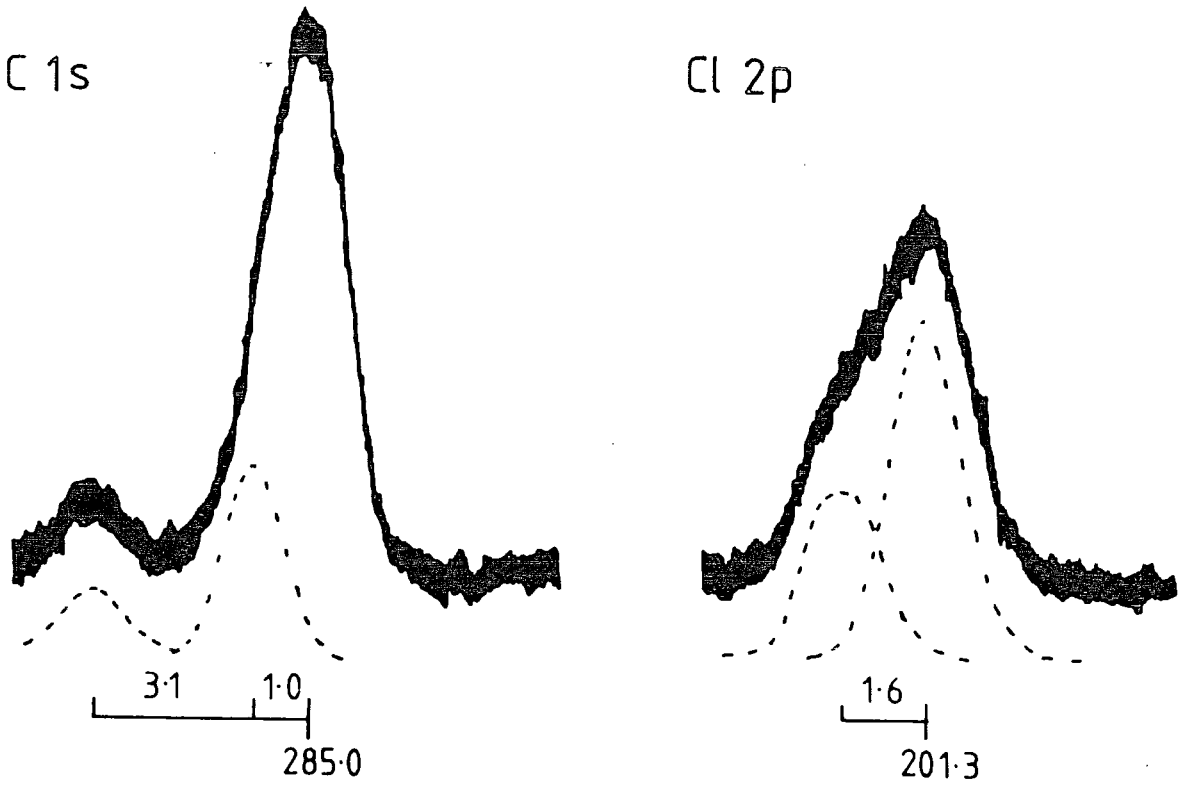


Figure 2.10 CORE HOLE SPECTRA OF A LOCALISED CARBOCATION (Binding energies, referenced to $C_{1s}$ at 285.0, and internal shifts in eV).

deposition of some species might be continuing during recording of the spectra, since the $Cl_{2p}$ level was observed after that of the $C_{1s}$ used to derive this stoichiometry. However this explanation of the low ratio is ruled out, because using another $C_{1s}$ spectrum recorded immediately after the $Cl_{2p}$, still gives a stoichiometry of <4 (2.5). The ratio again seems to be due to interaction leading to elimination of hydrogen chloride from the alkyl chloride. This inevitably leads to a complication in the spectral interpretation.

The small high binding energy peak in the $C_{1s}$ spectrum is ∿10% of the total intensity; thus 33%

of the low binding energy peak would arise from the methyl carbons of the trimethyl carbonium ion. The other 67% of this peak is due to a mixture of $C_{1s}$ intensities arising from unionised t-butyl chloride, alkene (possibly polymerised) derived from molecular interaction, and perhaps some contamination. Even if the third component is negligible, it is difficult to assign relative amounts to the other two; the $Cl_{2p}$ peak cannot be used to determine the total amount (ionised and unionised) of alkyl halide present since it itself arises from alkyl halide and hydrogen chloride, the latter perhaps having interacted with the Lewis acid. Thus a unique resolution of the $C_{1s}$ spectrum does not appear possible. The internal shift ($C_{1s}(C^+)-C_{1s}(\underline{C}-C^+)$, eV) of the t-butyl cation has been experimentally determined as 3.4eV,[18] and theoretically calculated as 3.7eV.[63] The separation of the two resolved peaks (Fig.2.10) is ∿4eV and because of the clear resolution of the two peaks it is possible to determine the minimum possible internal shift of the t-butyl cation by fitting a peak of intensity three times that of the high binding energy peak, to the low kinetic energy tail of the more intense peak; such a peak occurs 3.1eV away from the small resolved peak. The resolution could be completed by a single other peak at 4.2eV from the resolved high binding energy peak, and this could tentatively be assigned as a peak arising from carbon species with little or no positive charge. The shift between this latter peak and that arising from the methyl carbons of the cation is 1.1eV; this represents a maximum shift (corresponding to the minimum shift of the methyl carbons from the cation peak) and is in tolerable agreement with an earlier

deduced value of ∿1.5eV.[19] Comparison of this shift with that deduced from the theoretical results for the gas phase (∿7eV)[64] shows the effect of lattice potential, and differing relaxation enèrgies in the condensed phase.

In view of the probable presence of alkene it is possible that the cation is not the tertiary-butyl cation, but that formed by reaction of the t-butyl cation with iso-butylene; but this would still be a localised tertiary cation (VIII). Thus despite the experimental difficulties, it can be said that the internal shift of a carbon carrying a

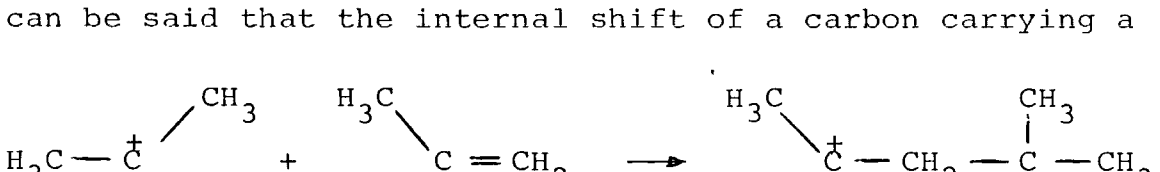

(VIII)

localised positive charge from an adjacent carbon, is at least 3.1eV.

The $Cl_{2p}$ peak can be resolved as a single doublet, with each component having a FWHM of ∿1.6eV. This comparatively narrow line width suggests that either the different $Cl_{2p}$ environments give rise to comparatively small shifts, or that the different species are present in significantly different amounts. Referenced to the $C_{1s}$ low binding energy component at 285.0, the $Cl_{2p^{3}/_{2}}$ level has a binding energy of 201.3eV.

The whole system could not be completely characterised since the second $C_{1s}$ spectrum (recorded immediately after the $Cl_{2p}$) already showed substantial change from the first, with decreasing intensity of the high binding energy

peak and broadening of the other. This rapid change suggests that the carbocation-containing surface was unstable even in the high vacuum environment.

Whilst the absolute binding energies have been quoted, it should be noted that charge referencing in these systems is a problem; they are essentially dynamic and variation of charging was observed in the course of other experiments with inevitable problems in the understanding of the binding energies determined; however it is considered that it is the relative internal shifts that are the most important feature of the spectra, because these are diagnostic of carbocation structure, and they can be accurately computed.

In view of the apparent side reaction occurring when using comparatively high pressures of reagents, particularly that of the alkyl halide, the possibility of reducing the inlet pressures was considered. Deposition of antimony pentafluoride on its own was studied using pressures of between $\sim 1 \times 10^{-6}$ and $2 \times 10^{-5}$T for times varying from 1 to 10 minutes. The quality of the deposited film could be roughly assessed by determining the purity ratio. Using pressures as low as $1 \times 10^{-6}$T yielded little deposition (gold substrate "visible") and the material was of low purity sometimes containing comparatively large amounts of silicon attributed to etching of glassware. Deposition was much more successful at $6 \times 10^{-6}$T yielding purity ratios of $\sim 1.7$ (*c.f.* $SbF_5$, Section 2.2.2), which seemingly was independent of the length of time of the deposition. This was judged to be the lowest pressure possible for this reagent.

For the alkyl halide, t-butyl bromide was studied, using pressures between $2x10^{-5}$ and $6x10^{-4}$T for times from 1 to 30 minutes. (Control of the alkyl halide flow had been improved by replacing the capillary tube with a needle valve). The purity of the deposited material was determined by calculating the $C_{1s}/Br_{3d}$ stoichiometric ratio which is obviously 4 for the pure compound. Below a pressure of $6x10^{-5}$T little bromine was observed, whilst even at this pressure the purity ratio was ∿12, and the gold substrate was"visible"showing that little deposition was achieved. Raising the pressure to ∿$2x10^{-4}$T was sufficient to produce a thin film (substrate "visible") of stoichiometric ratio ∿4.

Contamination is considered to come from the molecular beam jets and from inevitable build-up on the cooled probe of species present even in high vacuum. The possibility of the former was reduced as much as possible by pumping out the vacuum line and molecular beam jets before cooling down the probe, and routine baking was implemented to minimise the latter. Obviously the latter process becomes more of a problem as the length of deposition time is increased.

From the above results it appears that the minimum total pressure must be ∿$2x10^{-4}$T; however these results are for individual reagents and thus when attempting co-depositions lower pressures (particularly of the alkyl halides) were tried on the basis that the interaction of, for example, the organic halide with a gold surface, is probably different from that with a surface of antimony pentafluoride. Interaction of the two beams themselves would, of course, also make the codeposition different from the single beam experiment, but

this interaction is preferably avoided, since the idea of the molecular beam codeposition is to react the species at low temperature.

In an extensive series of experiments, having stabilised a flow of antimony pentafluoride at $2\times10^{-5}$T, t-butyl chloride was introduced to give total pressures ranging from $3\times10^{-5}$ to $6\times10^{-4}$T for times between 30 and 180 seconds. (The probe temperature was consistently -120°C). Lower pressures were explored partly for the reason outlined above and partly because it was anticipated that interaction between the beams would be decreased. However it was found that high binding energy peaks (associated with cation formation) only occurred in the $C_{1s}$ spectrum when the total pressure was $\sim6\times10^{-4}$T, never when the pressure was less than this. Even at this pressure though the preparation was not always successful, and the same resolution of the original experiment was not repeated. In these experiments, as in the first, the carbocation was not pure, and similar observations to those noted previously were made about the independence of the carbon and chlorine spectra.

In attempts to increase the amount of carbocation formed, both t-butyl fluoride and bromide were tried. Even with total pressures as high as $6\times10^{-4}$T ($SbF_5$ at $1\times10^{-5}$) and a probe cooled to its limit (~-170°C) no carbocation was observed using the fluoride. In the case of t-butyl bromide, deposition was observed when using the same conditions as those employed for the successful preparation from t-butyl chloride, but although the initial $^{C}/_{Br}$ stoichiometry (using a standard $^{C}/_{Br}$ sensitivity factor of 0.23) was ~3.7, no high

binding energy $C_{1s}$ peak was observed and upon standing the carbon signal intensity dramatically decreased, taking the $^{C}/_{Br}$ stoichiometry to less than one; again indicative of a halogen rich surface layer.

Conceivably interaction between the reagents occurs before condensing on a cold probe simply as a result of the beams crossing before reaching the substrate; thus a concentric codeposition apparatus was tried in which an inner tube carried a beam of the alkyl halide within a wider bore tube carrying antimony pentafluoride.[39] As with the previous experimental configurations with pressures of t-butyl bromide $\sim 1 \times 10^{-4}$T little deposition of the alkyl halide was observed and no evidence of ionisation was obtained even on allowing the sample to warm up to ambient temperature. Again using pressures of Lewis acid of $\sim 1 \times 10^{-5}$T and increasing the alkyl halide pressure to $\sim 6 \times 10^{-4}$T apparently led to the same side reaction occurring, as judged by a $^{C}/_{Br}$ ratio of 1.5 at the surface of the deposited material.

The fact that the same side reaction occurs independent of the experimental configuration of the beams shows that it is probably not caused by a crossing of the beams.

The observation that carbocations were formed when the total source pressure was high suggests that the pressure itself might be an important parameter, perhaps in enabling deposition of some of the alkyl halide which subsequently can react. However it appears that at higher pressures side reactions also occur. Thus the preparation of a pure carbocation might be possible using a lower pressure of the alkyl

halide but keeping the same total pressure by the introduction of an inert gas. Thus antimony pentafluoride was let in to a pressure of between $6x10^{-6}$ and $1x10^{-5}$, whilst t-butyl bromide was allowed in to a total pressure of between $2x10^{-5}$ and $5x10^{-5}$T. When these beams had been steadied, helium was introduced either through a separate port or premixed with the alkyl halide beam, to bring the total pressure in the source to $\sim 6x10^{-4}$T. The deposition time was limited to 1 minute because the high inert gas pressure increased the diffusion pump roughing pressure to such an extent that, because of the protection circuits, the diffusion pumps were "tripped-out". Very small amounts of deposition were observed (seen as low intensity bromine spectra) but there was no apparent carbocation formation. Thus, deposition is not simply a function of total pressure - the greater pressure of alkyl halide is necessary.

At a pressure of $6x10^{-4}$T the mean free path of the molecules is $\sim$5cm,[65] which is only 2-3 times the distance between the molecular beam nozzle and the cooled substrate. On emergence from the pipe, the beam can be expected to expand significantly and this increases the chance of gas phase reactions, rather than reactions occurring on the substrate when the molecules have been condensed at $-120^{o}$C.

The thermal decomposition of these alkyl halides is well documented[66-69] and is known to occur by unimolecular dehydrohalogenation with no appreciable side-reaction, though these particular reports are to studies at higher temperatures and pressures than used in the present work. However activation of the alkyl halides need not necessarily be achieved

thermally but could conceivably occur by collisional activation (certainly if there was interaction between "beams" of reagents). Deactivation can then occur by two routes, namely collision or elimination, with the latter route being favoured at low pressure. This formation of alkene and hydrogen chloride would certainly explain the present experimental observations, *viz* an independence of the carbon and

$$((CH_3)_3C\text{-}Cl)^* \xrightarrow{M} (CH_3)_3C\text{-}Cl$$

$$((CH_3)_3C\text{-}Cl)^* \longrightarrow (CH_3)_2C = CH_2 + HCl$$

halogen signals leading to $^{C}/_{\text{Halogen}}$ ratios significantly less than the pure compound.

The detailed study of the gas-phase chemiionisation reaction[48] (see Section 1.4.1) certainly does not rule out the possibility of this side-reaction occurring since in this a grid potential was used to draw products of the reaction into the mass spectrometer used for analysis; thus only ionic products, and not neutral molecules, were detected.

The observation noted above that ionisation only occurred using higher pressures of alkyl halides is consistent with a gas-phase ionisation due to interaction of the molecular "beams" since at lower pressures where interaction of the beams prior to condensing is less likely, ionisation was not readily apparent. Further evidence for the codeposition procedure leading to gas phase reaction is found by comparison with the bilayer experiments where reaction must occur in the condensed state (Section 2.1.3 and 2.3.3); in these ionisation either took a long time to occur or was not observed at all,

contrasting sharply with the immediate observation of cations in the codeposition experiments; the idea of a gas phase ionisation is not in disagreement with the results of the detailed study mentioned above; although t-butyl chloride was found not to react with the monomer or dimer of antimony pentafluoride,[48] higher oligomers are present under the conditions used in the present experiments (ambient temperature of nozzle), and indeed earlier results had shown that the chemiionisation of t-butyl chloride does occur.[47]

### 2.3.2 The Multilayer Method

Attempts to produce an intimate ion mix by co-deposition of the two reagents appeared to be problematical and results which did show carbocation formation were difficult to reproduce. Thus an alternative method of producing the ion mix was conceived, in which several thin layers of the reagents were alternately condensed onto the precooled substrate, and the sample then allowed to warm up.

For example antimony pentafluoride was let into the source, containing a substrate cooled to $-120^{o}C$, to a pressure of $1x10^{-5}T$ for $\sim$15 seconds. This beam was turned off, and when the pressure had returned to $\sim5x10^{-6}T$, t-butyl bromide was allowed in to $1x10^{-4}T$ for $\sim$15 seconds, then turned off; when the pressure had returned to $\sim5x10^{-6}$ this cycle was repeated a further three times; finally antimony pentafluoride was let in at $1x10^{-5}T$ for $\sim$5 seconds to provide a covering layer and preventing the alkyl halide from pumping-off. The whole deposition was performed over $\sim$5 minutes. Initially small amounts of carbon and bromine were present in the surface, but on allowing the sample to warm these

signals decreased until by ~+12°C they were of negligible intensity. Thereafter on further warming to +25°C and then to +45°C, these core level signals increased in intensity (Fig.2.11). Whilst the high binding energy peak

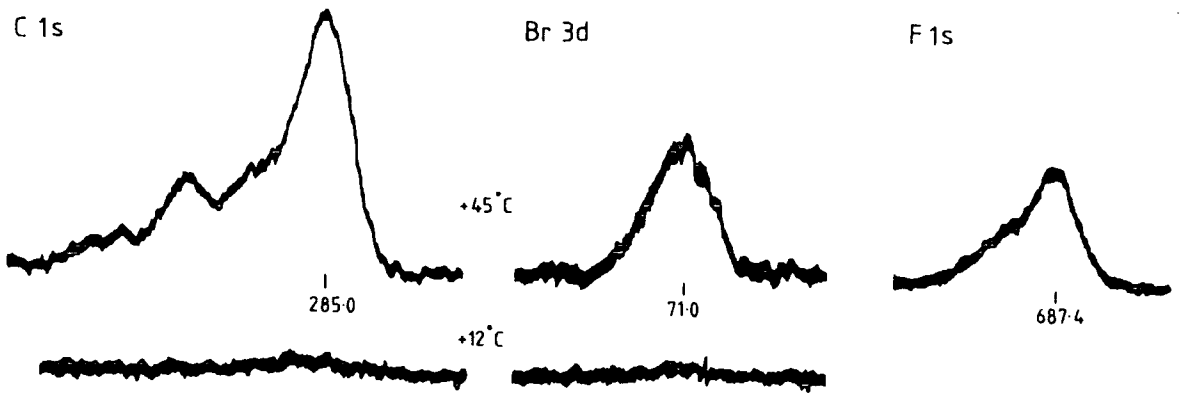


Figure 2.11 EFFECT OF TEMPERATURE ON SURFACE COMPOSITION OF MULTILAYER REACTION MIX - antimony pentafluoride and t-butyl bromide. (Binding energies, referenced to $C_{1s}$ at 285.0, in eV).

in the $C_{1s}$ spectrum, occurring some 4-5eV from the most intense component, might be due to the formation of the t-butyl cation, it is quite obvious that this is not the only species present. Confirmation of this latter fact is easily

deduced from the large $^{C}/_{Br}$ stoichiometry of the surface species, which is ∿13, and the $F_{1s}$ spectrum which shows a pronounced high binding energy shoulder attributable to the presence of organic fluorine.

The experiment shows that mixing of the reagent layers does not occur until ∿+15°C that is, after the antimony pentafluoride has melted; taken in conjunction with the bilayer reservoir shaft experiments it suggests that allowing reagent mixes to warm in high vacuum does not lead to successful ESCA observations of carbocations. This is because if it has not reacted at -120°C, most of the alkyl halide on the surface of the mixture appears to pump-off by ∿-80°C, and alkyl halide involved in an intimate reagent mix does not "appear" on the surface until the mix reaches a temperature of ∿+15°C, at which point the spectra show considerable contamination; also, of course, less stable carbocations would largely have rearranged. Experiments with cyclopentyl chloride yielded, upon melting of the layers at ∿+15°C, a $C_{1s}$ spectrum with essentially one component, even though the pressure was always allowed to drop below $5x10^{-6}$T between the deposition of layers. Hence assuming that gas phase reaction did not occur, it suggests that upon allowing the mixture to warm up, elimination of hydrogen chloride and polymerisation was observed rather than ionisation.

One approach which was not pursued in any of this work is the possibility of lowering the temperature of the probe. Deposition of the alkyl halide, using lower pressures, would be expected to be more facile if the substrate was further cooled. The temperature of -120°C normally used was a compromise; it was found that this temperature could be routinely attained whilst lower temperatures were more problematical not only in attaining them, but also because contamination is expected to increase as the probe temperature becomes comparable with that of the traps; this temperature however is considered to be low enough that less stable carbocations can be generated. The work on bilayers however suggests that alkyl halide deposition is not the limiting problem in forming carbocations, so that the effect of decreased probe temperature need not be considered further.

### 2.3.3 Bilayer (Norbornyl chloride and antimony pentafluoride)

When a low pressure of alkyl halide is used in codeposition experiments, deposition of the alkyl halide was found to be negligible, whilst although ionisation was sometimes observed when using higher pressures, so too were side-reactions. It is possible that only small amounts of alkyl halide are observed in the antimony pentafluoride surface, because of disproportionate rates of deposition of the two reagents, but significant lowering of the inlet pressure of the antimony pentafluoride leads to greater contamination as has already been noted (Section 2.3.1). In view of these difficulties bilayer experiments were carried out in which,

rather than codepositing the reagents, they were introduced successively so as to produce a thin layer of the organic halide on top of the Lewis acid layer. These experiments are therefore very similar to some of those performed with reservoir shafts (Section 2.1.3) but they have the advantage that the second reagent can be introduced in quick succession, whereas with reservoir shafts it had been necessary to withdraw the first ($SbF_5$ loaded) shaft and then reintroduce a second one for the alkyl halide. This obviously led to some delay and together with the necessary opening and closing of the insertion locks, could have led to contamination (hydrolysis, adventitious hydrocarbon) rendering the Lewis acid surface inactive. A distinct advantage of the bilayer method is that it permits a surface of the first reagent to be characterised before deposition of the second. Attempts to prepare the t-butyl cation by the bilayer method had failed (though this was with reservoir shafts, Section 2.1.3) and in these further bilayer experiments norbornyl chloride was used particularly since it is the norbornyl cation which is of such contemporary interest.

Antimony pentafluoride was allowed into the source for 30 seconds at a pressure of $\sim 1 \times 10^{-5}$T and condensed on a precooled substrate at -120°C. Characterisation of this surface (not including Auger peaks) took 30 minutes (Figure 2.12); analysis gives a "purity" ratio of 1.66 and $\frac{Sb_{3d^{3}/_{2}}}{F_{1s}}$ of 0.99. The surface was observed to be relatively free of contaminant carbon species. Norbornyl chloride was then introduced at a pressure of $\sim 1 \times 10^{-5}$T for 6 seconds. The carbon and chlorine

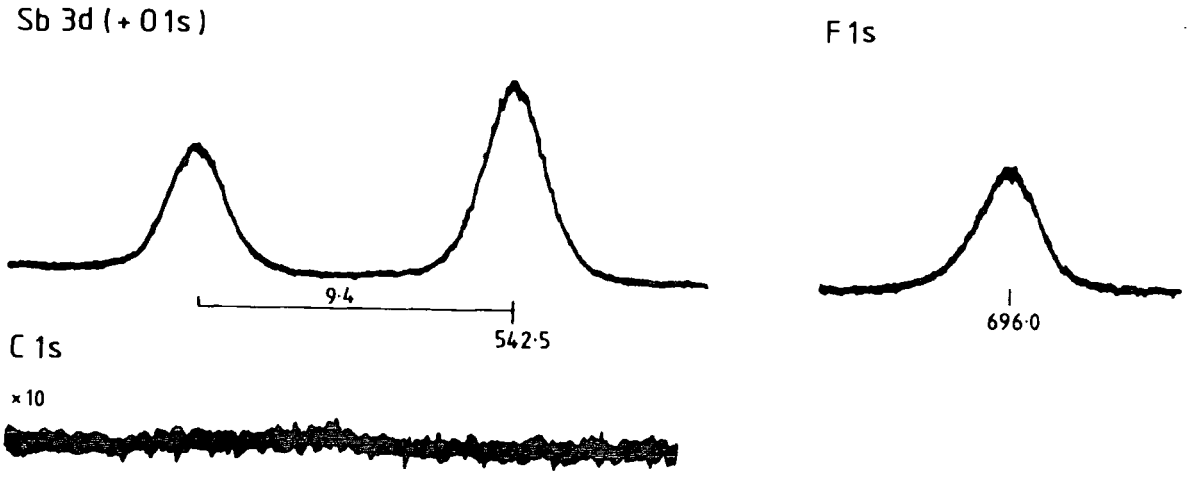


Figure 2.12 ANTIMONY PENTAFLUORIDE IMMEDIATELY BEFORE DEPOSITION OF NORBORNYL CHLORIDE (Binding energies and internal shift in eV).

---

core-level spectra observed immediately afterwards are shown in Fig.2.13. Whilst no discrete high binding energy peaks are apparent, resolution of the $C_{1s}$ spectrum by three peaks intensity ratio 1:2:4 (as for norbornyl chloride on a gold substrate, Section 2.2.2) suggests greater internal shifts for this bilayer system; hence the highest binding energy component is $\sim$1.9eV shifted from the most intense component, whilst the middle peak has a shift of $\sim$0.9eV. These shifts suggest that some polarisation of the organic halide may have occurred. The $Cl_{2p}$ spectrum though, can be resolved as a single doublet, intensity ratio 2:1 and with a separation of

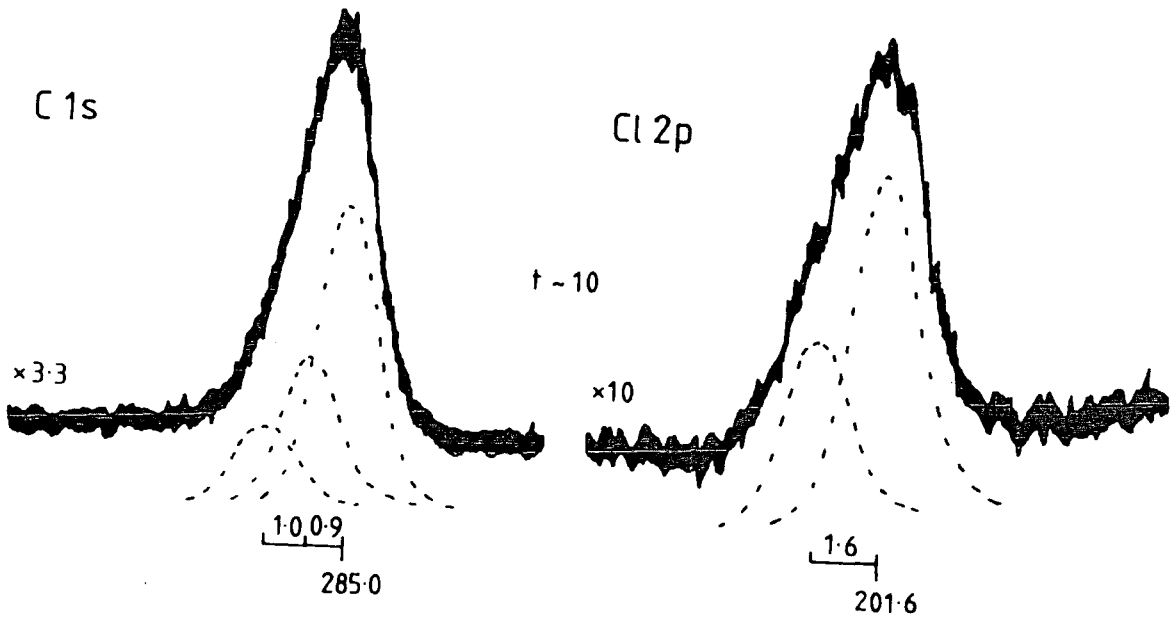


Figure 2.13 INITIAL SPECTRA OF NORBORNYL CHLORIDE DEPOSITED ON TOP OF A LAYER OF ANTIMONY PENTAFLUORIDE. $C_{1s}$ spectrum is recorded on the same scale as that used prior to the deposition of norbornyl chloride (Fig.2.12). (Time(mins.) from the norbornyl chloride deposition).

---

1.6eV; a binding energy of the $2p^3/_2$ component of 201.6eV (relative to the most intense component of the $C_{1s}$ spectrum at 285.0) is comparable with that determined for the organic chloride on a gold substrate. The $^C/_{Cl}$ stoichiometric ratio of 6.4 is in tolerable agreement with the expected value (7.0) and is consistent with that determined from analysis of the chloride (Section 2.2.2).

The deposition procedure can be seen as producing an overlayer of norbornyl chloride on top of an antimony

pentafluoride substrate; in terms of this basic model, it is of interest to consider the possible thickness of such an overlayer; two possible approaches have been tried:

(a) consideration of the ratio of the $Sb_{3d^{3}/_{2}}$ signal intensity before and after deposition. This ratio is 1.9 and employing the overlayer equation with $\theta \sim 30^{o}$ and $\lambda_{Sb_{3d}} \sim 12\text{Å}$, such a change in intensity would be caused by an overlayer of thickness $\sim 7\text{Å}$.

(b) consideration of the $^{Sb}/_{F}$ ratio before and after deposition (0.99 and 1.28 respectively). Using values of 12 and 10Å for $\lambda_{Sb_{3d}}$ and $\lambda_{F1s}$ respectively and with $\theta \sim 30^{o}$, the ratio of ratios (0.77) is well represented by a coverage $\sim 13\text{Å}$ thick.

It will be realised that in order to deposit reagents it was necessary to rotate the substrate through $\sim 120^{o}$. Consequently consideration of the intensity of a single peak represents a considerable approximation since the substrate angle (with respect to the X-ray source) may well not be exactly the same, and this in itself would alter the observed intensity. The second calculation based on $^{Sb}/_{F}$ ratios does not suffer from this defect since a ratio of intensities is used; also the ratio of mean free paths is likely to be more accurate than use of a single value. However it has already been established that the $^{Sb}/_{F}$ ratio will increase as hydrolysis progresses (Section 2.2.2); the calculation performed here assumes that the change in ratio is attributable solely to differential attenuation of core level signals by an overlayer, but since part of the change

may actually occur due to degradation of the acid bed, the result represents a maximum overlayer thickness. In view of the inherent approximations and assumptions, the results are in fair agreement, and suggest that the norbornyl chloride is ∿1-2 monolayers thick.

Approximately 30 minutes after the norbornyl chloride deposition, a low intensity peak was observed ∿4eV from the main $C_{1s}$ peak and not completely resolved from it. Over the following 40 minutes this peak was seen to grow in intensity, but never appeared completely resolved (Fig.2.14).

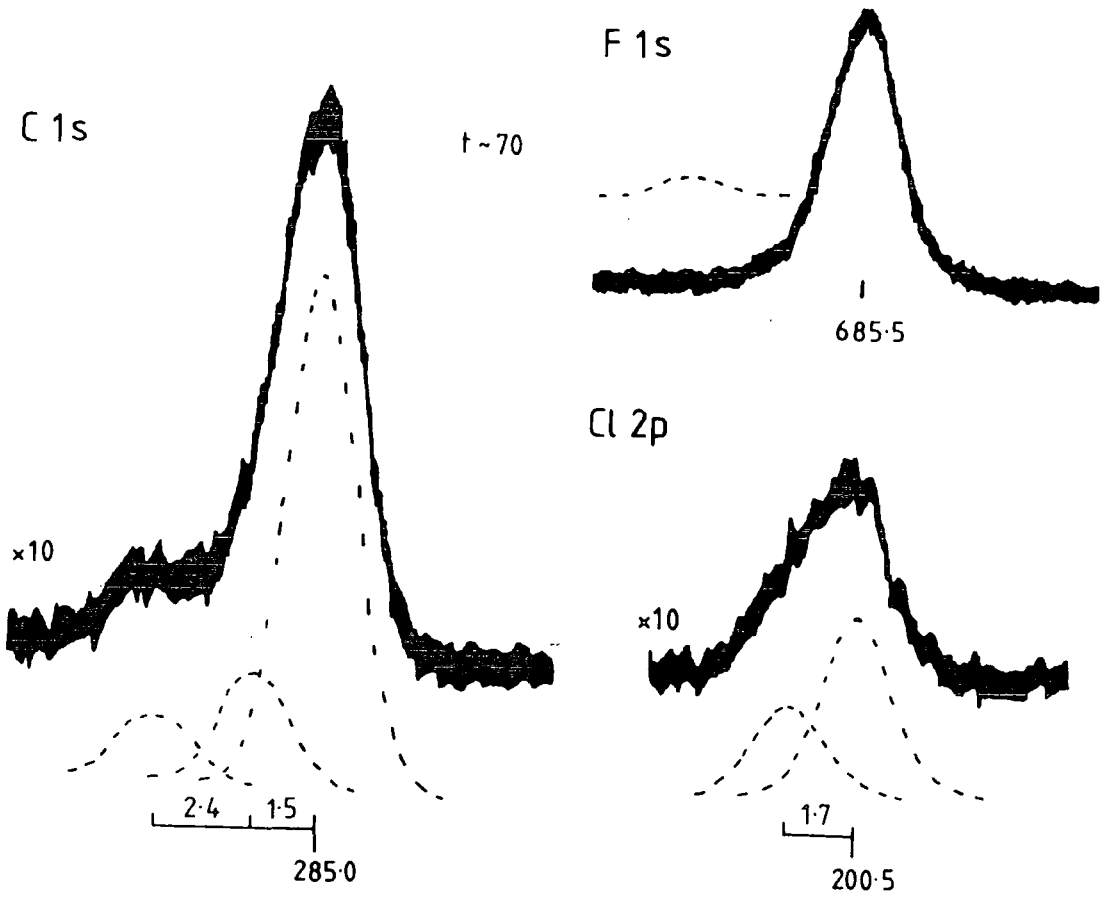


Figure 2.14 GROWTH OF HIGH BINDING ENERGY COMPONENT WITH TIME. (Time (mins.) from the norbornyl chloride deposition).

The minimum number of peaks required in the resolution of the $C_{1s}$ spectrum is 3; these have relative intensity 9:2:1 and the internal shifts are 1.5 and 3.9eV to higher binding energy of the main component. The $^{C}/_{Cl}$ stoichiometry is ~6.8; comparison of this value with that obtained previously (6.4) suggests that perhaps 6% of the total $C_{1s}$ spectrum is due to the presence of contamination. The $Cl_{2p}$ spectrum can still be adequately resolved as a single doublet. Ideally the determination of the chlorine binding energy would aid in the characterisation of ionic state; indeed (referenced to the low binding energy component of the $C_{1s}$ spectra at 285.0) the $Cl_{2p^{3}/_{2}}$ binding energy decreases from 201.6 to 200.5eV over the period from deposition of norbornyl chloride to observation of the high binding energy peak in the $C_{1s}$ spectrum. However it should be noted that during this time surface charging varies by ∿0.7eV. Also the subsequent demise of the $Cl_{2p}$ spectrum shows the loss of chlorine from the system and it is not clear at quite what stage the chlorine becomes dissociated from the carbon species. Hence caution is needed in interpreting the trend of decreasing $Cl_{2p^{3}/_{2}}$ binding energy as due to ionisation. In fact *a priori* it is not even certain whether the $Cl_{2p}$ binding energy should decrease in this process since the Lewis acid would be expected to drain electron density from the chlorine atom, and in this context it should be noted that the binding energy of the $Cl_{2p^{3}/_{2}}$ core level in the case of the localised tertiary cation (Section 2.3.1) was ∿201.4eV suggesting little change from organic chlorine. Similar attempts to correlate fluorine binding energies with ionisation were unsuccessful

since these were found to be inconsistent, and this exemplifies the problems encountered in the determination of absolute binding energies.

As has already been pointed out, high binding energy peaks appearing in the $C_{1s}$ spectra of these systems could arise from organic fluorine either from halogen exchange or from inherent organic contamination of the Lewis acid. The long time taken for the high binding energy component of the $C_{1s}$ spectrum to appear in the present experiment, would be equally consistent with the build up of contamination as with ionisation. The presence of organic fluorine is hard to detect in the $F_{1s}$ spectrum, because of the high intensity of the signal derived from the Lewis acid; from the intensity of the high binding energy peak of the $C_{1s}$ spectrum, assuming it to be totally attributable to C-F functional groups, the approximate intensity of the corresponding $F_{1s}$ signal can be estimated; this is represented (with a FWHM appropriate to the fluorine spectrum) in the inset to the $F_{1s}$ spectrum in Fig.2.14, though the position is <u>not</u> defined. Whilst the $F_{1s}$ core level could be resolved in this fashion as two peaks, the low intensity of the high binding energy peak defies accurate analysis; indeed it may be observed that the high binding energy tail in the present spectrum is similar to that of the $F_{1s}$ spectrum obtained <u>before</u> deposition of norbornyl chloride and this suggests that little can be deduced from the $F_{1s}$ spectrum concerning the presence or otherwise of organic fluorine. Two other factors however suggest that the high binding energy peak of the $C_{1s}$ spectrum is not due simply to C-F functionality; firstly, the internal shift

of this peak is ∿3.9eV and this is rather larger than the shift normally observed (∿3.3eV); secondly the $^{C}/_{Cl}$ ratio of 6.8, compared with the initial value of 6.4, suggests a maximum level of contamination of ∿6% of the total $C_{1s}$ intensity, whilst the high binding energy peak is ∿8-9%.

The other contamination problem of hydrolysis cannot be explicitly considered here since the antimony spectrum was not observed particularly close (in time) to the "best" $C_{1s}$ spectrum. However whilst hydrolysis can explain the absence of high binding energy peaks due to quenching of carbocations, it is not likely to explain their presence.

Thus whilst the possibility of side reaction cannot be rigorously ruled out, the spectra obtained at this point of the experiment suggests that ionisation of norbornyl chloride might have been achieved. The shift of the high binding energy peak from the most intense component of the $C_{1s}$ spectrum (∿3.9eV) is consistent with that expected for a localised carbocation.[70] Similarly the middle component, shifted by 1.5eV can be assigned to two carbons adjacent to that bearing the positive charge. Overall the $C_{1s}$ spectrum could be assigned as ∿60% arising from a classical carbocation and ∿40% from unionised chloride.

To promote further ionisation the sample was allowed to warm to -100°C (∿80 minutes after deposition of the chloride); initially there was little change in the $C_{1s}$ spectrum but over a further 70 minutes the high binding energy peak increased in intensity relative to the other, until in the final $C_{1s}$ spectrum recorded (Fig.2.15) it represented

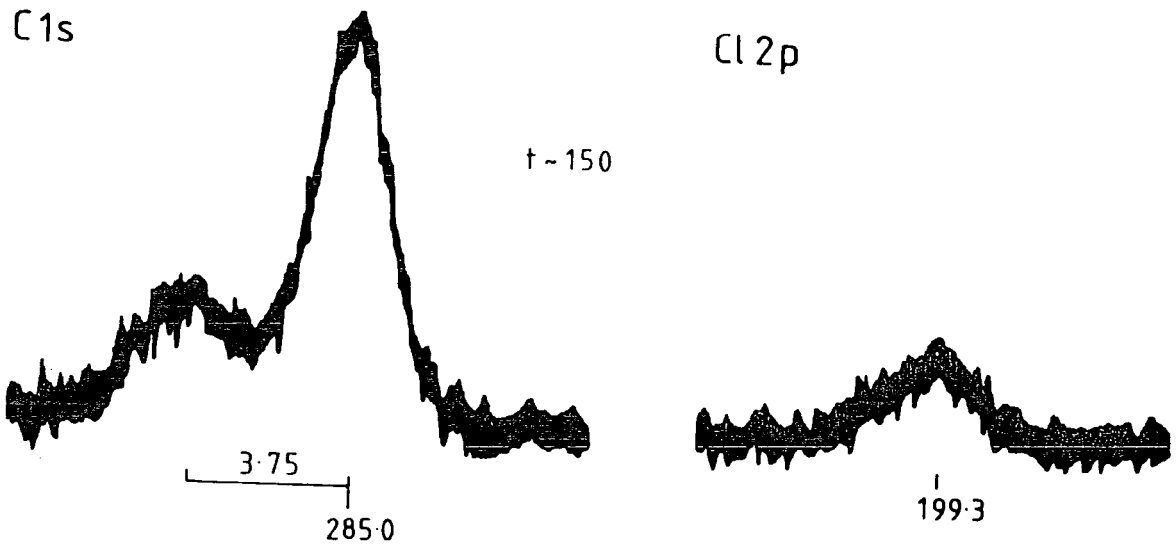


Figure 2.15 FINAL SPECTRA OF NORBORNYL CHLORIDE ON ANTIMONY PENTAFLUORIDE SURFACE (Binding energies, referenced to $C_{1s}$ at 285.0, and internal shift in eV)

---

∿25% of the total $C_{1s}$ signal intensity. The $^{C}/_{Cl}$ ratio at this point, ∿23, suggests that ∿70% of the $C_{1s}$ spectrum is not derived directly from norbornyl chloride (either ionised or unionised). Whilst the remaining $Cl_{2p}$ has a binding energy indicative of ionic chlorine (∿199.1eV), the $C_{1s}$ spectrum is not obviously related to carbocation forms, and is difficult to interpret.

In considering the interpretation of these results it is important to bear in mind the following:

Firstly, attempts to ionise tertiary butyl chloride in similar experiments were unsuccessful.

Secondly, the spectrum which is potentially consistent with some formation of a localised carbocation is intermediate between those showing little change from pure norbornyl chloride on its own and those which quite clearly derive from an impure norbornyl chloride-antimony pentafluoride system. Certainly the time of observation of this interesting $C_{1s}$ spectrum is sufficiently long after deposition of the two reagents that, on the basis of other experiments, degradation of the acid bed would be fairly well advanced.

Thirdly, ionisation is incomplete; the high binding energy component represents 8-9% of the spectrum, whereas if complete ionisation had occurred it should be ∿14%. The incompleteness of this supposed ionisation leaves open the possibility that the processes occurring may be incomplete. Even within solutions ion pairs are known to exist,[38] and since solvent is absent from the present system, separation of an ion pair might be expected to be problematical. Certainly the conclusion that ionisation may well be incomplete on the time-scale of this experiment is consistent with recent solid-state NMR observations which suggest that complete ionisation at temperatures in the range 150 to 200K requires time periods ranging from several hours to several days.[41] It is instructive to compare the present results with those obtained previously from which it was concluded that the 2-norbornyl cation had a nonclassical structure. If the spectrum recorded in this part of the present work derives from a classical cation, then that previously reported[19] cannot be a classical ion; Olah prepared the cation by the ionisation of norbornyl chloride but by the very nature of

the experiment there was a longer period of time between its formation outside the spectrometer and its ESCA observation, and this time difference might be crucial in obtaining complete ionisation.

In the light of this discussion it would be inappropriate to conclude that the $C_{1s}$ spectrum (Fig.2.14) derives from a "free" localised (classical) norbornyl cation, but this possibility cannot be definitely ruled out; even if it were the correct interpretation it would not be inconsistent with other results but would simply demonstrate that the cation structure is influenced by the surrounding matrix.

## 2.4 Summary

A localised carbocation $(CH_3)_2\overset{+}{C}(CH_2R)$, was prepared in the source of an ESCA spectrometer using molecular beams to codeposit antimony pentafluoride and t-butyl chloride. The internal $C_{1s}$ shift was found to have a minimum value of 3.1eV but accurate determination was not possible because the exact nature of the contamination of the spectrum was unknown. This contamination was considered to arise from a side reaction in which independent carbon and chlorine species are produced, the most likely explanation being the elimination of hydrogen chloride from the alkyl halide. Attempts to prepare a purer carbocation sample by using lower total pressures, which might reduce the extent of the side reaction, were unsuccessful. In experiments with concentric molecular beams the same independence of carbon and halogen

signals was observed suggesting that the side reaction is not a result of the beams crossing before they meet the cooled probe but that it is a result of the comparatively high pressures used. However the use of inert gas in some experiments to maintain a high total pressure during deposition has shown that pressure of itself is not the determining factor for cation formation. This has led to the conclusion that observation of the localised tertiary cation follows a gas phase ionisation. Further evidence for this conclusion lay in the fact that experiments in which a layer of an alkyl halide was deposited on top of a layer of the Lewis acid showed no ionisation at -120$^{o}$C. One possible exception to this was found in an experiment involving norbornyl chloride, but because of the length of time taken for potential carbocation peaks to occur it was pointed out that the integrity of the sample might not have been preserved. The length of time apparently required for solid-state ionisation appears to be a serious limitation on the use of this route in the preparation of carbocations for ESCA analysis.

Whilst the apparent gas phase ionisation of t-butyl chloride enabled the observation that the internal shift of a localised carbocation is > 3.0eV, such a route cannot be used for the preparation of less stable carbocations, which would invariably isomerise or fragment.

# CHAPTER THREE

## THE PROTONATION OF ALKENES

## 3.1 Experimental

### 3.1.1 Apparatus and Methods

The basic experimental set-up used for the protonation of alkenes is the same as that described in Chapter Two. Slight modifications were made for the alkene precursors, as detailed below. In the experiments described in this part of the work it is important to note that when two reagents are in use, deposition is sequential and not simultaneous.

(i) Norbornene

To prevent any deposition of this precursor in the vacuum line, the arm was heated by hot air and heating tape, and maintained at a temperature of $\sim+70^{o}C$ (Fig.3.1(b)). Thus after evacuating the vacuum line, and with T1 and SS-4H open, the arm was heated; small pressure rises were sometimes observed in the source, due to this bake-out; the probe was not inserted and cooled until the base pressure was re-attained, typically $\sim 2 \times 10^{-7}$ in the source. This sequence of operations is obviously necessary to ensure that in the experiments it is norbornene, and not extraneous hydrocarbon which is deposited. A needle valve was not required since it was found that a capillary (40x0.5mm) was sufficient, together with the SS-4H valve, to control the flow of alkene.

(ii) Cis-but-2-ene

Problems with the inconel valve led to the two reagent arms being changed around. Whilst the SS-4H valve was found to offer enough control of the acid beam, the

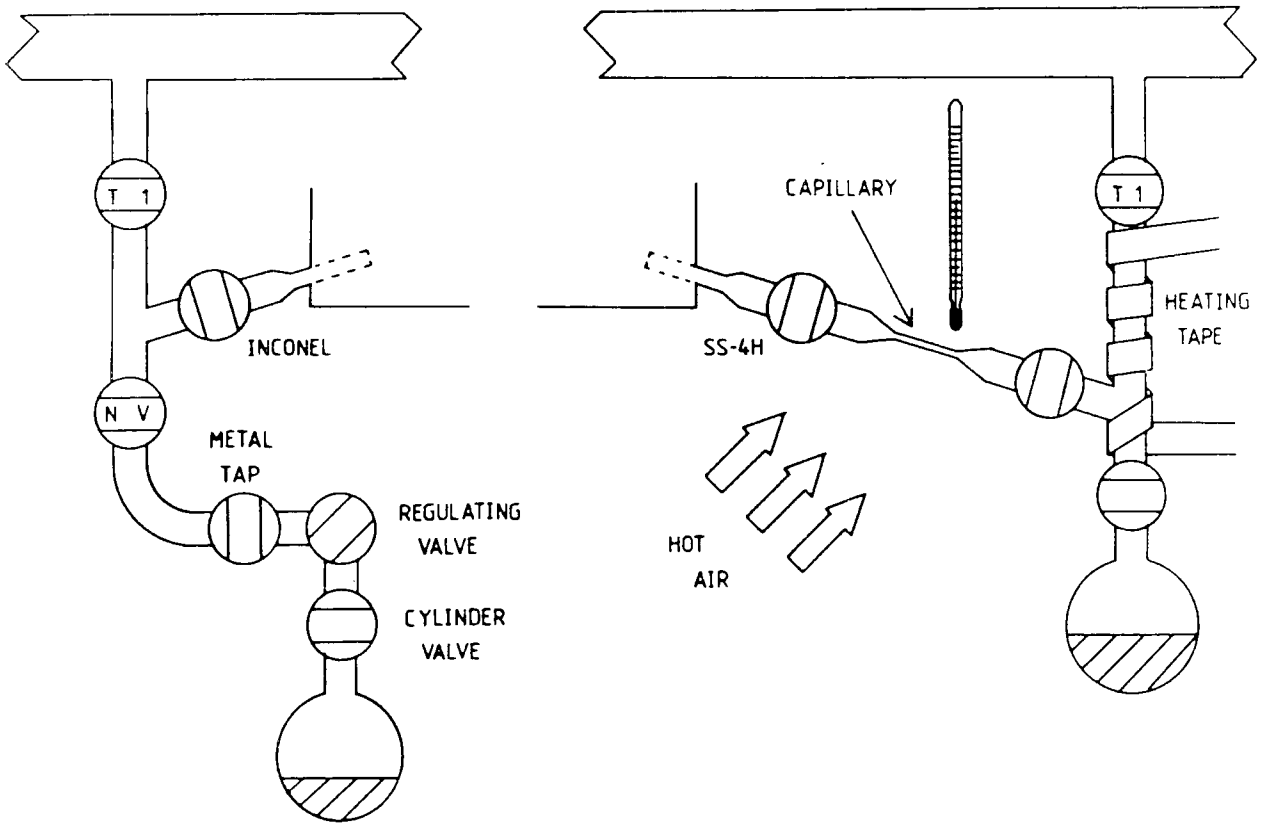


Figure 3.1 BUTENE "ARM" (left), NORBORNENE "ARM" (right)

alkene beam was controlled by a needle valve and the inconel valve was used simply as an on-off tap. Originally (for convenience) the butene cylinder was connected using a length of ¼" nylon tubing, but this was found to be difficult to pump out, and was later replaced by a 6" length of ½"-diameter flexible metal tubing (Fig.3.1a). With the metal tap closed and the needle valve open, the system was pumped down as previously described using rotary and diffusion pumps (Section 2.2.1). The inconel valve and needle valve were shut and butene allowed to fill the pipe up to the needle valve; then with the metal valve still closed, the needle valve was opened to allow the butene to be pumped away (rotary pump). The cycle of filling and evacuating was repeated three times and finally the flexible metal tubing was pumped out using the diffusion pump. During deposition the teflon valve (T1) was kept closed, inconel valve and metal tap fully open, and flow controlled by the needle valve.

### 3.1.2 Analysis of precursors

#### (i) "Magic" Acid

It has already been noted (Section 1.4.2) that the norbornyl cation has been prepared by protonation of norbornene by "Magic" acid (1:1 $SbF_5$-$FSO_3H$) in solution. In a move towards this method of preparation, attempts were made to deposit a layer of magic acid on to a gold substrate. Bath temperatures of +25 - +90°C and pressures ranging from $\sim 1 \times 10^{-5}$ to $\sim 1 \times 10^{-3}$ for times of 1 to 5 minutes were tried in attempts to deposit on a substrate at -120°C. Wide scan spectra presented in Figure 3.2, summarise the nature of the

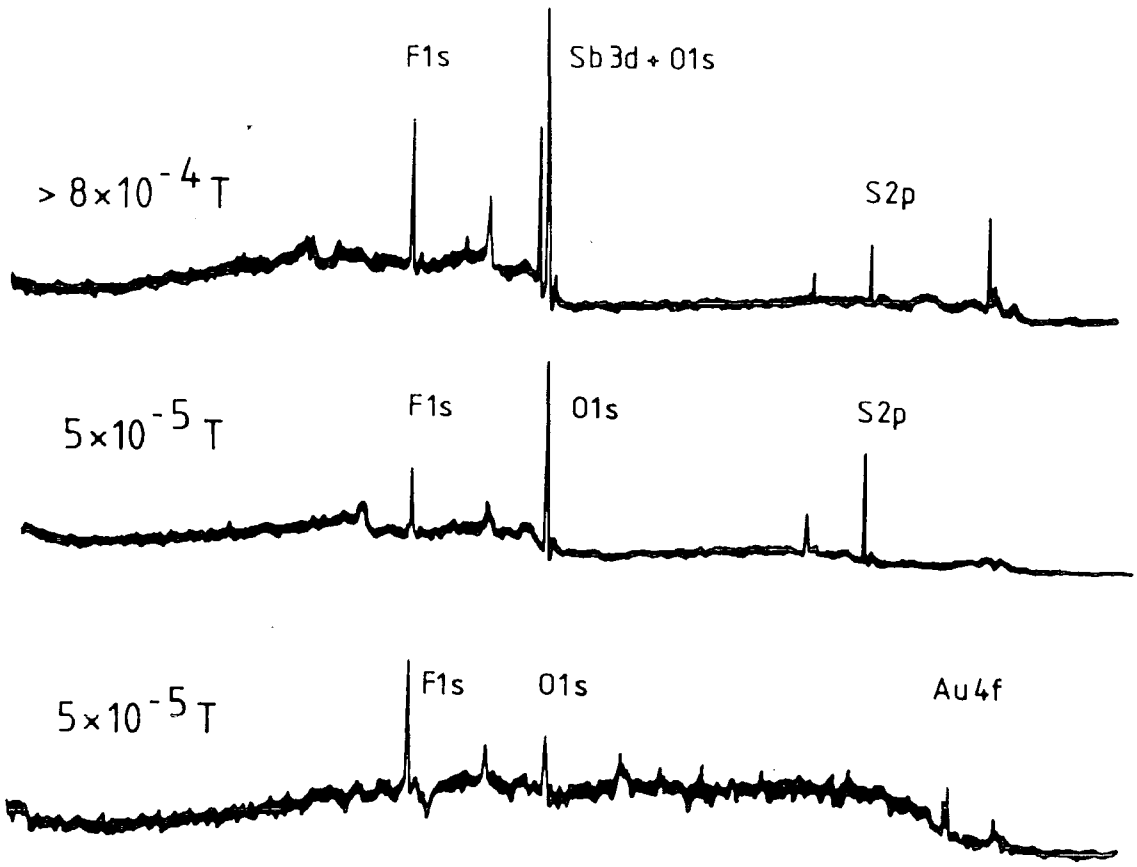


Figure 3.2 THE INCONSISTENCY OF THE SURFACE PRODUCED BY (TWO-COMPONENT) "MAGIC" ACID. (Acid bath temperature ∿+85°C; substrate temp -120°C; Deposition time 1 minute).

deposited films obtained. Fluorine and oxygen were sometimes the only elements obviously present suggesting that the layer was composed of water and hydrogen fluoride, the latter being produced from slight etching of the glassware in the presence of any moisture. Sulphur, oxygen and fluorine were frequently collectively present in the deposit, suggesting that distillation of only one component of the mixture into the source had occurred. It should be noted that the same deposition conditionssometimes led to a different deposited layer; that is, in one case it appeared that only hydrogen fluoride and moisture were present whilst in another fluorosulphuric

acid was deposited. Antimony was only detected in a layer deposited at (by accident) a pressure $>8\times10^{-4}$T, and this is unsuitable for routine use since it cannot be monitored.

Thus etching of glassware appears to be a problem in using magic acid in this experimental set-up. In addition the two component nature of the acid is problematical since different rates of distillation led to surfaces of differing composition and this defies the possibility of systematic experimentation.

(ii) Fluorosulphuric acid

It was found that this strong protonic acid could be readily distilled into the spectrometer. As a prelude to reacting it with alkenes the acid was introduced into the source containing a precooled probe ($-120^{o}$C) at a pressure of $\sim1\times10^{-4}$T for 1 minute, producing an acid covered gold substrate. The effect of the spectrometer environment on the acid was studied over six hours, after which the probe was allowed towarm to $-30^{o}$C, in order to allow those processes which were occurring to proceed more rapidly.

Initially hydrocarbon contamination on the acid surface could not be detected on a scale ten times more sensitive than that used to detect the other elements (F,O,S), suggesting a $^{S}/_{C}$ stoichiometry of >50:1; even at the end of the study there was no apparent build-up of hydrocarbon.

In the results of the study (Figures 3.3 and 3.4) the stoichiometric ratios used are derived from using bulk determined sensitivity factors, together with measured core

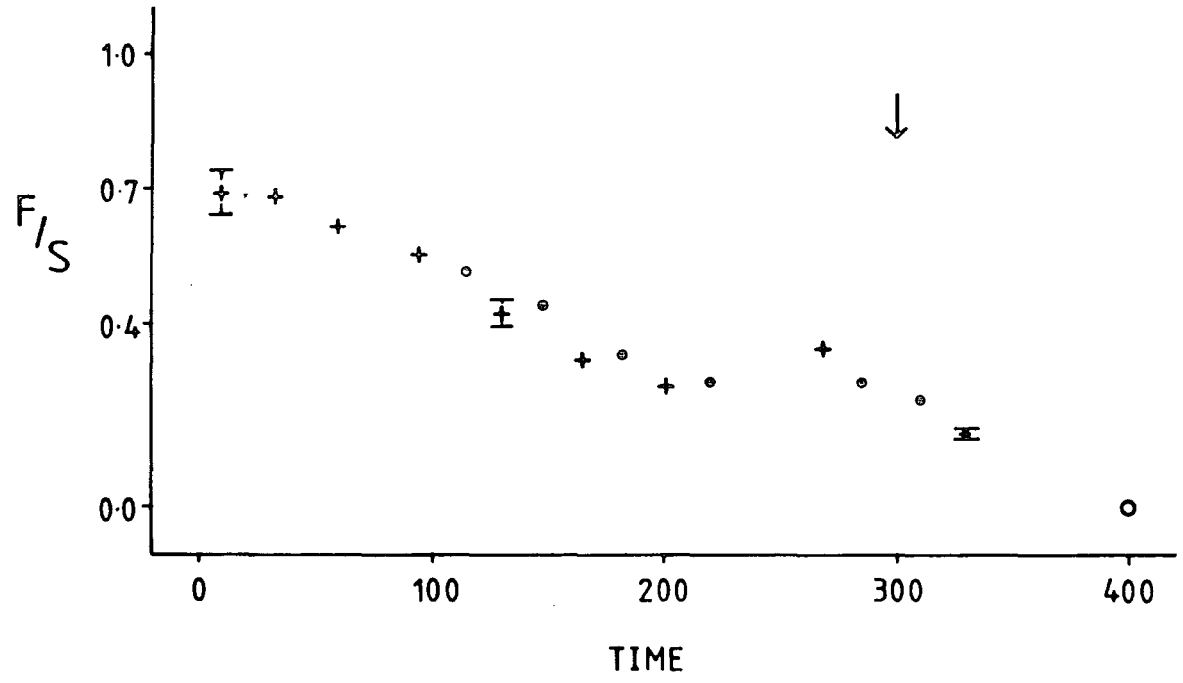


Figure 3.3 THE SURFACE HYDROLYSIS OF $FSO_3H$: F/S stoichiometry versus time (mins.) from deposition (+ : $\theta \sim 30^{o}$, T = $-120^{o}C$; ● : $\theta \sim 70^{o}$, T = $-120^{o}C$; O : $\theta \sim 30^{o}$, T = $-30^{o}C$; ↓ shows time of "dummy" alkene deposition).

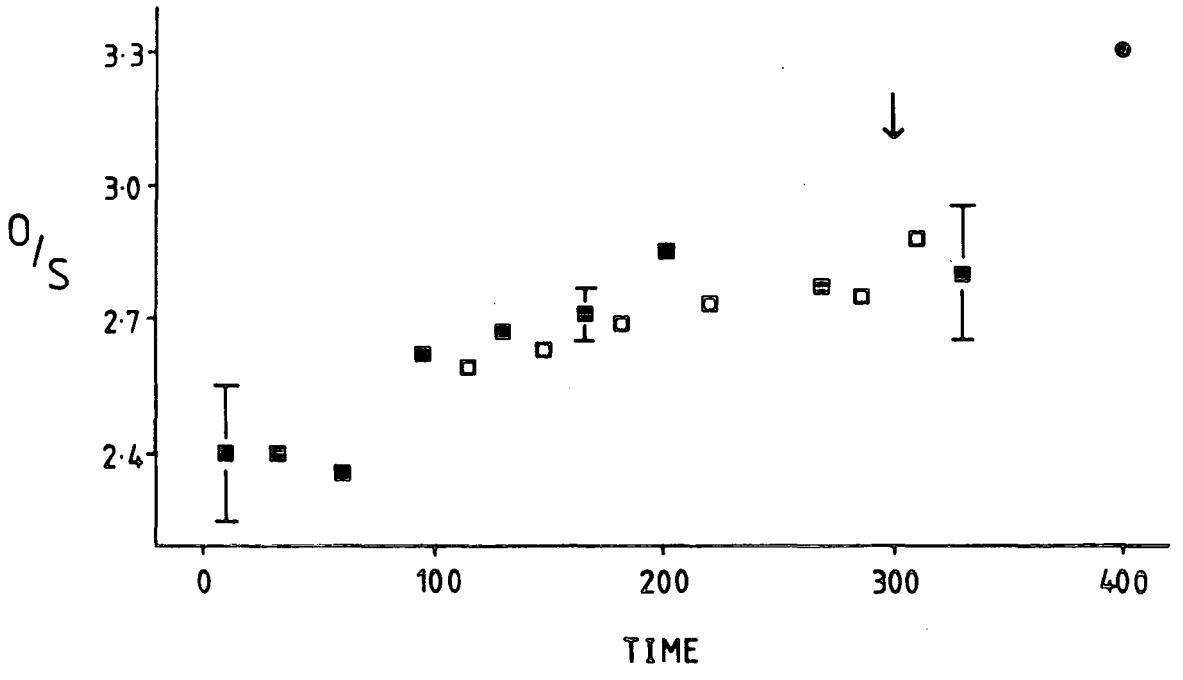


Figure 3.4 THE SURFACE HYDROLYSIS OF $FSO_3H$: O/S stoichiometry versus time (mins.) from deposition. (■ : $\theta \sim 30^{o}$, T = $-120^{o}C$; □ : $\theta \sim 70^{o}$, T = $-120^{o}C$; ⊙ : $\theta \sim 30^{o}$, T = $-30^{o}C$; ↓ shows time of "dummy" alkene deposition).

level intensities. An estimation of the errors in some of the points is included; the uncertainty in the time co-ordinate is derived from the time necessary to record the three relevant core level spectra (~10 mins.), whilst the errors in stoichiometry were derived from considering maximum and minimum values for the measured core level intensities. Clearly the trends observed are real and not within experimental error.

The hydrolysis of fluorosulphuric acid was briefly discussed in Section 1.4.2, and whilst complex, can be summarised by the equations

$$HSO_3F + H_2O \longrightarrow \begin{cases} HF + H_2SO_4 \\ H_3O^+SO_3F^- \xrightarrow{H_2O} H_3O^+HSO_4^- + HF \end{cases}$$

The trends shown (Fig.3.3, decreasing $^{F}/_{S}$ stoichiometry; Fig.3.4 increasing $^{O}/_{S}$) are consistent with these equations only by realising that in the high vacuum, hydrogen fluoride is continually pumped away from the surface; obviously this process complicates the interpretation of the results. Since hydrolysis of a compound is expected to be more advanced in the surface regions, one might expect that the data at a substrate angle of $70^{o}$ (more surface sensitive) would give a $^{F}/_{S}$ stoichiometry of less than, and an $^{O}/_{S}$ stoichiometry of more than, these ratios derived from data at $30^{o}$. Generally however the results, at first glance, suggest that hydrolysis is less advanced in the surface regions. This can be explained by considering the migration of hydrogen fluoride to the surface, prior to being pumped away, leading to a greater $^{F}/_{S}$ stoichiometric ratio than expected, (in the extreme we could consider a hydrogen fluoride overlayer); impurities in the

fluorosulphuric acid surface, such as hydrogen fluoride, would lead to a greater reduction of $O_{1s}$ signal intensity relative to that of $S_{2p}$ because of the differing kinetic energies and mean free paths of the photoionised electrons, explaining the smaller value of the $^{O}/_{S}$ stoichiometry found at the very surface. These results illustrate the complication of such a process on relative stoichiometries and it can only be suggested that this type of effect is responsible for the apparent discontinuity of the graphs.

After five hours a "dummy" alkene deposition was performed (marked by an arrow in Figs. 3.3 and 3.4) in which all the relevant valves were opened, the vacuum line having the normal status for a deposition. Though the increased $^{O}/_{S}$ stoichiometry (within experimental error the same) suggests the possible deposition of a small amount of moisture on the surface, this operation is seen not to have greatly contaminated the surface.

It is certainly pertinent to ask why the initially determined stoichiometry for the fluorosulphuric acid layer is $F_{0.7}S_{1.0}O_{2.4}$ (a generally obtained result) whereas the pure compound should, of course, be $F_{1.0}S_{1.0}O_{3.0}$. It appears that the deposited layer contains too much sulphur. The presence of elemental sulphur seems an unlikely possibility if for no other reason than that it would not be expected to distil across into the source, whilst any sulphur dioxide, if present, would be expected to pump off the surface, analogous to hydrogen fluoride. (However even if either of these substances were present, they would not be expected to affect the reaction of an alkene with the acid).

More important though is to ascertain whether the acid deposited is already partially hydrolysed, as might be inferred from an initial $^{F}/_{S}$ stoichiometry of 0.7, consistent with fluorine loss before the study begins. The negligible difference obtained for the first two sets of results suggests that little change is occurring in the surface over the first 30-40 minutes. Whilst this result is not conclusive because of the inherent error it certainly suggests that hydrolysis is not an on-going process initially.

As well as decreasing the $^{F}/_{S}$ stoichiometry, hydrolysis is also expected to increase the $^{O}/_{S}$ stoichiometry (*i.e.* it should be >3) whereas the initial ratio is seen to be 2.4. On allowing the substrate to warm to -30°C, the evident loss of hydrogen fluoride at -120°C appears to go to completion, with a $^{F}/_{S}$ stoichiometric ratio <0.02. On this basis it seems reasonable to assume that the processes inherent in the hydrolysis have gone to completion and so the $^{O}/_{S}$ stoichiometry should be between 4 and 5, the value being dependent on the exact hydrolysis pathway. However the final $^{O}/_{S}$ value is only ∿3.3. The ratio of the initial and final values therefore is 2.4 : 3.3, which is extremely close to 3:4.

From these arguments it would appear that the most likely reason for the initial determined stoichiometry of $F_{0.7}S_{1.0}O_{2.4}$ is due to the inapplicability of bulk sensitivity factors, rather than to obtaining a layer of degraded acid. In the experiments which follow the alkene is deposited within ∿30 minutes of the acid and over this period of time the acid surface appears to degrade very little.

The line shape of the initial $S_{2p}$ spectrum (Fig.3.5) is difficult to fit exactly, but can be adequately fitted by a single doublet (ratio 1:2, shift 1.3eV) leaving ∿3% of the spectrum unfitted, but within experimental error (estimated as ∿5% for curve resolution), it is concluded that all sulphur species present have the same core binding energy. The possibility of (elemental) sulphur contamination was briefly considered as a possible explanation for the apparently high amount of sulphur present in the surface (see above). This would be clearly distinguishable from the other sulphur species discussed, coming to 4-5eV higher kinetic energy (compared with sulphates); but there is no evidence for such a peak in the sulphur spectrum. The final $S_{2p}$ spectrum is very similar to that recorded initially. In contrast to this the initial and final $O_{1s}$ spectra (Figure 3.5) appear different; that recorded initially appears to be asymmetric and can be resolved as two components of separation 1.3eV and intensity ratio 1:2, whilst the final spectrum has lost most of the asymmetry and is resolved as two components of roughly comparable intensity and separation 1.5eV. Thus the $O_{1s}$ core level spectra seem consistent with the hypothesis that surface hydrolysis of fluorosulphuric acid is giving rise to sulphuric acid.

The absence of adventitious hydrocarbon makes the determination of binding energies problematical and the film is too thick to permit charge referencing from the gold substrate. Internal system shifts, *i.e.* the difference in kinetic energy of two core levels, are independent of sample charging and these have been determined for the initial and

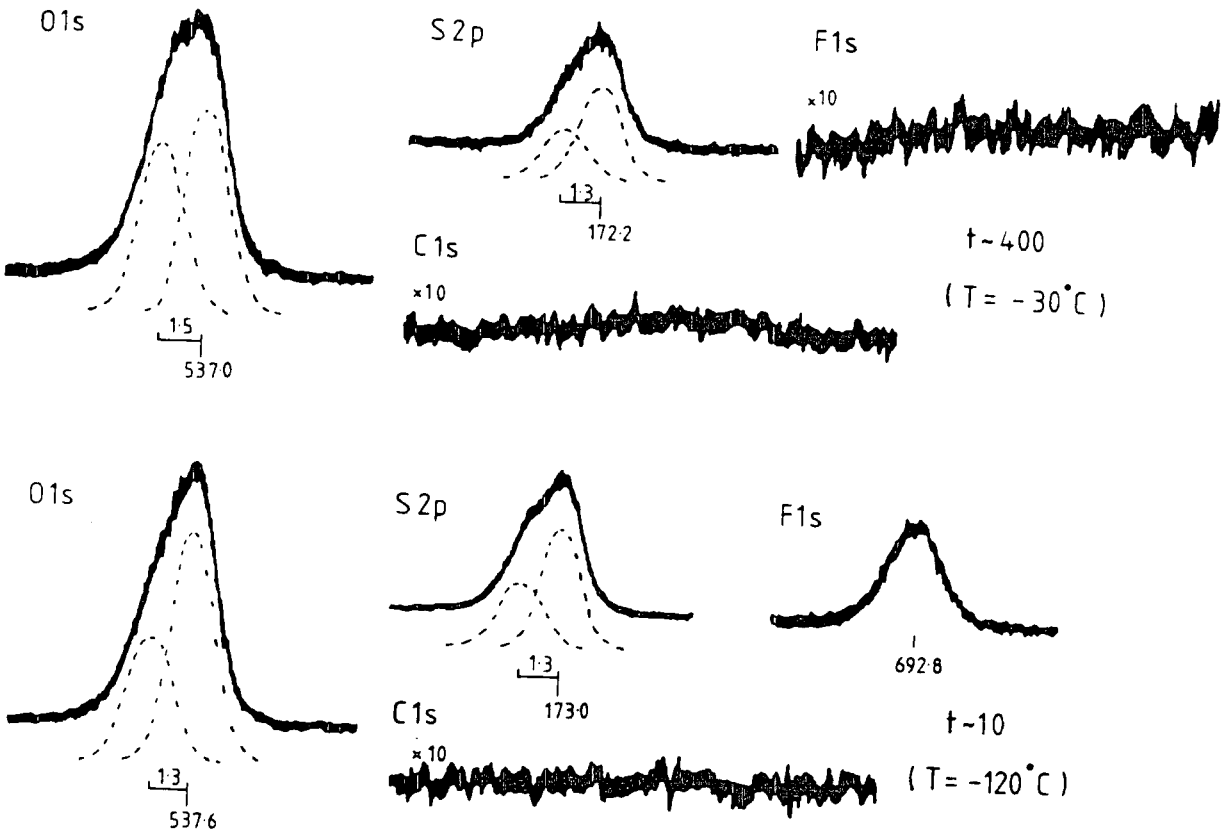


Figure 3.5 DEGRADATION OF $FSO_3H$ WITH TIME (mins.) (Binding energies in eV).

final compounds for the $S_{2p^{3}/_{2}}$ $-O_{1s}$ core levels, using the lower binding energy oxygen component. The similarity of the values (364.6 and 364.8eV), for the initial and final compounds respectively (which are thought to be fluorosulphuric and sulphuric acids), suggests however that this parameter may be too insensitive to be useful in characterising carbocation containing surfaces. Indeed in the experiments with alkenes, when the $C_{1s}$ spectrum indicated cation formation, this parameter had the same value as was found for the pure acid; either the ionised acid has the same value or it is obscured by an excess of the acid; the similarity of the fluorine, oxygen and sulphur spectra before and after alkene deposition certainly suggests that excess acid is present. Similar problems were encountered in determining a $S_{2p}$-$F_{1s}$ parameter. Such parameters would, of course, only be of limited use because, since the peaks are widely different in kinetic energy, they are somewhat calibration dependent.

(iii) Norbornene

Attempts were made to deposit norbornene onto a precooled substrate at -120°C, by allowing in the alkene to a pressure of $\sim 1 \times 10^{-4}$T for times up to 1 minute. Deposition was not achieved; this conclusion was based on the fact that there was no substantial increase of $C_{1s}$ intensity, and the (substrate) gold 4f core level signal was still observable. However deposition was possible when the substrate was maintained at -160°C, and a pressure of $1 \times 10^{-4}$T for 1 minute gave an apparently pure covering layer of norbornene (Figure 3.6). The absence of elements in the precursor other than carbon

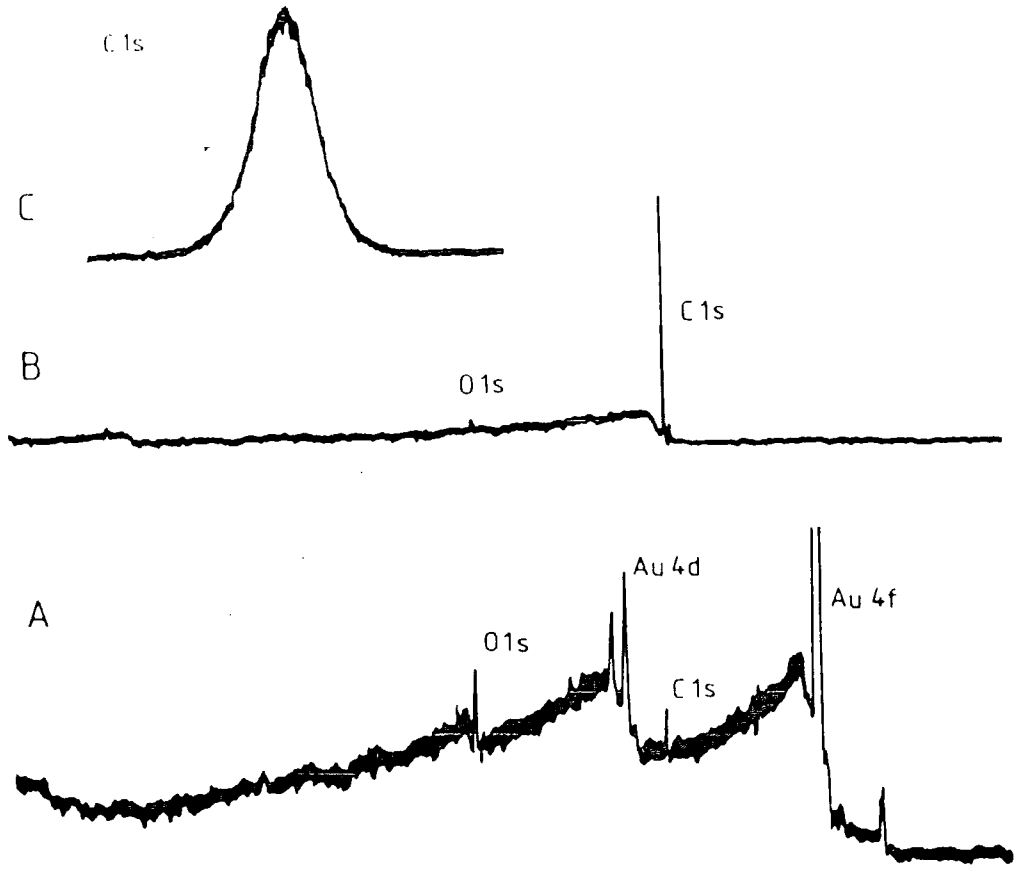


Figure 3.6 DEPOSITION OF NORBORNENE ON A GOLD SUBSTRATE; (A) substrate -120°C ($Au_{4f}$ not completely shown); (B) after deposition of norbornene ($1x10^{-4}$T, 1 min., -160°C); (C) High resolution $C_{1s}$ of (B).

precludes any estimation of purity, in contrast to the alkyl halide precursors where the halogen spectrum can give extra information about the deposited compound.

(iv) Cis-but-2-ene

With a substrate precooled to -120°C in the source, no deposition of this precursor was observed when pressures as high as $6x10^{-4}$T were used for a time of 1 minute. Even with a probe temperature of ∿-165°C (and using $6x10^{-4}$T for 1 minute) the amount of deposition achieved was insufficient to obscure the gold 4f signal (Figure 3.7, upper wide scan).

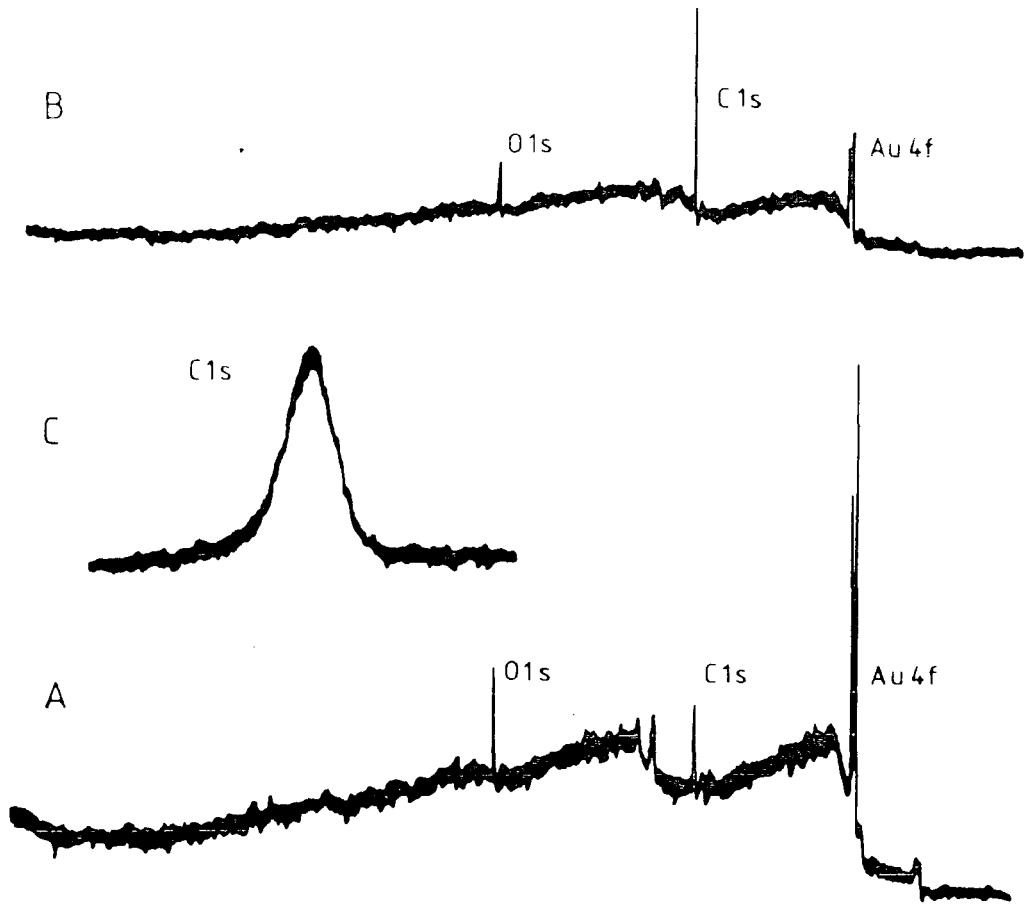


Figure 3.7 DEPOSITION OF CIS-BUT-2-ENE: (A) Substrate at -165°C prior to this deposition (deposition at -150°C had already been attempted); (B) After deposition ($6x10^{-4}$T, 1 min., -165°C); (C) High resolution $C_{1s}$ spectrum of (B).

The lower wide-scan spectrum shows the result of trying to deposit at -150°C, and by comparison, some deposition was achieved at the lower temperature of -165°C. The high resolution $C_{1s}$ spectrum is a single peak as expected, and whilst this particular spectrum suggests slight asymmetry, this feature is not borne out by a spectrum recorded on a more sensitive scale. The other apparent feature at this low temperature is the oxygen signal, showing the rapid acquisition of moisture on the cold surface.

## 3.2 The 2-Norbornyl Cation

### 3.2.1 Earlier work

#### (i) Experimental

The $^{1}H$ N.M.R. spectrum of the norbornyl cation in solution has been reported at increasingly lower temperature and higher field. Whilst at a temperature of $+3^{o}C$, the spectrum is a single peak[71] ($\delta \sim 3.1$ p.p.m.* in $SbF_5$-$SO_2$) significant changes occur on cooling. At $-100^{o}C$ the spectrum is three lines, $\delta$ = 1.93, 2.82 and 4.92, with intensity ratios of 6:1:4 respectively. Further cooling to $-158^{o}C$ leads to a splitting of the low field resonance into two peaks of equal intensity at 6.75 and 3.17 p.p.m., whilst the high field resonance splits into two peaks of ratio 2:1 at 2.13 and 1.37 p.p.m.[12] (These shifts were referenced to the single proton signal at 2.82 p.p.m.). This data is consistent with the successive freezing out of a 3,2 and a 6,2 (or 6,1,2) hydride shift. The question which the data does not answer though is whether a Wagner-Meerwein shift is not frozen out because it does not occur (*i.e.* the ion is non-classical), or if this shift occurring in classical cations, is still rapid enough at this temperature that not even substantial line broadening is observed.

Use of solution $^{13}C$ N.M.R.[12,20,56] has provided results which complement well the proton spectra so that at $-159^{o}C$ the hydride shifts are shown to be frozen out.[12] The equivalence of the signals attributed to $C_1$ and $C_2$ is again consistent with either a nonclassical ion, or classical ions undergoing rapid Wager-Meerwein shifts; the temperature of

---

* External TMS.

these studies probably represents the limit for solution work so that the conclusion that the spectra related to a non-classical ion had to be based on the application of the chemical shift analysis. A chemical shift difference of 168 p.p.m. is calculated for the norbornyl cation and norbornane and this contrasts with a value of ∿360 p.p.m. for the cyclopentane-cyclopentyl cation pair.

The advent of solid state N.M.R. has made it possible to study the norbornyl cation at temperatures down to 5K.[13,40] The conclusion reached from this experiment in which $C_1$ and $C_2$ were still observed to be equivalent was that if a Wagner-Meerwein shift was still occurring it must be doing so at a rate of at least $10^5$ $sec^{-1}$ and in classical rate theory this corresponds to an activation barrier of less than 0.2 kcal $mol^{-1}$.

The effect of isotopic perturbation on the N.M.R. spectrum of the 2-norbornyl cation has been studied.[72] Neither the 2-monodeutero nor the 3,3 dideutero ions revealed isotopic splitting of the downfield $C_1$, $C_2$ resonance. Such

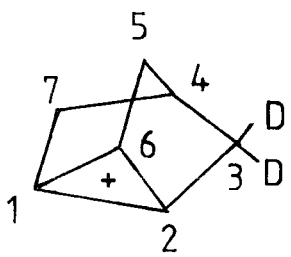


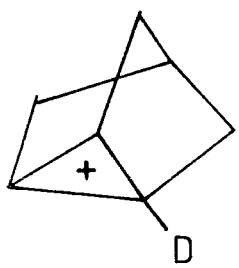


splitting was concluded to be < 2 p.p.m., but could not be determined more accurately since even at -150°C the 6,2 hydride shift causes broadening of the $C_1$, $C_2$ (and $C_6$) signals. However comparison with isotopic splittings of 105 p.p.m.

for the (equilibrating) dimethylcyclopentyl cation and <1 p.p.m. for the (static) cyclohexenyl cation leads to the conclusion that the norbornyl cation has a static (non-classical) structure.

The $C_{1s}$ E.S.C.A. spectrum of the 2-norbornyl cation has been reported following its preparation outside the spectrometer.[19,21] In contrast to the $C_{1s}$ spectra obtained of the cyclopentyl, methylcyclopentyl and 2-methylnorbornyl cations which exhibit two distinct peaks separated by ∿4eV, the spectrum of the 2-norbornyl cation shows a single broad peak with a shoulder. This was resolved as two peaks of intensity ratio 2:5 with an internal shift of ∿1.7eV. The conclusion that the cation was nonclassical followed mainly because of the absence of a high binding energy peak at some 4eV from the main peak, analogous to that seen in the $C_{1s}$ spectra of cations with localized positive charge. Subsequently though this data has been criticised, ranging from the suggestion that the spectrum is closer to two peaks of ratio 1:6,[9] to comments on the validity of the method since solutions of carbocations can involve several equilibria and thus there is no certainty of what species are frozen out and subsequently analysed.[73] Further criticism along these lines stemmed mainly from the publication of the norbornyl cation spectrum recorded at a different analyser pass energy.[20] In view of this discussion over the interpretation of the observed spectra, the results have not gained general acceptance.[3] Consequently it is one of the objectives of this work to establish the validity or otherwise of the published spectrum; more detailed discussion of the spectra to be expected for

the classical and nonclassical ions, and comparison with that experimentally observed, is delayed until Section (3.2.2).

Whilst the internal shifts of E.S.C.A. spectra are extremely important, it is regrettable that only the $C_{1s}$ spectra have been presented, since often it is the interdependence of the spectra which leads to a conclusive result, but in the present case this criticism is perhaps rather harsh because inevitably degradation of the moisture sensitive surface can be expected to occur rapidly.

(ii) Theoretical (Fig.3.8)

Dewar *et al* reported the results of a MINDO/3 (semi-empirical) geometry optimisation of the 2-norbornyl cation[74] in which they considered not only classical (A) and nonclassical (B, "π-complex") cations but also an unsymmetrical π-complex (G) and various edge protonated forms (C,D,E) two of which were seen as π-complexes. They do not appear to have considered a face protonated structure (F) but analogy with results of Pople *et al* for the $C_3H_7^+$ cation[75] suggests that this would be much higher in energy. Their results suggested that whilst the classical ion is more stable than the nonclassical (∿2 kcal/mol), the energy minimum might be the unsymmetrical π-complex (∿3.5 kcal/mol lower in energy than the classical ion). However the authors emphasized that the inherent accuracy of MINDO/3 was not great enough to allow definite predictions to be made from these results.

A complete *ab initio* (STO-3G) geometry optimisation was reported by Allen *et al*,[76] together with partial optimis-

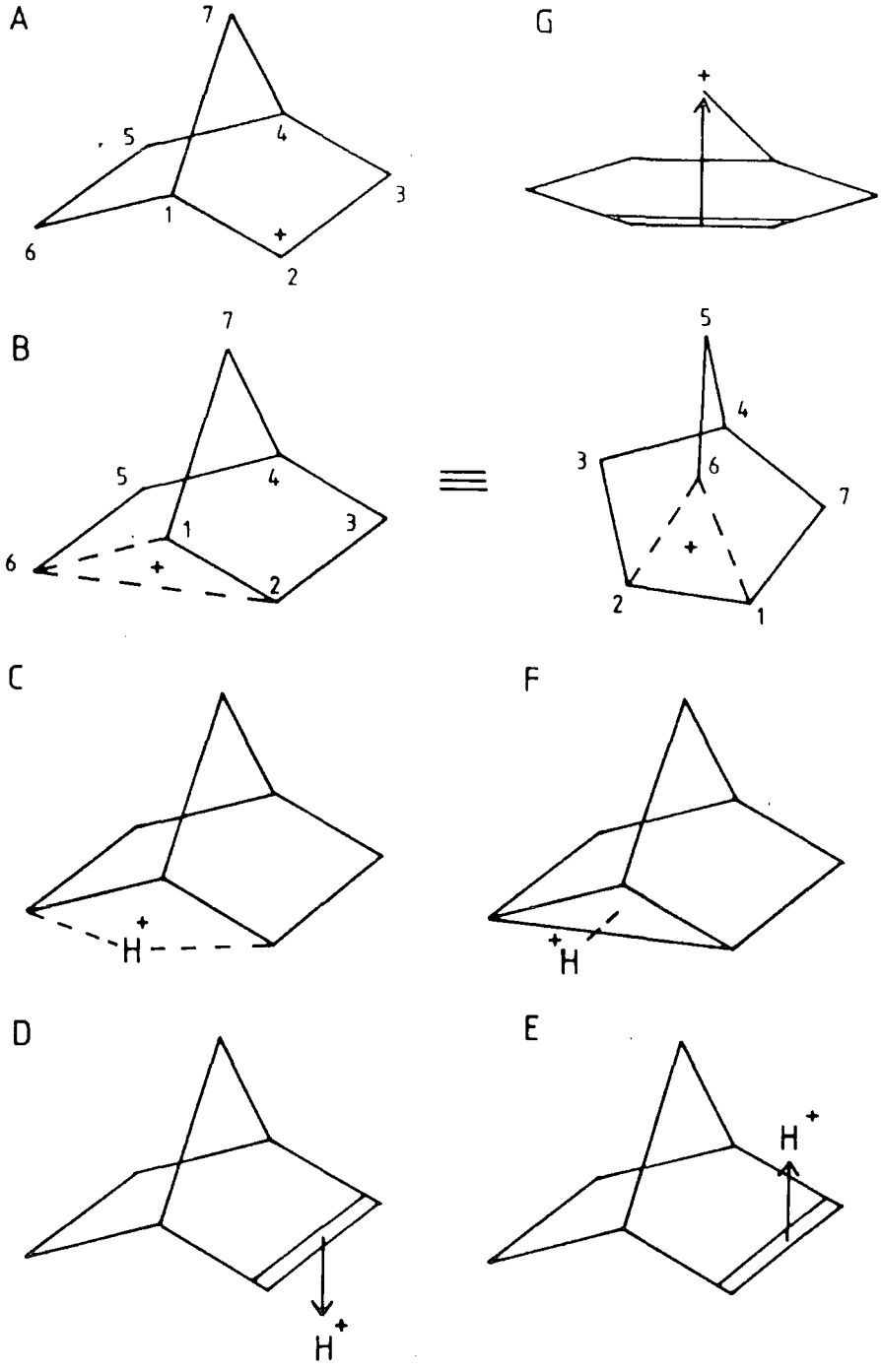


Figure 3.8 STRUCTURES PROPOSED FOR THE 2-NORBORNYL CATION; (A) Classical cation; (B) Nonclassical (corner protonated) cation; (C) Edge protonated; (D),(E) Endo and exo π-complexes; (F) Face protonated; (G) Unsymmetrical π-complex.

ation at the higher STO-4.31G level, of both the classical and nonclassical ions and the latter was described as the corner protonated form. Calculations of the total energy showed that whilst the classical form was 5.2 kcal/mol lower in energy at the STO-3G level, the higher level predicted it to be only 0.2 kcal/mol more stable than the nonclassical ion. The authors point out that this trend is similar to that found for the isomers of the ethyl cation; minimal basis set calculations predict the classical form to be more stable, but use of split valence basis sets, inclusion of polarization functions and correlation effects, successively lower the relative energy of the nonclassical form, predicting it to be the more stable.[77]

These results suggested that the ground states of the ions were very similar in energy; however the charge distributions obtained for the nonclassical ion differed significantly, for whilst the MINDO/3 results showed substantial charge on $C_6$, the *ab initio* calculations suggested that it was limited mainly to $C_1$ and $C_2$.

In order to aid the interpretation of the experimental data, E.S.C.A. chemical shifts were calculated from these two sets of optimised geometries. Dewar *et al* performed MINDO/3 equivalent core calculations[78] using their own geometries.[74] Whilst the internal shift calculated for the t-butyl cation (3.4eV) is in reasonable agreement with the observed experimental value (3.9eV), the values of 2.3 and 1.8eV obtained for the 2-methylnorbornyl and cyclopentyl cations respectively show that the method underestimates the

shift (*c.f.* experimental values of 3.7 and 4.3eV respectively). This is one example that using MINDO/3 and equivalent cores does not work well for shifts. The authors argue that relative peak intensity is far more important than internal shift, and it is on this basis that they reject the non-classical cation being the one observed experimentally; their simulated spectra for the nonclassical ion (two peaks of comparable intensity separated by ∿1eV) cannot give rise to the observed spectrum of a peak with a shoulder. Similar calculations and spectral simulation resulted in the conclusion that the classical ion would give a spectrum of two peaks separated by ∿1.4eV; this internal shift value was favourably compared with the experimentally observed value (∿1.47eV)[20] despite the fact that the authors have already acknowledged that the method underestimates the shifts!

Whereas Dewar *et al* argued that there was no really accurate theory of E.S.C.A. shifts, Clark *et al* suggest that this is not the case.[63] ΔSCF STO-4.31G calculations, whilst overestimating absolute binding energies, do reproduce internal shifts extremely well.[79] This method predicts an internal shift of 3.8eV for the t-butyl cation and later work by these authors using this level of theory, also rationalises the 4.3eV shift reported for the cyclopentyl cation.[80] Using the optimised geometries of Allen and Goetz, Clark *et al* calculated the ΔSCF shifts for both the classical and non-classical ions, noting in particular a larger span of binding energies for the classical ion (4.4 compared with 2.1eV for the nonclassical ion). Spectra synthesised using the core level shifts obtained showed that whilst the calculated

classical spectrum was very different, there was a striking resemblance between the calculated nonclassical and the experimental spectrum. It was further noted that the binding energy of $C_6$ was intermediate between that of $C_1, C_2$ and the remaining carbon atoms and this meant that deconvolution of the experimental spectrum into only two components would be incorrect.

Part of the difference in the results obtained in the two sets of calculated E.S.C.A spectra (MINDO/3 and STO-4.31G), will certainly be a reflection of the different charge distributions found for the ground state nonclassical ions. However an important difference between the results is the differing emphasis placed on the key spectral parameters, of internal shift and relative peak intensity, by the two groups. Whilst the work of Clark *et al* shows that E.S.C.A. shifts can be accurately calculated, relative intensities of carbon spectra can be questionable unless the sample is known to be free from adventitious hydrocarbon.

Further MINDO/3 calculations were reported by Wenke and Lenoir[81] suggesting that a 1-norbornyl cation was perhaps lower in energy than the unsymmetrical π-complex (G, identified as a possible minimum by Dewar *et al*), but STO-3G calculations, using partly optimised geometries at this level, yielded the classical cation (A) as the most stable with the bridged species (B) and edge-protonated (C) being some 4.3 and 4.4 kcal/mol higher respectively. They do not appear to have considered the 1-norbornyl cation, or unsymmetrical π-complex at this level, perhaps indicating that in the optimization procedure these structures were found not to correspond to energy minima.

Köhler and Lischka used completely optimised STO-3G geometries and performed single point calculations with contracted gaussian basis sets of double zeta quality, including some polarization functions.[82] From calculations involving electron correlations for smaller carbocations they estimated this correction for the norbornyl isomeric ions. Whilst they found that the classical structure was less stable than the nonclassical (∿13 kcal/mole) they also found that the edge protonated ion (C) was comparable in energy to this, being ∿8 kcal/mol more stable than the classical ion.

Single point calculations (STO-4.21P*) for the completely optimised geometry (STO-4.21P) reported by Schaefer *et al*,[83] gave the nonclassical ion as 0.2 kcal/mol more stable than the "classical", with the edge protonated form being 12.4 kcal/mol higher still. The optimised geometry for the nonclassical ion is in close agreement with that found by Allen and Goetz; however on close inspection the "classical" geometry suggested a degree of bridging. In other words in trying to find an optimised classical geometry, energy lowering occurs by involving some bridging. This appears to be reflected in the calculated $C_{1s}$ orbital energies particularly for $C_6$ which rises from 1.08eV (Allen *et al*, classical STO-4.31G) to 1.63eV (Schaefer *et al*, "classical" 4-21P*). Thus the "classical" form energy minimum, locked onto by Schaefer *et al*, appears to be an unsymmetrically bridged ion, and therefore nonclassical by very definition. The implication of this result is that the classical ion does not correspond

to an energy minimum and this has been confirmed by recent advanced level computations. Raghavachari *et al* [84] and Yoshimine *et al*[85] using fully optimised geometries at STO-4.21P levels and incorporating electron correlation showed that the only energy minimum on the potential energy surface was the symmetrically bridged norbornyl cation. Whilst the classical form so frequently found as an energy minimum in earlier work was considered an artefact of lower levels of computation, the edge protonated ion was found to be a saddle point ∿8 kcal/mol less stable than the nonclassical ion.

### 3.2.2 Results and Discussion

Fluorosulphuric acid was introduced into the source, containing a probe at -120°C, at a pressure of ∿1x10$^{-4}$T for 2 minutes. In view of the important time factor the surface was not characterised by a complete set of high resolution core level spectra; deposition was confirmed by a single wide-scan, and also the $C_{1s}$ core level was observed to determine the extent of adventitious hydrocarbon on the surface. Norbornene was then introduced at ∿1x10$^{-4}$T for 10 seconds and initially no deposition/reaction appeared to have occurred, but as the source pressure dropped over a period of thirty minutes the $C_{1s}$ signal grew and developed a shoulder (Figure 3.9). This spectrum (Fig.3.9d) was stable over ∿15 minutes - two consecutive spectra being identical. After this there was a gradual decrease of intensity followed by a loss of resolution leading to the final $C_{1s}$ spectrum, ∿1½ hours after the introduction of norbornene, and ∿2 hours after deposition of the acid bed. A repeat of this experiment yielded similar spectra.

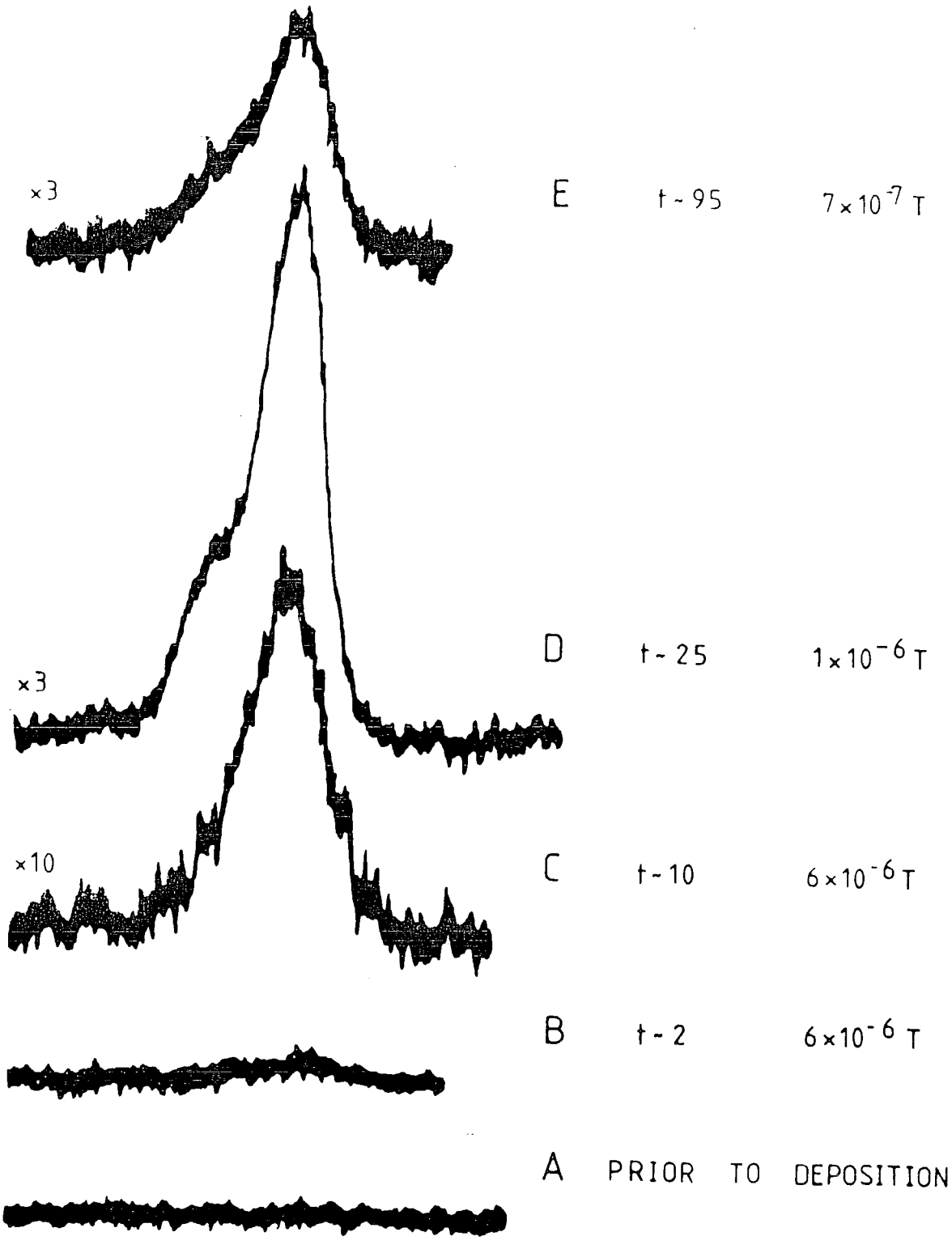


Figure 3.9 GROWTH OF $C_{1s}$ INTENSITY FOLLOWING INTRODUCTION OF NORBORNENE INTO THE SOURCE. Times (mins.) are from the introduction of alkene - approximately 30 minutes after introduction of the acid. Source pressures are given in Torr.

That any carbocation generated under the conditions of these experiments would not be stable for more than ∿1 hr., could be anticipated from the study of fluorosulphuric acid. On this basis the $C_{1s}$ spectrum which developed over the first thirty minutes (Fig.3.9d) can tentatively be assigned as attributable to the norbornyl cation; the subsequent demise of the carbocation then follows with that of the acid bed. Despite the lack of discrete high binding energy peaks in Fig.3.9c, interaction between the alkene and acid must have occurred since the alkene itself was found not to deposit under these conditions.

$F_{1s}$, $O_{1s}$ and $S_{2p}$ core level spectra (Figure 3.10) were run immediately after the two identical $C_{1s}$ spectra (Fig.3.9d), and a stoichiometry of $\sim F_{0.4}S_{1.0}O_{3.1}$ derived using standard sensitivity factors. This stoichiometry suggests

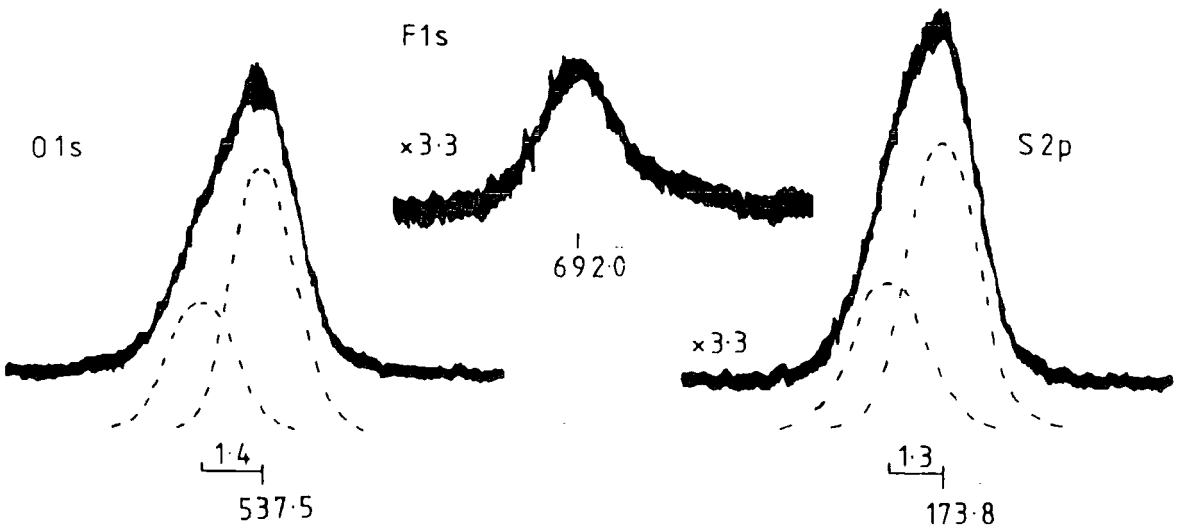


Figure 3.10 CORE LEVEL SPECTRA OF THE ACID BED AFTER DEPOSITION OF NORBORNENE

that hydrolysis is fairly well advanced; however the deposition procedure can be seen as yielding an overlayer of norbornene on an acid substrate and as such the $F_{1s}$, $O_{1s}$ and $S_{2p}$ signals will be attenuated by differing amounts. Assuming in the first instance that hydrolysis is negligible over the first hour (in fair agreement with the earlier data), the low value of the F/S ratio after norbornene deposition ($\sim$0.4), compared with that of the pure acid ($\sim$0.7), can be attributed entirely to differential attenuation by an overlayer of signals arising from photoelectrons of different energies. Using values for the mean free paths of $\lambda_{F_{1s}}$ $\sim$10Å and $\lambda_{S_{2p}}$ $\sim$18Å, the greater attentuation of the $F_{1s}$ core level signal is well modelled by a norbornene overlayer of $\sim$12Å, *i.e.* $\sim$2 monolayers. This represents a maximum overlayer thickness because it is calculated assuming that the low F/S ratio is entirely due to overlayer differential signal attenuation, whereas a part of this may be due to hydrolysis. Using $\lambda_{O_{1s}}$ $\sim$12Å, and calculating all core-level substrate attenuation factors leads to a possible acid stoichiometry of $F_{0.7}S_{1.0}O_{4.5}$. The calculations are of course only an approximation but they certainly give an order of magnitude to the correction needed for comparatively thin overlayers, when considering core-levels of widely different kinetic energies.

In considering the particularly high O/S ratio calculated here, several factors should be considered:

- in calculating this value all the oxygen signal was assumed to come from the substrate layer, but it is quite possible that moisture is present in, or even on, the very surface of the overlayer; if this were the case then applying

an overlayer intensity correction to this component of the $O_{1s}$ signal would lead to an overestimation of the oxygen present.

- with "pure" $FSO_3H$ it was found that bulk sensitivity factors overestimated the sulphur intensity, and one possible cause of this is a surface orientational effect; protonation of norbornene could conceivably necessitate a change of molecular orientation bringing, in particular, the hydroxyl group right to the surface. However this possibility is ruled out by the later results obtained for the sec-butyl cation (Section 3.3.2).

- the high ratio may of course be real, in which case it must be considered that hydrolysis of the acid has commenced. This of course to some extent invalidates the calculation based on no hydrolysis, but in these circumstances the overlayer would be less than two monolayers and consequently the attenuation factor would be different; thus an $^{O}/_{S}$ ratio of 4.5 again represents a maximum value. However, in the light of the stoichiometric ratios, which suggest that some hydrolysis of the acid bed may have occurred, it is necessary to consider whether quenching of carbocations excludes the possibility of their observation, and this is discussed in the interpretation of the $C_{1s}$ spectrum.

The $S_{2p}$ core level (Fig.3.10) is consistent with only one electronic environment, whilst a low binding energy component of the $F_{1s}$ spectrum suggests the possible presence of two different types of fluorine and the most likely origin would be the presence of some fluoride. Despite the possible

presence of moisture contamination, the $O_{1s}$ spectrum can be adequately resolved as two peaks of ratio 2:1, analogous to the acid when first deposited; in a "free" anion, all three oxygens would be expected to have equivalent binding energies due to charge delocalisation. It is possible that a free anion is not formed and that one of the oxygens is still associated with the carbocation, but it seems more probable that the observed spectra derive mainly from the unionised acid; indeed the internal shift of the two components of the $O_{1s}$ spectrum is found to be the same, within experimental error, for the two sets of data.

Thus the $O_{1s}$ and $S_{2p}$ spectra suggest that any ionised acid is not resolved from the signals arising from the excess acid present.

Perhaps the most striking feature of the $C_{1s}$ spectrum (Fig.3.9d) is its similarity with that reported previously. In view of the very different methods used to generate the norbornyl cation, it seems extremely unlikely that the spectrum is not what it is purported to be. The presence of the high binding energy shoulder shows that the spectrum is not attributable simply to polymerised norbornene, which would give a single peak.

Attempts have been made to deconvolute the $C_{1s}$ spectrum (Fig.3.9d) in a number of different ways; as classical or nonclassical, either simplistically or by reference to the core-hole calculations, and also with allowance for contamination of the pure spectrum. Possible contamination is considered to arise from the presence of excess alkene; it will be recalled that the overlayer calculation suggested that

coverage was a maximum of two monolayers of norbornene thick, but it seems unlikely that a second monolayer would react directly with the acid. Contamination, if present, has always been considered to contribute only to the lowest binding energy peak. Three different half-widths have been tried for deconvolution; consideration of the more intense, low binding energy peak suggests that a FWHM of ∿1.65eV would be correct, but ∿1.5 and 1.8eV have also been tried. The latter was found to be too broad however, and a reasonable line shape could not be produced when considering either a classical or nonclassical model. When more than two components were considered, two gaussians of appropriate intensities were initially fitted into the spectral lineshape, as far apart as possible, and the others then adjusted for position between these two. The most crucial and most difficult part of the spectrum to reproduce is the point at which the shoulder joins the lower binding energy peak.

The simplistic prediction of the norbornyl cation spectrum is along the lines that the nonclassical ion should give two peaks of intensity ratio 2:5, whilst the classical should give components of 1:6. It was found impossible to fit the spectrum with two peaks, of the same FWHM, that had intensity 2:5. The closest which could be achieved was two peaks (FWHM ∿1.7eV) with a ratio of 2:6, interpretable perhaps as "nonclassical with contamination", though here the shoulder appears overestimated (Fig.3.11B). The separation of the two peaks is ∿1.7eV and thus the result is virtually identical with that previously reported.[19] Two components (FWHM ∿1.7eV) with ratio of 1:6 and having the same total area as that of the spectrum observed, give a lineshape which is totally

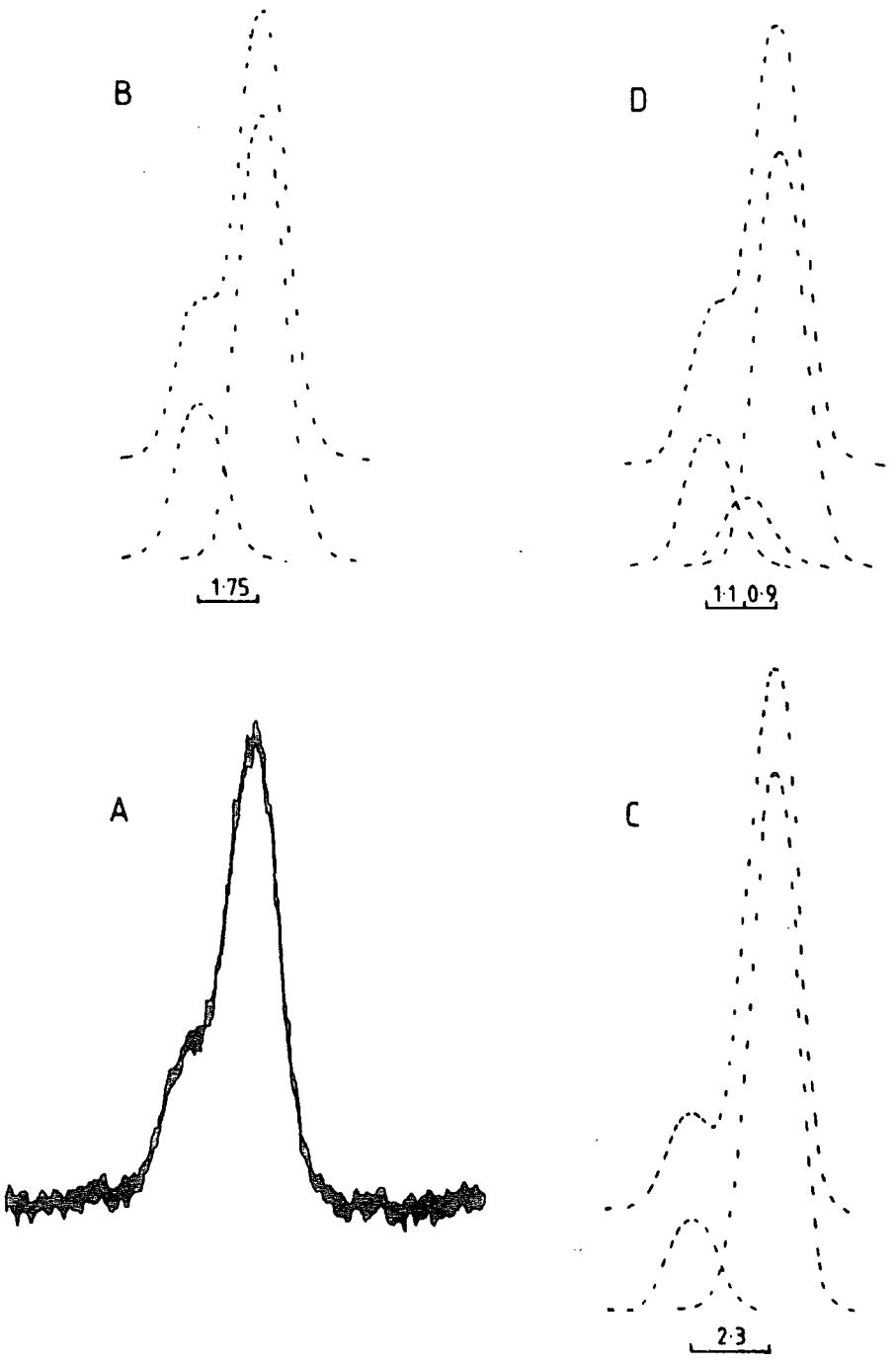


Figure 3.11 SIMULATED SPECTRA OF THE NORBORNYL CATION $C_{1s}$ SPECTRUM USING PEAKS OF FWHM ∿1.7eV

(A) Experimentally observed; (B) "Simplistic" nonclassical with contamination, (2:5+1); (C) "Simplistic" Classical (1:6); (D) Nonclassical with contamination (2:1:4+2.5).

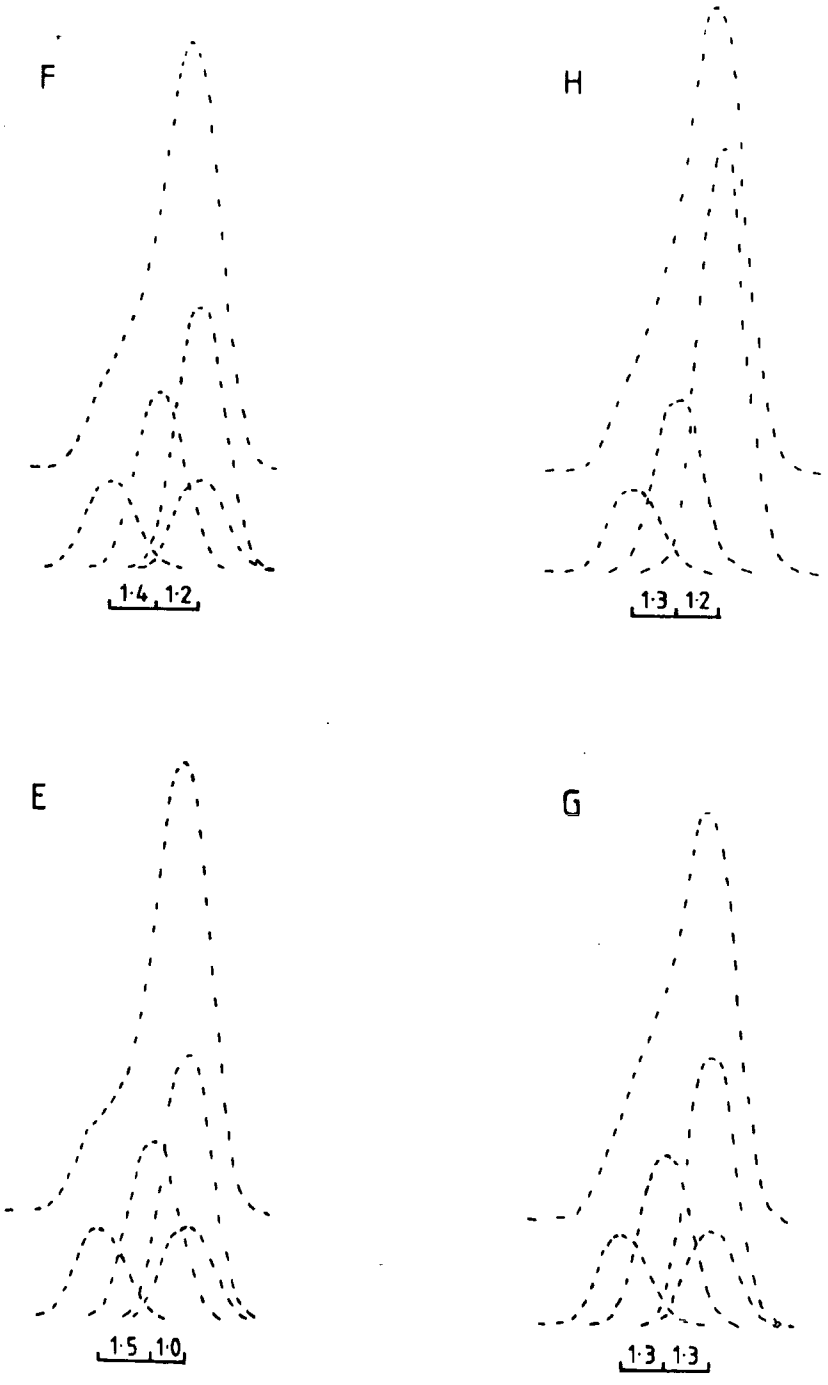


Figure 3.11 (contd.)

(E), (F), (G) Classical showing variation of position of second most intense peak (1:2:1:3); (H) Classical with contamination (1:2:4+1).

different, when the two peaks are spaced so as to fit the base of the observed spectrum (Fig.3.11C). One possible reason for the high $^{O}/_{S}$ ratio previously determined (see above) was the presence of moisture in the surface layers. Whilst all quenching of the carbocations cannot be ruled out, it is important to note that the failure of the simplistic classical model to reproduce the observed $C_{1s}$ lineshape also means that the spectrum is not simply due to exo-norborneol - the expected product of cation quenching. A norborneol spectrum would be two peaks ratio 1:6 with internal shift of ∿1.6eV.[86]

The simplistic cation model was the extent of data analysis by Olah, though in his unprecedented re-examination of the data Kramer suggested (rightly) that the situation was more complex. It was proposed that atleast three components would contribute to the spectrum and that whilst the classical ion spectrum contained peaks of ratio 1:2:4, the nonclassical should be 2:1:2:2. The best model though, on which to base an interpretation of the spectrum must be the *ab initio* core hole calculations.[63] These predict that the nonclassical ion spectrum would be well represented by three peaks relative area 2:1:4, whilst the classical ion could be as many as four peaks of intensity 1:2:1:3 (Table 3.1). A nonclassical resolution of the spectrum was found to be possible only if contamination was also included. The spectrum is well represented by three peaks (FWHM ∿1.7eV) of intensity ratio 4:2:13 (Fig.3.11d) which suggests ∿25% of the spectrum is "norbornene" as opposed to the cation. The internal shifts are∿2.0 and 0.9eV from the most intense component. Attempts

to reproduce the observed lineshape using a classical model and peaks (FWHM ∿1.7eV) of intensity ratio 1:2:1:3 were unsuccessful (Fig.3.11, E, F, G, H) It was found that the two peaks of lowest binding energy had to be coincident, and also that the lineshape derived was very dependent on the exact internal shift of the second most intense component (this change is shown in Figs. 3.11, E, F, G). But whatever the exact position of this peak, the essential shoulder characteristic of the observed spectrum cannot be reproduced. Allowance for some contamination by unreacted norbornene (Fig.3.11, H; peak ratios 1:2:5) did not improve the situation.

Altering the FWHM of the gaussians used for deconvolution to ∿1.5eV, a good fit could not be obtained based on a nonclassical model, either with or without consideration of some contamination. The "best" fit (Fig.3.12,B), grossly overestimates the shoulder dip, and three gaussians of this FWHM cannot accurately reproduce the base width of the observed spectrum. Whilst resolution of the spectrum on the basis of a pure classical ion leads to a poor simulation (Fig.3.12,C), the lineshape observed can be faithfully reproduced using four peaks (FWHM ∿1.5eV), of intensity ratio 2:4:2:11; that is, a classical model with ∿25% of the spectrum attributable to "norbornene" contamination (Fig.3.12,D). The internal shifts of this model are 0.3, 1.5 and 2.6eV from the most intense component.

Thus using either a classical or nonclassical model a good representation of the observed spectrum can be obtained (Figs.3.12, D and 3.11,D respectively). It is interesting to note that both of these simulations suggest that

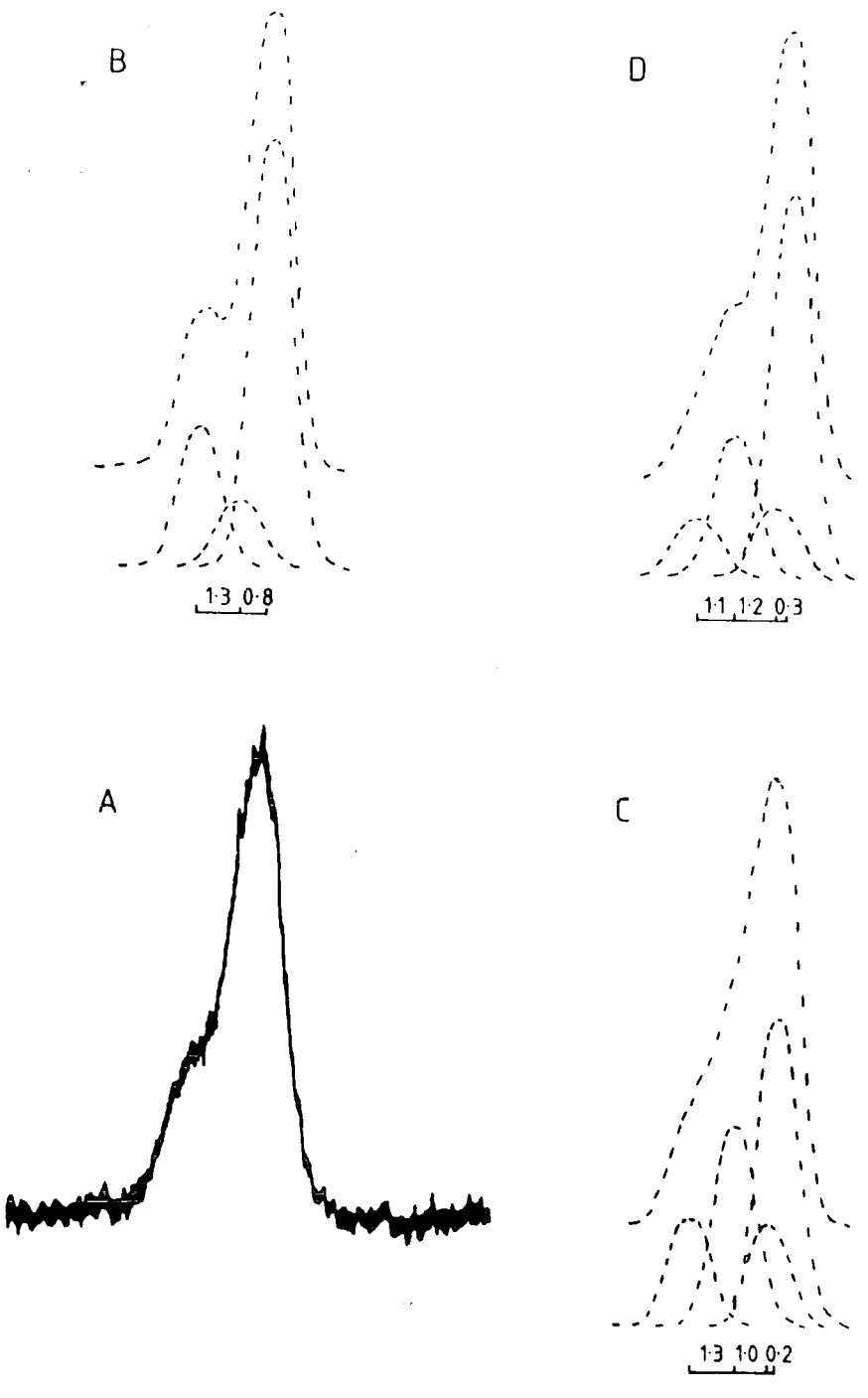


Figure 3.12 SIMULATED SPECTRA OF THE NORBORNYL CATION $C_{1s}$ SPECTRUM USING PEAKS OF FWHM ∿1.5eV. (A) Experimentally observed; (B) Nonclassical with contamination (2:1:4+2); (C) Classical (1:2:1:3), (D) Classical with contamination (1:2:1:3+2½).

∿25% of the observed spectrum may be due to contamination by "norbornene". It has already been noted that norbornene does not deposit under the conditions of the present experiment, and thus it seems most likely that the excess norbornene has reacted with some of the carbocations formed; this could lead to up to 30% of the norbornyl cations having a 3-norbornyl substituent, but substitution in this position is unlikely to affect the possibility of bridging, and at the temperature of this experiment the 3,2 hydride shift is frozen out.[12]

Up till this point the discussion has centred around simulating the observed lineshape from peaks of the predicted intensity ratios, and this is true of earlier work.[9,74] On this basis alone the observed spectrum cannot be considered to be diagnostic of either classical or nonclassical structure. However, as originally pointed out,[18] the single most important parameter of carbocation spectra is perhaps the internal shift. The t-butyl cation has been shown to have an internal shift of ∿3.9eV,[19] and in this work a localised tertiary cation had a shift of at least 3.1eV (Section 2.3.1). This is contrasted with the completely delocalised positive charge of, for example, the tropylium cation or the trityl cation (Section 2.1.1).[18] In addition to this the ΔSCF STO-4.31G core hole state calculations have been shown to be accurate in determining these internal shifts and, for example, have recently been used to rationalise the reported cyclopentyl cation spectrum.[80] Calculations on the norbornyl cation have predicted very different internal shifts for the classical and nonclassical species (Table 3.1); the carbon bearing a positive charge in the classical species is expected to be some 4.4eV to higher

TABLE 3.1

| | Relative $C_{1s}$ orbital energies (Allen *et al*)[76] (eV) | ΔSCF STO-4.31G shifts (Clark *et al*)[63] (eV) | Expected Peak Group intensities | Shift observed in simulation of observed spectral lineshape (eV) |
|---|---|---|---|---|
| Classical | | | | (Fig.3.12,D). |
| C2 | 4.58 | 4.44 | 1 | 2.6 |
| C3 | 1.32 | 1.45 | 2 | 1.5 |
| C1 | 1.50 | 1.28 | | |
| C6 | 1.08 | 0.80 | 1 | 0.3 |
| C4 | 0.58 | 0.27 | 3 | 0.0 |
| C7 | 0.39 | 0.31 | | |
| C5 | (0.0) | (0) | | |
| Non-classical | | | | (Fig.3.11,D) |
| C1,C2 | 2.48 | 2.01 | 2 | 2.0 |
| C6 | 1.96 | 1.25 | 1 | 0.9 |
| C3,C7 | 0.34 | 0.33 | 4 | 0.0 |
| C4 | 0.23 | -0.12 | | |
| C5 | (0.0) | (0) | | |

binding energy of the most intense spectral component. In all the simulated classical spectra of this work (see Figs. 3.11 and 3.12) this important internal shift is only ∿2.6eV; the 1.8eV difference between experimentally observed and theoretically calculated values being far beyond the expected error of the calculations. Similarly the calculated shift between the charge bearing carbon and the two adjacent carbon atoms, in the classical species is ∿3.0eV, whilst simulation

of the lineshape requires this shift to be only ∿1.1eV. In stark contrast to these inconsistencies between the theoretical calculated internal shifts, and those needed to simulate the observed spectral lineshape on the basis of a classical model, the nonclassical model simulation of lineshape suggests an internal shift of ∿2.0eV for $C_1$ and $C_2$, from the major component, in excellent agreement with the calculated value. Agreement between the calculated and observed shift for $C_6$ in the nonclassical ion (1.25 and 0.9eV respectively) is not quite as good, though it is much better than that found in the classical ion. Perhaps part of this discrepancy is because $C_6$ has a greater relaxation energy than $C_1$ and $C_2$, and though shifts are generally well reproduced at the STO-4.31G level, relaxation energies are underestimated, a feature which from consideration of orbital energies and ΔSCF shifts, might affect $C_6$ more than $C_1$ and $C_2$ (see Table 3.1). In addition, comparison of the MINDO/3 and *ab initio* results suggest that the charge at $C_6$ is geometry dependent.

Thus on the basis of lineshape and internal shift analysis, the $C_{1s}$ spectrum observed when norbornene is reacted with fluorosulphuric acid, is consistent with nonclassical models, and not with classical ones.

It is important to be quite certain why the spectrum obtained from protonation of norbornene has been interpreted as that of the norbornyl cation whilst that obtained using norbornyl chloride and antimony pentafluoride was dismissed. The latter spectrum did not appear as a stable form, but was very evidently a natural intermediate between two spectra (see Figs. 2.13, 2.14, 2.15), neither of which

corresponded to that expected for a cation; in other words in changing from the initial $C_{1s}$ to the final $C_{1s}$, it is inherently necessary to go through the form yielding the spectrum which potentially is that of a classical ion. This situation is contrasted with that in the reaction of norbornene and fluorosulphuric acid where the $C_{1s}$ spectrum assigned as that of the norbornyl cation was "static", in the sense that two $C_{1s}$ spectra were identical, and also it is less apparent that such a spectrum is an inherently necessary intermediate form between the initial and final $C_{1s}$ spectra (Fig.3.9).

Whilst potential ionisation of norbornyl chloride was observed only once and ionisation of t-butyl chloride was never observed, the essential nonclassical $C_{1s}$ spectrum obtained from protonation of norbornene was reproducible and also protonation of cis-but-2-ene appears to lead to cation formation (see Section 3.3.2).

It was pointed out (Section 2.3.3) that recent N.M.R. evidence suggests that the ionisation of halides at the temperature used for the experiments described in this work, was slow and might not be complete on the timescale of these experiments. This can again be contrasted with the potentially very fast protonation reaction; certainly the results obtained for the sec-butyl cation support this idea. The greater ionic mobility of a proton compared with a chloride ion in solution,[87] and the fact that ionic conduction in sodium and potassium chloride is mainly by the cation[88,89] (an effect attributed to the smaller size of the cation which could be greater still if comparing a proton and a halide ion) suggest that it is not

unreasonable to expect the proton to have an ionic mobility in the solid state which is greater than that of the chloride ion, and this would be consistent with the notion that protonation occurs more readily than ionisation. The other factor in consideration of different rates of reaction in the two methods of cation formation, is that whilst the ionisation reaction must occur in the solid phase (there was little evidence of substantial peak broadening immediately after deposition of norbornyl chloride), protonation might well be a gas-solid interface reaction.

## 3.3 The sec-butyl cation

### 3.3.1 Earlier work

#### (i) Experimental

Early attempts to prepare this cation were unsuccessful; the reaction of sec-butyl fluoride and antimony pentafluoride,[7] and n-butane[90] or sec-butyl alcohol[91] with "Magic" Acid, all led to the t-butyl cation. However, it was successfully prepared, without appreciable rearrangement by reaction of sec-butyl chloride with antimony pentafluoride in sulphuryl chlorofluoride at -110°C.[22] The $^{1}H$ N.M.R. spectrum showed two peaks, at $\delta$ = 2.7 and 6.8 p.p.m.,[91a] of ratio 2:1, and this was explained by assuming that the degenerate 2,3 hydride shift at this temperature was still rapid

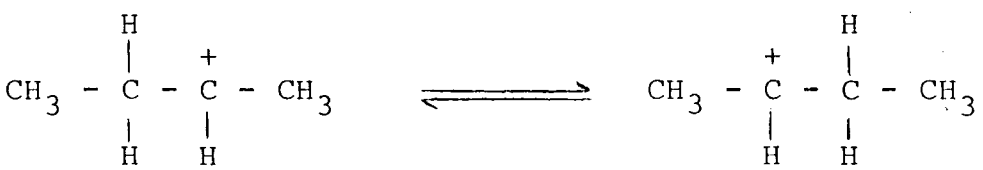

compared to the N.M.R. timescale. Lineshape analysis of the spectrum suggested that the process causing coalescence of the signals at higher temperature had an activation barrier of ∿7.5 kcal/mol. This value was significantly lower than that found for proton exchange in the isopropyl cation (∿16.4 kcal/mol) which was considered to occur *via* a 1-propyl cation; thus exchange in the sec-butyl cation was considered to occur *via* protonated methylcyclopropane intermediates.[92]

Early $^{13}C$ N.M.R. results suggested that the cation was equilibrating classical ions,[8] but this interpretation was refined in view of later work.[93] The $^{13}C$ spectrum showed two resonances at 21.0 and 171.6 p.p.m.* of equal intensity and these were assigned as the 1,4 and 2,3 carbon atoms respectively. Estimation of shifts from model systems suggested the values should be ∿30.2 and 191.4 p.p.m., showing that the carbons were more shielded than expected for a straightforward pair of equilibrating ions. Two possible courses were considered; the shielding might be due to strong β C-C hyperconjugation or the H-bridged intermediate was involved in the equilibration. The possibility of it being a hyperconjugation effect was dismissed, for whilst MO calculations showed that C-C hyperconjugation was important in substituted ethyl cations, the magnitude of this was similar in secondary and tertiary cations; thus the calculated N.M.R. shifts should not show extra shielding since the model systems used were tertiary cations. Whilst the coupling pattern of the $^{13}C$ spectrum was inconsistent with the ion being merely a static H-bridged ion, this criterion alone could not exclude the possibility of a rapidly exchanging H-bridged ion, in which the 3,2 hydride shift still occurred. A lack of suitable

* External $Me_4Si$

model systems precluded the possibility of estimating $^{13}C$ shifts for such an ion but it was suggested, by comparison with bridged halonium ions, that the carbons should be more shielded than those experimentally observed, so that the spectrum was not simply due to a rapidly exchanging H-bridged ion either. Since the spectrum could not be assigned as derived from one ion, it was concluded that the $^{13}C$ resonances observed were time-averaged ones and that their position would be consistent with equilibration between the hydrogen bridged and degenerate classical ions. Such a conclusion requires the assumption that these ions are of similar thermodynamic stability. In the light of more recent calculations, which show that with inclusion of electron correlation the H-bridged ion is some 8-10 kcal/mol more stable,[82] this conclusion appears to be invalid.

The isotopic perturbation of resonance method which has proved so diagnostic of single and double minima potential energy surfaces, applied to the sec-butyl cation gives an intermediate splitting value of 11 p.p.m.[94] (*c.f.* norbornyl <2 p.p.m., 1,2-dimethylcyclopentyl, >100 p.p.m.). Similarly the total chemical shift difference between the 2-butyl cation and butane, has a value of 309 p.p.m.[11] (*c.f.* norbornyl 175, 2-propyl 376 p.p.m.) showing it to be borderline in classical-nonclassical behaviour.

Solid state $^{13}C$ CPMAS N.M.R. of the sec-butyl cation at ∿190K[39] again showed two types of carbon, and the shifts of 22 and 170 p.p.m.* were in good agreement with the results of solution studies. However, even on cooling to 50K,[41] no further distinction was possible.

---

* $Me_4Si$

(ii) Theoretical (Fig.3.13)

Schleyer *et al* considered two open chain conformations, $C_1$ and $C_s$ forms[95] (Fig.3.13A and B); at the level of theory used (STO-3G) the $C_1$ form was predicted to be the more stable by ∿2.2 kcal/mol, and this was interpreted in terms of the possibility for this conformation of favourable C-C hyperconjugation with the vacant 2p orbital on the cation centre. In view of the large number of conformations considered for the $C_3H_7^+$ cation by these workers,[75] the investigation of only two for the sec-butyl cation is rather surprising.

Kohler and Lischka investigated the open chain ($C_s$) and hydrogen-bridged trans-2-butene (3.13C) conformations.[82] Single point calculations employing a contracted gaussian basis set were performed using STO-3G optimised geometries; whilst these gave the open chain isomer as that of lower energy, inclusion of an estimation of electron correlation reversed this, suggesting that the H-bridged structure was some 8-10 kcal/mol more stable.

Clark and Harrison considered protonated methylcyclopropane (3.13D) and partially methyl bridged (3.13E) structures as well as the $C_s$ conformation.[96] Using unoptimised estimated geometries they concluded that at the STO-4.31G level, the partially bridged structure was lowest in energy, being some 15 kcal/mol more stable than the $C_s$ form; the fully-bridged structure was only ∿0.6 kcal/mol below the open chain isomer. ΔSCF STO-4.31G core hole calculations for these conformations showed that the E.S.C.A. spectrum of this cation

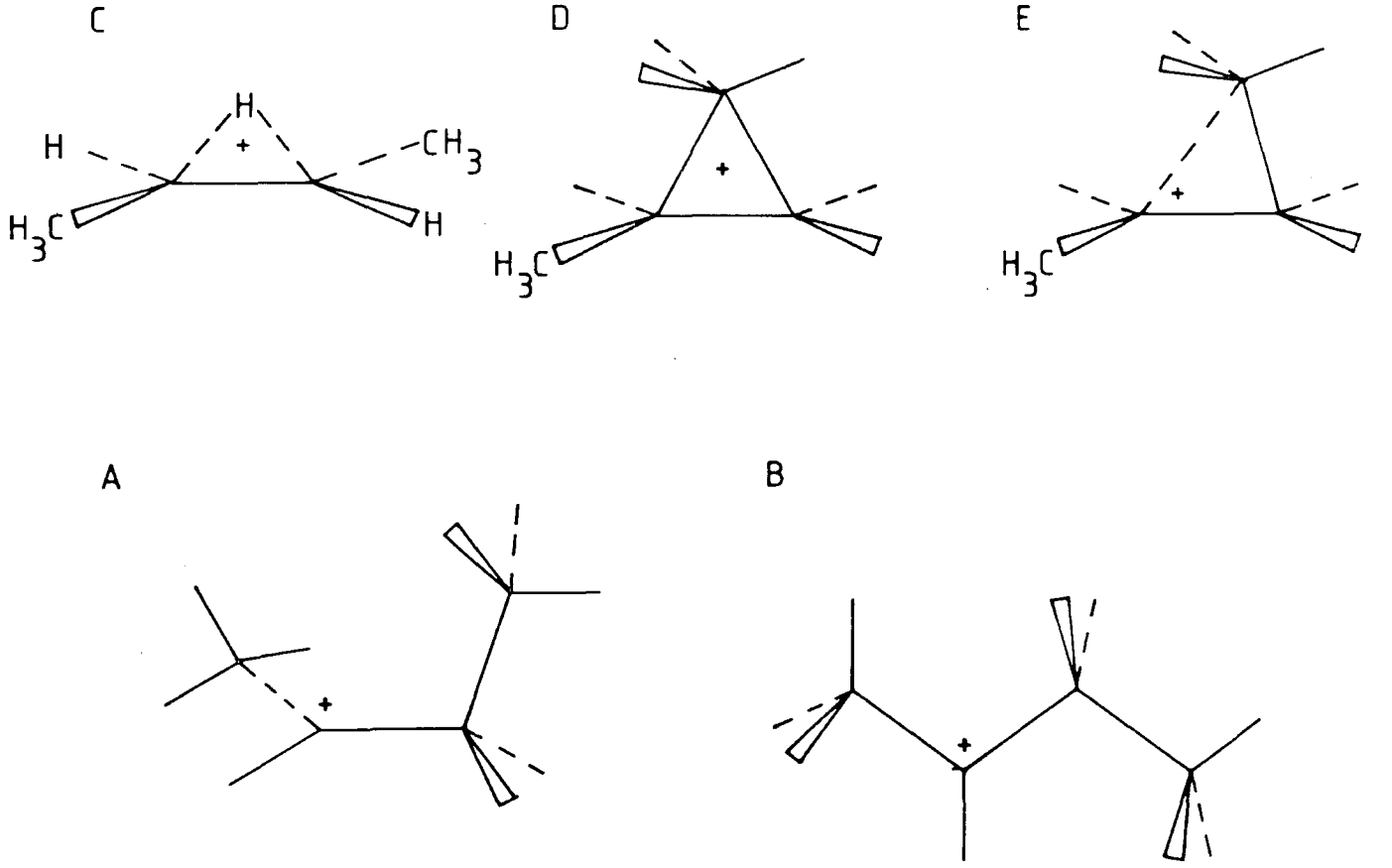


FIGURE 3.13 STRUCTURES PROPOSED FOR THE SEC-BUTYL CATION. (A) Open chain ($C_1$ form); (B) Open chain ($C_s$ form); (C) Hydrogen bridged trans-but-2-ene; (D) Fully bridged (methyl-substituted corner-protonated cyclopropane); (E) Partially bridged.

would be distinctive since the core electron binding energies were sensitive to the small geometrical differences between these conformations. Internal shifts calculated varied from ∿6.1eV for the $C_s$ cation to only 2.1eV for the fully bridged ion. Furthermore the structural determination would be aided by the observed peak intensity ratios since the predicted spectral lineshapes were significantly different.

### 3.3.2 Results and Discussion

Fluorosulphuric acid was introduced into the source to a pressure of $\sim 1 \times 10^{-4}$T for 1 minute, and the material deposited on a probe at -120°C was characterised (Wide Scan, $F_{1s}$, $O_{1s}$, $S_{2p}$, $C_{1s}$). The acid stoichiometry using bulk sensitivity factors was consistently in the region of $F_{0.7}S_{1.0}O_{2.4}$. Cis-but-2-ene was then introduced to $\sim 1 \times 10^{-4}$T for 15 seconds; the source pressure was $< 1 \times 10^{-6}$T before the alkene was introduced and rapidly returned to this when the reagent flow was stopped. The $C_{1s}$ spectrum was run immediately and is thus within ∿5 minutes of the alkene introduction and within ∿30 minutes of the acid deposition. The $C_{1s}$ spectra immediately before and after the butene introduction into the spectrometer are shown in Figure 3.14. After the $C_{1s}$ core level, the $F_{1s}$, $O_{1s}$ and $S_{2p}$ spectra were again recorded in order to determine the extent of hydrolysis. These three core level spectra, before and after the butene deposition are shown in Figure 3.15. About thirty minutes after introduction of the alkene ( ∿1 hr. after acid deposition), the $C_{1s}$ spectrum began to change, showing in particular the growth of another even higher binding energy peak (Fig.3.14C).

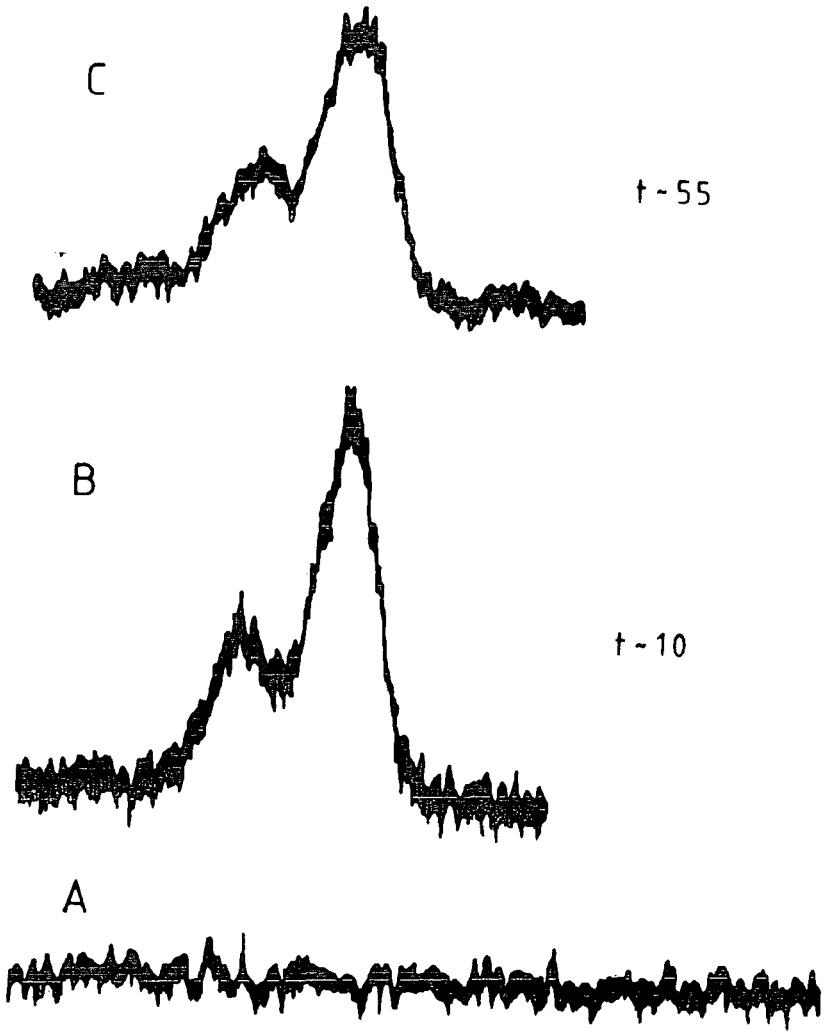


Figure 3.14 CIS-BUT-2-ENE AND FLUOROSULPHURIC ACID; CHANGE OF $C_{1s}$ SPECTRUM WITH TIME. (A) Prior to inlet of alkene; (B) immediately after alkene inlet. Time (mins.) from inlet of alkene - approximately 30 minutes after inlet of acid.

The first $C_{1s}$ spectrum obtained after the introduction of butene (3.14B) is considered to be that of the sec-butyl cation; at this point the butene must have reacted because it was previously shown that its deposition is problematical even at -160°C and also because the $C_{1s}$ spectrum is not that appropriate to the alkene precursor. Whatever reaction does occur obviously occurs quickly since this $C_{1s}$ spectrum is observed immediately after introducing the alkene, and this favours a protonation reaction. The later more complex $C_{1s}$ spectrum (3.14C) is considered to be a degraded form consistent with the growing hydrolysis of the acid bed,

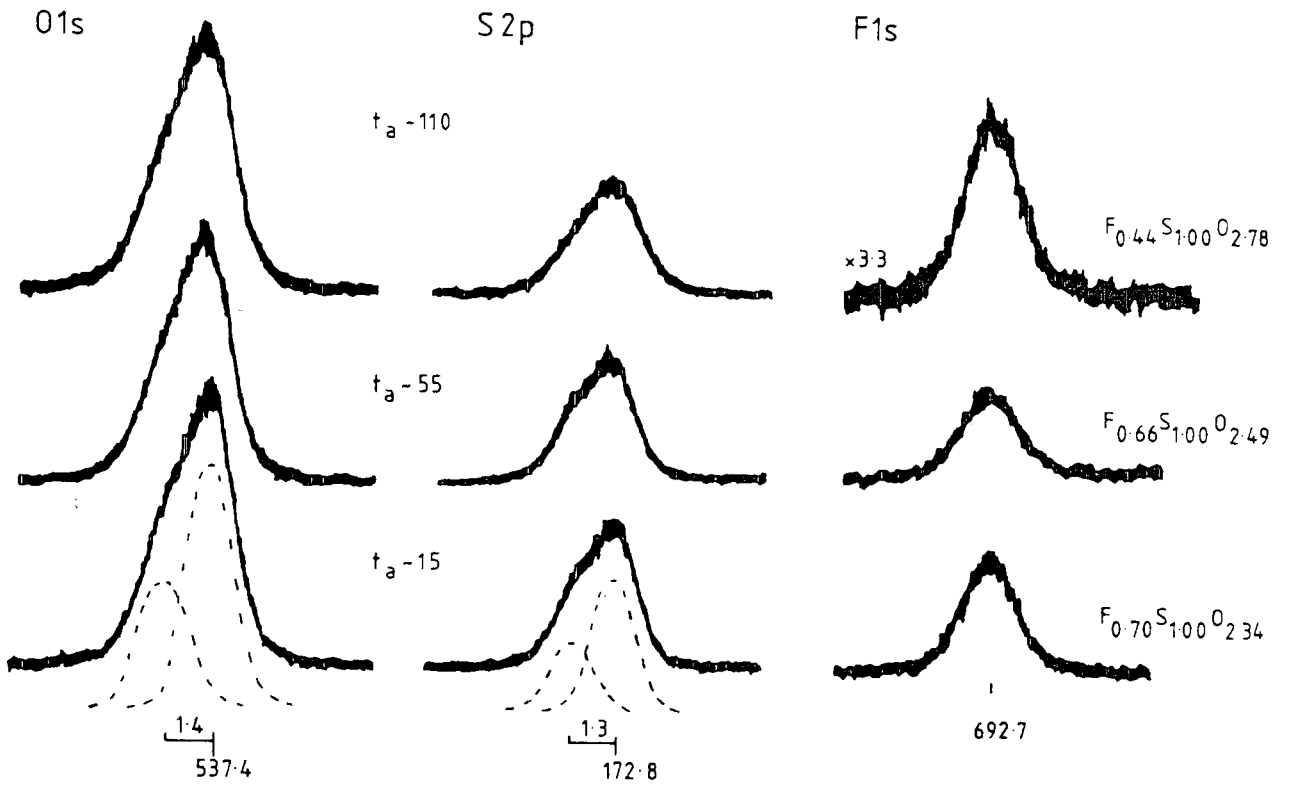


Figure 3.15 CHANGES IN THE CORE-HOLE SPECTRA OF THE $FSO_3H$ BED; Times (mins.) are from deposition of the acid; the three sets of data roughly correspond to the three $C_{1s}$ spectra of Fig.3.14. Binding energies (eV) are given for the initial spectra.

as is apparent from the significant decrease in the $^{F}/_{S}$ stoichiometry from 0.66 to 0.44 (both being determined after alkene deposition). The small change in acid stoichiometry observed before and just after alkene introduction shows that hydrolysis is negligible at the time of observation of the initial $C_{1s}$ spectrum; in fact the values obtained for the $^{F}/_{S}$ ratio are the same within experimental error. On the basis that the butene forms an overlayer, some differential attenuation of core level signals will occur; even if the total change in $^{F}/_{S}$ stoichiometry were due to this effect, an overlayer calculation (using $\lambda_{F_{1s}}$ = 10 and $\lambda_{S_{2p}}$ = 18Å) suggests that there is only fractional monolayer coverage of the surface; under these circumstances polymerisation of the alkene seems unlikely. The $C_{1s}$ spectrum attributed to the sec-butyl cation was found to be reproducible, suggesting that this spectrum does correspond to a discrete species, rather than to a mixture produced from quenching, fluorination or polymerisation since such side reactions would be expected to vary significantly in different experiments. In order to probe the possibility of polymerisation further the alkene inlet conditions were varied from $\sim 1 \times 10^{-5}$T to $\sim 1 \times 10^{-4}$T for 30 seconds, but the $C_{1s}$ spectra obtained were essentially the same. In one experiment the sec-butyl cation was not observed, the first $C_{1s}$ spectrum recorded being that of the degraded product; in this instance however, the acid stoichiometry had changed to $F_{0.16}S_{1.00}O_{3.01}$ over $\sim$80 minutes ($F_{0.69}S_{1.00}O_{2.40}$ initially) indicating a much faster rate of degradation in this particular experiment.

At first sight, the sec-butyl cation spectra (3.14B) appears to be simply two peaks, *i.e.* two carbon environments, but it is not possible to resolve the lineshape using only two gaussians, of the same FWHM. Resolution as two peaks (internal shift ∿2.1eV) requires that the peak to high binding energy has a half width some 40% greater than the other. Whilst the lifetime of a corehole state in a positively charged carbon atom might be different from that of a neutral carbon core hole, it certainly would not be expected to give rise to this substantial difference. Also the two peaks would have an intensity ratio of 1:2 which has no chemical meaning in relation to a four-carbon atom system. Thus a two peak resolution is purely a mathematical fit of the spectral lineshape, and the difference in peak FWHM, together with an uninterpretable intensity ratio shows that the resolution is more complex.

It should be noted that the spectrum is not consistent with polymerisation which would give only one peak, nor with quenching of the cation which would lead to two peaks of intensity ratio 1:3, with a shift of ∿1.6eV, attributable to butan-2-ol. Whilst the sec-butyl cation is known to easily undergo rearrangement to the tertiary cation, the spectrum is clearly inconsistent with this.

Using four gaussian peaks of equal half-widths and intensity to deconvolute the sec-butyl cation spectrum suggests that the maximum separation of the two of lowest binding energy is ∿0.2eV, and thus the lineshape can be well reproduced using only three peaks of ratio 1:1:2. The

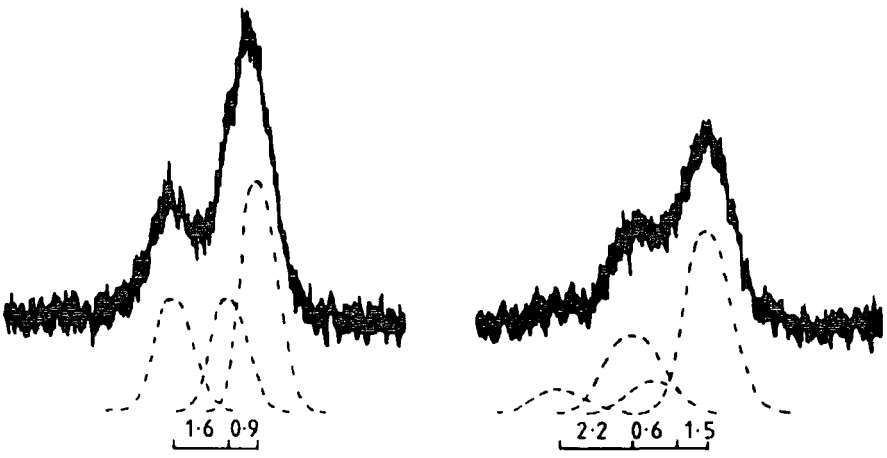


Figure 3.16 RESOLUTION OF SEC-BUTYL AND DEGRADED SEC-BUTYL CATION SPECTRA (Internal shifts in eV)

internal shifts are 2.5 and 0.9eV from the most intense component (Figure 3.16A). By comparison with the core-hole calculations the span of energies is clearly inconsistent with a localised positive charge, whilst the presence of three carbon environments rules out the possibility of the H-bridged cation structure. The shape of the observed spectrum suggests a partially bridged structure on the basis that the spectrum of this is predicted to have components of intensity ratio 1:1:2, in contrast to the fully bridged ion which should be 2:1:1 (high to low binding energy). The internal shift of $C_3$ from $C_1$ is calculated to be 0.3 and 1.9 in the partially bridged and fully bridged structures respectively, compared with the

experimental value of 0.8eV. The span of binding energies, experimentally determined as 2.5eV, is intermediate between those for the partially (3.1) and fully (2.1) bridged cations. From this it appears that the structure of the sec-butyl cation is intermediate between the partially and fully bridged isomers considered theoretically and might best be described as "heavily bridged".

The degraded spectrum was resolved on the basis that it mainly derived from the sec-butyl cation. Thus two peaks (of differing FWHM) were used to represent, in the simplest fashion, the contribution of this ion; the spectral lineshape then suggested that degradation involved two extra component peaks of approximately equal intensity with shifts of $\sim$1.5 and $\sim$4.3eV from the major low binding energy component (Fig.3.16B). Degradation spectra obtained in other experiments showed the same peaks, but there is no ready interpretation of them.

## 3.4 Summary

Less problem with organic fluorine contamination of fluorosulphuric acid was observed, than previously found with antimony pentafluoride, and this aids the assignment of observed high binding energy peaks as due to carbocations.

Protonation of norbornene using fluorosulphuric acid in the source of an E.S.C.A. spectrometer led to the observation of a $C_{1s}$ spectrum which was assigned as that of the norbornyl cation. Its preparation was contrasted against the results of attempts to ionise norbornyl chloride, and the similarity

of the present and previously reported norbornyl cation spectra was noted. Curve resolution of the spectrum on the basis of *ab initio* theoretical studies showed good correlation with a nonclassical, but not with a classical, model; it was noted that ∿25% of the spectrum might be attributable to contamination.

The $C_{1s}$ core-hole spectrum obtained following protonation of cis-but-2-ene was assigned as that of the sec-butyl cation. Deconvolution of the spectral lineshape suggested that this cation has a structure close to the partially methyl bridged model considered theoretically.

In the light of these results it is concluded that the protonation of alkenes, rather than the ionisation of alkyl halides, can be used to prepare *in situ* for E.S.C.A. observation, samples of carbocations of contemporary interest.

# CHAPTER FOUR

# AN INTRODUCTION TO "GLOW-DISCHARGE" PLASMAS AND THEIR CHEMICAL APPLICATIONS

## 4.1 Plasmas - definition, classification and production

"Plasmas" are partially ionized gases; as such they have been referred to as the fourth state of matter.[97] In essence they are composed of ions, electrons, atoms, radicals, metastables and photons as well as a large proportion of neutral ground state species, and they are an extremely reactive media.[98a,b] The many plasmas found in nature and the laboratory are usually classified according to their electron density and electron energy (Figure 4.1). A true "plasma" is electrically neutral, and for this condition to be met, the dimensions of the gaseous discharge must be significantly greater than a certain critical distance, known as the Debye length ($\lambda_D$ in Fig. 4.1). Plasmas can be divided into two distinct classes, the "hot" (or equilibrium) plasma in which the electron and gas temperatures are approximately the same, and the "cool" (or non-equilibrium) plasma in which the electrons have a much higher temperature than the surrounding gas.[99] "Glow-discharge" plasmas are an example of "cool" plasmas where typically the electron temperature is $\sim 1000^{o}C$ whilst that of the "sea" of partially ionised gas is little above ambient. The average electron energy lies in the range 1-10eV, but the distribution is (approximately) Maxwellian and a small proportion of the electrons have significantly higher energies (Figure 4.2). Plasmas can be produced by the action on a gas of either very high temperatures or strong electric or magnetic fields. Glow-discharges are conveniently produced using electric fields where the power input can be DC, AC (*i.e.* low frequency) or RF; "coupling" of the power to the plasma can be achieved by resistance, capacitance or inductive methods.

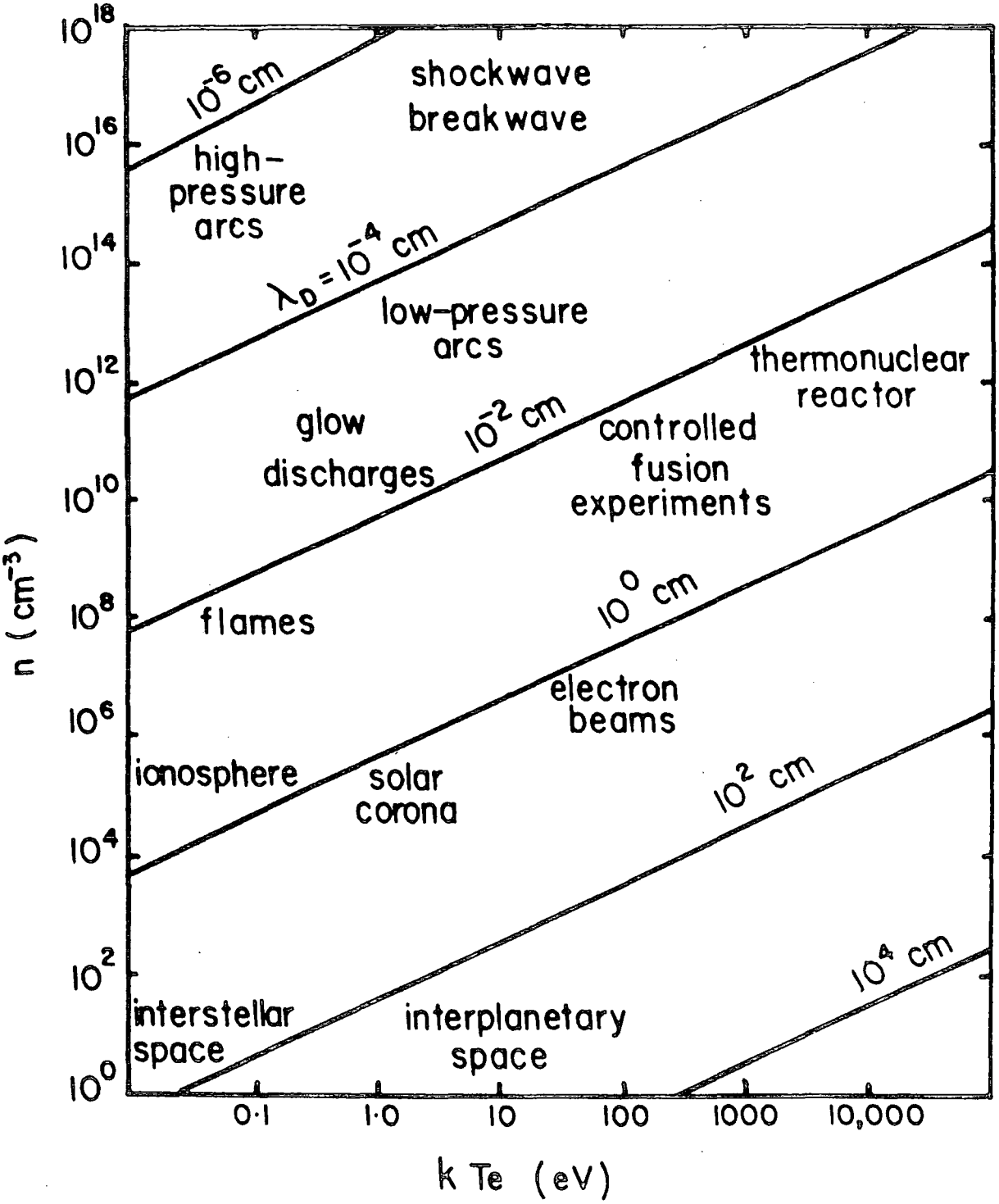


Figure 4.1 PLASMAS - CLASSIFIED ACCORDING TO THEIR ELECTRON DENSITY AND ELECTRON ENERGY

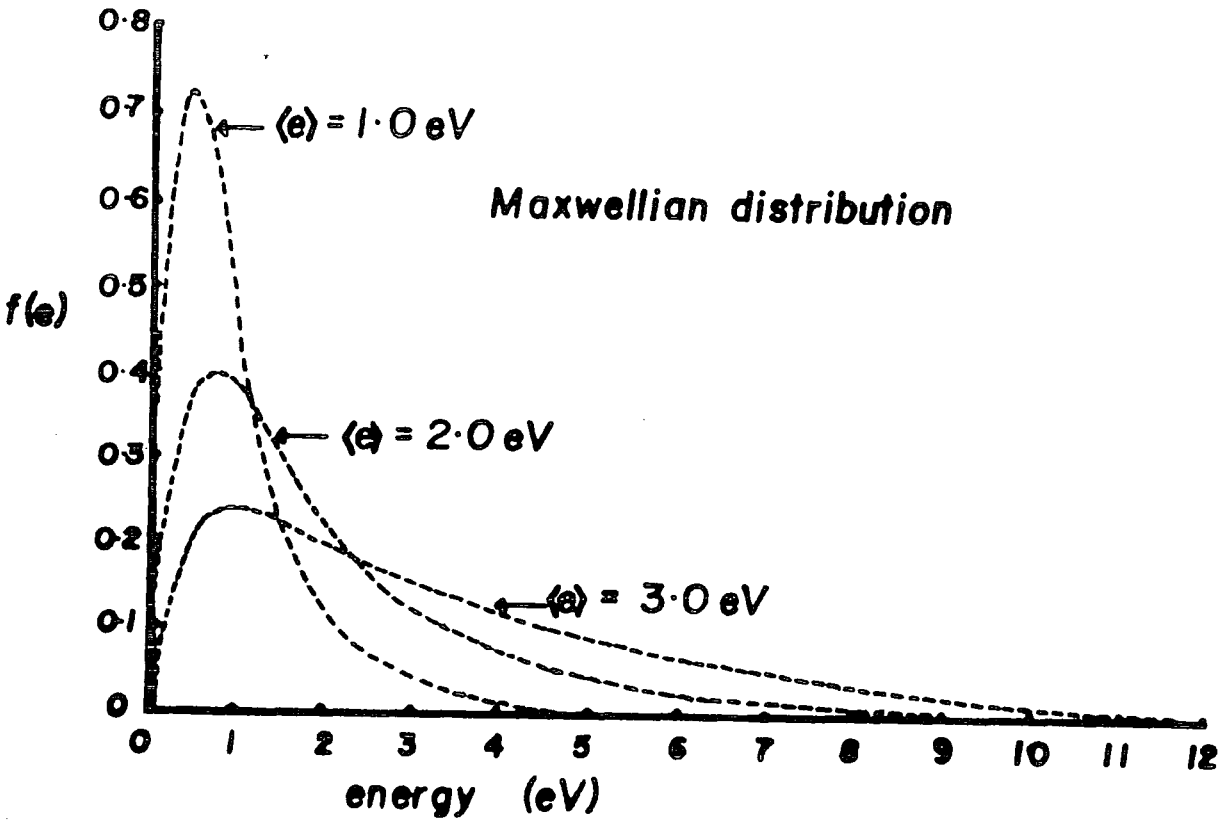


Figure 4.2 MAXWELLIAN DISTRIBUTION FUNCTION OF ELECTRON ENERGIES

---

Plasma media are complex environments and are, as yet, incompletely understood, but certain key processes are inevitably occurring. Following ionisation (natural or induced) electrons are accelerated by the externally applied electric field and acquire sufficient energy to induce ionisation, producing a second electron; *e.g.* $e^- + Ar \longrightarrow 2e^- + Ar^+$ this electron impact ionization is thought to be the most important process in maintaining the glow discharge.[100] Electrons which do not have enough energy to ionise species

may nevertheless cause electronic excitation (electron impact excitation). These processes are balanced by loss processes such as relaxation and recombination. The relaxation of excited states' leads to photon emission and it is this process which leads to the "glow", though it should be noted that the visible light is a relatively small proportion of the total radiation emitted. For ion-electron recombination a third body is necessary in order that momentum and kinetic energy can be conserved; typically then such processes will occur on the walls of the reactor, though the higher the pressure of the discharge the greater is the chance that the extra body may be another gas atom. Other processes occurring are electron attachment and electron impact dissociation of molecules.

## 4.2 Plasma applications

### 4.2.1 Organic Plasma Chemistry

Non-equilibrium plasmas have found use as a synthetic method in organic chemistry.[99,101,102] In more conventional (thermal and photochemical) methods of synthesis energy input tends to be in small steps whereas the electron collisions inherent in a plasma reaction allow a larger input of energy in a single event; thus, whilst in more conventional reactions, products are formed from the lowest energy reactive intermediate, the donation of large amounts of energy to the reagents may lead to unusual products formed

from a higher energy intermediate. For example, use of non-equilibrium plasmas allows the rearrangement of cycloheptatriene to toluene, which cannot be achieved thermally or photochemically.[101]

Since radicals are commonly found to be plasma intermediates, plasmas can be used as a source of these reactive species. For example in a perfluoroethane plasma, using minimal discharge power most of the active species are found to be trifluoromethyl radicals and these can be reacted with metal halides and organic halogen compounds.[103]

One of the largest areas of organic plasma chemistry is the field of elimination reactions involving leaving groups such as hydrogen, halogen and carbonyl. An example of where this type of reaction is a useful synthetic method is the reaction of o-biphenyl amine (I) in a plasma, to form carbazole (II) in 88% yield.[104] A related type of

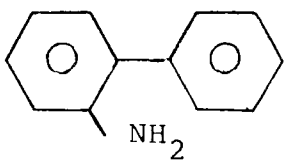


(I)

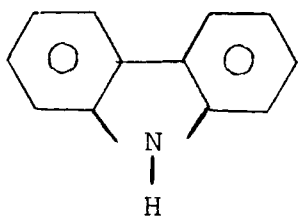


(II)

reaction is the desulphurization which readily occurs when organic sulphur compounds are subjected to glow discharges because of the weakness of the carbon-sulphur bond and potentially this might be of use as a method of removing sulphur from petroleum fractions.[101]

At its best therefore organic plasma chemistry

can provide useful "flick-of-a-switch" chemistry, and seen in context it provides a valuable addition to the arsenal of the organic chemist. However, the plasma process is difficult to control, in that it introduces energy into a compound in a fairly non-discriminatory fashion, and this can lead to complex mixtures of products; also the amount of energy introduced into a molecule is often enough for its complete destruction rather its subtle alteration.

### 4.2.2 Plasma etching

It is instructive to see how the process of plasma etching fits into the broad headings of etching and sputtering, terms found at the heart of many papers relating to surface chemistry. The process of sputtering is considered to be a purely physical process which relies upon energy transfer from incident to surface particles causing the ejection of the latter; as such it has often been compared to the break of a game of billiards.[100] The incident particles can be either ions or neutrals and as well as forming the basis for the formation of thin films by sputter-deposition of a target, sputtering is at the centre of techniques such as Fast-atom bombardment mass spectroscopy (FAB-MS)[105] and secondary-ion mass spectroscopy (SIMS).[106,107]

The process of etching is usually held to involve chemical combination of species.[100] Till very recently, etching of, for example, silicon dioxide was performed using (liquid) acids, a process known as wet-etching.[108] More recently it has been found possible to etch materials using (glow-discharge) plasmas, this being referred to as a dry etching process.

The most frequently encountered plasma etching processes are those used in the electronics industry. Both silicon and silicon dioxide can be etched using a tetrafluoromethane plasma. For example it is believed that etching of silicon is mainly by the attack of fluorine atoms, produced in the gaseous discharge; this leads to the formation of (volatile) silicon tetrafluoride as the major product and this is pumped away.[109-111] The selectivity of the etch (*i.e.* the ratio of etching of silicon/silicon dioxide) can be altered by adding either hydrogen or oxygen to the plasma feed; this arises because, amongst other effects, these gases affect the concentration of fluorine atoms.

Plasma ashing is another example of a plasma etching process.[112] In this, organic material is removed from a substrate through the action of an oxygen plasma, which reacts to form carbon dioxide and water and these are pumped away. This is a standard method for the removal of a photoresist in the semiconductor industry.

Plasma etching has two basic advantages when compared with wet-etching. Firstly it is a vapour phase technique, and this is readily compatible with the requirement of many (semiconductor) applications for high purity reagents. Secondly, in appropriate circumstances, plasma etching can give rise to anisotropic etching of a substrate. From an industrial point of view a third advantage would be the avoidance of solvent disposal.

### 4.2.3 Plasma Polymerization

As noted in the section on plasma chemistry

(Section 4.2.1), molecular fragmentation and film formation can occur in a glow discharge. Early workers considered this plasma polymerization to be a disadvantage of synthesis by plasma methods not least because these films were troublesome to remove from the reactors. However it is precisely this firm adherence to a substrate, along with other useful properties, which gives rise to potentially useful applications. The pin-hole free nature and chemical inertness of some polymers produced in this way enables them to be used as protective coatings;[113,114] not only can they be used as resists in the semiconductor industry[115] but also their low dielectric constant is made use of when they form an integral part of electronic devices;[116] their pin-hole free nature also enables their use as desalination and gas-separation membranes.[117] These properties of the films are coupled with the inherent property of the plasma process that polymers can be formed from monomers which cannot be polymerised conventionally, notably saturated hydro- and fluoro-carbons;[118] these features explain much of the current research interest in plasma polymer films.

The films produced by plasma polymerization are extensively cross-linked and the bulk of material is insoluble in conventional organic solvents. This makes characterization of the films problematical, but ESCA has proved to be an extremely good probe of polymer structure, particularly those films produced from fluorocarbons since the chemical shift range of the functional groups involved allows the determination of the contribution to the structure of $CF_3$, $CF_2$, CF groups, *etc.*[118-130b] Whilst it has been suggested that ESCA might be rivalled by the use of solid state NMR,[131a,b,132]

this has not yet occurred. The technique of pyrolysis - mass spectrometry,[132] whilst yielding valuable information, suffers from the problem associated with all destructive analytical techniques (*viz.* that the substance may change in the analysis procedure).

Often in plasma polymerization one of the discharge parameters (such as pressure or power) is varied, in an attempt to study the effect of this change on the rate or nature of the polymerization. However it has been pointed out that this is not ideal;[133] varying the power whilst keeping the flow rate constant (or *vice versa*) usually leads to glow-discharges of different volumes or intensities and true comparisons of discharge conditions and polymerization rate should be made under conditions of the same "glow-character". This can be achieved by replacing single system parameters by a composite discharge parameter and $W/FM$ is suggested (W = discharge power, F = monomer flow rate, M = molecular weight of the monomer). Essentially this parameter is a measure of the amount of energy introduced per unit mass of monomer.

The mechanism of plasma polymerization is incompletely understood, however certain key features have been identified. Whilst the fact that the concentration of radicals in a plasma is $\sim 10^5$-$10^6$ times that of the ions[134] does not of itself show that these are the polymerizing "monomer", the amount of polymer formed in some systems is too great for ionic species to be solely responsible.[131b] Positive ions do play a part in the plasma polymerisation process as evidenced by the fact that in a DC discharge deposition is almost exclusively

on the cathode,[135] but they are not considered to be the main polymerising species. Generally radicals are considered the most likely reactive intermediates and mechanisms involving them have been proposed, but the extent to which polymerisation occurs in the gas-phase or on a wall/substrate is not clearly elucidated.

It is considered that there is a range of polymerisation mechanisms.[136] Conventionally polymerisation occurs by "molecular" polymerisation, where no fragmentation is necessary in forming polymerisable monomers. Conversely plasma polymerisation can result from the reaction of molecular fragments, a process referred to as "atomic" polymerisation, and in these circumstances, the polymerising "monomer" will bear little resemblance to the plasma feed. Between these two extremes lie a range of polymerisation mechanisms and the importance of each of the extremes will be governed by the particular system investigated.

In fluorocarbon plasmas forming thin films it has been suggested that difluorocarbene is an important species and that reaction of this with unsaturated molecules ($C_2F_4$, $C_3F_6$, *etc.*) leads to $(CF_2)_n$ oligomers.[131b] These latter species have been detected in the gas phase (by mass spectroscopy) containing, for example, up to twelve carbon atoms in the case of a tetrafluoroethylene discharge. The stoichiometry of the film formed by plasma polymerisation of tetrafluoroethylene is $C_1F_{1.4}$ and this lower value of the $^F/_C$ stoichiometry compared with the supposed polymerising unit is explained in terms of the elimination of fluorine atoms following bombardment of the initially formed polymer by photons, ions and metastables.

Defluorination of polymers subjected to this type of treatment is becoming well established.[137,138]

It has been suggested that in mixed feed hydrogen-fluorocarbon plasmas CF radicals are possibly the most important species involved in the polymerisation in the discharge region;[139] whilst their presence in such plasmas is clear, as is that of $CF_2$ species, the relative importance of each is not clearly established. The suggestion of the greater importance of the CF radical appears to be largely based on the stoichiometry of the deposited polymer, which in the light of possible defluorination of an early formed polymer, by energetic bombardment, is not necessarily valid.

The plasma polymerisation of perfluorobenzene is thought to be largely "molecular" in nature,[140] and ESCA data support this idea in that the polymer stoichiometry is close to that of the monomer.[118] It has been shown how the well established isomerisation of the parent aromatic to benzvalene, Dewar benzene, prismane, fulvene and hexadienyne structures followed by appropriate cycloadditions can lead to the features observed in the ESCA spectrum of the plasma polymer.[123]

So far in this work etching and polymerisation have been considered as separate processes whereas, in fact, there are close links between them. This is well illustrated by the fluorocarbons, where the $^{F}/_{C}$ ratio present in the plasma has been found to correspond with whether the gaseous system etches or deposits.[131b] The formation of a plasma polymer is considered to be not simply the deposition of material but a dynamic struggle between the deposition and etching processes, and this is commonly called competitive-ablation-polymerisation (CAP).[141]

### 4.2.4 Surface Modification

Broadly speaking certain uses of etching and plasma polymerisation can be seen as forms of surface modification, and the three cannot be successfully separated completely. (The use of a plasma polymer as a protective coating on a metal can be viewed as a surface modification). The rather subtle distinction is that polymerisation is concerned with the production of a new surface by coating,etching produces a new surface by removal of material and modification alters the existing surface.

Modification of surfaces can be induced by the action of elemental gas plasmas such as oxygen, nitrogen, fluorine, hydrogen or the inert gases.[142a,b] Two distinct areas of application are metals and organic polymers.

The interaction of plasmas with organic polymer surfaces can be divided into those plasmas which chemically react with the surface and thus incorporate some of the plasma species (*e.g.* fluorine and oxygen plasmas) and those where the main interaction is physical in that it is the direct transfer of energy from the plasma to the polymer which leads to a chemically different surface without the inclusion of the reactive plasma species. This latter category is concerned with inert gas plasmas where bombardment of a polymer surface by cations, metastables, photons and electrons leads to bond cleavage and subsequently to cross-linking of polymer chains and effects such as defluorination of fluoropolymers.[143] As an example of the chemically active plasmas, oxygen is known to lead to oxidation of the outer few monolayers of a

polymer substrate;[144] this leads to a higher surface free energy and consequent increase of wettability. Polymer treatment by these methods is commercially important in, for example, the packaging and printing industries since they allow improved interaction of surfaces with inks, dyes and adhesives.

Metals exposed to plasmas similarly undergo surface modification such as oxidation, nitriding, *etc* .[145] As will become apparent, the nitriding of metal surfaces might be of some relevance to the work discussed in Chapter Five. The process leads to an increased hardness of the surface regions. Under certain conditions surface nitriding of various metals has been achieved using glow-discharges. A simple nitrogen gas feed does not lead to substantial nitride formation unless the substrate temperature is increased to $\sim 700^{o}C$,[146,147] and generally nitrogen-hydrogen mixtures or ammonia are used. Analysis of the gas plasma suggests that NH-species are important for efficient nitriding.[148]

## 4.3 Two contemporary lines of research

### 4.3.1 Plasma Diagnostics

Despite the already apparent technological importance of plasmas, comparatively little is known about the processes occurring within them and so plasma diagnostics is currently an important area of research. Various methods have been applied in order to probe the species and energy distributions present in gaseous discharges.

One approach is the direct analysis of plasma

particles in which the gaseous species emanating from the plasma form the inlet for an analytical technique.[149] For example, a differentially pumped mass spectrometer mounted downstream of various fluoro- and fluorohydro-carbon plasmas has been used to analyse the gaseous effluent.[150] In a similar fashion a mass-energy analysis has been carried out of ions bombarding a substrate in a plasma by using an experimental arrangement in which the inlet to the analysis system was a pin-hole in the substrate.[151]

Such methods are "*ex-situ*" methods in which a sample of the plasma is taken and analysed elsewhere; as such there is always the possibility that the sample, containing as it does many highly reactive species, may change during the journey either in component or energy distribution. "*In-situ*" techniques are therefore to be preferred, and the more non-intrusive they are, the better; in this respect a great deal of work has been done using optical techniques.[152-155] Probably the simplest non-intrusive *in situ* technique is the use of emission spectroscopy to study the (evident) radiation given out in gaseous discharges; whilst being qualitatively useful, the technique cannot give quantitative information because the intensity of emission from a species is not directly proportional to its concentration. This is not the case however with the technique of laser induced fluorescence which can be used to monitor the concentration of reactive species such as radicals and ions.[152]

Already optical techniques are contributing significantly in understanding plasma processes. In the commercially important silicon etching process using a $CF_4$-$O_2$ plasma, an

approximate correlation has been found between the fluorine atom emission and the etch rate.[156] Similarly optical emission spectroscopy has been used to monitor the emission of O and $O_2^+$ species in an etching discharge and it has been suggested that there is a correlation between the $^{O}/_{O_2}+$ emission intensity ratio and the degree of isotropy in the etching of the resist.[157]

The discussion so far has centred on the use of experimental techniques to determine the species present in a plasma; however theoretical chemistry can also play a role in plasma diagnostics in determining the relative energetics of species which might be present in the discharge and Chapter Six of this work presents an investigation of some reactive intermediate species in an attempt to assess their likely importance, or otherwise, in the formation of experimentally observed products.

### 4.3.2 Metal Incorporation into Plasma Polymers

#### (i) Methods

There are three basic methods which have been used to produce metal containing plasma polymers. These are (a) the plasma polymerisation of an organometallic starting material on its own or copolymerised with a second (organic) compound, (b) the etching of a metal substrate whilst polymerisation-incorporation occurs elsewhere in the reactor system, (c) the simultaneous evaporation of a metal and polymerisation of an organic material. The important features of these methods are elucidated below. Ion implantation of metals[158] can perhaps be considered as a fourth method though this is essentially

different in that in this method metal is incorporated into an already formed polymer, in contrast to the other three methods where incorporation occurs as the polymer film grows.

(a) The use of organometallics

The decomposition of organometallics by thermal and discharge means to form thin films of metals, oxides, carbides and nitrides is well established,[159,160] and it is only one step away to attempt the polymerisation of the organic components without total destruction of the starting material.

Organotin compounds, particularly tetramethyl tin (TMT) have received a lot of interest in the literature.[161-166] Tin containing thin films have been produced by the introduction of TMT into the coil region of an inductively coupled RF plasma, and the $^{C}/_{Sn}$ stoichiometry of the polymeric film has been studied as a function of position in the reactor by means of ESCA.[161,162] Minimum $^{C}/_{Sn}$ ratios of $\sim$3 were found for samples close to the precursor inlet, whilst downstream the ratio rose to $\sim$6. IR examination of an independently prepared sample ($^{C}/_{Sn}$ stoichiometry $\sim$2.8) in a reactor of slightly different design showed that as well as $CH_3$, $CH_2$ and CH groups, the film contained Sn-O-Sn and Sn-C functionalities.[163] Samples of tin-containing films produced in a capacitively coupled bell jar system have been found to contain in addition, tin dioxide and Sn-O-C groups,[164] and in a recent ESCA investigation, films formed by the inductively coupled RF polymerisation of TMT showed a high level of oxygen content (compared with organic plasma polymer systems) and this was taken as indicative of the presence of tin dioxide.[166] Copolymers of TMT

with methyl methacrylate[165] and perfluorobenzene[166] have also been prepared.

Analogous thin films containing Ge-$CH_3$, Ge-O-C and Ge-O-Ge functional groups were prepared by the glow-discharge polymerisation of tetramethylgermanium and analysed by IR.[167] ESCA analysis combined with argon ion etching was used in reaching the conclusion that whilst germanium dioxide was present in the outermost surface layers, the sub-surface ($\sim$100Å) contained germanium metal.

There has also been some interest in iron-containing plasma polymers. A recent publication concerns the copolymerisation of iron pentacarbonyl and the $C_2$-hydrocarbons;[168] it appears that copolymerisation was necessary to obtain reasonable polymers whilst the action of a plasma on $Fe(CO)_5$, or $Fe(CO)_5$ and hydrogen, was simply to produce "deposits". The films formed in an RF inductively coupled reactor were extensively characterised and studied as a function of distance from monomer inlet, which was downstream of the coil region. The polymers were found to contain carboxylate and carbonyl functionalities, and the iron present was assigned as being mainly iron (III) oxide; this oxide was shown to be highly dispersed within the polymer matrix. Lowering the energy imput per unit mass led to the observation of some carbon monoxide complexed to iron being retained in the plasma polymer. The greatest amount of iron was incorporated closest to the monomer inlet and here values of 27 and 46 weight per cent of iron were found for the plasma polymer (from $Fe(CO)_5$ and $C_2H_6$), and the plasma deposit ($Fe(CO)_5$ on its own), respectively.

Study of a series of ferrocenes[169] showed that whilst iron oxides were present in the plasma polymers, a fair proportion of ferrous ($Fe^{2+}$) environments were retained suggesting that some of the ferrocene units were incorporated into the polymer, *i.e.* that polymerisation was probably a combination of "molecular" and "atomic" polymerisation. The fact that the $^{Fe}/_{C}$ ratio of ferrocene and its plasma polymer are similar also suggests the importance of "molecular" polymerisation, though some "atomic" processes are necessary to account for the iron (III) species. The susceptibility of the polymer films to oxidation was pointed out.

(b) The Etching-Polymerisation incorporation of metal

This method has been extensively reported and investigated by Kay and coworkers and relates exclusively to fluorocarbons as the organic monomer.[131b, 170-175] The mechanism of incorporation is envisaged as occurring because of the combination of the two basic processes of etching and polymerisation which occur simultaneously in different parts of the reactor. The etching capability of certain fluorocarbon plasmas is well established as too is the possibility of forming plasma polymers from fluorocarbon feeds. In this respect, it is considered that the $^{F}/_{C}$ ratio of the reagent gas is probably the most important parameter in determining which process occurs; typically $^{F}/_{C}$ ratios $\geq 2$ lead to etching whilst $^{F}/_{C} < 2$ lead to polymerisation. However which process prevails also depends upon the voltage of the substrate; for example, application of a negative bias of 200V changes the role, of a feed of $^{F}/_{C}$ stoichiometry $\sim 2.5$, from one of polymerising deposition to

etching, and this is explained in terms of more energetic ion bombardment of the substrate.[131b] Thus, by making a metal target the cathode in a plasma reactor and using a fluorocarbon gas such as perfluoropropane ($^{F}/_{C}$ ~2.7), etching of the metal can occur;[171] however, polymerisation can occur on a grounded substrate elsewhere in the reactor and it is found that some of the etched metal is incorporated into the growing polymer film.

Differences in mechanism of incorporation have been postulated for those metals which form volatile and involatile fluorides.[171] Use of a molybdenum target is considered to lead to volatile molybdenum hexafluoride which readily desorbs from the target surface, whilst sputtering of involatile fluorides is probably the main process for the inclusion of copper into a plasma polymer. Somewhat anomalous, and as yet not fully explained, is the behaviour of germanium which is not incorporated despite the formation of a volatile fluoride.

Change of the typical plasma parameters has been found to be relatively ineffective at controlling the amount of metal incorporation and this is a result of the inherent connection between the etching and polymerising processes.[173] It is well established that the addition of other gases to the fluorocarbon feed affects its behaviour within a plasma, an effect explained again in terms of the $^{F}/_{C}$ ratio;[131b] addition of oxygen leads to the formation of carbon monoxide and carbon dioxide effectively increasing the $^{F}/_{C}$ ratio of the active species so that addition of small quantities of oxygen enhances the etching capability of a fluorocarbon feed. Conversely hydrogen is

seen as a fluorine atom scavenger and its addition to a plasma feed can qualitatively be seen as lowering the $^{F}/_{C}$ ratio, thus enhancing polymerisation. Mixed feeds have been shown to be an effective way of controlling the metal content of the plasma polymers.[172] Addition of oxygen enhances the fluorocarbon's etching capability and this leads to greater metal etching at the target and slower polymerisation at the grounded substrate; consequently a higher degree of metal incorporation is obtained. Lower metal incorporation is found when hydrogen is added since the rate of etching of the metal is decreased and that of polymerisation is increased; in fact the etching capability can easily be suppressed altogether, leading to polymer formation on the metal target.

Following their preparation, the metal-containing films are stored in air before analysis. The ESCA spectra for the metal containing films show that the metal is in a high oxidation state (*e.g.* Mo assigned as +5/+6, Cu as +2). Whilst a small peak, assigned as fluoride ion, was sometimes detected in the $F_{1s}$ core hole spectrum (in addition to the intense signal from organic fluorine) this was not of sufficient intensity for the metal to be present solely as its fluoride. Metal incorporated polymers revealed a much higher $^{O}/_{C}$ ratio than straightforward plasma polymers of the same feed material and therefore much of the metal is considered to be present as oxides and hydroxides. The explanation for this is that, upon exposure to air, hydrolysis occurs of the metal-fluorine bonds formed in the etching process.[171]

The incorporation of gold, a relatively inert metal, has also been achieved using a mixed fluorocarbon-inert gas feed

($C_3F_8$-Ar).[174] ESCA showed that the gold was in a metallic state, despite several days storage in air; this shows the purely physical nature of the metal incorporation (*i.e.* sputtering) in this particular case. The work has been extended to aluminium and cobalt, metals which form involatile fluorides, and it has been shown that variation of the fluorocarbon-inert gas ratio determines the percentage of metal in the plasma deposit.[175]

Perhaps the most significant part of a paper concerning the incorporation of tin into a plasma polymer of tetrafluoroethylene, by using tin foil, is the investigation of the metal surface following its use.[176] ESCA analysis revealed that the surface was completely covered to a depth of at least 100Å by a tin fluoride compound of unknown composition other than that the $^{Sn}/_{F}$ stoichiometry was 1. The low binding energy component of the $F_{1s}$ core-hole spectrum, found for the metal incorporated plasma polymer, was of sufficient intensity to yield the same 1:1, Sn:F stoichiometry. This appears to be the only instance where the metal target has been analysed in an effort to understand the nature of the sputtering/etching processes involved in this type of metal incorporation.

(c) Metal Evaporation

Metal Vapour Synthesis has become a well established route to organometallics,[177-179] and it appears logical to try to extend its use to metal incorporation into plasma polymers, yet this method has not received much attention in the literature.

Probably the earliest use of metal vapour as the method of metal inclusion was the vaporisation of tin into a benzene (capacitively coupled) plasma.[180] Mössbauer spectroscopy was used to characterise the products and show that in a film of Sn/C stoichiometry of 1:1 the tin had formed four Sn-C bonds, giving spectra very like those of organo-tin compounds.

Both bismuth and tellurium have been evaporated into a carbon disulphide plasma and the latter metal also into a styrene plasma.[181] IR measurements, made only on the $CS_2$-Te film, showed the presence of C=S and S-S bonds whilst it was suggested that a third band, appearing only in the composite film and not in the single component films of $CS_2$-plasma polymer, or tellurium, resulted from some (unspecified) interaction between the carbon disulphide film and the tellurium. Other physical measurements (electron and X-ray diffraction and differential scanning calorimetry) were used to show that the metal was present in an amorphous state.

The simplest metal to generate in the vapour phase is mercury, and recently incorporation of this into a perfluoro-benzene plasma polymer has been reported.[182] In this a mercury reservoir was included upstream of the coil region of an RF inductively coupled flow system. The Hg/C stoichiometry of $\sim$0.04 for the polymer was found to be independent of the mercury distillation temperature, provided this exceeded a certain minimum. Whilst the binding energy of the Hg4f level (as determined by ESCA) was $\sim$3eV higher than that for pure mercury, and the oxygen content of the polymer film was too low for the metal to be present as an oxide, pyrolysis mass spectrometry results suggested that the mercury was chemically bonded within

the polymer matrix. Comparison of the $^{F}/_{C}$ stoichiometries for perfluorobenzene plasma polymer films with and without mercury incorporation, led to the conclusion that mercury vapour was affecting the gas phase rearrangements of perfluorobenzene.

(ii) Applications of metal incorporated plasma polymers

It is widely expected that metal incorporation will yield materials with interesting electrical, optical and magnetic properties, and already some of these expectations are starting to be fulfilled. Variation of the metal content in a gold-fluorocarbon plasma polymer system has been shown to affect its electrical resistivity,[174] and under the correct conditions polymerisation of tetramethyl-tin or -germanium leads to photoconducting films.[164] Whereas many plasma polymers are yellowish or golden-brown the inclusion of metal dispersionscan lead to coloured films, of obvious commercial importance; incorporation of gold, copper or aluminium in a hexamethyldisiloxane polymer leads to red, yellow and blue films respectively.[183] Not so artistic perhaps but of considerable technological significance is the preparation, by plasma copolymerisation of tetramethyltin and methylmethacrylate, of a self-developing electron-beam resist with an increased sensitivity compared with polymethylmethacrylate - an established resist material.[184]

# CHAPTER FIVE

# THE INCORPORATION OF MOLYBDENUM INTO A PERFLUOROBENZENE PLASMA POLYMER

## 5.1 Introduction

Most of the detailed investigations of metal-incorporated plasma polymers to date have concerned the use of organometallics and the etching-polymerisation mechanism. The third route, of metal evaporation, has not yet been sufficiently investigated that it can be discounted as a viable alternative. The inherent simplicity of the metal evaporation method argues for its development; organometallics have obviously to be synthesised prior to use, whilst the etching-polymerisation method may be confined to well chosen combinations of metal and organic. Metal evaporation has potential applicability to virtually all metals. Therefore the object of this work is to present a preliminary investigation of various experimental parameters, of a metal vapour-glow discharge system, which might have an effect on the amount of metal incorporation in a plasma polymer.

## 5.2 Experimental

The reactor used comprises the simplest system thought *a priori* feasible for the work (Figure 5.1).

The reactor (approximately 43 cm. long and 5 cm. in diameter) is of pyrex glass with two FG50 ground glass flanges, one for mounting the evaporation unit and one for ease of sample manipulation. A conventional liquid nitrogen trap separates the reactor from the ED50 two-stage rotary pump; the system pressure is monitored by a pirani gauge located near the monomer inlet, and typically the base pressure of the reactor is $\sim$0.06T.

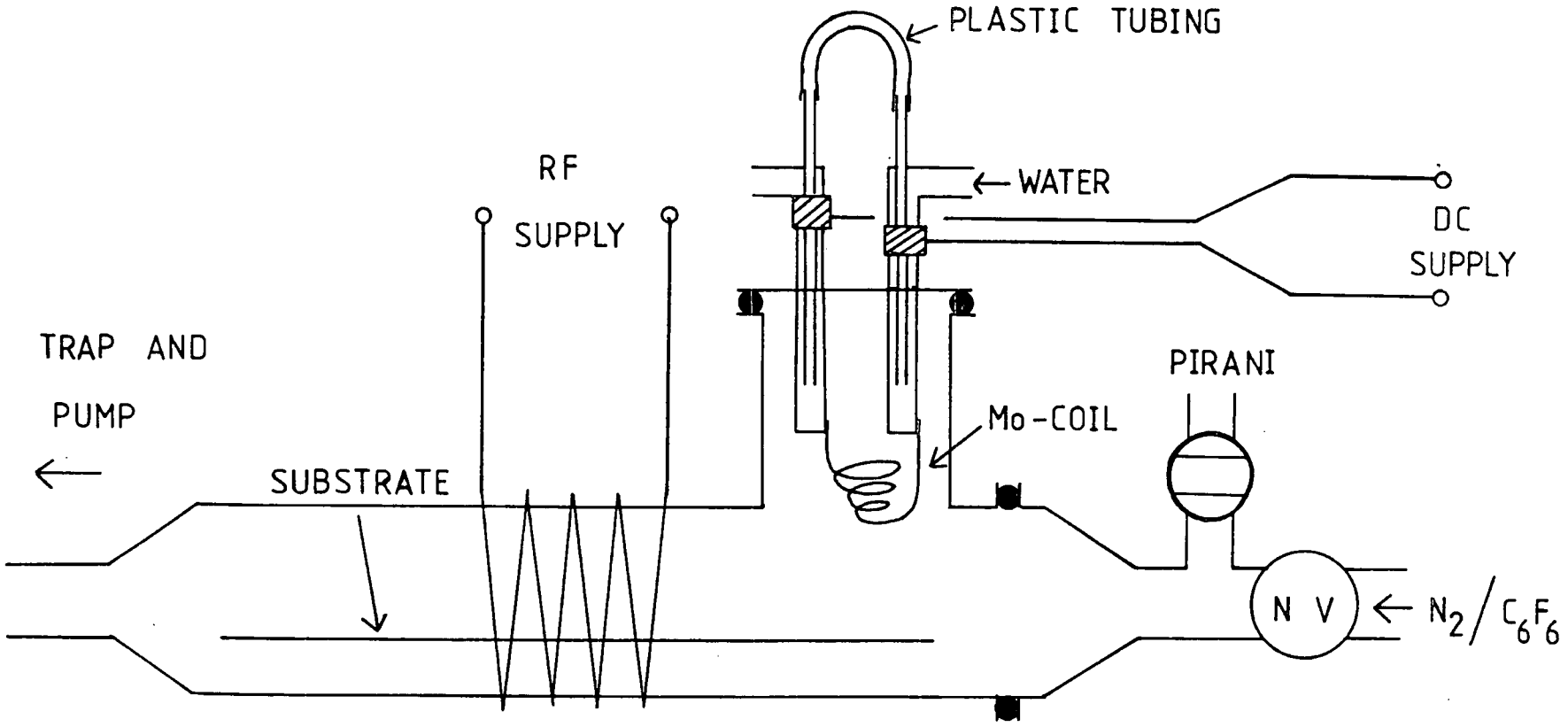


Figure 5.1 SCHEMATIC OF REACTOR

The Glow Discharge was excited by an inductively coupled copper coil connected to a Tegal Corporation 13.56 MHz RF generator, with maximum power output of 100W. Tuning of the RF power was by an L-C matching network monitored by a Heathkit HM 102RF power meter. (This part of the reactor is as previously described).[118]

For complete simplicity of these initial experiments a molybdenum filament resistive heater was used as the metal evaporation unit. (This is often referred to as the "atomiser"). This is water cooled and mounted in a stainless steel flange compatible with an FG 50. Power to this unit is supplied by a 9V, 60A source which could be varied by a Variac controlling the input (mains) voltage.* The unit is similar to one described earlier.[185]

The substrate used was aluminium foil mounted on an aluminium former and prior to use it was cleaned by wiping with acetone. Typically the resistive heating coil was $\sim 2\frac{1}{2}$ cm. above the substrate.

The standard operating procedure was as follows. The reactor was pumped out to 0.06T and then let up to a pressure of 0.2T of nitrogen and subjected to a 100W plasma of 30 minutes' duration. During the nitrogen plasma the coil input voltage was increased from 0 to 180V and left at this setting for 2-3 minutes in an attempt to clean off any surface contamination. When the plasma had been switched off the substrate was introduced under a positive pressure of nitrogen. The reactor was then allowed to pump down overnight.

---

* The power used in each experiment is generally given as the Variac setting; this is later correlated to approximate temperatures of the filament (Section 5.4.1).

The experiment itself consisted of setting the atomiser voltage to the required value and allowing the heater ∿5 minutes to reach an equilibrium temperature. Usually there was a brief rise in pressure to ∿0.08T. The organic feed stock was allowed in to the required pressure and then the plasma was initiated. Usually the plasma was balanced at this stage, except when short plasma deposition times (≲2 mins.) were used when balancing at the required power setting was achieved at the end of the 30 minute nitrogen plasma and the matching network and power control were not adjusted subsequently. The plasma was sustained for the parametric time period, and then the discharge and atomiser were turned off and the reactor was let up to nitrogen. The samples were kept in air prior to ESCA analysis.

The procedure calls for a few explanatory comments. The nitrogen plasma was intended as a method of cleaning the reactor and more especially the heater filament; the latter can be expected to have a surface layer of oxide as well as adventitious hydrocarbon and it was desired to clean this off prior to insertion of the substrate into the reactor. Nitrogen was used because of its ready availability and low cost. The radiative heat of the filament imposed a limitation of not operating the Variac supply above ∿180V in this glass system. There was an obvious time-delay for the coil to reach its equilibrium temperature and this is why the heater was allowed a warming-up period. Whilst Metal Vapour Synthesis has usually been carried out at pressures $<10^{-3}$T, glow-discharge polymerisation is generally performed in the pressure range $10^{-3}$ - $10^{-1}$T; the slightly higher end of this range was used because of the large amount of readily available data pertaining to plasma polymers prepared under these conditions.

The "standard" experiment involves the following values for the five parameters investigated: atomiser voltage 90V; plasma parameters of power, pressure and time, 20W, 0.2T and 10 minutes; resistive heater coil - RF inductance coil ("atomiser-coil") separation, 3½ cm. Whilst four parameters were kept constant the fifth was varied as follows: five values for the atomiser voltage (0, 40, 90, 140, 180V); three values of power (20, 50, 100W); two values of pressure (0.1, 0.2T); four values of time (0.16, 2, 10, 30 mins.); three values of the "atomiser-coil" separation (3½, 13½, 23½ cm.).

Samples for ESCA analysis were taken from three positions along the substrate; these were, directly below the atomiser, the (atomiser) end of the coil region, and the middle of the coil region (samples 1, 2 and 3 respectively). In addition, in the experiments in which the atomiser-coil separation was varied a total of seven samples were taken in each case, corresponding to the middle and end of the three coil positions as well as one from beneath the resistive heater (Figure 5.4).

Prior to use, perfluorobenzene (Bristol Organics) was degassed to $6 \times 10^{-4}$T using a series of freeze-thaw cycles. The molybdenum heating coil was made from 30x0.1 cm. wire (Goodfellow) purity 99.95%.

## 5.3 Results and Discussion

An experiment attempting to incorporate Chromium into a perfluorobenzene plasma polymer by simultaneous plasma deposition and vaporisation of the metal from the molybdenum basket

was unsuccessful; but whilst chromium was not present in the sample surface, a wide-scan ESCA spectrum showed that molybdenum was. This metal incorporation was studied as a function of the five variables outlined above. Not only is the incorporation of molybdenum interesting in its own right, by virtue of the fact that it is such a refractory metal, but also such a study appeared to be a necessary preliminary to determine whether molybdenum incorporation might be prevented in order that other metals might be individually introduced by this method.

Visually the prepared (substrate) samples are rather uninteresting being yellowish or golden-brown; the material collected in the trap was brownish or reddish brown. These colours are typical of perfluorobenzene plasma residues. On exposure of the substrate to air there was never any evidence of pyrophoric metal particles. The samples taken from the middle and end of the RF coil region were film-like whilst those taken from beneath the atomiser were powdery in nature and adhered less strongly to the substrate; charring of these latter samples particularly at higher atomiser voltages shows the damage caused to them by radiative heat.

Typical core-level spectra of the molybdenum-incorporated plasma polymer are shown in Figure 5.2.

The well established procedure for the deconvolution of the $C_{1s}$ core-level envelope was followed by assigning components at ∿285.0, ∿286.7, ∿288.3, ∿289.1, ∿291.3, ∿293.7 and ∿295.5 to $\underline{C}$-H, $\underline{C}$-$CF_n$, $\underline{C}$F-CF, $\underline{C}$F-$CF_n$, $\underline{C}F_2$, $\underline{C}F_3$ and $\pi \rightarrow \pi^*$ shake-up satellite of =CF.[118] The $^F/_C$ intensity ratios presented in the tables are derived from two core-levels* comparison then

---

* Where ionic fluorine is present, the intensity of this component is not included in the reported F/C ratios.

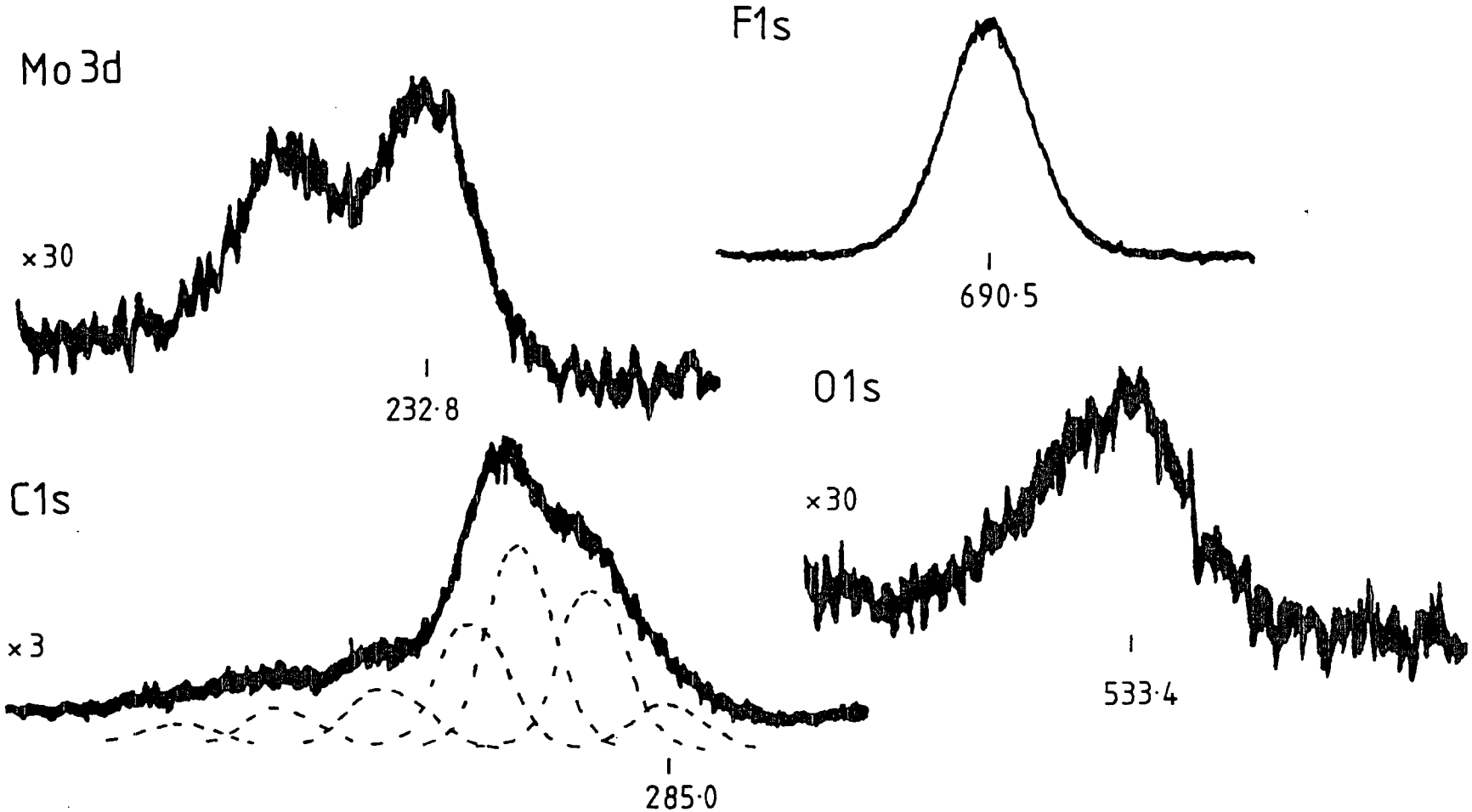


Figure 5.2 TYPICAL CORE LEVEL SPECTRA OF A MOLYBDENUM INCORPORATED PERFLUOROBENZENE PLASMA POLYMER; Conditions, 90V, 0.2T, 10 mins. 20W, 3½ cm., sample position 2 (Binding energies in eV)

being made where appropriate, with the $^{F}/_{C}$ ratio derived from the $C_{1s}$ envelope component analysis. Stoichiometries are derived using a standard $^{C}/_{F}$ instrument sensitivity factor of 0.52.[60]

In the following discussions attention is usually focussed on samples taken from the atomiser end of the coil region, with supporting evidence drawn from the results of the other two sampling positions.

### 5.3.1 Variation of Atomiser Voltage

The changes in gross element intensity ratios occurring with change in atomiser voltage, are shown in Table 5.1.

The $^{F_{1s}}/_{C_{1s}}$ intensity ratio appears to decrease as the atomiser voltage is increased; this trend is greatest for sample 1 and smallest for sample 3. It is tempting to suggest that the hot filament causes some defluorination of the polymer precursors, but the situation is probably more complex than this simple trend suggests.

The $^{F}/_{C}$ ratios shown in Table 5.1 are derived by consideration of the intensity of the covalent fluorine signal and the total $C_{1s}$ signal intensity; for sample 2 they correspond to $^{F}/_{C}$ stoichiometries of 0.75, 0.78, 0.72, 0.60 and 0.52 (for atomiser voltage of 0, 40, 90, 140, 180V respectively). Curve resolution of the $C_{1s}$ spectra (Figure 5.3) allows determination of the $^{F}/_{C}$ stoichiometry from consideration of the intensity of the various components, $CF_3$, $CF_2$, *etc*. This method leads to stoichiometries of 0.95, 0.97, 0.86, 0.82 and 0.67; whilst the

TABLE 5.1 VARIATION OF GROSS INTENSITY RATIOS WITH ATOMISER VOLTAGE

| | Ratio | $F_{1s}/C_{1s}$ (c) | | | $Mo_{3d}/C_{1s}$ | | | $Mo_{3d}/F_{1s}$ (d) | | | $O_{1s}/C_{1s}$ | | | $Mo_{3d}/O_{1s}$ | | |
|---|---|---|---|---|---|---|---|---|---|---|---|---|---|---|---|---|
| | Sample Position (b) | 1 | 2 | 3 | 1 | 2 | 3 | 1 | 2 | 3 | 1 | 2 | 3 | 1 | 2 | 3 |
| Atomiser Voltage (a) (volts) | 0 | 1.47 | 1.44 | 1.51 | ∿0 | ∿0 | ∿0 | ∿0 | ∿0 | ∿0 | 0.04 | 0.04 | 0.03 | ∿0 | ∿0 | ∿0 |
| | 40 | 1.49 | 1.50 | 1.43 | 0.02 | 0.01 | 0.01 | 0.01 | 0.01 | 0.01 | 0.05 | 0.04 | 0.05 | 0.42 | 0.33 | 0.20 |
| | 90 | 1.41 | 1.39 | 1.56 | 0.14 | 0.11 | 0.04 | 0.10 | 0.08 | 0.02 | 0.10 | 0.07 | 0.05 | 1.41 | 1.47 | 0.74 |
| | 140 | 1.11 | 1.16 | 1.34 | 0.55 | 0.26 | 0.02 | 0.50 | 0.22 | 0.01 | 0.27 | 0.14 | 0.05 | 2.07 | 1.82 | 0.38 |
| | 180 | 0.78 | 1.00 (e) | 1.32 | - | 1.06 | 0.23 | - | 0.89 | 0.17 | - | 0.38 | 0.12 | - | 2.75 | 1.86 |

(a) Other parameters: Power, 20W; Time, 10 mins.; Pressure, 0.2T; atomiser-coil separation 3½ cm.

(b) 1: Below atomiser; 2: atomiser end of coil region; 3: middle of coil region.

(c) Covalent fluorine/carbon ratio.

(d) Molybdenum/total fluorine ratio.

(e) Sample for which ionic fluorine is present as well as covalent fluorine.

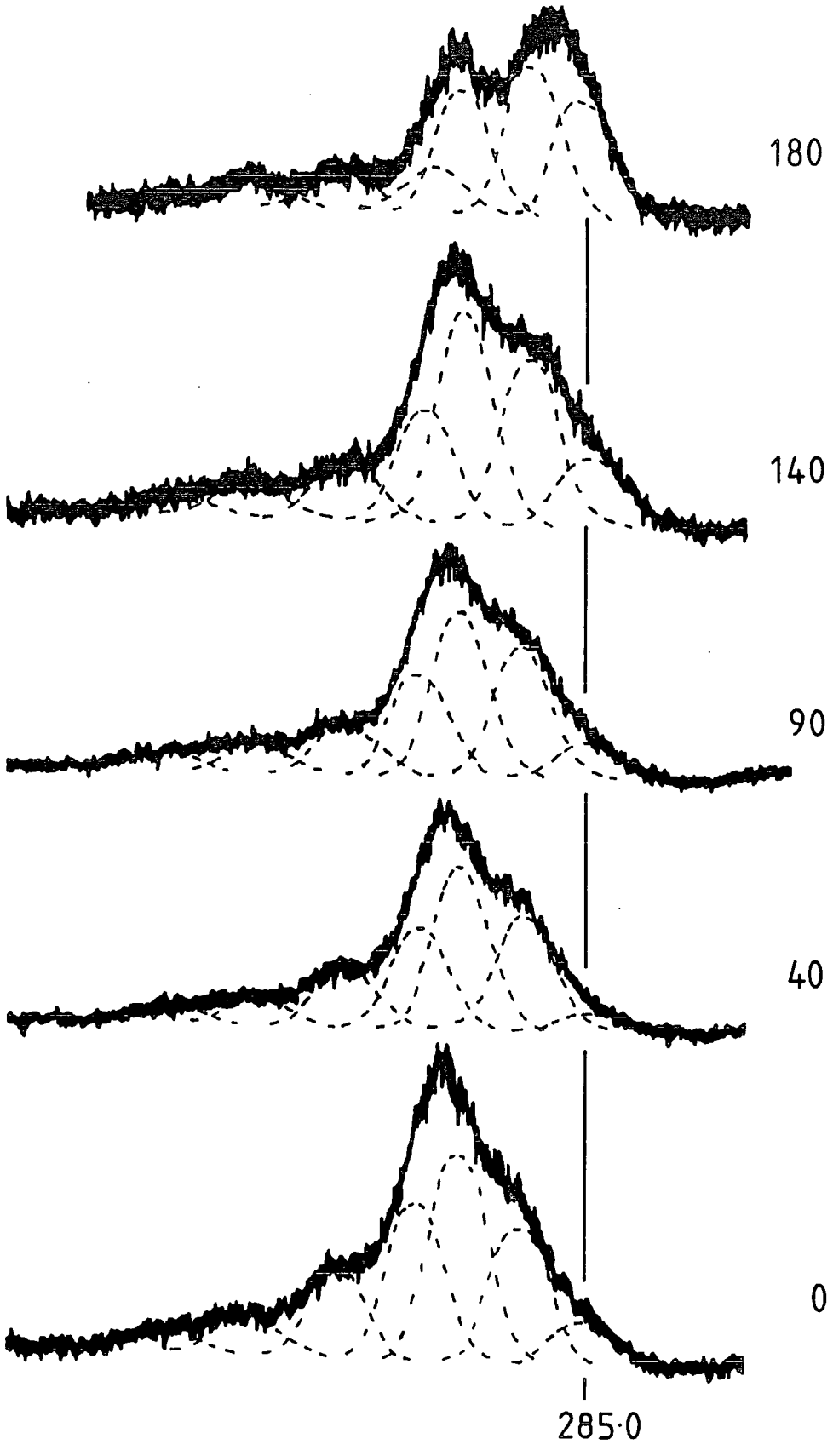


Figure 5.3 VARIATION OF $C_{1s}$ SPECTRUM WITH ATOMISER VOLTAGE

(Filament Voltage in Volts)

values are consistently higher the same trend is apparent. Previously it has been explained that the component analysis leads to a higher value of the $^{F}/_{C}$ stoichiometry because part of the peaks assigned to highly fluorinated sites ($CF_3$ and $CF_2$) may actually arise from $\pi \rightarrow \pi^*$ shake-up transitions of sites involving a much lower degree of fluorination.[118] In the event of vertical inhomogeneity of the sample this could lead to a more substantial difference between the two sets of $^{F}/_{C}$ ratios; for example, if there was a hydrocarbon overlayer, whilst both sets of values would decrease because of the extra carbon intensity, the ratio calculated from two core levels would also decrease because of differential attenuation of the lower kinetic energy electrons arising from the $F_{1s}$ level. The comparatively large difference between the $^{F}/_{C}$ ratios calculated by the two methods in the present case reveals the vertical inhomogeneity of the analysed samples.

The component analysis of the $C_{1s}$ envelopes allows an estimation of the contribution from carbon atoms without either α or β fluorine substituents. This peak represents 7, 4, 8, 11 and 24% of the carbon sites in the polymers prepared when operating the atomiser at different voltages (0-180V; Figure 5.3); if this component is subtracted out then the $^{F}/_{C}$ stoichiometries, derived from core-level ratios, become 0.80, 0.81, 0.78, 0.68 and 0.69. Whilst these figures still suggest that some defluorination may be occurring the values are much closer to being the same, within experimental error, and show that a large part of the changing $^{F}/_{C}$ stoichiometry is caused by the single component at 285.0. Support for this comes from the rest of the component analysis of the $C_{1s}$ envelope; the contributions from the $CF_3$ and $CF_2$ components in this series

of spectra vary over less than 5% and with the exception of the spectrum recorded for the experiment using an atomiser voltage of ∿18OV, the same is true for the CF components. The error associated with peak intensities obtained by analogue curve resolution is usually placed at ±5%,[118] and so within this margin, the plasma polymers produced appear to be little affected by the atomiser voltage. Indeed, visually, the high binding energy side of the $C_{1s}$ spectra obtained appear very similar and they differ only in the lower binding energy regions. This was also found to be true for the plasma polymers produced in regions 1 and 3.

The intensity of the component at 285.0eV in the analysed samples does appear to be related to the atomiser voltage; extraneous contamination arising during transport of the sample to the spectrometer would be expected to vary randomly, but here the intensity of this component appears to increase with the atomiser voltage. Also this component is generally found to be greatest in sample 1 and then to successively decrease in samples 2 and 3, so that whilst the $^{F}/_{C}$ ratios for samples 1 and 3 are very similar when no voltage is applied to the atomiser, higher voltages of 140 and 180V lead to substantial differences in this ratio for these two sampling positions (Table 5.1).

The fact that plasma polymerisation of perfluorobenzene in a wide variety of conditions (not involving an atomiser) leads to only a small intensity component at 285.0eV[118,125,166] supports the suggestion that in the present instance its intensity is related to the use of the atomiser.

Whilst there does seem to be some correlation between increasing atomiser voltage and decreasing $^{F}/_{C}$ ratios it is not possible to separate out the trends of defluorination

of polymerising precursors and hydrocarbon contamination. Also if this trend is due to hydrocarbon contamination it is not clear whether this is intrinsic to the use of a heated metal filament; certainly if hydrocarbon arises inside the reactor during the plasma, due to the use of a heated metal filament, then it will most likely be incorporated and become an integral part of the plasma polymer rather than being confined to an overlayer. An alternative explanation, of the presence of hydrocarbon, might lie in disparate rates of polymer deposition along the substrate due to greater (radiative) heating of some parts of the substrate; in this case extraneous hydrocarbon present on the substrate prior to deposition might be a significant source of $C_{1s}$ signal intensity in certain instances where polymer deposition is minimal.

Despite the difficulties of deciding the cause of the trend in $^{F}/_{C}$ ratios, what can be said is that the plasma-deposits prepared in this system exhibit ratios which are significantly lower than those previously reported for perfluorobenzene plasma polymers.[118,125]

The increasing $^{Mo}/_{C}$ ratio as the atomiser voltage is increased (Table 5.1) shows the increasing incorporation of metal into the plasma-deposits as the temperature of the filament is increased. Obviously this trend would be accentuated if the "hydrocarbon" component at 285.0eV were subtracted out, but in the light of the above discussion on the uncertainty over the origin of this peak, this would be somewhat false. The increasing metal incorporation is greatest for region 1 and smallest for region 3, reflecting the distance from the filament.

Concomitant with the increasing $^{Mo}/_{C}$ ratio is an increasing $^{O}/_{C}$ intensity ratio and this suggests that the two might be linked and that molybdenum oxides may be present in

the analysed surfaces. If this was the case one might anticipate a fairly constant value for the $^{Mo}/_{O}$ ratio, which is obviously not so. These points are discussed below (Section 5.3.4).

### 5.3.2 Variation of Plasma Parameters

#### (i) Time

Times of plasma discharge of 10 secs., 2, 10 and 30 minutes were used to determine the effect of time. The gross intensity ratios are presented in Table 5.2.

The derived $^{F}/_{C}$ stoichiometries of 0.56, 0.74, 0.72 and 0.63 (t = 0.16, 2, 10, 30; sample 2) show no systematic change of stoichiometry with time of deposition; exclusive of hydrocarbon these stoichiometries are 0.67, 0.78, 0.78 0.68. Either with or without inclusion of the component at 285.0eV, the component distributions, derived from the $C_{1s}$ envelopes of these samples, are very similar showing virtually no variation of polymer structure with time of deposition (the same result was found for earlier work).[125] The most significant difference between the $C_{1s}$ spectra is that the plasma polymer prepared by a 10 second discharge shows substantially more hydrocarbon, some 2-3 times that found in the other samples. This is most likely because the shorter deposition time leads to a much thinner film[125] and the extraneous hydrocarbon present on the substrate prior to deposition contributes to the signal intensity. Samples from regions 1 and 3 show a similar invariance of fluoropolymer composition with time, the only exception being the sample taken from region 1 after the 10 second plasma preparation. The low $^{F}/_{C}$ stoichiometry of this sample arises

TABLE 5.2 VARIATION OF GROSS INTENSITY RATIOS WITH TIME OF DEPOSITION

| | Ratio | $F_{1s}/C_{1s}$ (c) | | | $Mo_{3d}/C_{1s}$ | | | $Mo_{3d}/F_{1s}$ (d) | | | $O_{1s}/C_{1s}$ | | | $Mo_{3d}/O_{1s}$ | | |
|---|---|---|---|---|---|---|---|---|---|---|---|---|---|---|---|---|
| | Sample Position (b) | 1 | 2 | 3 | 1 | 2 | 3 | 1 | 2 | 3 | 1 | 2 | 3 | 1 | 2 | 3 |
| Time (a) (min.) | 0.16 | 0.47[e] | 1.08 | 1.28 | 2.35 | 0.47 | 0.17 | 3.00 | 0.43 | 0.14 | 1.06 | 0.24 | 0.10 | 2.22 | 1.91 | 1.69 |
| | 2 | 1.32 | 1.43 | 1.47 | 0.14 | 0.09 | 0.05 | 0.11 | 0.07 | 0.03 | 0.11 | 0.09 | 0.07 | 1.26 | 1.07 | 0.78 |
| | 10 | 1.41 | 1.39 | 1.56 | 0.14 | 0.11 | 0.04 | 0.10 | 0.08 | 0.02 | 0.10 | 0.07 | 0.05 | 1.41 | 1.47 | 0.74 |
| | 30 | 1.18 | 1.21 | 1.30 | 0.04 | 0.08 | 0.01 | 0.04 | 0.07 | 0.01 | 0.06 | 0.07 | 0.03 | 0.71 | 1.12 | 0.27 |

(a) Other parameters: Power, 20W; Atomiser Voltage 90V; Pressure, 0.2T; Atomiser-coil separation, 3½ cm.

(b) 1: Below atomiser; 2: atomiser end of coil region; 3: middle of coil region.

(c) Covalent fluorine/carbon ratio.

(d) Molybdenum/total fluorine ratio.

(e) Sample for which ionic fluorine is present as well as covalent fluorine.

from the fact that the component at 285.0eV is ∿30% of the total $C_{1s}$ signal. Taken in conjunction with the fact that for this sample the characteristic plasma fluoropolymer structure has not developed suggests that the rate of deposition is lower in this (non-coil) region.[118]

The observed $^{Mo}/_{C}$ ratio clearly decreases with length of time of plasma deposition (Table 5.2). In particular the ratio is far higher for the shortest plasma time used, where it has been suggested by consideration of the $^{F}/_{C}$ ratio that the polymer film is sufficiently thin to permit the extraneous hydrocarbon present on the substrate, to contribute to the observed signal. Thus the much higher $^{Mo}/_{C}$ ratio observed for the shorter plasma times is consistent with the idea that deposition of molybdenum species onto the substrate occurs largely independently of polymer deposition.

The $^{O}/_{C}$ ratio follows the same trend as the $^{Mo}/_{C}$ ratio and whilst this again suggests an interdependence of the molybdenum and oxygen species it is noted that the $^{Mo}/_{O}$ ratio is far from constant.

(ii) Variation with pressure

The results of experiments performed at two monomer pressures of 0.1 and 0.2T are given in Table 5.3.

The $^{F}/_{C}$ ratios determined are very similar. The most significant variation is found for the sample in region 1, prepared at the lower pressure, and this lower ratio is caused by the high intensity of the hydrocarbon component (∿30% of the total $C_{1s}$ spectrum); in addition the characteristic high binding energy peaks of the plasma polymer are not well estab-

TABLE 5.3 VARIATION OF GROSS INTENSITY RATIOS WITH PRESSURE

| | Ratio | $F_{1s}/C_{1s}$ (c) | | | $Mo_{3d}/C_{1s}$ | | | $Mo_{3d}/F_{1s}$ (d) | | | $O_{1s}/C_{1s}$ | | | $Mo_{3d}/O_{1s}$ | | |
|---|---|---|---|---|---|---|---|---|---|---|---|---|---|---|---|---|
| | Sample Position (b) | 1 | 2 | 3 | 1 | 2 | 3 | 1 | 2 | 3 | 1 | 2 | 3 | 1 | 2 | 3 |
| Pressure[a] | 0.1 | 0.93[e] | 1.32 | 1.37 | 0.88 | 0.11 | 0.02 | 0.79 | 0.08 | 0.01 | 0.48 | 0.15 | 0.13 | 1.85 | 0.71 | 0.12 |
| (Torr) | 0.2 | 1.41 | 1.39 | 1.56 | 0.14 | 0.11 | 0.04 | 0.10 | 0.08 | 0.02 | 0.10 | 0.07 | 0.05 | 1.41 | 1.47 | 0.74 |

(a) Other parameters: Power, 20W; Atomiser Voltage, 90V; Time, 10 mins.; Atomiser-coil separation, 3½ cm.

(b) 1: Below atomiser; 2: atomiser end of coil region; 3: middle of coil region.

(c) Covalent fluorine/carbon ratio.

(d) Molybdenum/total fluorine ratio.

(e) Sample for which ionic fluorine is present as well as covalent fluorine.

lished, showing that in this region for this pressure, deposition is somewhat slower. (Earlier results established that deposition at 200μ is substantially greater than at 100μ.[125] Also region 1 is outside the coil region[118]). The $^{F}/_{C}$ stoichiometries, inclusive of hydrocarbon and determined from gross core level intensities for region 2, are 0.69 and 0.72 for the lower and higher pressures respectively. Despite this similarity in overall $^{F}/_{C}$ stoichiometries the polymer prepared at lower pressure contains far more $CF_2$ groups than does that prepared at higher pressure, a result which has been alluded to before.[118]

The high $^{Mo}/_{C}$ ratio found for region 1 of the lower pressure plasma, where polymer deposition is comparatively slow, again shows the independence of the metal incorporation and the polymer deposition. Other than this, little can be deduced concerning the variation of metal incorporation with pressure, from this limited data set.

The $^{O}/_{C}$ ratios of the resultant polymers are consistently higher for the samples prepared at lower pressure, which probably reflects the relatively greater concentration of impurities in the lower pressure plasma. This would explain the low $^{Mo}/_{O}$ ratios found for the polymers prepared at lower pressure, in regions 2 and 3; region 1 is anomalous because of the significantly lower rate of polymer deposition as noted above. The greater importance of impurities in the lower pressure discharge is also reflected in the incorporation of nitrogen in the polymeric product; the binding energy (∿401eV) is too high for a metal nitride and is indicative of organic nitrogen species.[186]

(iii) Variation with Power

The results obtained using different RF input powers (20, 50 and 100W) are shown in Table 5.4.

The overall $^{F}/_{C}$ intensity ratios suggest that higher powers lead to a fluoropolymer of lower fluorine content, the relevant stoichiometries determined from total core level intensities being 0.72, 0.60 and 0.56 (20, 50, 100W; sample 2). This trend has been noted before.[125] However the $C_{1s}$ spectra are remarkably similar and curve resolution shows that percentage contributions, to the total intensity, of $CF_3$, $CF_2$ and CF groups are very similar for all powers; this leads to $^{F}/_{C}$ stoichiometries, determined by $C_{1s}$ somponent analysis, which are approximately the same for the three powers (0.86, 0.89 and 0.92). It is interesting to note that the discrepancy between the $^{F}/_{C}$ stoichiometries determined by the two methods increases with increasing power; as noted earlier such a trend could be explained if there were successively greater hydrocarbon or defluorinated layers on the three samples. Electron bombardment of a perfluorobenzene polymer showed the growth, in the $C_{1s}$ spectra, of carbonaceous peaks,[138] so it is not inconsistent to suggest that the greater electron bombardment of the surface by a higher power plasma may lead to the formation of a defluorinated overlayer.

Consideration of the $^{Mo}/_{C}$ and $^{Mo}/_{F}$ ratios for the samples prepared at 20W shows the decrease in metal incorporation in going from region 1 to 2 to 3. This again emphasises the independence of the metal incorporation and polymer deposition. The ratios obtained for samples, prepared in any of the three regions, suggest that metal incorporation decreases as power

TABLE 5.4 VARIATION OF GROSS INTENSITY RATIOS WITH POWER

| | Ratio | $F_{1s}/C_{1s}$ | | | $Mo_{3d}/C_{1s}$ | | | $Mo_{3d}/F_{1s}$ | | | $O_{1s}/C_{1s}$ | | | $Mo_{3d}/O_{1s}$ | | |
|---|---|---|---|---|---|---|---|---|---|---|---|---|---|---|---|---|
| | Sample Position(b) | 1 | 2 | 3 | 1 | 2 | 3 | 1 | 2 | 3 | 1 | 2 | 3 | 1 | 2 | 3 |
| Power (a) (Watts) | 20 | 1.41 | 1.39 | 1.56 | 0.14 | 0.11 | 0.04 | 0.10 | 0.08 | 0.02 | 0.10 | 0.07 | 0.05 | 1.41 | 1.47 | 0.74 |
| | 50 | 1.19 | 1.14 | 1.16 | 0.10 | 0.10 | 0.01 | 0.09 | 0.08 | 0.01 | 0.11 | 0.08 | 0.05 | 0.90 | 1.27 | 0.24 |
| | 100 | 1.13 | 1.08 | 1.14 | 0.04 | 0.03 | ∿0 | 0.03 | 0.03 | ∿0 | 0.06 | 0.05 | 0.04 | 0.62 | 0.70 | ∿0 |

(a) Other parameters: Time, 10 mins.; Atomiser voltage 90V; Pressure 0.2T; atomiser-coil separation 3½ cm.

(b) 1: Below atomiser; 2: atomiser end of coil region; 3: middle of coil region.

is increased. The trend could be interpreted as showing that plasma sputtering of the metal is not the major method of incorporation since it would be anticipated that increased power would increase sputtering. However such a straightforward interpretation is probably invalid because the power also affects the rate of polymer deposition. Earlier results suggested an increase in rate of deposition up to ∿40W[125] after which ablation became more prominent and the rate of deposition started to decrease, behaviour which is to be anticipated from the CAP mechanism of polymer formation. But the power corresponding to maximum deposition rate will be reactor-dependent and the more important parameter is the composite paremeter W/FM. It is one of the omissions of this work that the flow rate of the reactor used was not established and therefore the composite parameter cannot be determined.

### 5.3.3 Variation of the atomiser-coil separation

Since the distribution of molybdenum along the total reactor length was to be studied the highest acceptable atomiser voltage of ∿180V was used for these experiments. Other parameters were 20W, 10m, 0.2T.

Three different atomiser-coil separations were tried, of 3½, 13½ and 23½ cm, these being the distances between the atomiser and the end of the coil itself; 3½ and 23½ represent the minimum and maximum possible distances - limits imposed by the size of the reactor. Seven sampling positions were considered for each separation distance, corresponding to the middle of the coil and mouth of the coil for each of the three coil positions, as well as one from immediately below

the atomiser unit (O, 3½, 8, 13½, 18, 23½ and 28 cm. from the atomiser; samples X.1 - X.7 respectively; see Figure 5.4). The intensity ratios derived from these samples are shown in Table 5.5.

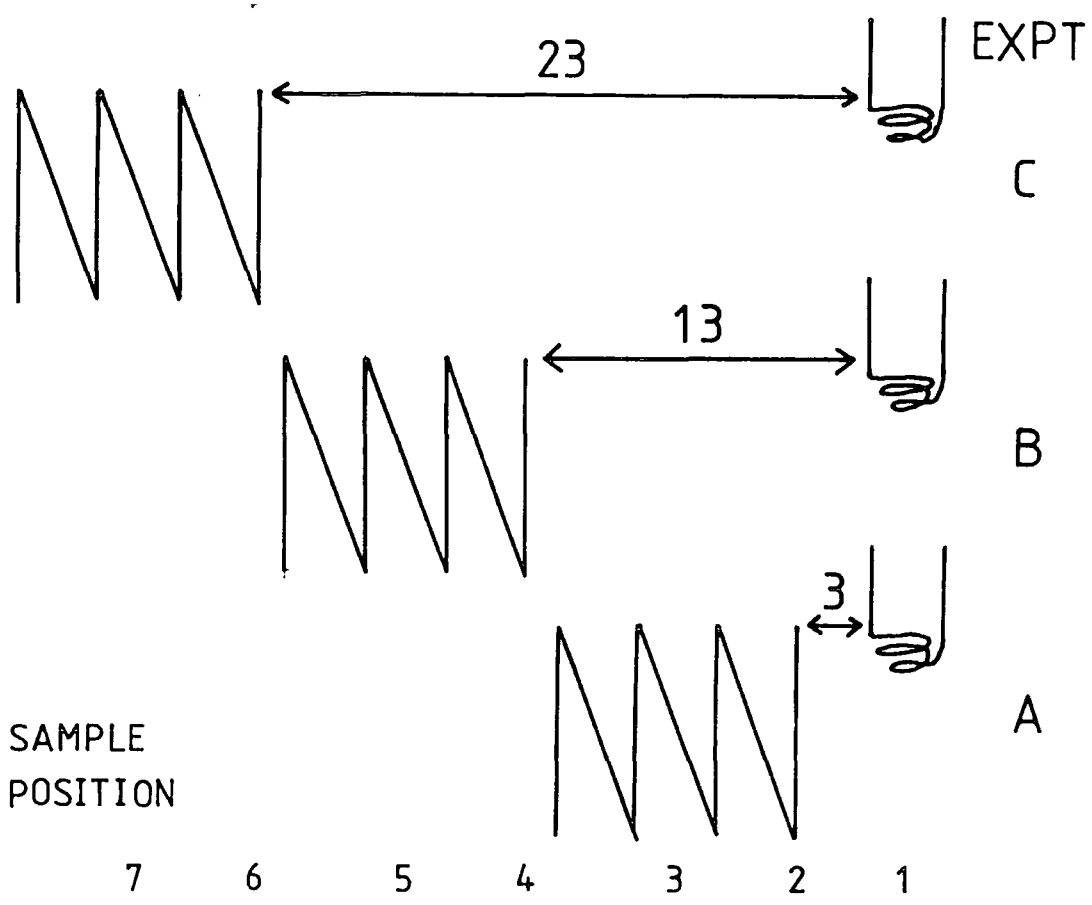


Figure 5.4 SCHEMATIC OF SAMPLING POSITIONS

---

Notes to Table 5.5 (shown on following page)

(a) For Atomiser-coil separation see Schematic Figure 5.4.
Other parameters: Atomiser voltage 180V; Pressure, 0.2T; Power 20W; Time 10 min.

(b) Sampling positions, see schematic - thick lines in Table represent limits of coil region.

(c) Covalent fluorine/carbon ratio.

(d) Molybdenum/total fluorine ratio,

(e) Samples for which ionic fluorine is present in addition to covalent fluorine.

TABLE 5.5 VARIATION OF GROSS INTENSITY RATIOS WITH ATOMISER-COIL SEPARATION

| Sample[a][b] | Plasma Polymer? | $F_{1s}/C_{1s}$[c] | $Mo_{3d}/C_{1s}$ | $Mo_{3d}/F_{1s}$[d] | $O_{1s}/C_{1s}$ | $Mo_{3d}/O_{1s}$ |
|---|---|---|---|---|---|---|
| A1 | No | 0.54[e] | 2.48 | 2.75[e] | 0.87 | 2.84 |
| A2 (coil) | No | 0.59[e] | 1.92 | 2.53[e] | 0.78 | 2.45 |
| A3 (coil) | Yes | 0.87 | 0.38 | 0.43 | 0.19 | 2.01 |
| A4 | Yes | 0.95 | 0.06 | 0.07 | 0.06 | 1.10 |
| A5 | Yes | 0.93 | 0.08 | 0.08 | 0.08 | 0.99 |
| A6 | Yes | 0.93 | 0.06 | 0.06 | 0.07 | 0.79 |
| A7 | Yes | 0.92 | 0.05 | 0.05 | 0.06 | 0.78 |
| B1 | No | 0.20[e] | 2.95 | 5.18[e] | 1.04 | 2.83 |
| B2 | No | 0.44[e] | 1.83 | 3.10[e] | 0.72 | 2.54 |
| B3 | Yes | 0.70 | 0.86 | 1.22 | 0.35 | 2.45 |
| B4 (coil) | Yes | 0.84 | 0.63 | 0.75 | 0.25 | 2.52 |
| B5 (coil) | Yes | 0.79 | 0.15 | 0.19 | 0.09 | 1.61 |
| B6 | Yes | 0.74 | 0.04 | 0.05 | 0.05 | 0.82 |
| B7 | Yes | 0.79 | 0.06 | 0.08 | 0.06 | 0.93 |
| C1 | No | 0.12[e] | 3.25 | 5.71[e] | 1.01 | 3.22 |
| C2 | No | 0.41[e] | 1.83 | 3.3[e] | 0.81 | 2.25 |
| C3 | Yes | 0.66 | 1.26 | 1.91 | 0.47 | 2.70 |
| C4 | Yes | 0.72 | 0.97 | 1.35 | 0.35 | 2.77 |
| C5 | Yes | 0.75 | 0.83 | 1.10 | 0.34 | 2.46 |
| C6 (coil) | Yes | 0.69 | 0.71 | 1.03 | 0.28 | 2.50 |
| C7 (coil) | Yes | 0.67 | 0.07 | 0.10 | 0.07 | 0.91 |

Column 1 of this table indicates whether the $C_{1s}$ exhibited the high binding energy peaks characteristic of the plasma polymer. The thick lines indicate the samples formed in the coil region in each experiment.

Before discussing the results in general, attention is focussed on the samples taken from the mouth of the coil in each case (A2, B4, C6) which are comparable with those discussed in previous sections. For these samples the $^{F}/_{C}$ stoichiometries are 0.31, 0.44 and 0.36 and considerable hydrocarbon appears to be present in all cases. This is evident not only from the $C_{1s}$ component analysis but also the low $^{F}/_{C}$ ratio which is far lower than previously found for these polymer systems.[125] For the minimum atomiser-coil separation the sample analysed shows minimal plasma fluoropolymer formation; whilst CF and C-CF functional groups are clearly present, the characteristic high binding energy tail comprising $CF_3$ and $CF_2$ functions is not observable. The component at 285.0eV represents ∿60% of the total $C_{1s}$ signal, and taken in conjunction with the other facts it appears that in this experiment minimal deposition occurred in the mouth of the coil. This result can be contrasted with the two larger separations where the characteristic $CF_3$ and $CF_2$ groups of the plasma polymer were observed, though the 285.0eV component in both these cases was still relatively high (∿20% in each case).

For both the $^{Mo}/_{C}$ and $^{Mo}/_{F}$ ratios it can be seen that the sample prepared using the minimum atomiser-coil separation contains significantly more molybdenum than either of the other two; to some extent though this observation is probably linked with the suggestion that film deposition in this position is rather limited; this is discussed more fully below.

The $^{O}/_{C}$ ratios of the samples follow the same pattern as the $^{Mo}/_{C}$ and this is not surprising considering the remarkable similarity of the $^{Mo}/_{O}$ ratios which are all $\sim$2.5.

More generally, in all three experiments the $^{F}/_{C}$ ratios obtained for samples taken from regions 1 and 2 are particularly low. It is difficult to be certain that this low ratio is not due to defluorination of the polymer, but the observation of fluoride for many of the relevant samples is consistent with the suggestion (see Section 5.4.2) that deposition is minimal and that extraneous hydrocarbon contributes significantly to the overall $C_{1s}$ signal intensity leading to low values of the $^{F}/_{C}$ ratio. This is borne out by the more detailed component analysis of the $C_{1s}$ envelopes which show the main component at 285.0 with some small contributions from C-CF and CF. Although deposition is generally greater in the coil region than outside it,[118] this alone does not explain the results obtained. Indeed sample A2 (which is inside the mouth of the coil) exhibits little plasma polymer structure whilst conversely analysis of samples B3, C4 and C5 (outside the coil region) do show $C_{1s}$ envelopes characteristic of the polymer. Thus the minimal deposition in the first two sampling regions appears to be attributable to the higher temperature of these regions.

With the exception of certain regions noted above, the $^{F}/_{C}$ ratios seem to be generally fairly similar, both inside and outside the coil region, for individual experiments though the variation between experiments suggests slightly higher fluorine incorporation for samples prepared using the minimum atomiser-coil separation.

It is difficult to gauge accurately the extent of molybdenum incorporation. The plasma polymer deposited in certain regions of the reactor may be defluorinated compared to other regions, and for such samples the $^{Mo}/_{F}$ ratio would overestimate the amount of metal incorporation per "unit" of polymer. Conversely low deposition rates in certain areas of the reactor may mean that the $C_{1s}$ signal recorded contains a significant contribution from extraneous hydrocarbon present at the substrate-polymer interface; this would lead to an underestimate of the metal incorporation per polymer "unit".

The greatest metal incorporation appears to be in the first two sampling regions where it has been suggested that polymer deposition is slow. The $^{Mo}/_{C}$, $^{Mo}/_{F}$ ratios of 2.48, 2.75; 2.95, 5.18 and 3.25, 5.71 for sample A1, B1 and C1 increase as distance from the coil increases and this can be seen in the light of the probable decreasing rate of polymer deposition along the series.[124,128] Similarly the increasing ratios 0.38, 0.43; 0.86, 1.22 and 1.26, 1.91 for samples A3, B3 and C3, which are in the middle of the coil region and 10 and 20 cm. from it respectively, increase in the order for which polymer deposition is expected to decrease. These results support the idea that a large part, if not all, of the metal incorporation occurs independently of the polymer formation.

From the results obtained for C1-C5 ($^{Mo}/_{C}$, $^{Mo}/_{F}$) it might be supposed that the amount of molybdenum incorporated is a direct function of the distance from the atomiser, but the trend could simply be the result of increasing polymer deposition closer to the coil region. For this reason an independent experiment was performed to try to determine the molybdenum

distribution along the substrate in the absence of a glow discharge. In this experiment the atomiser was simply operated for the length of time normally used for the plasma experiments. It is difficult to assess the amount of molybdenum in each sample position because there is little with which to compare the signal intensity but using an aluminium substrate the $^{Mo}/_{C}$ ratios of 4.39, 2.62 and 0.04 and the $^{Al}/_{Mo}$ ratios of $\sim$0, 0.01 and 6.18, for sample positions 1, 2 and 3, lend credence to the suggestion that there is greater metal deposition closer to the coil. This experiment was performed at base pressure of the reactor without a flow of gas and clearly this is another variable which might affect the result; certainly in the plasma experiments metal can be detected at reasonable distances from the atomiser (*e.g.* A6 and A7) albeit at low levels.

Perhaps the most interesting region investigated is that from which samples C3-C6 are taken, that is, the area between the atomiser and the coil. In these samples there is significant molybdenum content but also the plasma polymer is formed. In "earlier" regions, under and close to the atomiser there is minimal polymer formation, the samples contain high proportions of hydrocarbon and are powdery in nature. In the "later" regions of the middle of the coil the rate of polymer deposition is greatest and comparatively low molybdenum content is observed (A3, B5, C7). Further downstream, beyond the coil, though the rate of deposition is slower, the amount of metal reaching these areas is also much smaller. Samples C3-C6 are interesting because they give rise to high $^{Mo}/_{C}$ ratios and the $C_{1s}$ spectra show the characteristic plasma polymer structure. Much higher $^{Mo}/_{C}$ ratios have been found for other samples but the $C_{1s}$ spectra reveals that the polymer is not formed (*i.e.* such

samples are better described as molybdenum containing deposits). Sample C3 has the highest $^{Mo}/_{C}$ ratio of all the polymer samples analysed; its stoichiometry of $C_{6.0}F_{2.1}Mo_{0.6}O_{1.7}$ corresponds to a sample containing 29 weight per cent of molybdenum (*c.f.* 18-26% produced in a Mo-$C_3F_8$ etching-polymerisation reactor[173]).

### 5.3.4 The molybdenum/oxygen ratio and molybdenum chemical state

Whilst the $^{Mo}/_{O}$ ratio for these samples varies over a wide range it has been noted that very often over a series of results increase in the $^{O}/_{C}$ ratio is concomitant with an increase in the $^{Mo}/_{C}$ ratio. Thus it seems quite likely that molybdenum oxides might be present in the analysed samples.

A sample of molybdenum trioxide was analysed and the spectra are shown in Figure 5.5. Using the extraneous hydrocarbon peak as energy reference (285.0eV) the $Mo_{3d_{5/2}}$ binding energy of ∿233.4eV is in fair agreement with a literature value of ∿232.5eV[187] and is considerably higher than that of molybdenum dioxide (∿229.4).[187] The $O_{1s}$ is a single peak with a binding energy of 532.4eV. The (total) $Mo_{3d}$ doublet/$O_{1s}$ intensity ratio is ∿2.5; since the compound has a stoichiometry of 1:3 this implies a $Mo_{3d}/O_{1s}$ sensitivity factor ∿7.4, and a $Mo_{3d}/C_{1s}$ ∿12.3. Extraneous hydrocarbon present on the sample surface would lead to a greater attenuation of the $O_{1s}$ signal compared with the $Mo_{3d}$ doublet and this would mean that the derived sensitivity factor is too high but conversely any adsorbed oxygen on the surface would give too low a value. However despite these possible errors it has been established that for molybdenum trioxide the $Mo_{3d}/O_{1s}$ intensity ratio is approximately 2.5.

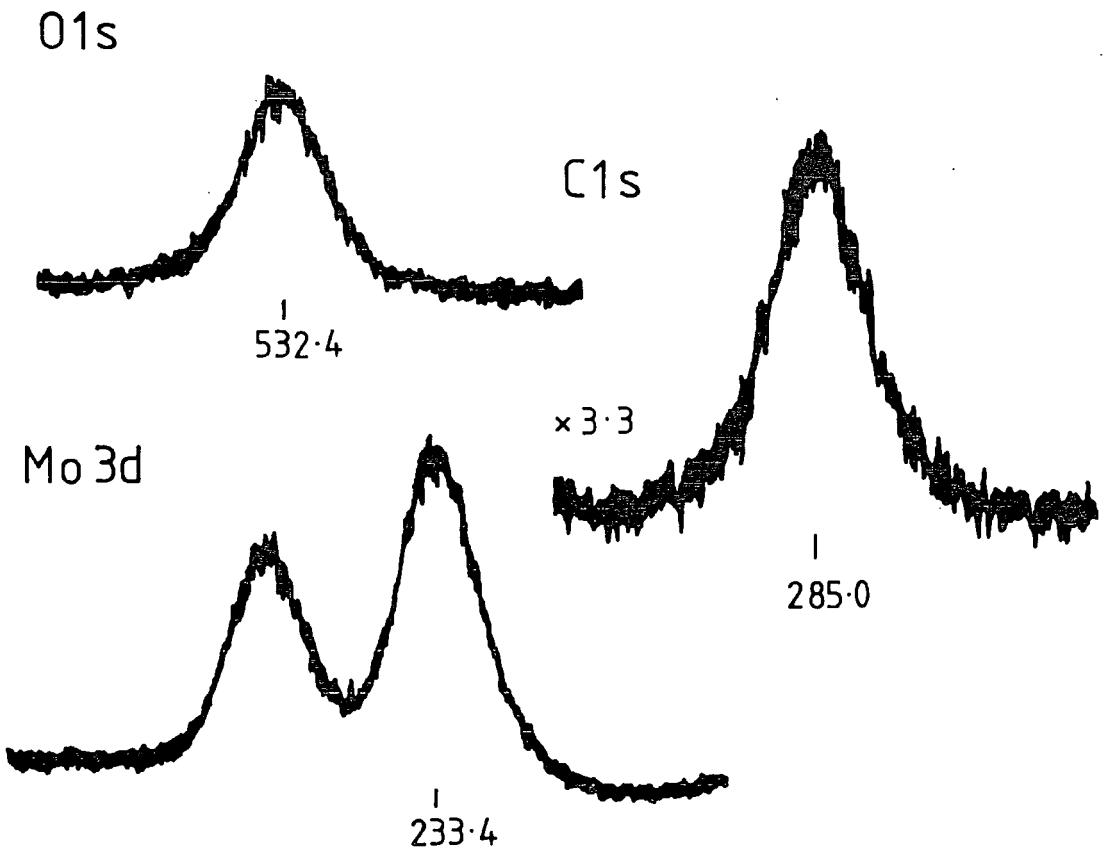


Figure 5.5 CORE HOLE SPECTRA OF MOLYBDENUM TRIOXIDE POWDER SAMPLE. (Binding energies referenced to $C_{1s}$ at 285.0eV).

---

In the incorporation of metal into the plasma polymer, the $O_{1s}$ signal is often asymmetric. In all cases where significant amounts of metal are incorporated this core level extends over regions including low binding energies of ∿532eV so that it is perfectly feasible that molybdenum trioxide contributes to the $O_{1s}$ signal. Certainly the asymmetry of many of the oxygen spectra recorded shows that at least two distinct oxygen environments are present in these systems. In earlier

work it has been noted that oxygen rapidly reacts with free radical sites in a plasma polymer surface when this is exposed to the atmosphere. The two oxygen components in the present asymmetric spectra have binding energies ∿535.2 and ∿533.2eV. Within this two component analysis the higher binding energy component might be assigned as arising from organic oxygen functionalities and the other from molybdenum trioxide. There is a trend that as the $^{Mo}/_{O}$ ratio increases, the binding energy of the centroid of the $O_{1s}$ signal decreases (Figure 5.6).

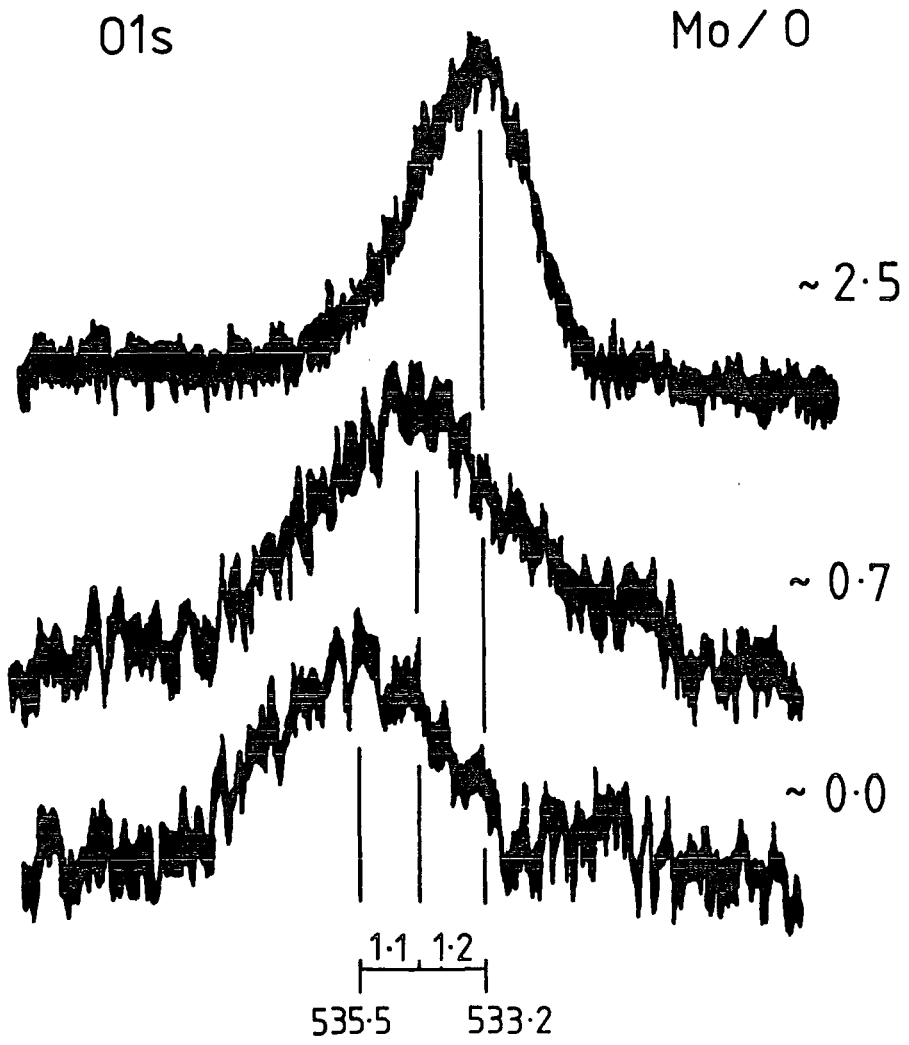


Figure 5.6 VARIATION OF $O_{1s}$ BINDING ENERGY WITH $^{Mo}/_{O}$ INTENSITY RATIO. (Binding energy in eV)

This simple trend is not totally general because of more complex factors; since the metal oxide is incorporated into the polymer, overlayer effects will complicate the observed $^{Mo}/_{O}$ intensity ratio. Also it is quite probable that the oxygen signal may be the sum of more than two components. Earlier work suggested at least two distinct organic oxygen signals, at ∿535.3 and 534.1eV. In the simplistic idea of a two component oxygen spectrum this lower binding energy organic oxygen peak would partially contribute to that assigned as "molybdenum trioxide" and this might explain why the binding energy of this component (∿533.2eV) is somewhat higher than that determined from the metal oxide sample. Another complicating factor would, of course, be the presence of other molybdenum-oxygen compounds.

The reason for the wide ranging $^{Mo}/_{O}$ ratios is now apparent, even if only molybdenum trioxide and a single organic oxygen species are considered. The amount of organic oxygen, related as it is to the free radical sites in the plasma polymer, is a fairly constant proportion of the $C_{1s}$ signal intensity, typically ∿5%. When the amount of molybdenum incorporation is low, the organic oxygen forms a significant part of the total oxygen signal, leading to very low $^{Mo}/_{O}$ ratios; with increasing metal in the system the metallic oxide becomes the major component and the $^{Mo}/_{O}$ ratio tends towards ∿2.5, approximately that expected for molybdenum trioxide. Values of this ratio higher than 2.5 are referred to in Section 5.4.1.

For a large number of samples (∿60) the binding energy of the molybdenum present in the plasma deposits, falls in the range 232.8-233.8eV. By comparison with the binding

energy of the $Mo_{3d_{5/2}}$ core level in the molybdenum trioxide sample analysed in the present work (∿233.4eV) it can be seen that the incorporated metal is in a high oxidation state of +5/+6 and this is consistent with the conclusion that much of the molybdenum is present as the trioxide with perhaps some contribution from $MoO_X$ species ($2<X<3$) in which the binding energy of the molybdenum is expected to be only ∿1eV less.[188] Certainly the binding energy of the incorporated molybdenum rules out the possibility of there being significant amounts of molybdenum metal or dioxide in the analysed surfaces.

### 5.3.5 Summary of the results

The major points revealed by this investigation can be summarised as follows:

(i) The $^{F}/_{C}$ ratio of the plasma polymer decreases with increase in filament temperature, though whether this is due to defluorination of the normal polymer precursors or to the presence of extraneous hydrocarbon (arising perhaps from the use of the filament) is not clear.

(ii) The $^{Mo}/_{C}$ ratio increases with increase in temperature of the filament.

(iii) The rate of deposition of fluoropolymer is lower close to the atomiser.

(iv) The metal incorporation and polymer deposition are independent.

(v) The molybdenum present in the analysed surfaces is in a high oxidation state and is probably mainly the trioxide.

(vi) Samples formed between the plasma coil and molybdenum heater are potentially the most interesting.

## 5.4 The Nature of the Metal Incorporation

### 5.4.1 The evaporation of molybdenum

The aim of the present series of experiments was to incorporate metal by evaporation and so it is pertinent to ask whether molybdenum is evaporated from the filament, incorporated into the growing polymer, and subsequently oxidised when the samples are stored in air.

If molybdenum metal rather than molybdenum oxides was present in the analysed polymer surfaces the $^{Mo}/_{O}$ ratio would rapidly become >2.5 (*i.e.* that determined for molybdenum trioxide) as the ratio of metal to metal oxide increased. Whilst bearing in mind that this ratio is an approximate value (Section 5.3.4) one or two samples do show $^{Mo}/_{O}$ ratios higher than that found for the trioxide; these samples are those prepared using the highest atomiser voltages of ∿140 or 180V and suggest that metal evaporation might just be starting to be of significance at the highest voltages used. However there was never any evidence of pyrophoric metal particles when bringing the substrate into air. Also if the temperatures used were insufficient for molybdenum evaporation then it would be anticipated that there would have been no problem in evaporating chromium.

Use of an optical pyrometer to measure the approximate filament temperatures at the various supply voltages (Table 5.6) effectively resolves this problem showing that metal evaporation is not likely to be significant at these supply voltages; the temperatures used are well below that necessary for significant evaporation of molybdenum metal (∿2, 500$^{o}$C).[177]

TABLE 5.6

| Supply Voltage (V) | Approximate Filament Temperature ($^{o}C$) |
|---|---|
| 60 | 760 |
| 90 | 870 |
| 120 | 1030 |
| 150 | 1220 |
| 180 | 1280 |

### 5.4.2 Plasma Etching

The introduction of molybdenum into a fluoropolymer using a metal target cathode has been explained in terms of the formation of a volatile fluoride ($MoF_6$) which is incorporated into the growing polymer. The known hydrolysis of molybdenum hexafluoride would explain why, after standing in air, ESCA analysis suggested that molybdenum was present mainly as its oxides. From the available data then, can it be determined whether plasma etching of the filament is the main route to metal incorporation?

Firstly, when no voltage is applied to the atomiser there is no molybdenum incorporation into a perfluorobenzene plasma polymer (Table 5.1) and this argues against a purely etching mechanism of incorporation, though a temperature-assisted mechanism is not ruled out by this result. The fact that (as has already been mentioned, Section 5.3.3) molybdenum can be deposited on an aluminium substrate by heating the atomiser, in the absence of a plasma, shows that processes other

than etching can occur, though the amounts of molybdenum deposited in this experiment are difficult to correlate with the other results. One of the conclusions of the study was that metal incorporation and polymer deposition were occurring independently and this appears inconsistent with the etching polymerisation mechanism; certainly the observation of molybdenum species separate from the plasma polymer (*e.g.* directly under the atomiser in certain cases) is strong evidence that the trapping of volatile fluorides by the polymer matrix is not the mechanism of metal incorporation in such regions.

However, in the present work some of the $F_{1s}$ spectra recorded clearly exhibit two different fluorine environments, and from their binding energies of ∿689 and ∿686eV these can readily be assigned as covalent fluorine and fluoride. The former obviously derives from fluorine in the perfluorobenzene polymer, and this component is always present. It is the fluoride peak which is only sometimes present; it is certainly tempting to assign this peak to the presence of metal fluorides in the polymer surface. This would be in agreement with earlier assignments of metal incorporated plasma polymers; the variable nature could then be explained by the hydrolysis of the fluoride in storing the sample in air (the ease of hydrolysis of $MoF_6$ has already been noted).[171] However, in the present work two fluorine environments are only observed for those samples where it has already been suggested that deposition is slow (judged mainly by the low $^{F}/_{C}$ ratio and the prevalence of C-H and perhaps C-CF environments contrasting with the plasma polymer's characteristic structure containing $CF_2$ and $CF_3$ groups). For example in the results obtained from

the experiment employing an atomiser-coil separation of 23½ cm., whilst two fluorine environments were evident for samples 1 and 2 only one was observed for sample 3; conversely the characteristic plasma polymer structure was evident in the $C_{1s}$ spectrum of sample 3 but not in the spectra recorded for samples 1 and 2. Previously, from the observation of two fluorine environments for a perfluorobenzene plasma polymer it has been suggested that the fluoride anion may be formed at the substrate-polymer interface.[121,122] In view of the correlation in the present work of, low $^{F}/_{C}$ ratios and high percentage intensity of the $C_{1s}$ component at 285.0eV, with observation of the fluoride signal, it seems likely that the fluoride derives from the substrate-polymer interface, rather than from the incorporation of metal fluorides. This is in accord with the observation that the $^{Mo}/_{F_{ionic}}$ ratio was far from constant.

The conclusion, that metal etching is not an important part of the metal incorporation process, is in agreement with the theory that the $^{F}/_{C}$ ratio of the active species needs to be $\geq 2$; not many such species are expected to be present in a perfluorobenzene plasma since the stoichiometry of the feed is 1:1 and because polymerisation is thought to be largely molecular in nature.

### 5.4.3 The formation of Molybdenum Trioxide

It is well known that molybdenum trioxide sublimes readily and since it is fairly clear from the preceding two sections that metal incorporation is not by evaporation of molybdenum or by the formation of volatile fluorides, the most likely method is one in which the oxide is formed on the filament

surface and is then sublimed off. The important question then is, what leads to the formation of the oxide layer?

There are two ways in which the molybdenum surface could be oxidised. Molybdenum metal does not react with oxygen at ambient temperature, but at red heat ($\sim$6-700$^{o}$C) readily combines to give the trioxide;[189] so the use of a hot filament in low vacuum could lead to oxide formation. An alternative method of oxidation could be plasma oxidation due to any oxygen species present either in the nitrogen or perfluorobenzene plasmas. For either process to occur there must be oxygen in the reactor; if at the base pressure of $\sim$0.06T (a limit imposed by any leaks in the reactor and the vapour pressure of the pump oil) there is sufficient oxygen to oxidise the filament then this is a fundamental problem of this method of metal incorporation and the only solution is to move into a lower pressure regime. However there are other possible sources of oxygen species and attempts may be made to eliminate some of these in order to determine whether this decreases the amount of molybdenum trioxide present in the prepared surface. With the standard method, outlined in Section 5.2 there appear to be four possible sources of oxygen species:

(i) that in leaving the reactor after cleaning with a nitrogen plasma, oxygen/moisture accumulate again overnight;

(ii) that oxygen species are introduced with the substrate and that since the nitrogen plasma was run prior to its introduction, these are not eliminated from the reactor;

(iii) the sputtering of the reactor walls may lead to reactive oxygen species. For example it has been suggested that bombardment of the reactor wall by $N_2^+$ ions formed in a nitrogen plasma can lead to the formation of nitrous oxide (NO) by the

sputtering of molecular silica ($SiO_2$) into the plasma; this is the explanation given for the oxidation of silicon in a nitrogen plasma;[190]

(iv) despite degassing, there might be sufficient oxygen in the organic feed to cause some oxidation. (This might be a contributory source but it cannot be the sole one since molybdenum can be detected on a substrate following heating of the coil, in the absence of plasma).

To gain some insight into the possible cause of molybdenum oxidation a different experimental procedure was tried. The substrate was introduced, the reactor cleaned with a nitrogen plasma as before but the coil was not heated up. The experiment was done immediately after this with the coil being allowed to equilibrate for ∿5 minutes before the perfluorobenzene was introduced and the plasma deposition commenced. The two different procedures were compared using values of 3½ cm., 90V, 0.15T, 50W and 10 mins. for the parameters. This procedure almost totally eliminates the first possible source of contaminating oxygen species (i). The nitrogen plasma, run before heating the coil, should cause desorption of most oxygen species so that thermal oxidation by species introduced with the substrate should be greatly reduced (ii); plasma oxidation by these species can theoretically occur in both the procedures used and there does not appear to be an easy method of eliminating such a process (ii). (This second procedure introduces a different problem, that sputtering of the oxide surface might become an important method of deposition on to the substrate). Sputtering of the reactor walls (iii) is inherent in the use of plasmas and if this was the main mechanism of molybdenum oxid-

ation it would also be a fundamental problem of this method. This second procedure also leaves open the possibility of dissolved gases in the organic feed (iv). The results of the two experiments are shown in Table 5.7. The conditions used correspond to significantly higher power input per unit

TABLE 5.7 (Molybdenum/Carbon Intensity Ratios)

| Sample Position | 1 | 2 | 3 |
|---|---|---|---|
| Standard Procedure | 0.24 | 0.05 | ∿0 |
| Modified Procedure | 0.07 | ∿0 | ∿0 |

monomer than for the standard experiments (*c.f.* 20W, 0.2T before; 50W, 0.15T here) but whether or not deposition is decreased due to the increased competitiveness of ablative processes, the $C_{1s}$ spectra still show the characteristic structure of the plasma polymer. The results indicate that the revised procedure leads to a reduction of the amount of molybdenum incorporation, but total elimination has not been obtained and experiments attempting to incorporate a different metal (Al, Cr) still led to samples containing significant amounts of molybdenum in comparison with the other metals.

## 5.5 The Importance of the Work

Considering the aim of the experiment, the fact that molybdenum trioxide sublimation appears to be responsible for the molybdenum incorporation is perhaps a disappointing result. However the work does draw attention to several important points.

One feature which has not been given due attention in the literature pertaining to metal incorporated plasma polymers is the importance of pre-deposition procedures for plasma reactors containing a metal target or filament, and in particular, the chemical state of these metal surfaces. For example, whilst acknowledging the presence of an oxide layer on their molybdenum target surface,[173] Kay and Dilks have made no assessment of whether sputtering of this layer might significantly contribute to the metal incorporated in the polymer; in view of the fact that they offer little information on the thickness of the polymer samples prepared this is a notable omission since it is evident from the present work that in preparing thin films with low metal content, such processes could be significant.

In respect of the importance of pre-deposition procedures it should be noted too, that the use of a nitrogen plasma for cleaning the reactor is potentially problematical. It was remarked upon earlier (Section 4.2.4) that nitriding of metals has been achieved using glow-discharges.[145-149, 190,191] Usually this is only found to be efficient when using mixtures of nitrogen and hydrogen; some nitriding has been possible in a nitrogen plasma but this occurs when using higher pressure ($\sim$1T), higher power ($\sim$300W) and over a much longer period of time ($\sim$6-8 hrs.). Therefore whilst it is possible that the filament surface may have been nitrided the extent to which this might have occurred is uncertain and probably minimal; more important though, is the fact that whether or not the surface may have been nitrided to some degree, the oxide consistently forms.

This work has led to the incorporation of molybdenum oxide rather than the metal. In this respect the samples analysed here are similar to many others where the metal is thought to be present as the oxide, and there has been some interest in the literature specifically in surfaces modified by the inclusion of metal oxides.[192] The field of incorporation of metals into plasma polymers is now clearly divisible into those methods incorporating a metal compound into a polymer matrix and those which lead to the metal being chemically bound into the polymer. If the inclusion of a metal oxide into the plasma polymer were the main objective then the processes occurring might be enhanced by deliberately trying to oxidise the metal surface prior to plasma deposition. To this end two experiments were performed (using the modified start-up procedure of introducing the substrate right at the beginning of the experiment, and then cleaning with a nitrogen plasma) in which, following the nitrogen plasma, a 100W, 0.2T oxygen plasma was struck and continued for 10 minutes. In the first of these experiments (0.1) the coil was heated up (A.V.=90V) and allowed to equilibrate for about 5 minutes before allowing in perfluorobenzene to 0.15T and initiating a 50W plasma lasting for 10 minutes. When the coil was first heated up the pressure rose substantially to ∿0.09T but then dropped back to ∿0.06T during the equilibration period. Another experiment was carried out using an oxygen plasma treatment (0.2) in which the atomiser voltage was not applied until the tenth minute of the plasma deposition. The $^{Mo}/_{C}$ ratios of these two experiments, together with a reference run using no oxygen plasma treatment, are given in Table 5.8. It is obvious that the oxidation treatment leads to higher molybdenum oxide

TABLE 5.8 (Molybdenum/Carbon ratios)

| Sample Position | 1 | 2 | 3 |
|---|---|---|---|
| - No $O_2$ plasma | 0.07 | ∿0 | ∿0 |
| 0.1 - $O_2$ plasma | 0.12 | 0.04 | ∿0 |
| 0.2 - $O_2$ plasma (10th minute) | 0.54 | 0.17 | ∿0 |

incorporation. It also appears that, as would be expected, the plasma treatment leads to a surface oxide[188] which is rapidly sublimed on heating the coil. The results suggest that if the oxidation/sublimation were made a dynamic process then it might be possible to obtain continuous metal oxide incorporation into a growing polymer film.

## 5.6 Summary

Attempts to incorporate metal by evaporation into a plasma polymer, by introducing a simple resistively-heated molybdenum basket into a plasma flow-reactor of well-established design, were unsuccessful, but instead molybdenum (V/VI) oxides were found to be present in the analysed samples. Variation of five system parameters led to the conclusion that the processes of metal incorporation and polymer deposition were occurring independently. The mechanism by which molybdenum is transferred from the filament to the substrate was discussed, and it was concluded that the mechanism is largely the straightforward sublimation of molybdenum trioxide from the filament surface. The work is discussed in terms of the importance of pre-deposition reactor cleaning procedures which,

in this type of system, have previously been ignored in the literature. The highest molybdenum/carbon ratio determined for metal incorporated into a plasma polymer (as opposed to a plasma deposit) was for a sample prepared between the glow-discharge coil and the resistive heater, and corresponded to a film with 29 weight per cent molybdenum. If the inclusion of molybdenum oxide is a desired result then it was suggested that increase of this value is probably possible by making the formation and sublimation of oxide a continuous process.

# CHAPTER SIX

## AN MNDO SCF MO INVESTIGATION OF SOME STRUCTURAL ISOMERS OF THE PERFLUORO DIAZINES (PYRIMIDINE, PYRAZINE AND PYRIDAZINE) OF RELEVANCE TO THEIR PLASMA POLYMERIZATION

## 6.1 Introduction

ESCA studies of plasma polymers produced from the three isomeric tetrafluorobenzenes showed that whilst the component structural features of the $C_{1s}$ envelope were consistent with substantial rearrangement of the feed compounds, the gross structure and the rates of deposition for the isomers were essentially the same and this was taken as evidence of the interconversion of the isomers during the plasma process.[123] This experimental conclusion is in accord with earlier results which showed that positional isomers of substituted benzenes could be obtained by passing them through a plasma reactor, and it was suggested that this ring-scrambling most likely occurred through the intermediacy of valence isomers.[99]

In an MNDO SCF MO investigation,[123] the heats of formation calculated for the Benzvalene, Prismane and Dewar benzene valence isomers (*i.e.* those associated with ring scrambling processes) suggested that these species could be readily formed from the first and second excited singlets of the tetrafluorobenzenesand that a significant percentage (∿40%) of the electrons in a "cool" plasma, with an estimated average energy of ∿2eV, would be capable of producing these states. The heat of formation of Benzyne intermediates was considered to be too great for elimination prior to reaction to be significant in the plasma polymerisation of the tetrafluorobenzenes,and this was used to explain the similarity of the $^{F}/_{C}$ stoichiometries of the starting compound and the polymers. Fulvene isomers were found to be the closest in energy to the parent aromatic in both the ground state and cation manifolds,[126] and the investigation revealed that the possible tetrafluorofulvenes were all of similar energies. The Hexadienynes were somewhat

higher in energy than the fulvenes. The involvement of these two lowest energy valence isomers (*viz.* the fulvenes and hexadienynes) in the plasma polymerisation of the tetrafluorobenzenes readily accounted for the presence of $CF_2$ structural features, whilst $CF_3$ functional groups were considered to arise from fluorine migration. The large excess of the parent aromatic present in the partially ionised gaseous medium means that this species is likely to be involved in polymer formation and it was shown how cycloaddition reactions of the parent aromatic structure with valence isomers such as fulvene, hexadienyne and benzvalene, could lead to the formation of highly cross-linked structures.

In a study of the perfluorodiazines it was found that the isomers (pyridazine, pyrimidine and pyrazine) exhibited distinctively different rates of deposition,[129] and from this it was suggested that ring scrambling prior to polymerisation is of less importance for this series than for the homocyclic analogues. The existence of perfluoroalkyldiazine valence isomers is well established experimentally[193-196] and it is reasonable therefore to assume *a priori* that these isomers may well be of importance in the plasma polymerisation of the perfluorodiazines. The present work considers some aspects of the relative energetics of the neutral (ground and excited state) and cationic species of the isomeric perfluorodiazines. For comparison purposes consideration has been given to acyclic as well as heterocyclic structures. The emphasis is on the potential explanation of differences in plasma behaviour with respect to the corresponding tetrafluorobenzenes.

## 6.2 Computational Details

Geometry optimisations of the ground states of all the species in Figure 6.1 have been performed using the MNDO method[197,198] incorporating the DFP optimisation routine.[199] Initial geometries were estimated from standard bond lengths and angles[200] where possible.

Single SCF calculations using the optimised ground state geometries were carried out for the cation, first excited singlet and first excited triplet states for one of each of the isomers containing nitrogens at 1,3 positions.

The calculations were carried out on a CDC7600 at UMRCC. Typically the C.P.U. time for a complete geometry optimisation was about 300 seconds. Full details of the optimised geometries are not essential to the discussion presented but salient features are pointed out.

## 6.3 Results and Discussion

### 6.3.1 Ground States

It is convenient in discussing the data to briefly consider the overall energetics (and where appropriate comments on the geometries) for each of the aza substituted isomers of a given structural type.

#### (i) Parent perfluoro heteroaromatics

Although there have been a number of theoretical studies at a variety of levels of sophistication of the parent ring systems of pyrazine, pyrimidine and pyridazine[197,201-204]

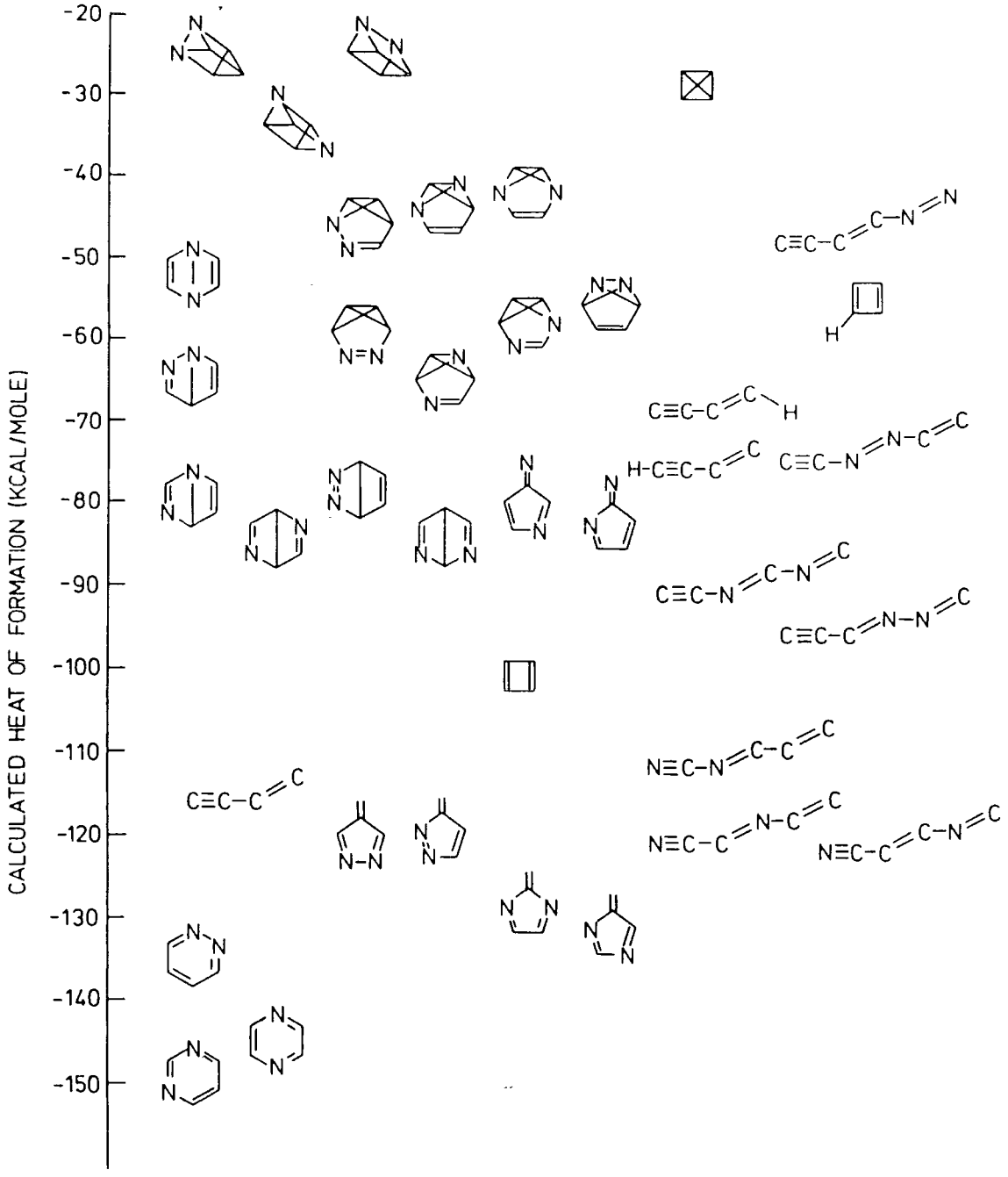


Figure 6.1 Heats of formation of the perfluorodiazines, some of their structural isomers and related compounds

there have been no previous studies of the relative energies for the geometry optimised perfluorinated derivatives. For the hydro series the relative heats of formation fall in the order 1,4∿1,3>1,2 diazine, the pyrimidine (1,3) and pyrazine (1,4) being the more stable by ∿20 kcal/mole.[205] The data displayed in Figure 6.1 indicate a relative stabilizing effect of fluorine substitution (with respect to the pyrimidine) for the pyridazine and a relative destabilizing effect for the pyrazine; the predicted stability order therefore being pyrimidine>pyrazine>pyridazine.

As expected the optimised geometries give planar systems in all three cases; the computed bond lengths in each case closely following those that might have been anticipated on the basis of tables of standard bond lengths.[200]

(ii) Diazafulvenes

It was previously noted that for fluorinated benzenes the valence isomer closest in energy terms to the planar aromatic system is that appropriate to the fulvene structure.[123] In the particular case of the tetrafluorofulvenes MNDO SCF MO computations indicate that the various possible isomers have closely similar energies.[123] In this respect the introduction of nitrogens into the system provides a striking contrast. In this study 6 of the possible diazafulvenes were investigated and the results are displayed in Figure 6.1. It is clear from this that structures involving N-F bonds are thermodynamically unstable with respect to isomers having nitrogen as part of the five-membered ring system; the energetic preference typically

being ∿40-50 kcal/mole. For structures involving ring nitrogen there is again a small energetic preference for the 1,3 disposition.

The optimised structures were planar with C-C and C=C bond lengths where appropriate of ∿1.49Å and 1.37Å indicating a degree of conjugation in these isomers.

(iii) Diazadienynes

The previous investigation of isomers of the tetrafluorobenzenes[123] indicated that fluorodienynes were at higher energy than the fulvene valence isomers but lower in energy than the Dewar benzene, prismane, and benzvalene isomers. The data in Figure 6.1 reveal that the energies of the diazadienynes are strongly dependent on the position of nitrogen substitution with particular preference being for structures encompassing -C≡N. By contrast the structure involving N-F bonds is destabilized whilst structures involving N-N bonds also tend to be relatively unfavourable. The net effect is that for the isomers involving the thermodynamically favourable -C≡N group the energies are comparable with those for the most favourable fulvene structures.

The most interesting feature arising from the optimisation of these isomers is the non-planarity of 3 of the 7 structures considered. The relevant twist angle, abcd (180° in the planar isomers) was found to be ∿147° when b and f are nitrogen, and ∿40° when either b and d or d and f are nitrogen. Heats of formation calculated for five values of this twist angle indicate that there is a balance of two main factors. The loss

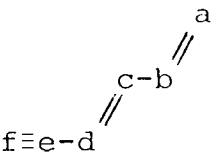


of conjugation energy caused by deviation from planarity, is balanced by a decrease in repulsive interaction of non-bonded atoms, predominantly fluorine-fluorine and nitrogen-fluorine. A plot of these interactions and the variation of heat of formation with twist angle is shown for one of the isomers in Figure 6.2. In this case a twist angle of 180° is clearly

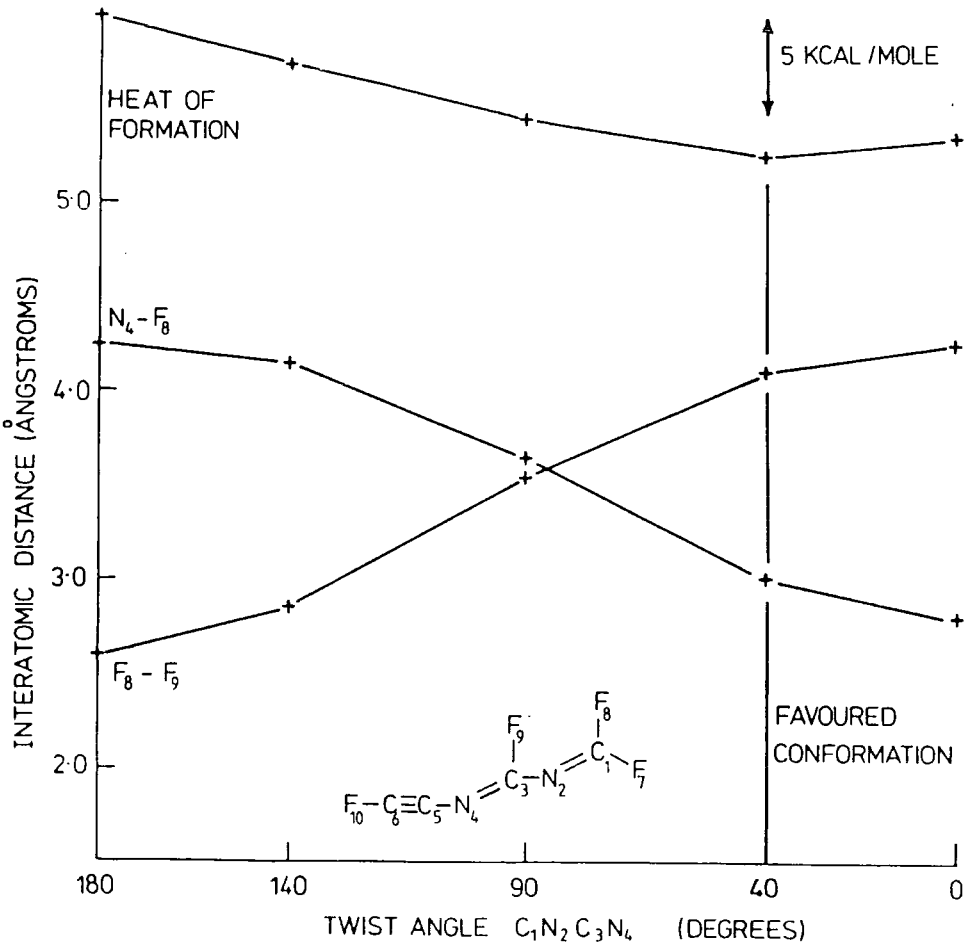


Figure 6.2 Effect of varying twist angle in a hexadienyne system

unfavourable since the F-F interatomic distance is only 2.58Å, significantly lower than twice the crystallographically determined Van der Waal's radius for $F_2$ (1.5-1.6Å). However, the potentially favourable conformation, in terms of F-F interactions and conjugative stabilisation, with zero twist angle, involves an N-F distance of 2.78Å, again, lower than would be expected from Van der Waal's radii. Thus the twist angle of $40^{\circ}$ in the fully optimised geometry can be rationalised, since the N-F interatomic distance is 3.02Å, the F-F distance is still favourable, and the conjugation energy is not significantly decreased.

(iv) Diaza Dewar Benzenes

In the tetrafluorobenzene series the valence isomers next in energy after the hexadienynes are the Dewar benzenes.[123] As might have been anticipated whilst the various positional isomers for the tetrafluoro derivative span a very small energy range, the introduction of the nitrogen substituents has a substantial influence on the overall pattern. Structures involving >C=N tend to be energetically favourable with respect to those which involve nitrogen in a bridgehead position. It is interesting to note that there is again a preference for structures involving nitrogen in a 1,3 disposition with respect to those involving a 1,2 arrangement, however, the preference is small. For the most favourable cases the total span in energy for 1,2, 1,3 and 1,4 substitution patterns is only 6kcal/mole which is substantially less than for the heteroaromatic ring systems themselves.

The optimised structures for the Diaza Dewar benzenes have an average carbon-carbon bridgehead bond length of ~1.64Å which seems large until compared with the experimentally determined value of 1.63Å for the hexamethyl Dewar benzene.[206] The dihedral angle in these systems is also close to an experimental value of 117.7°, [207] determined for perfluoro-Dewar Benzene.

(v) Diazabenzvalenes

Seven positional isomers have been studied and their heats of formation are shown in Figure 6.1. A straightforward correlation between the positions of nitrogen substitution and the heats of formation is not apparent, though there appears to be preference for nitrogen at the bridgehead position joining the two cyclopropyl rings, the bond angles of about 60° at this strained position being less unfavourable to nitrogen where lone pair-bond pair repulsions are involved, rather than the bond pair-bond pair repulsions of a C-F unit.

The range spanned by these nitrogen substituted isomers is again greater than the tetrafluorobenzvalene analogues.

In all the isomers the C-C or C-N bond common to the two cyclopropyl rings is shorter than the others involved in the bicyclobutyl ring system overall. This was also found for the tetrafluorobenzvalenes, but of course contrasts with the result for bicyclobutane itself. The dihedral angle of the bicyclobutyl ring was found to increase with increasing nitrogen substitution of that ring, which reflects the increasing bond lengths along the series N=N, C=N, C=C, involved in the "pendant group".

(vi) Diazaprismanes

The 1,3 substituted isomer is again energetically preferred by ∿9 kcal/mole. This again emphasises the fact that a ring nitrogen substituent gives rise to a greater spread in energies for a given structural isomer than fluorine substitution.

The optimised structures for the prismanes indicate a highly strained system with all interatomic distances corresponding to regular single bonds.

(vii) Summary of Ground State Results

Although there is a spread in the heats of formation for each isomer, the general trend of parent<Dewar benzene<benzvalene<prismane is the same as that observed experimentally for the hexamethyl[208] and perfluoromethyl[209] homocyclic analogues, and observed in various theoretical treatments of the parent benzene isomers.[210-212] This ordering was also found for the MNDO study of the tetrafluorobenzenes[123] in which the difference between the most and least stable isomers was ∿100 kcal/mole compared to ∿125 kcal/mole in the present investigation. Relative to the parent aromatic systems the diaza Dewar benzenes and benzvalenes are destabilised by ∿10 kcal/mole compared to the tetrafluorobenzene series, whilst for the prismanes the destabilisation is ∿20 kcal/mole. However, the heats of formation of the diazafulvene isomers show a slight stabilisation compared to the tetrafluorofulvenes. The greatest difference between the results of Figure 6.1 and the tetrafluorobenzenes is the large range of energies spanned by the diazahexadienynes, the origin of which was discussed in Section (iii).

### 6.3.2 Excited States

#### (i) Cations

First ionisation potentials calculated by Koopmans' Theorem,[213] hence corresponding to a 'frozen' final state, for the heteroaromatic systems tend to be over estimated by about 0.4 eV compared to experimentally determined UPS values.[214] Heats of formation have been calculated for the 1,3 isomers in the cation manifold using ground state optimised geometries which for the perfluoro-pyrimidine gives a ΔSCF relaxation energy of 0.3eV. The data displayed in Figure 6.3 show that

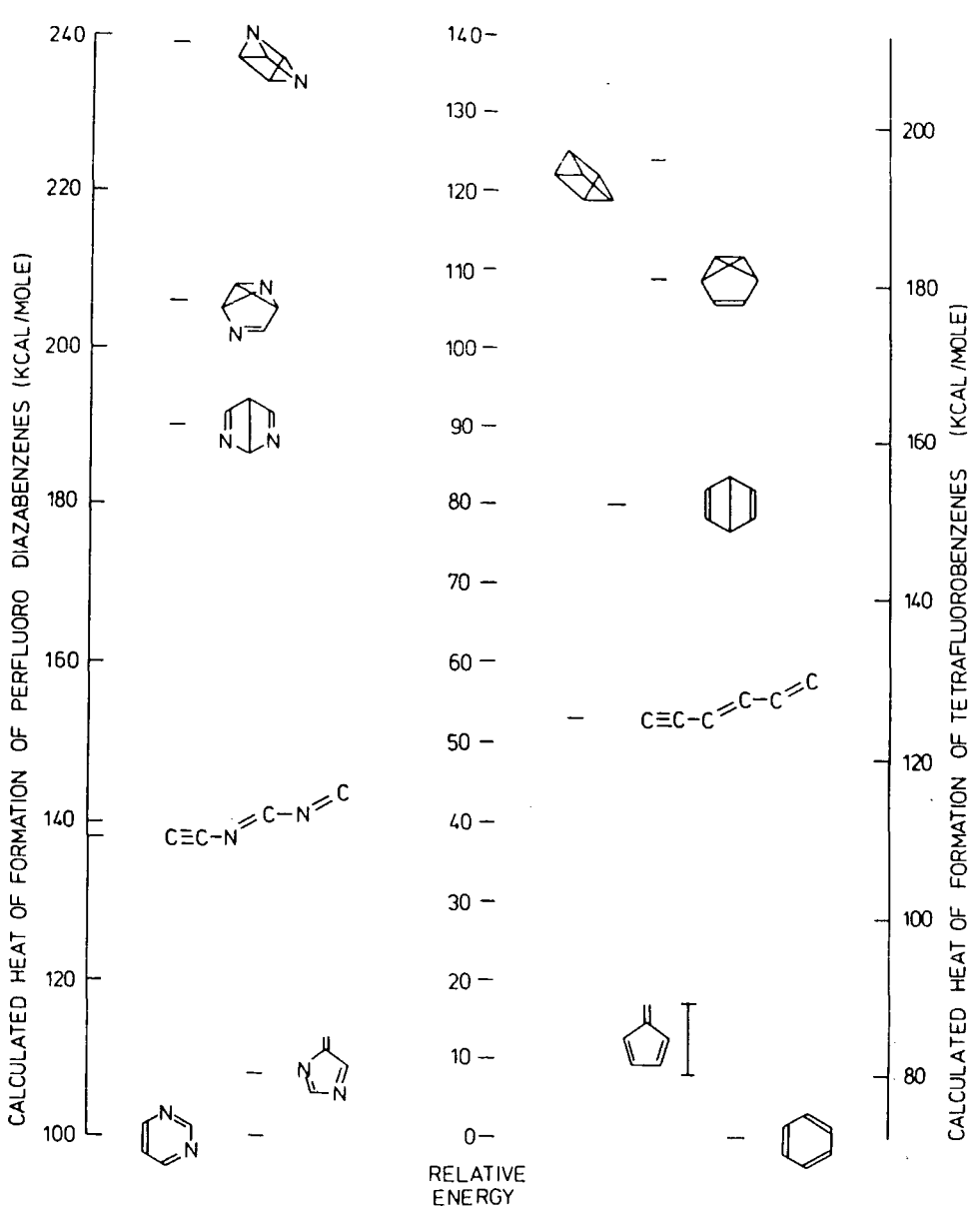


Figure 6.3 Heats of formation of the cations of the perfluoro 1,3-diazabenzenes and some of the tetrafluorobenzene structural isomers.

although the ordering is the same as for the neutral species, the energy separation between the isomers is different. In particular, the fulvene is stabilised with respect to the hetero-aromatic system compared to the ground state manifold. This observation is consistent with UPS data for homocyclic benzene and fulvene[215] where the ionisation potential of fulvene is ∿0.7eV lower than benzene, indicating an increased stability of fulvene in the cation manifold.

Of the other isomers whilst the prismane, Dewar benzene and benzvalene are destabilised by about 25 kcal/mole by cation formation, the hexadienyne, significantly, is stabilised by 18 kcal/mole, with respect to the parent. It is interesting to compare these results with those for the tetrafluoro-benzene analogues (Figure 6.3) where the cation heats of formation show destabilisation of ∿25 kcal/mole for prismane and benzvalene cations, ∿16 kcal/mole for the Dewar isomer and no significant change for the hexadienyne, compared with the parent. The stabilisation for the fulvene system is comparable with that noted for the heterocyclic system.

(ii) Singlet and triplet states

First excited singlet and triplet state heats of formation were calculated for the same 1,3 isomers as were investigated in the cation manifold, and the results are shown in Figure 6.4. Singlet-triplet splittings of about 50 kcal/mole and wave function analysis for the two singly occupied MOs indicate that the MNDO SCF procedure has locked onto a $\pi\pi^*$ configuration for the aromatic, fulvene, hexadienyne and benzvalene isomers. In contrast for the prismane and Dewar benzene

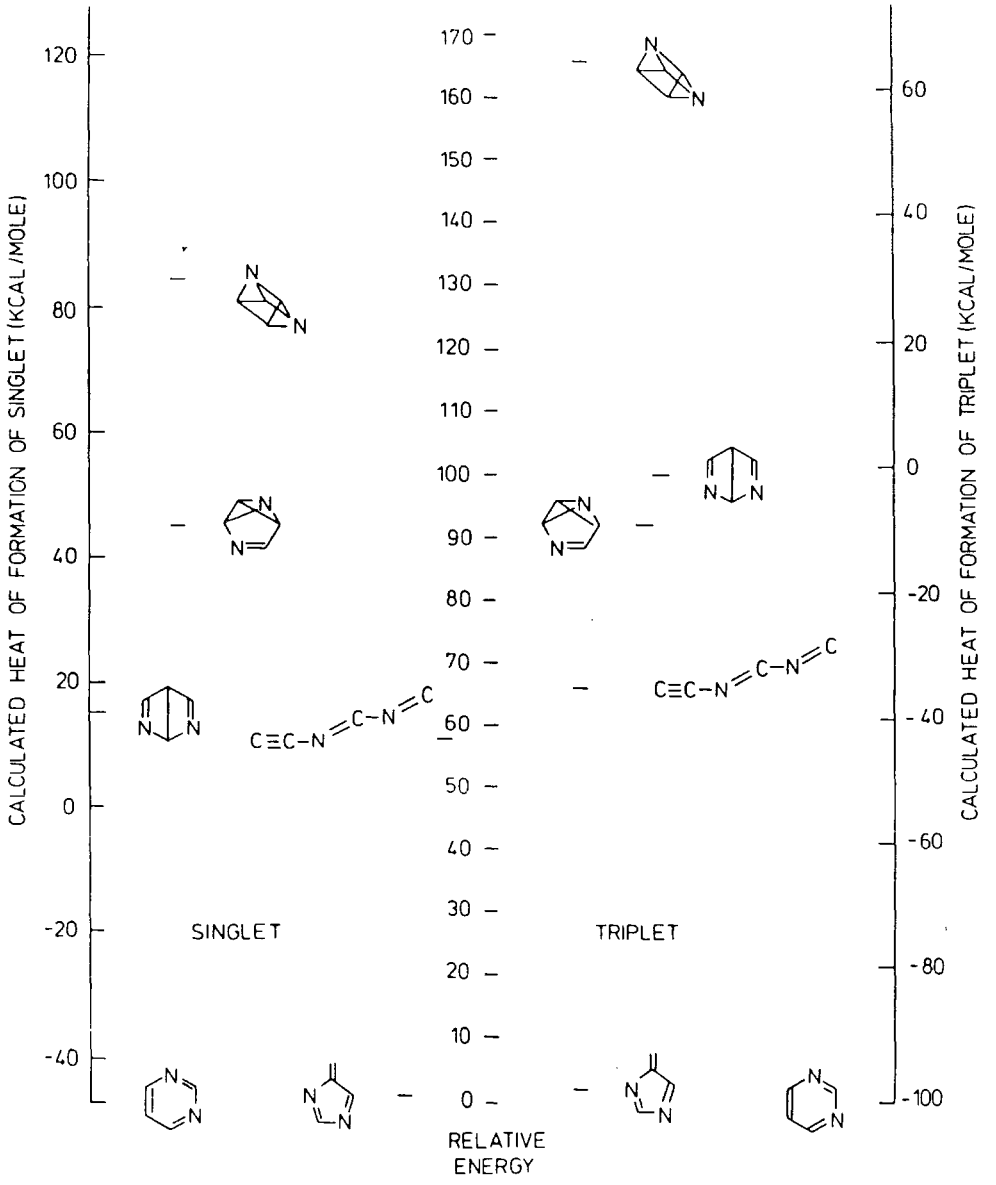


Figure 6.4 The heats of formation of the singlet and triplet excited states of the perfluoro 1,3-diazabenzenes

the lower singlet-triplet splitting and σ-π inseparability means that the nature of the excited state cannot be assigned in a clear cut manner. The singlet and triplet $\pi\pi^*$ states of perfluoropyrimdine are calculated to be 4.45 and 2.07 eV above the ground state respectively. The experimentally observed band maximum for the $\pi \rightarrow \pi^*$ transition involving singlet states is at 241 nm[216] corresponding to an energy separation of 5.14 eV, in tolerable agreement with that calculated theoretically.

A calculation on perhydropyrimdine again gives the first excited singlet as $^1\pi\pi^*$ whereas it is well known to be $^1n\pi^*$.[217] Similarly MNDO predicts the first triplet to be $^3\pi\pi^*$, some 2.7eV above the ground state, whereas the first triplet is known to be $^3n\pi^*$ at 3.6eV,[218] with the $^3\pi\pi^*$ being some 0.1-0.2 eV higher still.[219] However, we will not consider these points further, since our main theme is the relative energetics of these species.

The benzvalene is found to be slightly destabilised with respect to the heteroaromatic (∿8 kcal/mole) in both singlet and triplet manifolds. The hexadienyne is similarly destabilised in the triplet state, but in the singlet its relative energy is the same as that in the ground state. Thus these two isomers are useful markers by which to identify the relative changes in energy of the others. The major difference between the ground and excited state manifolds is the stabilisation (by 15-20 kcal/mole) of the fulvene isomer with respect to the heteroaromatic, in both the singlet and triplet states, bringing it to within 2 kcal/mole in the latter case, *i.e.* certainly within the error limits of MNDO.[197,198] The Dewar benzene on the other hand, whilst having the same relative energy in the ground and singlet states, is considerably destabilised in the triplet state (∿35 kcal/mole), so that its energy becomes comparable with that of benzvalene. The prismane is destabilised in both excited states, but the effect is much greater in the triplet (∿49 kcal/mole) than in the singlet (∿14 kcal/mole).

Thus the overall pattern in the excited states is a destabilisation of the prismane and a stabilisation of the fulvene structures, whilst the other isomers are relatively unchanged.

### 6.3.3 Application to Plasma Polymerisation of these Compounds

The object of these calculations is to attempt to rationalise experimental data obtained on the structure and composition of plasma polymers obtained from the isomeric perfluorodiazines in comparison with the isomeric tetrafluorobenzenes.

It is important to consider that the electron distribution in a cool plasma is typically Maxwellian[98b] with an average electron energy of ~2 eV and a tail extending beyond the ionisation potential of these systems. The electron flux will interact with the monomer flux in three primary ways giving rise to electron attachment, excitation and ionisation. From the typical distribution pattern of electron energies the typical electron flux involved in each of these 3 processes is approximately in the ratio 60:40:0.4[123] respectively. However, for purposes of comparison only the ground state manifold has been considered in this discussion of the relative energetics of the perfluorodiaza- (Figure 6.1) and tetrafluorobenzene (Figure 6.5) isomers relevant to the plasma polymerisation of these compounds.

#### (i) Interconversion of parent isomers

Table 6.1 details the energetics of the most favourable routes of interconversion between the parent isomers[220-223]

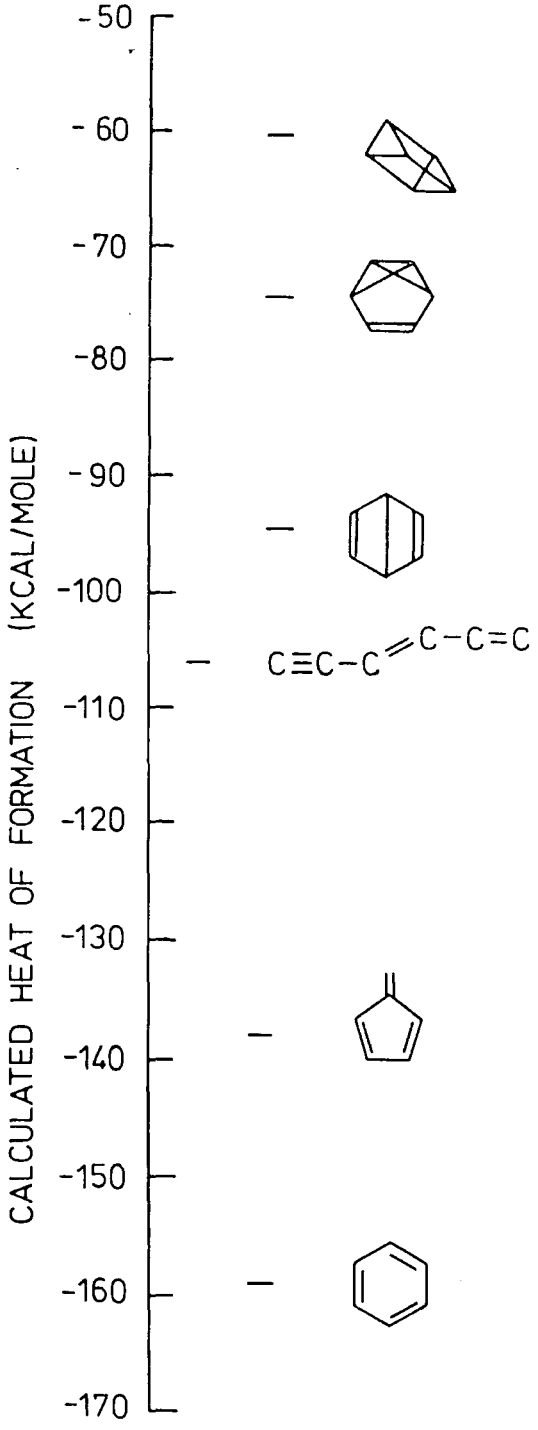


Figure 6.5 The heats of formation of some of the tetrafluorobenzene structural isomers.[123]

TABLE 6.1 Energetics of Parent Isomerisation (kcal/mole)

| TETRAFLUOROBENZENES | $\Delta H_{eb}$ | $\Delta H_R$ |
|---|---|---|
| *via* Dewar | + 64.5 | ∿ 0 |
| *via* Dewar and prismane | + 98.5 | ∿ 0 |
| *via* Benzvalene | + 84.5 | ∿ 0 |

| DIAZABENZENES | $\Delta H_{eb}$ | $\Delta H_R$ |
|---|---|---|
| 1,2 - 1,3 *via* Dewar and prismane | + 103 | - 14 |
| *via* Benzvalene | + 89 | - 14 |
| 1,2 - 1,4 *via* Dewar | + 51 | - 10 |
| *via* Benzvalene | + 89 | - 10 |
| 1,3 - 1,4 *via* Dewar and prismane | + 117 | + 4 |
| *via* Benzvalene | + 91 | + 4 |

---

and these are shown schematically in Figure 6.6. The value $\Delta H_{eb}$ is simply the difference between the calculated heats of formation of the starting compound and the least stable isomer involved in the conversion. Similarly $\Delta H_R$ is the energy separation of the initial and final isomers thus, a value of $\Delta H_{eb}$ for the reverse process is formed from $\Delta H_{eb}$ (forward) - $\Delta H_R$. Comparison with the tetrafluorobenzene data is facilitated by taking an average of the $\Delta H_{eb}$ values for the forward and reverse processes of the diaza series. This indicates that the interconversion of the parent isomers *via* the prismane (which also involves Dewar benzene intermediates) is approximately 14 kcal/mole less favourable for the diaza-compounds, compared with the corresponding tetrafluorobenzene positional isomerisation. Similarly, interconversion involving just benzvalenes is of the

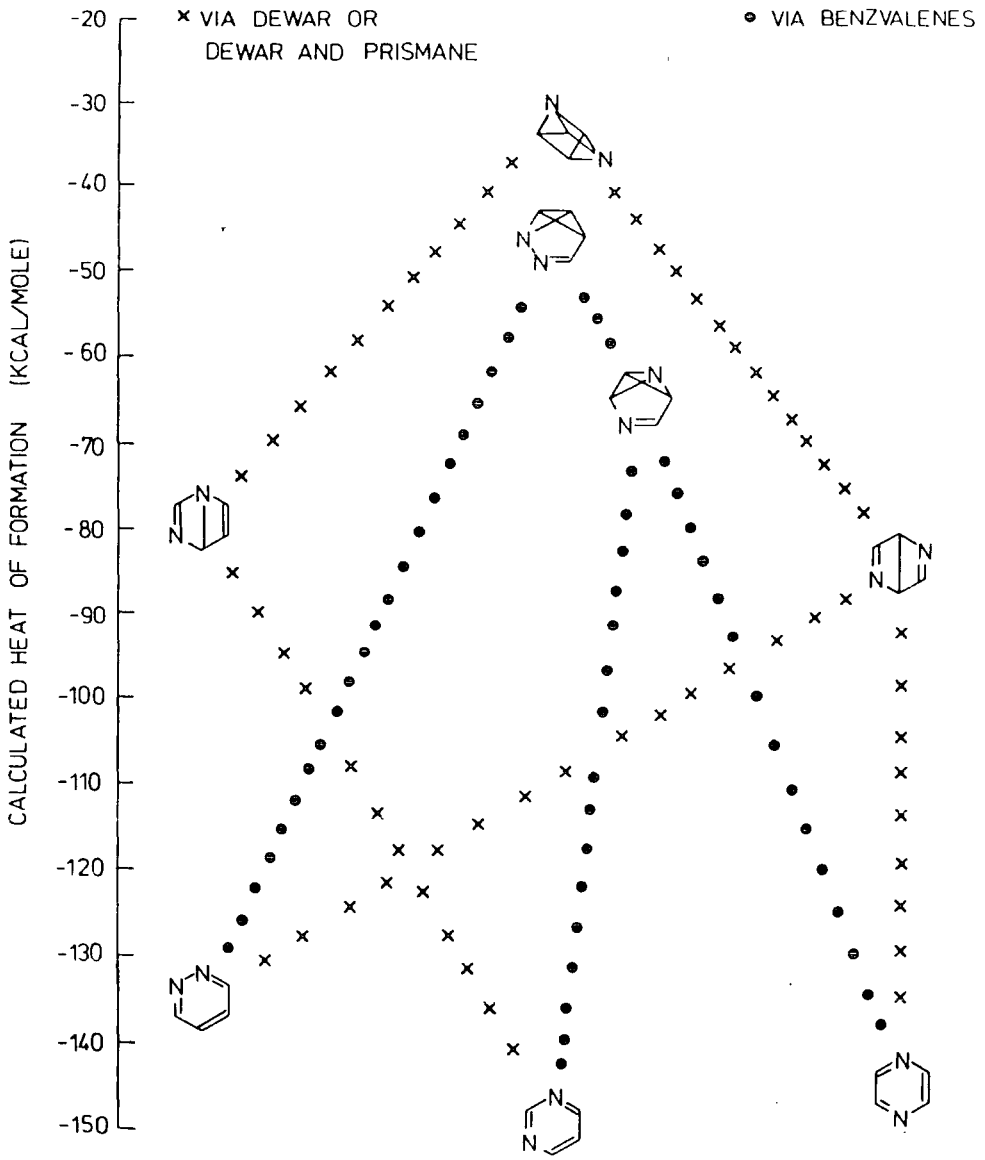


Figure 6.6 Energetically most favourable routes of parent isomerisation

order of 10 kcal/mole less favourable. The 1,2-1,4 diaza transformation, the only one to involve Dewar benzenes alone, is seen to be more facile (∿10 kcal/mole) than the equivalent process in the homocyclic series, a result which is not surprising when one considers the large body of literature concerning the mechanism of this process for the diazabenzene case.[193] Thus in general formation of isomers which would be expected to be involved in ring scrambling is energetically more favourable in the case of the tetrafluorobenzene series. However, isomers which are not involved in ring scrambling processes,

*viz.* the fulvenes and hexadienynes, are predicted to be formed more easily in the diaza- series as can be seen from the $\Delta H_R$ values in Table 6.2, the formation of the diazahexadienyne isomers being more favourable by an average of ∿20 kcal/mole.

TABLE 6.2 Energetics of Polymer-Precursor Formation (kcal/mole)

| TETRAFLUOROBENZENES | | $\Delta H_R$ |
|---|---|---|
| | to fulvene | + 21 |
| | to hexadienyne | + 53 |
| DIAZABENZENES | | $\Delta H_R$ |
| 1,2 | to fulvene | + 15 |
| | to hexadienyne | + 39 |
| 1,3 | to fulvene | + 17 |
| | to hexadienyne | + 37 |
| 1,4 | to fulvene | + 16 |
| | to hexadienyne | + 24 |

(ii) Polymerisation

Plasma polymerisation has previously been considered to involve cycloaddition of parent and valence isomer systems.[123] Using this idea the data suggest that cycloaddition of the parent isomer with the fulvenes and hexadienynes is comparatively favourable energetically for the diaza compounds. This is consistent with the experimental observation of substantially higher levels of $CF_2$ groups present in the perfluorodiazabenzene

plasma polymers compared with the tetrafluorobenzene polymers[126,129], since this group only arises from the participation of fulvene and hexadienyne in the cycloaddition reactions. The proximity of the $\Delta H_{eb}$ values (about 20 kcal/mole) of the hexadienyne and Dewar benzene/benzvalene isomers in the tetrafluorobenzenes contrasts with the larger separation (about 50 kcal/mole) in the diaza analogues. This supports the experimental evidence concerning the rates of plasma polymerisation since it shows the relative unimportance of interconversion of the diaza-parent isomers in comparison with hexadienyne formation. For the homoaromatics on the other hand the energetics of inter-conversion are favourable, thus giving rise to similar rates of deposition and structures.

Consideration of the cation manifold gives a similar trend. Fulvene formation especially is greatly eased in both homoaromatic and heteroaromatic systems, but particularly so in the latter case where it is within $\sim$3 kcal/mole of the parent.

(iii) Elimination

It is of interest to consider the possibility of the elimination of a small stable molecule from these compounds, since plasma polymerisation of fluoroethylene was shown to be accompanied by elimination of HF. However, in the tetrafluoro-benzene case, experiment showed that HF elimination was not significant, a fact interpreted theoretically by the high energy of the resulting benzyne.[123]

On this basis the equivalent elimination (of $F_2$) has not been considered here. However, the possibility of nitrogen

elimination from the diaza series and analogous elimination of acetylene from the tetrafluorobenzenes has been investigated.

Elimination of $N_2$ from a $C_4N_2F_4$ molecule yields a $C_4F_4$ fragment for which there are three structural isomers, *viz.* the tetrahedrane, the cyclobutadiene and the tetraenyne. The most stable of these is the perfluorotetraenyne (see Figure 6.1). It is readily apparent that pyridazine could eliminate nitrogen without any other rearrangement with a heat of reaction of 27 kcal/mole. Conversely elimination of $N_2$ from the 1,3 and

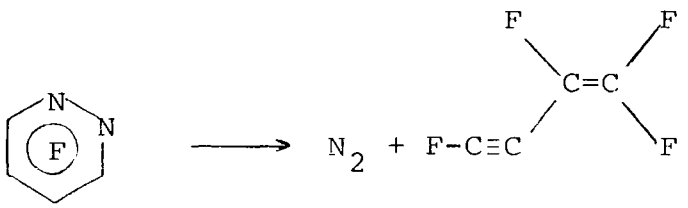


1,4 diazines must occur *via* either a Dewar benzene, prismane or benzvalene thus making $N_2$ loss as unfavourable as interconversion of the parent systems.

Bulk and surface N/C ratios determined for the plasma polymers of the diazines[129] support the prediction of greatest $N_2$ loss from the 1,2 diazine. By comparison the elimination of a similar stable molecule from the tetrafluorobenzenes yields heats of reactions of ∿98 kcal/mole for fluoroacetylene and ∿100 kcal/mole for acetylene.

## 6.4 Summary

Extensive MNDO SCF MO calculations have been performed to calculate the heats of formation of the ground state of the geometry optimised perfluorodiazabenzenes (pyridazine, pyrimidine, pyrazine) and some of their structural isomers (Dewar

benzene, benzvalene, prismane, fulvene and hexadienyne). The heats of formation of the cation, singlet and triplet states have been determined for the ground state geometry of the 1,3-diaza isomers in order to gain some insight into the excited state manifolds. These results are used in an attempt to interpret various experimental observations relating to the plasma polymerisation of the diazines. In particular the interconversion of the parent heteroaromatic, the relative energies of interconversion and polymerisation and the possibility of the elimination of a small stable molecule are considered. Comparison is made with previously reported results for the tetrafluorobenzenes.

# APPENDIX A

# ELECTRON SPECTROSCOPY FOR CHEMICAL APPLICATIONS

## A.1 Introduction

The acronym ESCA stands for Electron Spectroscopy for Chemical Applications (originally designated, for Chemical Analysis). The same technique is alternatively referred to as X-ray Photoelectron Spectroscopy (XPS) and, less commonly as, High Energy Photoelectron Spectroscopy (HEPS), Induced Electron Emission Spectroscopy (IEES) or Photoelectron Spectroscopy of the Inner Shell (PESIS).

The basis of the technique is that, bombardment of a surface by soft X-rays, *in vacuo*, leads to the emission of electrons whose kinetic energy is characteristic not only of the elemental core-level from which it was ejected but also the chemical state of that element.

The advent in the 1950s of high resolution *beta*-ray spectrometers (for nuclear structure research) was fundamental in the development of the technique since electrons could then be energy analysed to a high enough precision that core-electron chemical shifts could be observed. In the late sixties Siegbahn and coworkers published their classic texts[224,23] which can be seen as the basis of a great deal of research in both fundamental and applied chemistry. Historical accounts of the work have since been given.[225,226]

Application of the technique to organic materials has been pioneered by Clark and coworkers and has proved valuable in the study of polymer surfaces,[227,230] in this the "Polymer Age".

## A.2 Instrumentation

The basic components of an electron spectrometer are shown in Figure A.1 and consist of an X-ray source, a sample chamber, a system for analysing the electron energies and electron detection and display equipment. The following discussion relates directly to the AEI ES 200B used in this work.

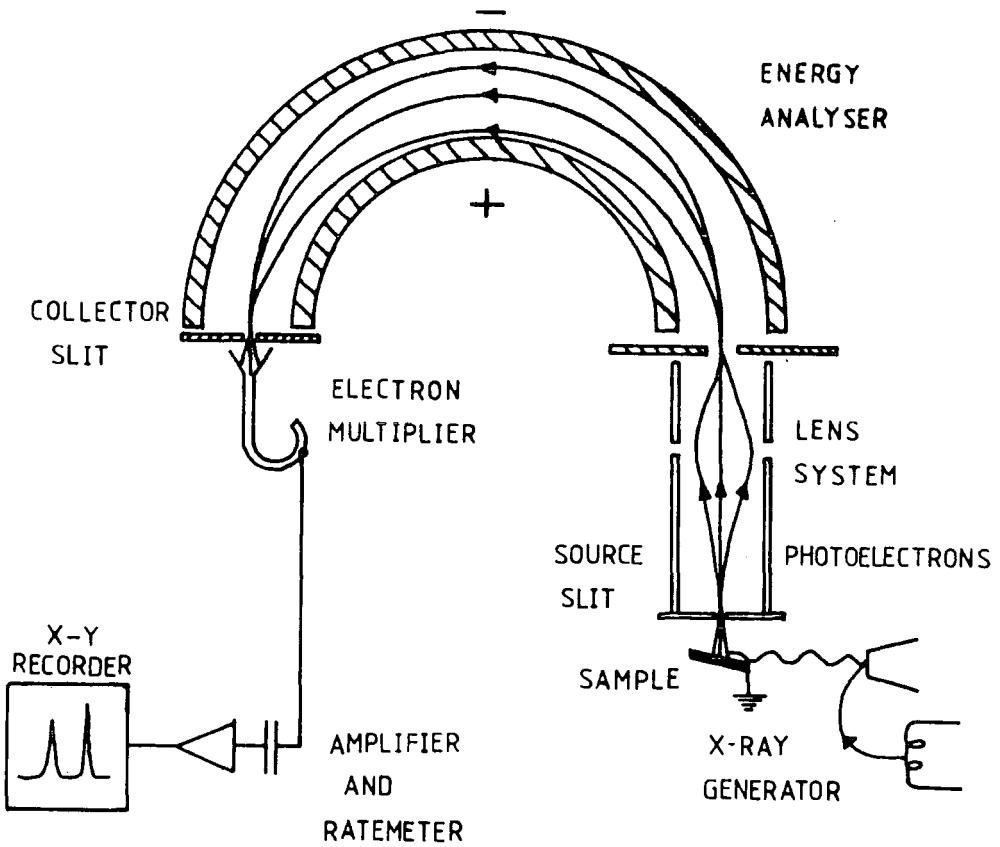


Figure A.1 SCHEMATIC OF AN ESCA SPECTROMETER

### A.2.1 The X-ray Source

The X-ray gun is based on the Henke hidden filament design[231] (which reduces contamination of the target by tungsten evaporated from the filament) and the X-ray beam is

produced by bombardment of an anode with high energy electrons. The filament is grounded and a positive potential is applied to the anode; this is supplied by a Marconi-Elliott GX5 high voltage generator with an integrally variable voltage and current output of 0-60kV and 0-80mA respectively. The instrument used in this work has a single magnesium anode and the gun was operated at 8kV, 14mA. This gives an X-ray flux of ~0.1 millirad/s[232] which is sufficiently low to avoid radiation damage of most samples. To prevent electrical breakdown, operation of this gun requires a pressure $<10^{-5}$T in the X-ray source.

The X-ray gun is separated from the source by an aluminium foil window (~0.003" thick) which prevents stray electrons from the filament from entering the sample chamber as well as preventing material from this chamber contaminating the anode. The high voltage is applied to the anode rather than the filament since this stops high energy electrons hitting the window and exciting $Al_{K\alpha}$ X-rays.

An X-ray gun of this type produces characteristic X-ray emission lines super-imposed on a continuous background of radiation known as the *Bremstrahlung*. The magnesium anode gives rise to a characteristic $K\alpha_{1,2}$ line, with a natural width of 0.7eV, and an energy of 1253.6eV which is an unresolved doublet arising from $2p_{3/2} \rightarrow 1s$ and $2p_{1/2} \rightarrow 1s$ transitions.[233] A photon energy of 1253.6eV is sufficient for photoionisation of the 1s core level of the first period elements, the 2s and 2p for the second period, and so on (Table A.1); little advantage is gained by using photon sources of sufficient energy to ionise deeper core levels since these have shorter life times

TABLE A.1 Approximate core binding energies of first and second row elements

| | Li | Be | B | C | N | O | F | Ne |
|---|---|---|---|---|---|---|---|---|
| 1s | 55 | 111 | 188 | 284 | 399 | 532 | 686 | 867 |
| | Na | Mg | Aℓ | Si | P | S | Cℓ | Ar |
| 1s | 1072 | 1305 | 1560 | 1839 | 2149 | 2472 | 2823 | 3203 |
| 2s | 63 | 89 | 118 | 149 | 189 | 229 | 270 | 320 |
| $2p_{1/2}$ | 31 | 52 | 74 | 100 | 136 | 165 | 202 | 247 |
| $2p_{3/2}$ | 31 | 52 | 73 | 99 | 135 | 164 | 200 | 245 |

and this leads to greater uncertainty in the energy of the core-level. For example the Au 1s peak would have a Full-width at Half-Maximum (FWHM) of 54eV! As will be explained (Section A.2.3) the X-ray line-width is often one of the major limitations to the observed line widths and magnesium is also a useful anode because of the comparatively narrow line-width of the $K\alpha_{1,2}$ line ($\sim$0.7eV) enabling its use without mono-chromatisation.

### A.2.2 The Sample Chamber

The base pressure of the sample chamber is $\sim 1 \times 10^{-7}$T. A vacuum system is required for two reasons.[233] Firstly the pressure must be sufficiently low that the emitted electrons can pass from the sample to the analyser without making too many collisions; this requires a vacuum of better than $10^{-5}$T. Secondly the sample surface needs to be maintained free from contamination over the time necessary to acquire spectra; (assuming a sticking probability of unity, a surface

would be covered by a monolayer of residual gas in 0.2s at $10^{-5}$T, or ∿2000s at $10^{-9}$T).

Sample probes enter the chamber by means of insertion locks based on Viton O-ring seals and ball valves; it is these which impose the major limitation on the vacuum attainable within the sample chamber, but they allow fairly rapid sample insertion and rotation of the sample with respect to the analyser.

The sample requirements of the technique are extremely modest requiring ∿1mg of solid, 0.1μl of liquid or ∿0.5 $cm^3$ of gas (at STP). Sheet or thick film samples may be screwed onto the probe-tip whilst powder and thin film samples are routinely mounted using two-sided Scotch tape; though this latter method will lead to sample charging this can be compensated for by suitable referencing (Section A.4.1). Techniques have been developed for studying liquids and gases *per se* but generally analysis is carried out by using a reservoir shaft to introduce the sample which is then condensed onto a cooled inert substrate, typically gold. (This is the method used in this work). The sample probes can be cooled to liquid nitrogen temperature by pumping liquid nitrogen through metal capillary tubing or if circumstance requires may alternatively be (resistively) heated to ∿400°C.

The geometry of the sample chamber is such that the analyser is at right angles to the X-ray gun and both are at right angles to the axis of probe entry. The argon-ion gun fitted for spectrometer cleaning purposes is not at the same height as the sample and thus cannot be easily used for sample cleaning or depth-profiling.

### A.2.3 The Electron Energy Analysis System

The electron energy analysis system comprises a hemispherical double-focussing dispersive electrostatic analyser (based on the principle first proposed by Purcell[237]), enclosed within two mu-metal shields for magnetic shielding, preceded by a lens system. The relative resolution ($^{\Delta E_o}/_{E_p}$) of the analyser is given by equation A.1.[238] (The term resolving power, commonly encountered, is the reciprocal relative resolution, *i.e.* $^{E_p}/_{\Delta E_o}$).

$$\frac{\Delta E_o}{E_p} = \frac{0.63w}{R} \qquad \text{(eqn. A.1)}$$

where $\Delta E_o$ is the FWHM of the observed line and is known as the absolute resolution. From a practical point of view this is the term of most interest to the chemist.

$E_p$ is the kinetic energy of the electron as it traverses the analyser (the "pass energy" - note that a pass energy of, for example, 65eV means that an electron exiting the lens and entering the analyser with an energy of 65eV will be focussed onto the collector slit).

W is the width of the source slit or collector slit, whichever is the larger.

R is the radius of the hemispheres.

From equation A.1 it can be seen that the absolute resolution can be improved by:

(i) decreasing the slit width; this will also decrease the signal intensity;

(ii) increasing the radius of the hemispheres; this will increase engineering costs and pumping requirements.

(iii) decreasing the energy of the electrons prior to their entry into the energy analyser (*i.e.* decreasing $E_p$; see below).

The absolute resolution itself ($\Delta E_o$) is affected by various factors, which are

(i) the width of the X-ray radiation line ($\Delta E_x$);

(ii) the natural line-width of the core-level being studied ($\Delta E_{Cl}$). This is governed by the uncertainty principle[239] (as is the X-ray line-width) which relates the lifetime of the core-hole state with its energy and therefore with the energy of the emitted electron; the equation is

$$\Delta E = \frac{6.6 \times 10^{-16}}{\Delta t} \quad \text{(eV - second units)} \qquad \text{(eqn.A.2)}$$

so that for a hole-state life-time of $\sim 6.6 \times 10^{-16}$ seconds the linewidth ($\Delta E_{Cl}$) *i.e.* the uncertainty in energy is $\sim$1eV. Typically the lifetimes of the core-hole states involved in ESCA fall in the range $10^{-14}$ - $10^{-17}$ seconds.[228] In respect of the use of ESCA to study carbocations, its most important feature is that the photoionisation event central to the technique, is rapid by comparison with nuclear motion.[236,240]

(iii) The line broadening due to spectrometer irregularities ($\Delta E_s$). This varies with the electron pass energy ($E_p$) and slit-widths (and is also the component affected by changing R).

(iv) The line broadening due to solid state effects in the sample ($\Delta E_{ss}$) caused, for example, by different crystallographic environments for a given element.

Generally it is the natural widths of the X-ray line and core-hole state which control the observed FWHM. All these terms ($\Delta E_j$) are the FWHM of the various components and are related to the observed FWHM ($\Delta E_o$) by equation A.3.

$$(\Delta E_o)^2 = (\Delta E_x)^2 + (\Delta E_{Cl})^2 + (\Delta E_s)^2 + (\Delta E_{ss})^2 \qquad \text{(eqn. A.3)}$$

This is only approximate since it assumes that the contributions are Gaussian in form whereas, in fact, those of the X-ray line-width ($\Delta E_x$) and core-level ($\Delta E_{Cl}$) are essentially Lorentzian.[241] The convolution of these factors for an observed peak is essentially Gaussian with Lorentzian character in the tails but it has been shown[23] that analysis of experimental spectra of insulating samples using a pure Gaussian (or Lorentzian) lineshape introduces minimal error and therefore the spectra in this work have been resolved by generating Gaussian functions on a Du Pont 310 analogue curve resolver. A discussion on more detailed data analysis has been given.[242]

The lens system preceding the analyser serves two purposes.[233] Firstly it allows electrons to be decelerated prior to entering the analyser, thus allowing the same absolute resolution to be obtained with an analyser of inferior resolving power. Secondly it permits the analyser to be located at a convenient distance from the sample and this allows greater flexibility in the positioning of samples.

There are two basic methods of operating the electron energy analysis system, known as FAT (Fixed Analyser

Transmission) and FRR (Fixed Retarding Ratio). In FAT a constant voltage is applied to the analyser plates and the voltage applied to the lens optics is scanned so that electrons of differing energies are consecutively brought to a focus at the collector slit. In FRR the voltages applied to the lens and analyser are scanned simultaneously, maintaining a constant ratio between the two and retarding the electrons to ∿4% of their initial energy. Since in FAT the pass energy of the analyser is the same, no matter what the energy of the electron leaving the sample, this mode of operation gives the same absolute resolution across the whole kinetic energy range. In this mode the absolute resolution can be improved by using a lower pass energy (that is $E_p$ is de-decreased, so $\Delta E_o$ is decreased; Eqn. A.1) as claimed by Olah.[243] Conversely in FRR the pass energy of the electrons focussed at the collector slit increases as the spectrum is scanned (*i.e.* as $E_p$ increases) and therefore the absolute resolution increases for peaks of higher kinetic energy.

The sensitivity of a mode of operation of the electron energy analysis system is related to its ability to detect a signal of a certain intensity; that is, the lower the intensity of a signal which can just be detected (*i.e.* resolved from the noise) the higher the sensitivity. It is generally held[244] that the sensitivity for the two modes of operation of the ES200B analysis system follow the form

$$S_{FAT} \propto \frac{1}{KE}$$

$$S_{FRR} \propto KE$$

and that FAT is more sensitive than FRR for electrons of

kinetic energy less than ∿500eV. However Castle has suggested[245] that the relationship for the sensitivity in FAT mode is

$$S_{FAT} \simeq \text{constant.}$$

The sensitivity is affected by two factors:

(i) the transmission efficiency of the analysis system (analyser, lens optics and detector) for electrons of a certain kinetic energy;

(ii) the absolute resolution; the relationship between resolution and sensitivity is well-known.[246]

Perhaps it is the failure to distinguish sensitivity and transmission which has led to the dichotomy of opinion, since as was discussed above, for FAT the absolute resolution is constant whilst in FRR it increases with kinetic energy. However, having noted this disagreement, the sensitivity for the FAT mode is not of further interest since all the spectra recorded in this work employed the FRR mode of operation.

### A.2.4 Electron detection and display

Electrons focussed at the collector slit pass from the analyser into a single channeltron electron multiplier which gives amplification of the signal by a factor of $\sim 10^7$. Pulses obtained are amplified and fed to the counting electronics. There are two ways of generating the spectra:

(i) the continuous scan; in this the energy of the electrons collected is increased continuously at a known rate from a preset starting kinetic energy. The electron count from the ratemeter is plotted *versus* the kinetic energy on an X-Y recorder. This is the mode employed throughout this work;

(ii) the step-scan; in this the energy of the electrons collected is increased by preset increments (*e.g.* O.leV) and at each increment either the counts are measured for a fixed length of time, or a fixed number of counts are timed. The data is then fed into a multichannel analyser or, more recently, into a mini-computer.

## A.3 Processes involved in ESCA

### A.3.1 Photoionisation (Figure A.2)

The irradiation of atoms by soft X-rays causes the ejection of electrons which have binding energies less than the photon energy; this is the process of photoionisation. The ejected electrons may originate from either the core or valence levels and, for an isolated molecule or atom, they have specific kinetic energies which are governed by the equation[224]

$$h\nu = KE + BE + E_r$$

(initial energy = final energy)

where $h\nu$ is the photon energy; h is Planck's constant,

$\nu$ is the frequency of the X-rays

KE is the kinetic energy of the ejected electron

BE is the binding energy of the ejected electron

$E_r$ is the recoil energy of the atom or molecule.

When soft X-rays are being used the recoil energy is negligible[224] so the equation reduces to

$$KE = h\nu - BE$$

### A.3.2 Relaxation (Figure A.2)

If photoionisation occurred in total isolation of other events (*i.e.* a one-electron process) then the binding energy of the electron would simply be the energy of the orbital from which the electron is removed,

$$BE = -\varepsilon_i \qquad \text{(eqn. A.4)}$$

($-\varepsilon_i$ is the orbital energy of the ejected electron)

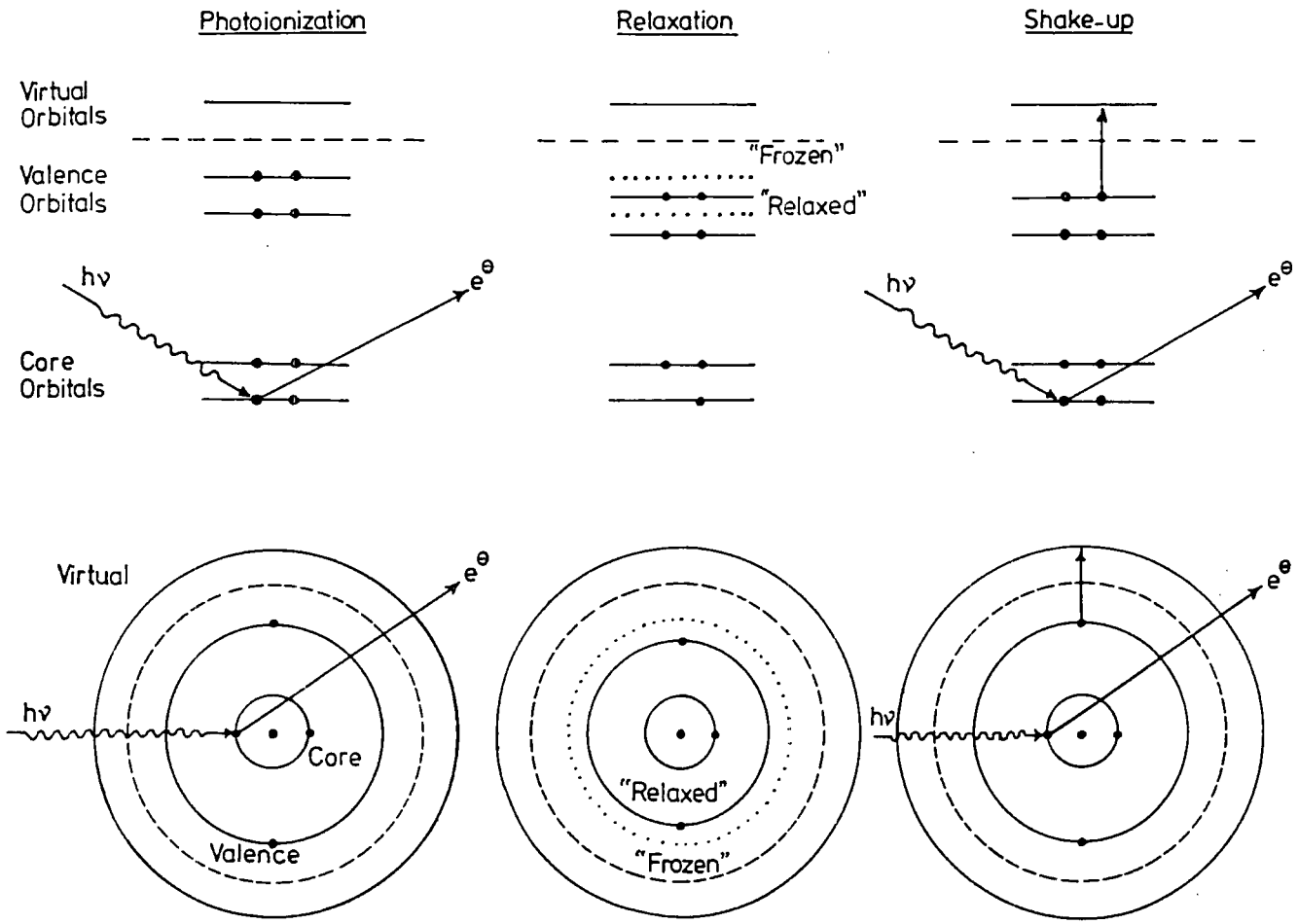


Figure A.2 SCHEMATIC OF PHOTOIONISATION, RELAXATION AND SHAKE-UP

This is Koopman's Theorem.[213] However the final state is not "frozen" since photoionisation is accompanied by a "relaxation" process. Although core electrons do not take part in bonding they are sensitive to the valence-electron distribution.[228] The process of core ionisation leads to an effective increase in nuclear potential and this causes a substantial electronic reorganisation termed "relaxation".[247-251] This electronic relaxation occurs on a timesacle comparable to the photoionisation event and therefore it affects the energy of the ejected electron, thus the binding energy is more accurately given by the equation,

$$BE = -\varepsilon_i - RE \qquad \text{(eqn. A.5)}$$

(RE is the relaxation energy)

### A.3.3 Shake-up and Shake-off processes (Figure A.2)

The sudden perturbation to the valence cloud accompanying core ionisation gives rise to a finite probability for photoionisation to be accompanied by simultaneous excitation of a valence electron to a virtual orbital (known as "shake-up").[229,248,252] A similar process involves the complete ejection of a valence electron to the vacuum level, simultaneous with photoionisation ("shake-off"). Both shake-up and shake-off processes result in excited states of the core ionised species and because they essentially occur simultaneously with photoionisation they result in a modification of the kinetic energy of the photoejected electron, by an amount ($\bar{E}$) equal to the energy needed to excite the valence electron (equation A.6). The occurrence of such processes may lead to

$$KE = h\nu - (BE + \bar{E}) \qquad \text{(eqn. A.6)}$$

the observation of satellite peaks to the low kinetic energy side of the main photoionisation peak.

### A.3.4 The Fate of Core-Holes

The two mechanisms of de-excitation of core-holes are Auger emission[241b,253] and X-ray fluorescence[254] (Figure A.3) both of which form the basis for important analytical techniques in their own right. In both processes the core-hole is filled by an electron from a higher occupied level and the energy released by this results either in the simultaneous emission of another electron giving rise to a doubly ionised final state (the Auger process) or in the emission of a photon in the X-ray region of the electromagnetic spectrum (X-ray fluorescence). For de-excitation of a K-shell vacancy (*i.e.* a 1s core-hole), Auger emission is the predominant process for elements of low atomic number while fluorescence becomes dominant for heavier elements; the cross-over comes at an atomic number of ∿33(Arsenic).

De-excitation of the core-hole is much slower than the initial photoionisation and Auger emission and X-ray fluorescence do not affect the kinetic energy of the photo-ejected electron.

## A.4 Features of ESCA Spectra

### A.4.1 Binding Energies and Energy Referencing

Core electrons are essentially localised on atoms and therefore their binding energies are characteristic for any element.[255] This is illustrated for the first and second row elements in Table A.1. The corollary of this is that determination of the binding energy of peaks appearing

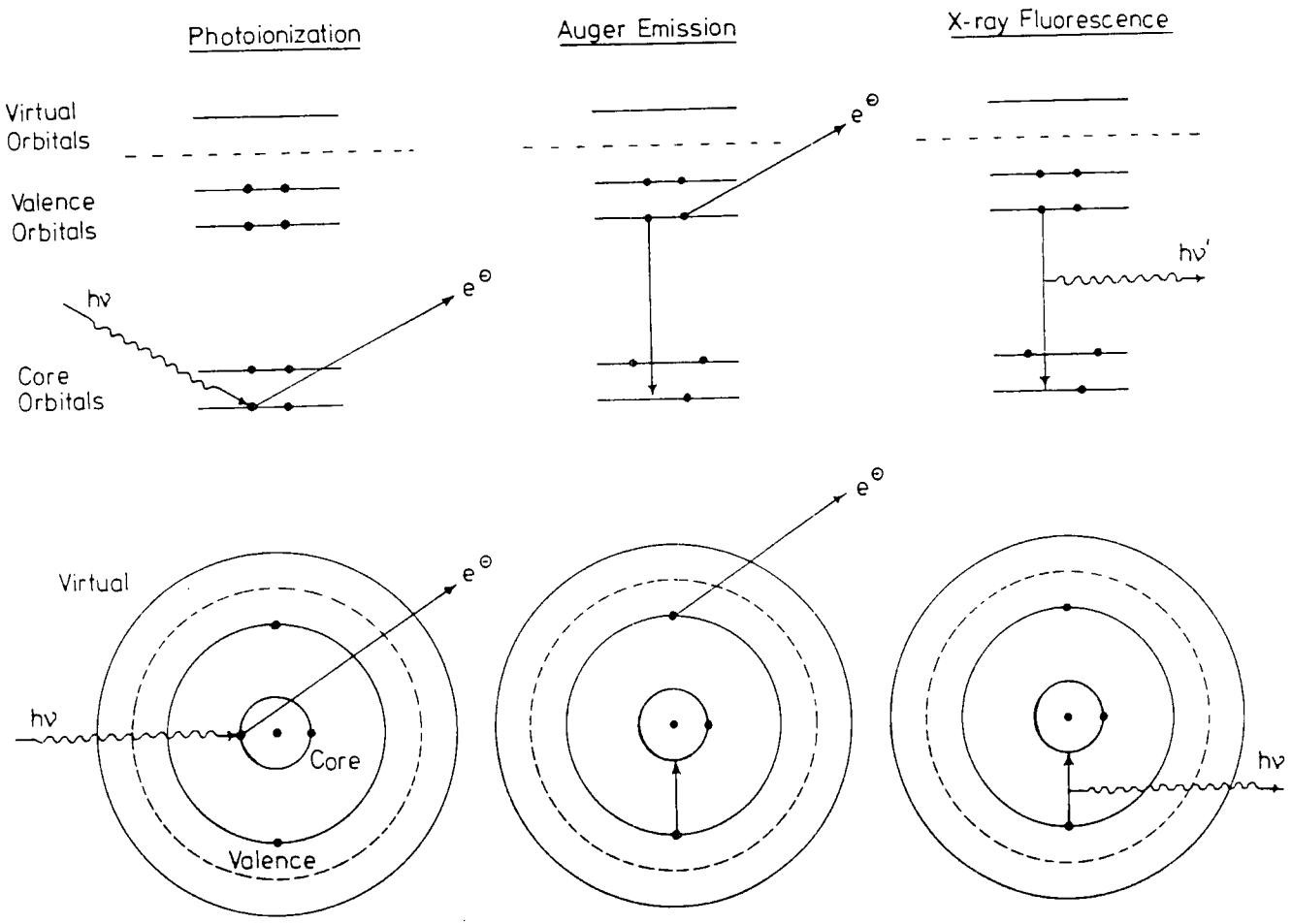


Figure A.3 SCHEMATIC OF PHOTOIONISATION, AUGER EMISSION AND X-RAY FLUORESCENCE

in the observed spectrum leads to identification of the elements composing the sample.

Binding energies in ESCA are referenced to the Fermi level. (The more correct energy zero is the vacuum level which differs from the Fermi level by an amount of energy termed the work function). For a metal, the Fermi level is defined as the highest occupied level at absolute zero.[256] For a conducting sample in electrical contact with the spectrometer the Fermi levels of both will "line-up" (*i.e.* they will be at equal potential; Figure A.4). The energy gap between

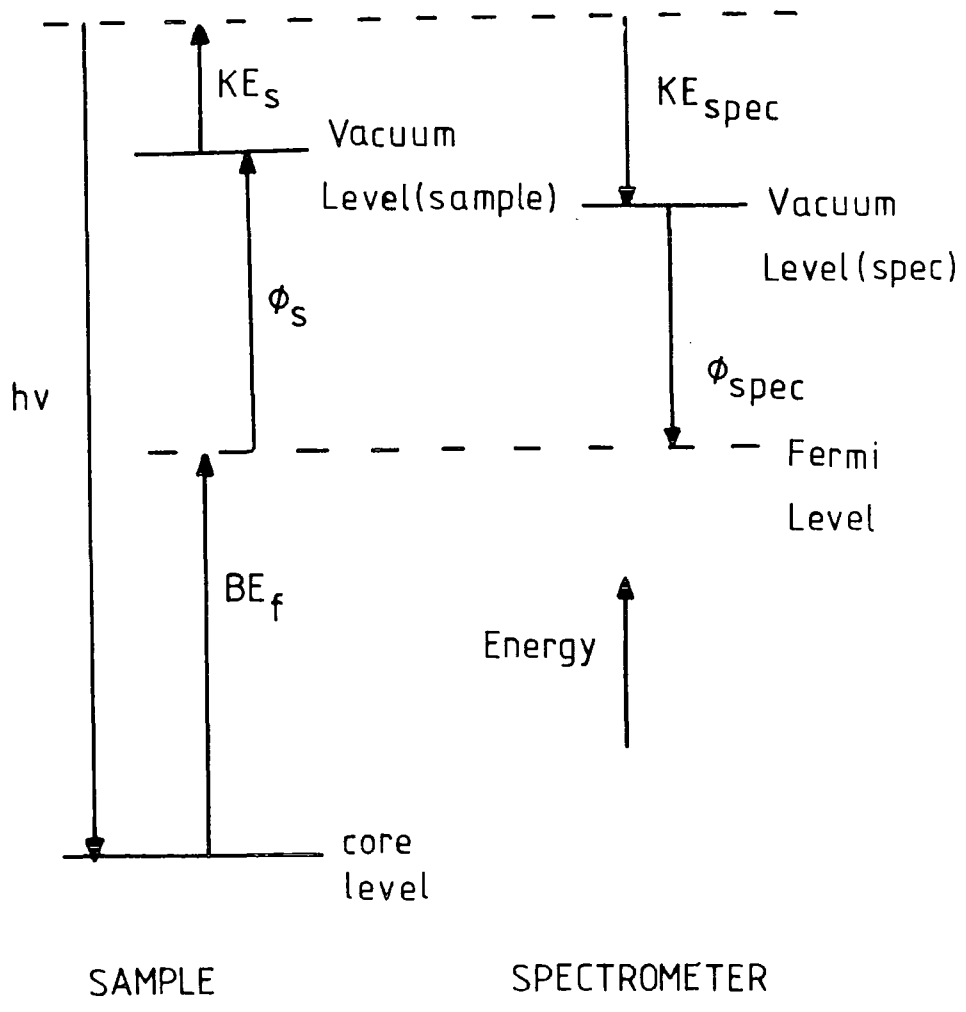


Figure A.4 ENERGY LEVEL DIAGRAM FOR A SAMPLE IN ELECTRICAL CONTACT WITH THE SPECTROMETER

the vacuum and Fermi levels (the work function) may not be the same for the sample and the spectrometer[255] leading to a difference in energy of the vacuum levels (termed the "contact potential"). An electron escaping from the sample with a kinetic energy $KE_s$ is detected at the spectrometer with a kinetic energy $KE_{spec}$ where

$$KE_{spec} = KE_s + (\phi_s - \phi_{spec}) \qquad \text{(eqn. A.7)}$$

($\phi_s$ = the work function of the sample,
$\phi_{spec}$ = the work function of the spectrometer)

From Figure A.4 it is seen that,

$$h\nu = BE_F + \phi_s + KE_s \qquad \text{(eqn. A.8)}$$

where $BE_F$ is the binding energy referenced to the Fermi level (the binding energy referenced to the vacuum level, $BE_v$, is equal to $BE_F + \phi_s$). Combining equations A.7 and A.8

$$KE_{spec} = h\nu - BE_F - \phi_{spec} \qquad \text{(eqn. A.9)}$$

Again, this is seen to be true from Figure A.4. Therefore it can be seen that referencing binding energies to the Fermi level means that they can be specified without a knowledge of the work function of the sample; the work function of the spectrometer is always involved but even if its value is not known this is not a problem because it simply represents a constant correction to all binding energies.

In an insulator the Fermi level is less well defined; the (filled) valence band is separated by an energy gap from the (empty) conduction band and the Fermi level is intermediate between these bands. Insulators also represent a further problem because of the static charging which occurs;

this charging phenomenon occurs because electrons lost through the photoemission process are not replaced by a flow from earth (as happens for a conductor) so that the sample becomes positively charged and this potential leads to a retardation of all electrons leaving the sample. Effectively then both $KE_s$ and $KE_{spec}$ are reduced by the charging potential (C) so that equation A.9 for a charged sample becomes,

$$KE^{SC}_{spec} = h\nu - BE_F - \phi_{spec} - C \quad \text{(eqn.A.10)}$$

In practice, binding energies (independent of spectrometer work function and static charging) are determined by referencing to peaks of known binding energy; usual standards are

(i) for thin films deposited onto a gold substrate, the $Au4f_{7/2}$ signal which has a binding energy of 84.0eV;

(ii) for organic systems, or systems left in the spectrometer long enough to acquire an adventitious overlayer of hydrocarbon, the $C_{1s}$ (C-H) level, which has a binding energy of 285.0eV.

### A.4.2 Chemical Shifts

#### (i) Origin of Chemical Shifts

Although they are essentially localised, tightly bound and non-participatory in bonding, core electrons are sensitive to the valence electron distribution, which is dependent on the chemical state of the atom. Thus changes in the chemical environment of an atom give rise to shifts in core electron binding energies and these are often measurable (*i.e.* >0.1eV). A dramatic example of this is the $C_{1s}$ core-hole

spectrum of ethyl trifluoroacetate (Figure A.5). It will be noted that the signal is proportional to the number of carbon atoms giving rise to it; since the core electrons are localised, the photoionisation cross-section is independent of the chemical environment of the four carbon atoms, and other factors affecting signal intensity (Section A.4.4(i)) are the same.

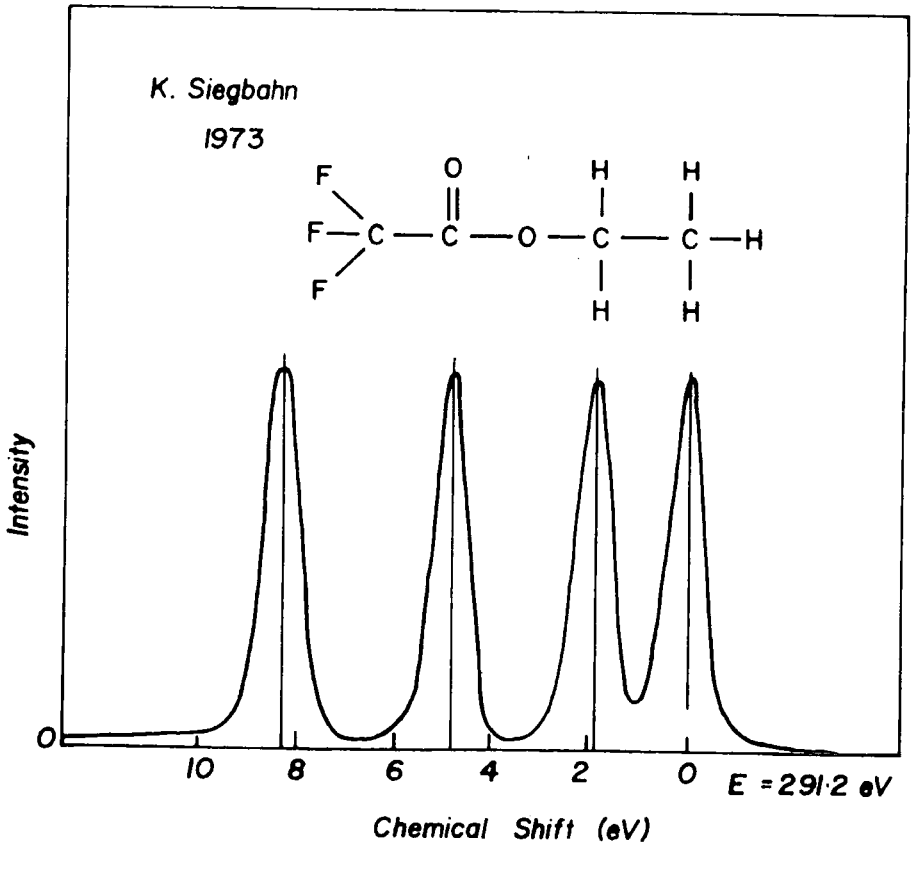


Figure A.5 HIGH RESOLUTION CORE LEVEL SPECTRUM ($C_{1s}$) OF ETHYL TRIFLUOROACETATE.

Tables of chemical shift data are available[186] but are often compilations from many sources and potentially offer problems with charge referencing. Whereas such tabulations are a good and useful guide, it is always preferable to "run" compounds along with unknown samples.

(ii) Methods of calculating chemical shifts

Various theoretical methods have been employed to calculate chemical shifts; the most widely used (and probably conceptually easist) are

(a) Koopmans' Theorem[213]

(b) The Ground State Charge Potential Model[23]

(c) The Equivalent cores model[257-259]

(d) ΔSCF methods[247,260].

These, and other methods (the Transition State model[261,262] and Quantum Mechanical Potential Model[263-265]) have been reviewed.[266] More recently binding energies have been calculated using Green's Function.[267]

For the experimental chemist the important points to realise are that not only can the chemical shift be readily interpreted by theoretical models, but also that an acceptable level of accuracy is obtained using comparatively low levels of theory.

(iii) The Auger Parameter and Two-dimensional chemical state plots

The excitation of many elements by soft X-rays gives rise to Auger transitions emitting electrons which are detected in addition to photoionised electrons in a conventional ESCA "wide scan" spectrum. Wagner has suggested[268] that Auger electron signals usefully complement photoelectron binding energies in determining the chemical state of an element, and has defined the "Auger parameter" (α) as

$$\alpha = KE_{(Auger)} - KE_{(photoelectron)} \quad \text{(Eqn. A.11)}$$

where $KE_{(photoelectron)}$ is the kinetic energy of the most intense photoelectron,

and, $KE_{(Auger)}$ is the kinetic energy of the most intense Auger electron signal. Ideally narrow Auger transitions are used, that is those not involving valence electrons.

The reason for defining such a parameter is that the chemical shifts associated with Auger electrons are frequently greater than for photoelectrons so that its numerical value is related to the chemical state of the element; because two lines are used the static charging, which occurs for insulating samples, cancels so that the value of the parameter can be more precisely defined than either of the two component kinetic energies. However, as originally defined it suffered from two disadvantages, namely that the parameter was often negative and was dependent upon photon energy; this led to the definition of the modified Auger parameter ($\alpha'$) as the sum of the photon energy and the Auger parameter,

$$\alpha' = KE_{(Auger)} - KE_{(photoelectron)} + h\nu \quad \text{(eqn. A.12)}$$

$$= KE_{(Auger)} + BE_{(photoelectron)}$$

The modified Auger parameter is still a one-dimensional parameter and for this reason two-dimensional chemical state plots have been suggested as an aid to chemical state identification. In these the Auger kinetic energy is plotted against the photoelectron binding energy, giving two-dimensional resolution. For the photoelectron spectroscopist the advantage of such procedures is evident from a cursory glance of the plots presented, particularly for elements such as Sodium and Magnesium where the Auger electron energies span a range of $\sim$8eV compared with only $\sim$2eV for the photoelectron.

### A.4.3 Other Fine Structure

#### (i) Spin-Orbit Splitting

When photoionisation occurs from a filled orbital of orbital quantum number (L) greater than zero a doublet structure is observed in the resultant spectrum which arises from a coupling of the spin (S) and orbital (L) angular momenta of the final state unpaired electron giving two states of different total momenta (J);[224] so for example, ionisation of a p-electron ($\ell$=1) results in a doublet arising from states with total angular momentum of $^1/_2$ and $^3/_2$. Typical ESCA spectra displaying this splitting are shown in Figure A.6.

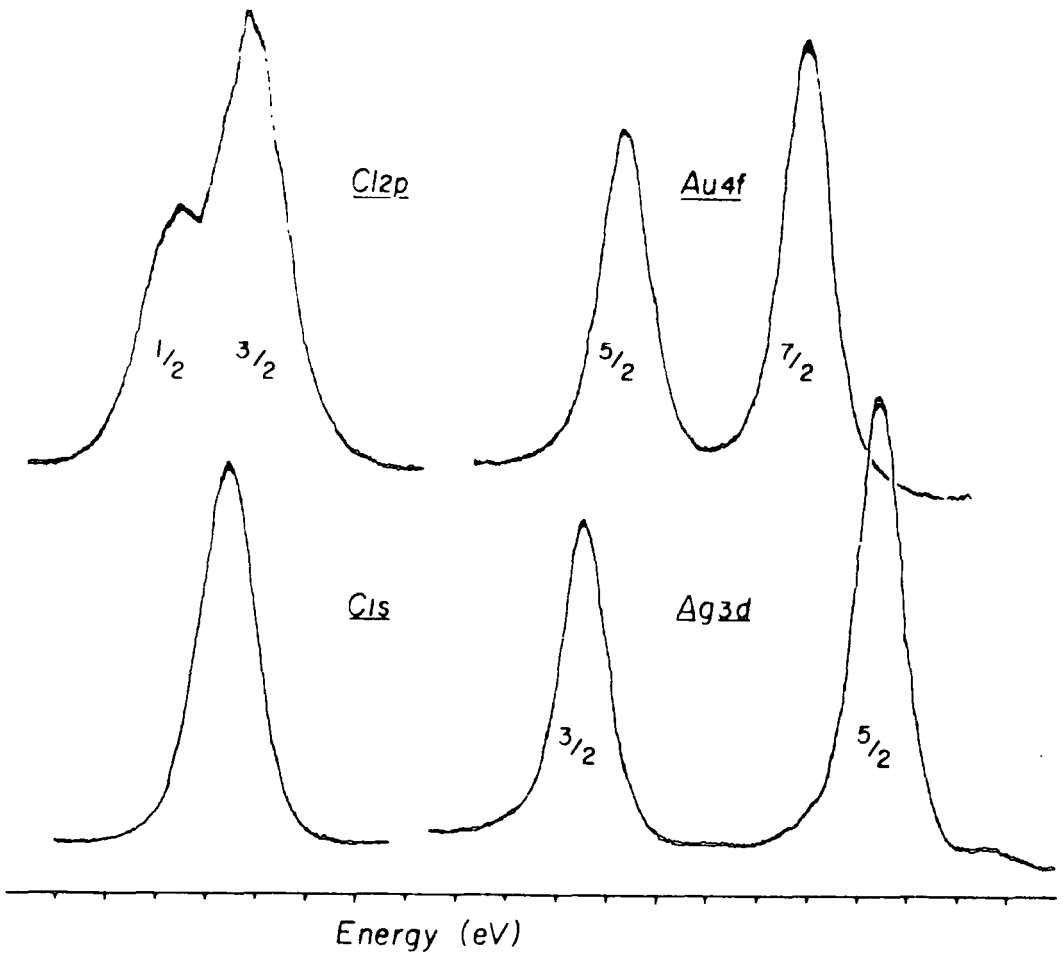


Figure A.6 SPIN-ORBIT SPLITTINGS IN $C_{1s}$, $Cl_{2p}$, $Ag_{3d}$ AND $Au_{4f}$ CORE LEVELS

The relative intensities of the doublets are proportional to the degeneracies of the states; the degeneracy of a state of total momenta J is (2J+1). The states arising for orbitals of different quantum numbers and the intensity ratios are summarised in Table A.2.

TABLE A.2 Spin orbit splitting degeneracies and intensities

| Orbital | Orbital Quantum No. | Total Quantum No. | Intensity Ratio |
|---|---|---|---|
| | $\ell$ | $J = (L \pm S)$ | $(2J + 1) : (2J + 1)$ |
| s | 0 | $^1/_2$ | singlet |
| p | 1 | $^1/_2$ , $^3/_2$ | 1 : 2 |
| d | 2 | $^3/_2$ , $^5/_2$ | 2 : 3 |
| f | 3 | $^5/_2$ , $^7/_2$ | 3 : 4 |

(ii) Multiplet Splitting

Following the photoionisation of a system containing unpaired electrons, coupling occurs between them and the unpaired core electron.[269] An interesting example of multiplet splitting is given by the comparison of the core hole spectra of nitrogen, nitrous oxide and oxygen[23] (Figure A.7). Whereas the ground state of nitrogen has all electrons paired giving rise to a single photoionisation peak, the oxygen diatomic contains two unpaired electrons and coupling with an unpaired core electron left after photoionisation leads to two energy states and these are partially resolved in the ESCA spectrum. The initial state of nitrous oxide has a single unpaired electron and splitting is observed in the $N_{1s}$ core hole spectrum but not the oxygen (*i.e.* the splitting in the $N_{1s}$ spectrum is greater than that for the $O_{1s}$). The size of multiplet

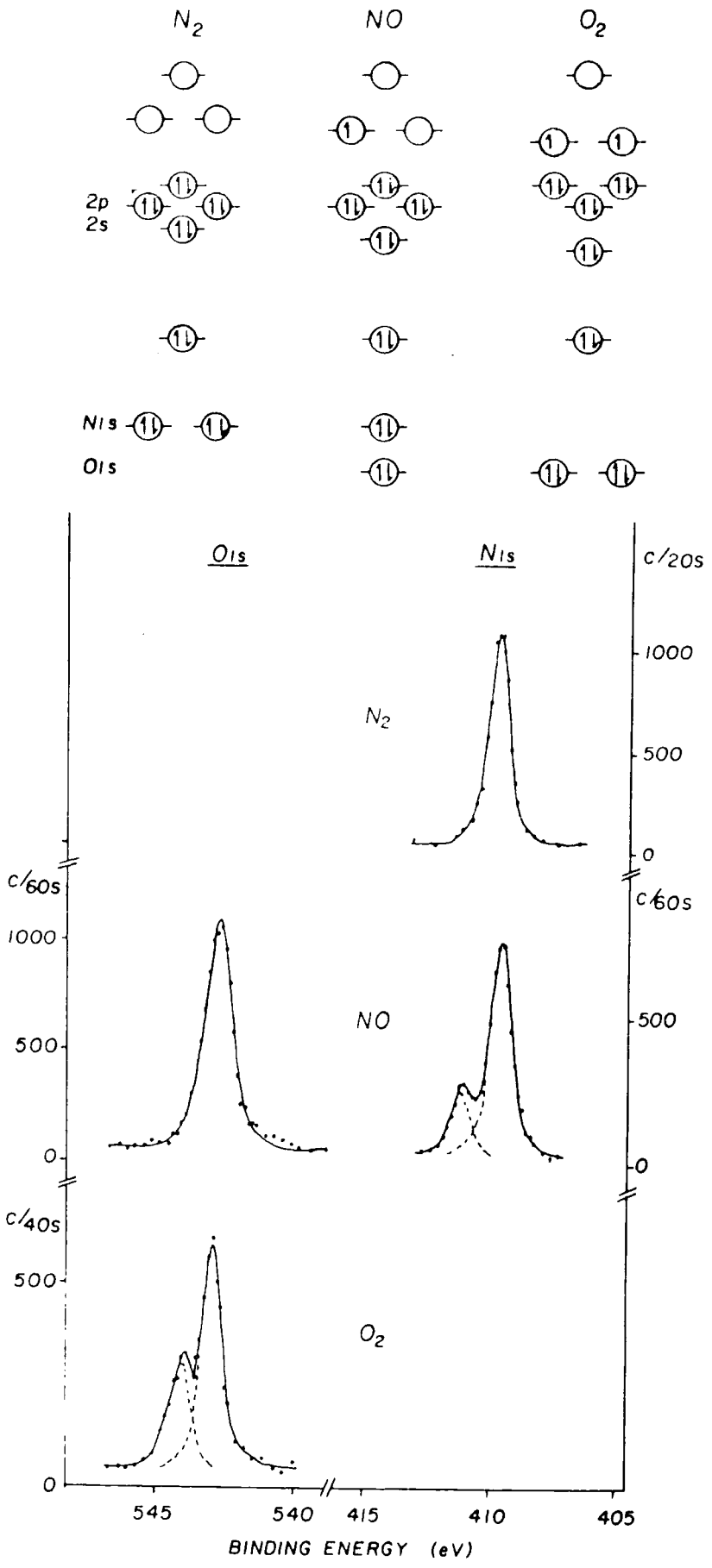


Figure A.7 CORE HOLE SPECTRA OF $N_2$, NO and $O_2$ ILLUSTRATING MULTIPLET SPLITTING

splitting can be shown (theoretically) to be related to the unpaired spin density on an atom so that the spectra indicate that most of the unpaired spin density is on the nitrogen atom.

This type of splitting is commonly found in the spectra of transition metals.[269-272]

(iii) Electrostatic Splitting

Splitting of the $5p_{3/2}$ levels of uranium and thorium in the metals themselves and their compounds has been observed[273,274] and this is attributed to the electrostatic field within the material, causing a non-degeneracy of the spin state. Such splitting can be compared with the Zeeman effect, that is, the splitting of these levels within a magnetic field. Similar splittingshavebeen observed in compounds of gold and tin;[274,275] they are not likely to be observed in systems such as polymers which have an inherently amorphous structure.

A.4.4 Signal Intensities

The sample geometry with respect to the analyser and photon source is shown in Figure A.8. The X-rays enter the sample at an angle $(\phi-\theta)$ and emerge at an angle $\theta$ (both defined relative to the normal to the sample). For the spectrometer used in this work the angle $\phi$ between the analyser and X-ray source is fixed at $90^{\circ}$. For photoionisation events which occur at a depth d, electrons which are to be detected by the analyser must travel a distance $d/\cos\theta$ before escaping from the sample surface.

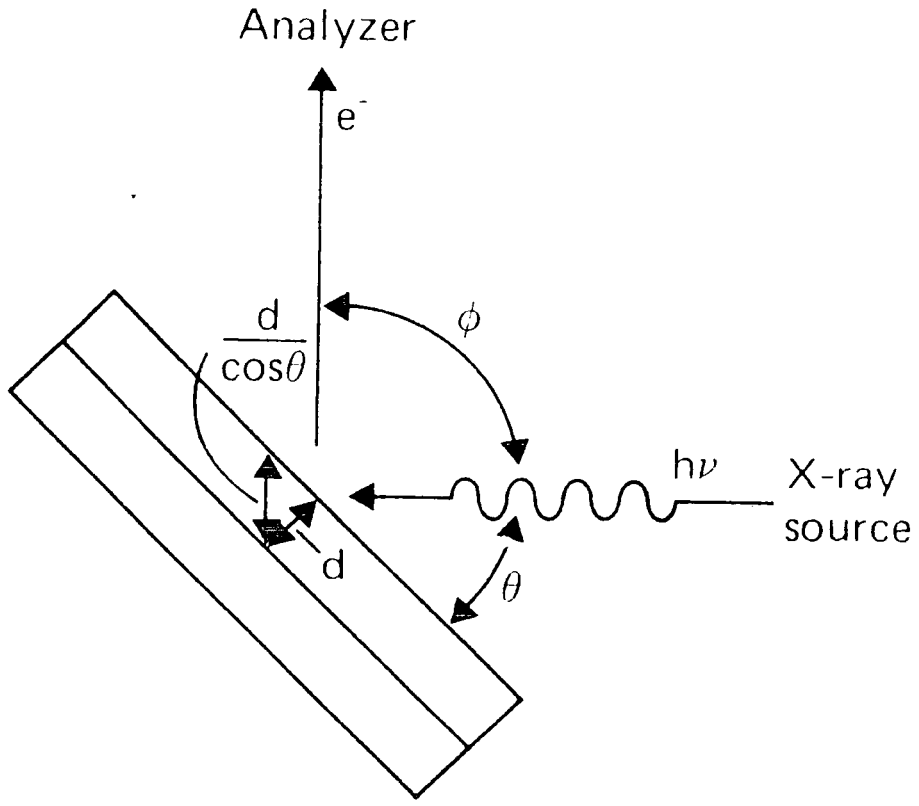


Figure A.8 SAMPLE GEOMETRY WITH RESPECT TO THE ANALYSER AND PHOTON SOURCE

(i) Homogeneous Samples

For an infinitely thick homogeneous sample, the intensity ($I_i$) of the elastic peak arising from photoionisation of core level i is given by the differential equation[276,277]

$$dI_i = F\alpha_i N_i k_i e^{-x/\lambda i} dx \qquad \text{(eqn. A.13)}$$

where x is the depth of photoionisation of core level i; (note that the intensity decreases exponentially with depth)

F is the X-ray flux; this is primarily dependent on the power applied to and the efficiency of the X-ray gun. Over the depth sampled by ESCA attenuation of the X-ray flux is considered to be unimportant.

$\alpha_i$ is the photoionisation cross-section; this is a measure of the probability of core level i being ionised when "hit" by a photon, and of the electron being emitted in a direction favourable for its detection. The cross-section is a function not only of the core-level and the photon energy but also varies with $\phi$ (the angle between the X-ray flux and analyser). Photoionisation cross-sections may be calculated[59] and for most elements are within two orders of magnitude of that for the $C_{1s}$ level (when using conventional X-ray sources) so that ESCA has suitable sensitivity to be used in the study of most elements.

$k_i$ is a spectrometer factor which depends on analyser transmission characteristics and detector efficiencies (both of which vary with the kinetic energy of the analysed electron) and also on the spectrometer (analyser/sample) geometry since this affects the solid angle of acceptance of the analyser. The transmission characteristics are dependent on the mode (FRR or FAT) of operation.

$\lambda_i$ is the inelastic mean free path (sometimes known as the "escape depth") which is defined as the distance through which electrons will travel before $^1/_e$ of them have not suffered energy loss. The mean free path of an electron depends upon its kinetic energy and for the energies appropriate to ESCA (*i.e.* >100eV) there exists the approximate relationship[266]

$$\lambda_i \propto (KE)^{\frac{1}{2}} \qquad \text{(eqn. A.14)}$$

Typically for electrons of kinetic energy between 500-1000eV $\lambda_i$ lies in the range of 10-20Å (but see Section A.4.4(ii) for a discussion of ESCA "sampling depth")

$N_i$ is the number density of the sample and relates to the number of atoms of (core-level) i within the analysed volume; it is not directly related to density though higher density materials do generally give rise to more intense signals. Its importance in this equation is that the signal intensities of core levels are directly related to the overall stoichiometry of an analysed surface (see equation A.16).

Integration of equation A.13, with respect to the depth of photoionisation (x),

$$I_i = \int_0^\infty F\alpha_i N_i k_i e^{-x/\lambda i} \, dx$$

is straightforward because for a homogeneous sample, F, $\alpha_i$, $N_i$, $k_i$ and $\lambda_i$ are independent of this parameter; the integrated form is

$$I_i = F\alpha_i N_i k_i \lambda_i \qquad \text{(eqn. A.15)}$$

Using this equation the stoichiometry (ratio of number densities) of a sample containing two core levels i and j is

$$\frac{N_j}{N_i} = \frac{I_j}{I_i} \times \frac{\alpha_i k_i \lambda_i}{\alpha_j k_j \lambda_j} \quad \text{(F cancels)} \qquad \text{(eqn. A.16)}$$

For any spectrometer the term $\frac{\alpha_i k_i \lambda_i}{\alpha_i k_j \lambda_j}$ is a constant which is known as the instrumental sensitivity factor and this can be determined by using standard compounds of known stoichiometry. If i and j are the same core-level but in different environments then $\alpha_i k_i \lambda_i = \alpha_j k_j \lambda_j$ so that

$$\frac{N_j}{N_i} = \frac{I_j}{I_i} \qquad \text{(eqn. A.17)}$$

and this is clearly of use when interpreting spectra such as the $C_{1s}$ envelope of a plasma polymer (see Chapter Five).

(ii) Substrate-Overlayer Model and Non-destructive Depth Profiling

A situation of common occurrence in ESCA analysis is of an inhomogeneous sample, typically a bulk sample with a modified surface or with an adventitious layer of hydrocarbon. It is appropriate therefore that a model has been developed[278,279] which gives insight into the effect of such overlayers on determined stoichiometries. Further, the model also aids understanding of why variation of substrate angle can enhance surface features and of the relatively greater contribution of the surface (compared with the subsurface) features to the observed signal.[280]

Consider a homogeneous overlayer of thickness d covering a homogeneous substrate which is infinitely thick (Figure A.9). From equation A.13 the intensity of the over-

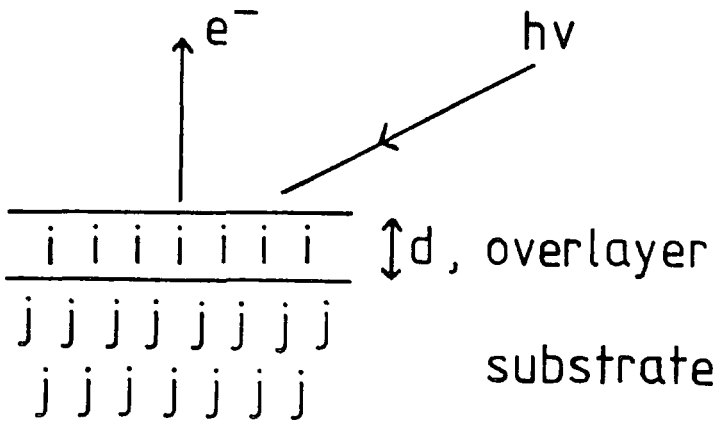


Figure A.9 SCHEMATIC OF THE SUBSTRATE-OVERLAYER MODEL

layer signal is given by

$$I_i^{over} = \int_o^d (F\alpha_i N_i k_i)\ e^{-x/\lambda i}\ dx$$

$$= (F\alpha_i N_i k_i \lambda_i)\ (1 - e^{-d/\lambda i}) \qquad \text{(eqn. A.18)}$$

and that from the substrate is

$$I_j^{subs} = \int_d^{\infty} (F\alpha_j N_j k_j)\ e^{-x/\lambda j}\ dx$$

$$= (F\alpha_j N_j k_j \lambda_j)\ (e^{-d/\lambda_j}) \qquad \text{(eqn. A.19)}$$

In practice these equations are modified slightly since the detected electrons are not emitted normal to the surface, but at an angle $\theta$ to the surface normal; thus the electron must actually travel a distance $d/\cos\theta$ to escape from the surface. Therefore the integration limit d is replaced by $d/\cos\theta$ and the equations are then

$$I_i^{over} = (F\alpha_i N_i k_i \lambda_i)\ (1 - e^{-d/\lambda i\ \cos\theta}) \qquad \text{(eqn. A.20)}$$

$$I_j^{subs} = (F\alpha_j N_j k_j \lambda_j)\ (e^{-d/\lambda j\ \cos\theta}) \qquad \text{(eqn. A.21)}$$

One method of depth profiling which is commonly used is to vary the substrate angle ($\theta$), samples typically being analysed at $30^{\circ}$ and $70^{\circ}$. Increasing $\theta$ leads to a decrease of the exponential term and therefore a decrease in the intensity of the substrate-derived signal and an increase in that from the overlayer. This is the rationalisation of the "enhancement of surface features upon increasing the angle of X-ray incidence ($\theta$)" which is commonly referred to.

Insight into the sampling depth of ESCA can be gained by considering a homogeneous sample within the substrate-overlayer model. Since the same core level is to be considered for both the overlayer and substrate the factors F, $\alpha$, N, k and $\lambda$ are equal and it may also be noted that the combination of these factors is equal to $I_\infty$, the signal intensity from a homogeneous sample (either from equation A.15 or by putting d=0 into equation A.21)

$$I_i^{over} = I_\infty (1 - e^{-d/\lambda i \cos\theta}) \qquad \text{(eqn. A.22)}$$

$$I_i^{subs} = I_\infty (e^{-d/\lambda i \cos\theta}) \qquad \text{(eqn. A.23)}$$

These equations represent the signal intensity derived from the top layer thickness d ($I_i^{over}$) and that originating below this top layer ($I_i^{subs}$). For example the amount of signal intensity derived from a top layer of thickness $\lambda_i$ (assuming for convenience that $\theta=90^o$) is

$$I_i^{over} = I_\infty (1 - e^{-1}) = 0.63\ I_\infty.$$

This means that 63% of the signal intensity of a core level arises from a layer of depth equal to the mean free path of the emitted electron; similarly 86% and 95% derive from depths of $2\lambda$ and $3\lambda$ respectively. The sampling depth of ESCA is usually taken to be that from which 95% of the signal intensity originates, *i.e.* $3\lambda$.

Since the sampling depth depends upon the mean free path of the emitted electron and this depends upon its kinetic energy, signals derived from different core levels of the same element will originate from different depths within the sample. A dramatic illustration of this is found for Germanium covered with an oxide layer[281] (Figure A.10); the lower kinetic energy electrons emitted from the Ge2p core level originate more from the oxide layer than do the higher kinetic energy electrons emitted from the Ge3d core level.

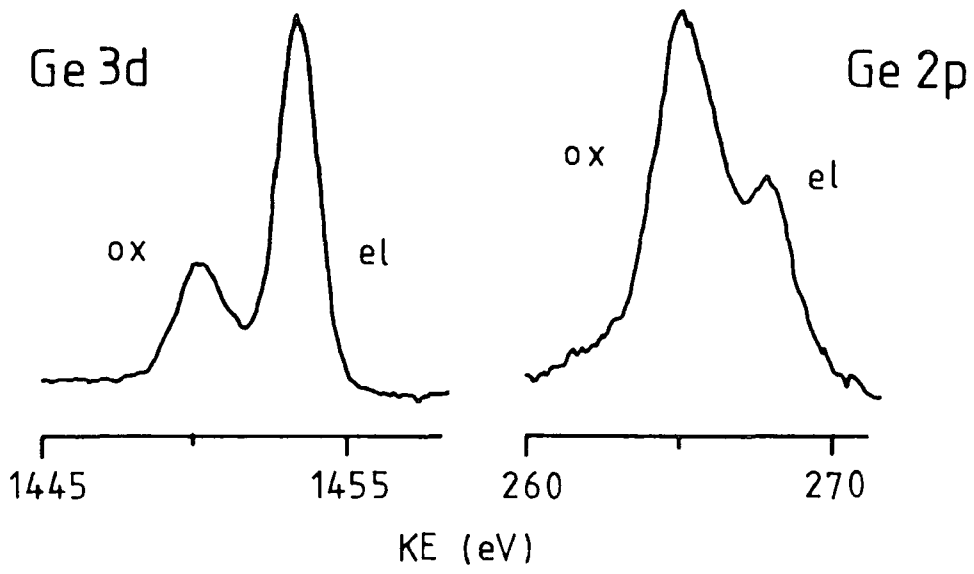


Figure A.10 $Al_{K\alpha}$ EXCITED CORE HOLE SPECTRA DERIVED FROM A GERMANIUM METAL TARGET WITH AN OXIDE OVERLAYER

# APPENDIX B

## COLLOQUIA AND CONFERENCES

The Board of Studies in Chemistry requires that each postgraduate research thesis contains an appendix, listing:

(A) all research colloquia, research seminars and lectures arranged by the Department of Chemistry during the period of the author's residence as a postgraduate student;

(B) all research conferences attended and papers presented by the author during the period when research for the thesis was carried out;

(C) details of the postgraduate induction course.

(* indicates attendance)

## (A) RESEARCH COLLOQUIA, SEMINARS AND LECTURES

1. Durham University Chemistry Department Colloquia.

14.10.81* Prof. E. Kluk (Katowice)
"Chemoluminescence and photo-oxidation"

28.10.81* Dr. R.J.H. Clark (U.C.L.)
"Resonance Raman Spectroscopy"

6.11.81* Dr. W. Moddeman (Monsanto)
"High energy materials"

18.11.81* Prof. M.J. Perkins (London)
"Spin-trapping and nitroxide radicals"

25.11.81 Dr. M. Baird (Newcastle)
"Intramolecular reactions of carbenes and carbenoids"

2.12.81* Dr. G. Beamson (Durham)
"Photoelectron spectroscopy in a strong magnetic field"

20. 1.82* Dr. M.R. Bryce (Durham)
"Organic metals"

27. 1.82 Dr. D.L.H. Williams (Durham)
"Nitrosation and nitrosoamines"

3. 2.82* Dr. D. Parker (Durham)
"Modern methods of determining enantiomeric purity"

10. 2.82 Dr. D. Pethrick (Strathclyde)
"Conformation of small and large molecules"

17. 2.82* Prof. D.T. Clark (Durham)
"Plasma Polymerization"

24. 2.82 Prof. R.D. Chambers (Durham)
"Recent reactions of fluorinated internal olefins"

2. 3.82* Dr. L. Field (Oxford)
"Applications of NMR to biosynthetic studies on pencillin"

3. 3.82* Dr. P. Bamfield (I.C.I. Organics)
"Computer aided design in synthetic organic chemistry"

17. 3.82 Prof. R.J. Haines (Natal)
"Clustering around Ruthenium, Iron and Rhodium"

7. 4.82* Dr. A. Pensak (Dupont, U.S.A.)
"Computer aided synthesis"

5. 5.82 Dr. G. Tennant (Edinburgh)
"Exploitation of the aromatic nitro-group in the design of new heterocyclisation reactions"

7. 5.82* Dr. C.D. Garner (Manchester)
"The structure and function of molybdenum centres in enzymes"

26. 5.82 Dr. A. Welch (Edinburgh)
"Conformation patterns and distortion in carbometalloboranes"

14. 6.82 Prof. C.M.J. Stirling (UCW, Bangor)
"How much does strain affect reactivity?"

28. 6.82* Prof. D.J. Burton (Iowa, USA)
"Some aspects of the chemistry of fluorinated phosphonium salts and their phosphonates"

2. 7.82 Prof. H.F. Koch (Ithaca College, Cornell, USA)
"Proton transfer to and elimination reactions from localized and delocalized carbanions"

13. 9.82 Prof. R. Neidlein (Heidelberg, FRG)
"New aspects and results of bridged annulene chemistry"

24. 9.82* Prof. G. Hoflund (Florida, USA)
"Electron Spectroscopy"

27. 9.82 Dr. W.K. Ford (Xerox, Webster, N.Y.)
"The dependence of the electron structure of polymers on their molecular architecture"

13.10.82* Dr. W.J. Feast (Durham)
"Approaches to the Synthesis of Conjugated Polymers"

14.10.82* Prof. H. Suhr (Tübingen, FRG)
"Preparative Chemistry in Nonequilibrium Plasmas"

27.10.82* Dr. C.E. Housecroft (Oxford High School/Notre Dame)
"Bonding capabilities of butterfly-shaped $Fe_4$ units. Implications for C-H bond activation in hydrocarbon complexes"

28.10.82 Prof. M.F. Lappert, FRS (Sussex)
"Approaches to Asymmetric Synthesis and Catalysis using electron-rich olefins and some of their metal complexes"

15.11.82* Dr. G. Bertrand (Toulouse, France)
"Curtius Rearrangement in Organometallic Series: A route for new hybridised species"

24.11.82* Prof. F.R. Hartley (R.M.C.S., Shrivenham)
"Supported Metal-Complex Hydroformylation Catalysts"

24.11.82* Prof. G.G. Roberts (Applied Physics, Durham)
"Langmuir-Blodgett films: Solid state polymerisation of diacetylenes"

8.12.82* Dr. G. Wooley (Trent)
"Bonds in transition metal-cluster compounds"

12. 1.83 Dr. D.C. Sherrington (Strathclyde)
"Polymer-supported phase transfer catalysts"

9. 2.83 Dr. P. Moore (Warwick)
"Mechanistic studies in solution by stopped flow F.T.-NMR and high pressure NMR line broadening"

21. 2.83* Dr. R. Lynden-Bell (Cambridge)
"Molecular motion in the cubic phase of NaCN"

2. 3.83 Dr. D. Bloor (Queen Mary College, London)
"The solid-state chemistry of diacetylene monomers and polymers"

8. 3.83 Prof. D.C. Bradley, FRS (Queen Mary College, London)
"Recent Developments in Organo-Imido-Transition Metal Chemistry"

9. 3.83* Dr. D.M.J. Lilley (Dundee)
"DNA, Sequence, Symmetry, Structure and Supercoiling"

11. 3.83* Prof. H.G. Viehe (Louvain, Belgium)
"Oxidations on Sulphur" and
"Fluorine substitutions in radicals"
(The W.K.R. Musgrave Lecture)

16. 3.83* Dr. I. Gosney (Edinburgh)
"New extrusion reactions: Organic synthesis in a hot-tube"

25. 3.83 Prof. F.G. Baglin (Nevada, USA)
"Interaction induced Raman Spectroscopy in supracritical ethane"

21. 4.83* Prof. J. Passmore (New Brunswick, Canada)
"Novel selenium-iodine cations"

4. 5.83 Prof. P.H. Plesch (Keele)
"Binary ionisation equilibria between two ions and two molecules. What Ostwald never thought of"

10. 5.83 Prof. K. Burger (Munich, FRG)
"New reaction pathways from trifluoromethyl-substituted heterodienes to partially fluorinated heterocyclic compounds"

11. 5.83 Dr. N. Isaacs (Reading)
"The Application of high pressures to the theory and practice of organic chemistry"

13. 5.83 Dr. R. de Koch (Michigan/Amsterdam)
"Electronic structural calculations in organometallic cobalt cluster molecules. Implications for metal surfaces"

16. 5.83* Prof. R.J. Lagow (Texas, USA)
"The chemistry of polylithium organic compounds. An unusual class of matter"

18. 5.83 Dr. D.M. Adams (Leicester)
"Spectroscopy at very high pressures"

25. 5.83 Dr. J.M. Vernon (York)
"New heterocyclic chemistry involving lead tetraacetate"

15. 6.83 Dr. A. Pietrzykowski (Warsaw/Strathclyde)
"Synthesis, structure and properties of Aluminoxanes"

22. 6.83 Dr. D.W.H. Rankin (Edinburgh)
"Floppy molecules - the influence of phase on structure"

5. 7.83 Prof. J. Miller (Camfinas, Brazil)
"Reactivity in nucleophilic substitution reactions"

5.10.83* Prof. J.P. Maier (Basel, Switzerland)
"Recent approaches to spectroscopic characterization of cations"

12.10.83* Dr. C.W. McLeland (Port Elizabeth, Australia)
"Cyclization of aryl alcohols through the intermediacy of alkoxy radicals and aryl radical cations"

19.10.83 Dr. N.W. Alcock (Warwick)
Aryl tellurium (IV) compounds, patterns of primary and secondary bonding"

26.10.83* Dr. R.H. Friend (Cavendish, Cambridge)
"Electronic properties of conjugated polymers"

30.11.83* Prof. J .M.G. Cowie (Stirling)
"Molecular interpretation of non-relaxation processes in polymer glasses"

2.12.83 Dr. G.M. Brooke (Durham)
"The fate of the *ortho*-fluorine in 3,3-sigmatropic reactions involving polyfluoro-aryl and -heteroaryl systems"

14.12.83* Prof. R.J. Donovan (Edinburgh)
"Chemical and physical processes involving the ion-pair states of the halogen molecules"

10. 1.84* Prof. R. Hester (York)
"Nanosecond laser spectroscopy of reaction intermediates"

18. 1.84* Prof. R.K. Harris (UEA)
"Multi-nuclear solid state magnetic resonance"

8. 2.84* Dr. B.T. Heaton (Kent)
"Multi-nuclear NMR studies"

15. 2.84 Dr. R.M. Paton (Edinburgh)
"Heterocyclic syntheses using nitrile sulphides"

7. 3.84 Dr. R.T. Walker (Birmingham)
"Synthesis and biological properties of some 5-substituted uracil derivatives; yet another example of serendipity in antiviral chemotherapy"

21. 3.84* Dr. P. Sherwood (Newcastle)
"X-ray photoelectron spectroscopic studies of electrode and other surfaces"

23. 3.84* Dr. A. Ceulemans (Leuven)
"The Development of Field-Type models of the Bonding in Molecular Clusters"

2. 4.84* Prof. K. O'Driscoll (Waterloo)
"Chain Ending reactions in Free Radical Polymerisation"

3. 4.84* Prof. C.H. Rochester (Dundee)
"Infrared Studies of Adsorption at the Solid-liquid interface"

25. 4.84* Dr. R.M. Acheson (Biochemistry, Oxford)
"Some Heterocyclic Detective Stories"

27. 4.84* Dr. T. Albright (Houston, U.S.A.)
"Sigmatropic Rearrangements in Organometallic Chemistry"

14. 5.84* Prof. W.R. Dolbier (Florida, USA)
"Cycloaddition reactions of fluorinated Allenes"

16. 5.84* Dr. P.J. Garratt (UCL)
"Syntheses with Dilithiated Vicinal Diesters and Carboximides"

22. 5.84* Prof. F.C. de Schryver (Leuven)
"The use of Luminescence in the study of micellar aggregates" and
"Configurational and Conformational control in excited state complex formation"

23. 5.84* Prof. M. Tada (Waseda, Japan)
"Photochemistry of Dicyanopyrazine Derivatives"

31. 5.84* Dr. A. Haaland (Oslo)
"Electron Diffraction Studies of some organometallic compounds"

11. 6.84* Dr. J.B. Street (IBM, California)
"Conducting Polymers derived from Pyrroles"

19. 9.84* Dr. C. Brown (IBM, California)
"New Superbase reactions with organic compounds"

21. 9.84* Dr. H.W. Gibson (Signal UOP, Illinois)
"Isomerization of Polyacetylene "

2. Durham University Chemical Society Lectures

22.10.81* Dr. P.J. Corish (Dunlop)
"What would life be like without rubber?"

29.10.81* Miss J.M. Cronyn (Durham)
"Chemistry in Archaeology"

12.11.81* Prof. A.I. Scott (Edinburgh)
"An organic chemist's view of life through the NMR tube"

19.11.81* Prof. B.L. Shaw (Leeds)
"Big rings and metal-carbon bond formation"

26.11.81 Dr. W.O. Ord (Northumbrian Water)
"The role of the Scientist in a Regional Water Authority"

3.12.81* Dr. R.E. Hester (York)
"Spectroscopy with Lasers"

28. 1.82 Prof. I. Fells (Newcastle)
"Balancing the Energy Equations"

11. 2.82* Dr. D.W. Turner (Oxford)
"Photoelectrons in a strong magnetic field"
(The RSC Liversidge Lecture)

18. 2.82* Prof. R.K. Harris (UEA)
"NMR in the 198Os"

25. 2.82* Prof. R.O.C. Norman, FRS (York)
"Turning points and Challenges for the Organic Chemist"

4. 3.82 Dr. R. Whyman (ICI, Runcorn)
"Making Metal Clusters Work"

14.10.82* Mr. F. Shenton (County Analyst, Durham)
"There is death in the pot"

28.10.82* Prof. M.F. Lappert, FRS (Sussex)
"The Chemistry of some unusual Subvalent compounds of the Main Group IV and V Elements"

4.11.82* Dr. D.H. Williams (Cambridge)
"Studies on the Structures and Modes of Action of Antibiotics"

11.11.82* Dr. J. Cramp (ICI)
"Lasers in Industry"

25.11.82* Dr. D.H. Richards (PERME, MOD)
"Terminally Functional Polymers - their Synthesis and Uses"

27. 1.83* Prof. D.W.A. Sharp (Glasgow)
"Some Redox Reactions in Fluorine Chemistry"

3. 2.83* Dr. R. Manning (Zoology, Durham)
"Molecular Mechanisms of Hormone Actiom"

10. 2.83* Sir Geoffrey Allen, FRS (Unilever)
"U.K. Research Ltd."

17. 2.83* Prof. A.G. MacDiarmid (Pennsylvania, USA)
"Metallic Covalent Polymers: $(SN)_x$ and $(CH)_x$ and their Derivatives"
(The RSC Centenary Lecture)

3. 3.83* Prof. A.C.T. North (Leeds)
"The Use of a Computer Display System in Studying Molecular Structures and Interactions"

20.10.83* Prof. R.B. Cundall (Salford)
"Explosives"

3.11.83* Dr. G. Richards (Oxford)
"Quantum Pharmacology"

10.11.83 Prof. J.H. Ridd (UCL)
"*Ipso*-Attack in Electrophilic Aromatic Substitution"

17.11.83* Dr. J. Harrison (Sterling Organic)
"Applied Chemistry and the Pharmaceutical Industry"

24.11.83* Prof. D.A. King (Liverpool)
"Chemistry in two-dimensions"

1.12.83* Dr. J.D. Coyle (Open University)
"The Problem with Sunshine"

26. 1.84* Prof. T.L. Blundell (Birbeck, London)
"Biological Recognition: Interactions of Macromolecular Surfaces"

2. 2.84* Prof. N.B.H. Jonathan (Southampton)
"Photoelectron Spectroscopy - a Radical Approach"

16. 2.84* Prof. D. Philipps (Royal Institution)
"Luminescence and Photochemistry - a light entertainment"

23. 2.84* Prof. F.G.A. Stone, FRS (Bristol)
"The Use of Carbene and Carbyne Groups to Synthesise Metal Clusters"
(The Waddington Memorial Lecture)

1. 3.84* Prof. A.J. Leadbetter (Rutherford Appleton Labs.)
"Liquid Crystals"

8. 3.84* Prof. D. Chapman (Royal Free Hospital, London)
"Phospholipids and Biomembranes, Basic Science and Future Techniques"

28. 3.84* Prof. H. Schmidbaur (Munich, FRG)
"Ylides in Coordination Sphere of Metals: Synthetic, Structural and Theoretical Aspects"
(The RSC Centenary Lecture)

(B) RESEARCH CONFERENCES ATTENDED

21. 4.82 Graduate Symposium, Durham

15. 4.83 Graduate Symposium, Durham

28. 4.83 "Organic Reaction Paths: Theory and Experiment" RSC (Faraday and Perkin), London.

8-9.9.83 "Photooxidation and Photostabilisation of Polymers" Polymer Degradation Discussion Group, Durham.

11. 4.84 Graduate Symposium, Durham

Partial attendance at:
16-20.7.84 "Chemistry of Carbanions" RSC (Perkin), Durham.

(C) POSTGRADUATE INDUCTION COURSE

In each part of the course, the uses and limitations of the various services available were explained.

Departmental Organisation - Dr. E.J.F. Ross.

Electrical appliances and infrared spectroscopy - Mr. R.N. Brown.

Chromatography - Mr. J.A. Parkinson.

Microanalysis - Mr. T.F. Holmes and Mrs. M. Cocks.

Atomic absorption spectrometry and inorganic analysis - Mr. R. Coult

Mass spectroscopy - Dr. M. Jones.

N.m.r. spectroscopy - Dr. R.S. Matthews.

Glassblowing techniques - Mr. R. Hart and Mr. G. Haswell.

Safety matters - Dr. M.R. Crampton.

## REFERENCES


1. G. Olah, G. Prakash, M. Saunders, Acc.Chem.Res. (1983), 16, 440 .

2. H. Brown, Acc.Chem.Res. (1983), 16, 432.

3. C. Walling, Acc.Chem.Res., (1983), 16, 448.

4. C. Grob, Acc.Chem.Res., (1983), 16, 426.

5. V. Barkhash in Top.Curr.Chem., Vol.116/117, Ed.: F. Boschke, Springer-Verlag, Berlin, (1984).

6. H. Brown, P. Schleyer, "The Nonclassical Ion Problem", Plenum Press, New York, (1977).

7. G. Olah *et al*, J.Am.Chem.Soc., (1964), 86, 1360.

8. G. Olah, A. White, J.Am.Chem.Soc., (1969), 91, 5801.

9. G. Kramer, Adv.Phys.Org.Chem., (1975), 11, 177.

10. D. Farnum, Adv.Phys.Org.Chem., (1975), 11, 123.

11. P. Schleyer *et al* J.Am.Chem.Soc., (1980), 102, 683.

12. G. Olah *et al* J.Am.Chem.Soc., (1982), 104, 7105.

13. C. Yannoni, V. Macho, P. Myhre, J.Am.Chem.Soc., (1982), 104, 7380.

14. M. Saunders in "Stereodynamics of Molecular Systems", Ed.: R. Sarma, Pergamon, Elmsford (1979).

15. M. Saunders, L. Telkowski, M. Kates, J.Am.Chem.Soc., (1977), 99, 8070.

16. M. Saunders, M. Kates, J.Am.Chem.Soc., (1977), 99, 8071.

17. H. Brown, Tetrahedron, (1976), 32, 179.

18. G. Olah *et al*,
J.Am.Chem.Soc., (1970), 92, 7231.

19. G. Olah, G. Mateescu, J. Riemenschneider,
J.Am.Chem.Soc., (1972), 94, 2529.

20. G. Olah *et al*,
J.Am.Chem.Soc., (1973), 95, 8698.

21. G. Mateescu, J. Riemenschneider in
Proc.Int.Conf.Electron Spectrosc.,
Ed.: D. Shirley, (1971).

22. M. Saunders, E. Hagen, J. Rosenfeld,
J.Am.Chem.Soc., (1968), 90, 6882.

23. K. Siegbahn *et al*,
"ESCA applied to free molecules",
North-Holland Publishing Co., Amsterdam, (1969).

24. U. Gelius *et al*,
J.Electron Spectrosc.Relat.Phenom, (1972), 1, 285.

25. L. Radom, D. Poppinger, R. Haddon in
"Carbonium Ions", Vol.V,
Eds.: G. Olah, P. Schleyer,
Wiley-Interscience, New York, (1976).

26. W. Hehre in
"Modern Theoretical Chemistry", Vol.IV,
Ed.: H. Schaefer,
Plenum, New York, (1977).

27. W. Jorgensen,
J.Am.Chem.Soc., (1977), 99, 280.

28. W. Jorgensen,
J.Am.Chem.Soc., (1977), 99, 4272.

29. W. Jorgensen,
J.Am.Chem.Soc., (1978), 100, 1049.

30. W. Jorgensen, J. Munroe,
Tetr.Lett., 1977, 581.

31. M. Saunders, J. Chandrasekhar, P. Schleyer in
"Rearrangements in Ground and Excited States", Vol.I,
Ed.: P. Mayo,
Academic Press, London, (1980).

32. H. Mayr, W. Förner, P. Schleyer,
J.Am.Chem.Soc., (1979), 101, 6032.

33. M. Cournoyer, W. Jorgensen,
J.Am.Chem.Soc., (1984), 106, 5104.

34. D. Bethell, V. Gold,
"Carbonium Ions; an introduction",
Academic Press, London, (1967).

35. J. March,
"Advanced Organic Chemistry",
McGraw-Hill, Kogakusha, Tokyo, (1977).

36. G. Olah *et al*,
J.Am.Chem.Soc., (1963), 85, 1328.

37. G. Olah, D. Donovan,
J.Am.Chem.Soc., (1978), 100, 5163.

38. R. Alder, R. Baker, J. Brown,
"Mechanism in Organic Chemistry",
Wiley-Interscience, Chichester, (1971).

39. P. Myhre, C. Yannoni,
J.Am.Chem.Soc., (1981), 103, 230.

40. C. Yannoni, V. Macho, P. Myhre,
J.Am.Chem.Soc., (1982), 104, 907.

41. P. Myhre, C. Yannoni, V. Macho,
Prepr. - Am.Chem.Soc., Div.Pet.Chem., (1983), 28, 271.

42. M. Saunders, D. Cox, W. Ohlmstead,
J.Am.Chem.Soc., (1973), 95, 3018.

43. M. Saunders, D. Cox, J. Lloyd,
J.Am.Chem.Soc., (1979), 101, 6656.

44. K. Moss, M. Smith in
"International Review of Science (Inorganic Chemistry
Series 2)", Vol.II,
Ed.: D. Sowerby,
Butterworths, London, (1975).

45. J. Bacon, P. Dean, R. Gillespie,
Can.J.Chem., (1969), 47, 1655.

46. G. Olah,
"Halonium Ions",
Wiley-Interscience, New York, (1975).

47. A. Auerbach, R. Cross, M. Saunders,
J.Am.Chem.Soc., (1978), 100, 4908.

48. L. Lee *et al*,
J.Am.Chem.Soc., (1981), 103, 5031.

49. K. Alben *et al*,
J.Am.Chem.Soc., (1978), 100, 3274.

50. G. Olah *et al*,
J.Am.Chem.Soc., (1964), 86, 5679.

51. R. Gillespie,
Acc.Chem.Res., (1968), 1, 202.

52. J. Barr, R. Gillespie, R. Thompson,
Inorg.Chem., (1964), 3, 1149.

53. R. Thompson in
"Inorganic Sulphur Chemistry",
Ed.: G. Nickless,
Elsevier, Amsterdam, (1968).

54. A. Jache,
Adv.Inorg.Radiochem., (1974), 16, 177.

55. G. Olah, G. Prakash, J. Sommer,
Science, (1979), 206, 13.

56. G. Olah *et al*,
J.Am.Chem.Soc., (1970), 92, 4627.

57. J. Larsen *et al*,
J.Am.Chem.Soc., (1974), 96, 2284.

58. D. Quarroz, P. Vogel,
Helv.Chim.Acta (1979), 62, 335.

59. J. Scofield,
J.Electron Spectrosc.Relat.Phenom, (1976), 8, 129.

60. H. Thomas,
Ph.D. Thesis, University of Durham (1977).

61. G. Olah,
Science, (1970), 168, 1298.

62. L. Schmerling,
J.Am.Chem.Soc. (1946), 68, 195.

63. D. Clark, B. Cromarty, L. Colling,
J.Am.Chem.Soc., (1977), 99, 8120.

64. B. Cromarty,
Ph.D.Thesis, University of Durham, (1978).

65. J. Beynon, A. Brenton,
"An Introduction to Mass Spectrometry",
Univ.Wales Press, Cardiff, (1982).

66. A. Maccoll,
Chem.Rev., (1969), 69, 33.

67. K. Howlett,
J.Chem.Soc., 1952, 4487.

68. W. Tsang,
J.Chem.Phys., (1964), 40, 1498.

69. D. Brearley *et al*,
J.Am.Chem.Soc., (1936), 58, 43.

70. See, for example, reference 63.

71. M. Saunders, P. Schleyer, G. Olah,
J.Am.Chem.Soc., (1964), 86, 5680.

72. M. Saunders, M. Kates,
J.Am.Chem.Soc., (1980), 102, 6867.

73. H. Brown, K. Liu,
J.Am.Chem.Soc., (1975), 97, 600.

74. M. Dewar *et al*,
J.Am.Chem.Soc., (1977), 99, 377.

75. P. Hariharan *et al*,
J.Am.Chem.Soc., (1974), 96, 599.

76. D. Goetz, H. Schlegel, L. Allen,
J.Am.Chem.Soc., (1977), 99, 8118.

77. J. Pople in
"Molecular Ions", NATO ASI Series B, Vol.90,
Eds.: J. Berkowitz, K. Groeneveld,
Plenum Press, New York, (1983).

78. W. Jolly,
J.Am.Chem.Soc., (1970), 92, 3260.

79. D. Clark, B. Cromarty in
"Progress in Theoretical Organic Chemistry", Vol.II,
Ed.: I. Csizmadia,
Elsevier, Amsterdam, (1977).

80. D. Clark, A. Harrison,
J.Electron Spectrosc.Relat.Phenom., (1982), 27, 57.

81. G. Wenke, D. Lenoir,
Tetrahedron, (1979), 35, 489.

82. H. Köhler, H. Lischka,
J.Am.Chem.Soc., (1979), 101, 3479.

83. J. Goddard, Y. Osamura, H. Schaefer,
J.Am.Chem.Soc., (1982), 104, 3258.

84. K. Raghavachari *et al*,
J.Am.Chem.Soc., (1983), 105, 5915.

85. M. Yoshimine *et al*,
J.Am.Chem.Soc., (1983), 105, 6185.

86. A. Dilks in
"Electron Spectroscopy", Vol.IV,
Ed.: C. Brundle, A. Baker,
Academic Press, London, (1981).

87. P. Atkins,
"Physical Chemistry",
Oxford University Press, Oxford, (1978).

88. N. Greenwood,
"Ionic Crystals, Lattice Defects and Nonstoichiometry",
Butterworth, London, (1968).

89. F. Blatt,
"Physics of electronic conduction in solids",
McGraw Hill (Materials Science and Engineering Series),
New York, (1968).

90. G. Olah, J. Lukas,
J.Am.Chem.Soc., (1967), 89, 2227.

91. G. Olah, J. Sommer, E. Namanworth,
J.Am.Chem.Soc., (1967), 89, 3576.

91a. E. Bittner, E. Arnett, M. Saunders,
J.Am.Chem.Soc., (1976), 98, 3734.

92. M. Saunders *et al*,
Acc.Chem.Res., (1973), 6, 53.

93. G. Olah, D. Donovan,
J.Am.Chem.Soc., (1977), 99, 5026.

94. M. Saunders *et al*,
J.Am.Chem.Soc., (1977), 99, 8072.

95. L. Radom, J. Pople, P. Schleyer,
J.Am.Chem.Soc., (1972), 94, 5935.

96. D. Clark, A. Harrison,
Chem.Phys.Letts. (1981), 82, 143.

97. W. Crookes,
Phil.Trans. (1879), 1, 135.

98a. "Techniques and Applications of Plasma Chemistry",
Ed.: J. Hollahan, A. Bell,
J. Wiley, New York, (1974).

98b. A. Bell, Chapter 1 in reference 98a.

99. H. Suhr, Chapter 2 in reference 98a.

100. B. Chapman,
"Glow Discharge Processes",
J. Wiley, New York, (1980).

101. H. Suhr,
Plasma Chem.Plasma Process, (1983), 3, 1.

102. L. Miller,
Acc.Chem.Res., (1983), 16, 194.

103. R. Lagow, J. Morrison,
Adv.Inorg.Chem.Radiochem., (1980), 23, 177.

104. H. Suhr, U. Schöch, G. Rosskamp,
Chem.Ber., (1971), 104, 674.

105. L. Taylor,
Ind.Res.Dev., (1981), 23. 124.

106. D. Hercules, S. Hercules,
J.Chem.Ed., (1984), 61, 592.

107. "Secondary Ion Mass Spectrometry SIMS II",
(Chemical Physics, No.9),
Ed.: A. Benninghoven *et al*,
Springer-Verlag, New York, (1979).

108. J. Curran,
Phys.Technol., (1983), 14, 283.

109. H. Winters, J. Coburn, T. Chuang,
J.Vac.Sci.Technol., (1983), B1(2), 469.

110. D. Flamm, V. Donnelly, D. Ibbotson,
J.Vac.Sci.,Technol., (1983), B1(1), 23.

111. G. Turban,
Pur.Appl.Chem., (1984), 56, 215.

112. R. Kirk, Chapter 9 in reference 98a.

113. H. Yasuda,
J.Membr.Sci., (1984), 18, 273.

114. W. Freitag, H. Yasuda, A. Sharma,
Org.Coat.Appl.Polym.Sci.Proc., (1982), 47, 449.

115. S. Hattori *et al*,
Org.Coat.Appl.Polym.Sci.Proc., (1982), 47, 136.

116. D. Allam, C. Stoddard,
Chem.Brit., (1965), 1, 410.

117. H. Nomura, P. Kramer, H. Yasuda,
Thin Solid Films, (1984), 118, 187.

118. D. Clark, D. Shuttleworth,
J.Polym.Sci., Polym.Chem.Ed., (1980), 18, 27.

119. D. Clark, D. Shuttleworth,
*ibid*, (1978), 16, 1093.

120. D. Clark, D. Shuttleworth,
*ibid*, (1979), 17, 1317.

121. D. Clark, D. Shuttleworth,
*ibid*, (1980), 18, 407.

122. D. Clark, M. Abrahman,
*ibid*, (1981), 19, 2129.

123. D. Clark, M. Abrahman,
*ibid*, (1981), 19, 2689.

124. D. Clark, M. Abrahman,
*ibid*, (1982), 20, 691.

125. D. Clark, M. Abrahman,
*ibid*, (1982), 20, 1717.

126. D. Clark, M. Abrahman,
*ibid*, (1982), 20, 1729.

127. D. Clark, M. Abu-shbak,
*ibid*, (1983), 21, 2907.

128. D. Clark, M. Abu-shbak,
*ibid*, (1984), 22, 1.

129. D. Clark, M. Abu-shbak,
*ibid*, (1984), 22, 17.

130a. "Plasma Polymerization",
ACS Symposium Series No. 108,
Ed.: M. Shen, A. Bell,
Am.Chem.Soc., Washington, D.C., (1979).

130b. M. Pender, *et al*, p.147 in reference 130a.

131a. Top.Curr.Chem.No.94,
Ed.: S. Veprek, M. Venugoplan,
Springer-Verlag, Berlin Heidelberg, (1980).

131b. E. Kay, J. Coburn, A. Dilks, p.1 in reference 131a.

132. A. Dilks, S. Kaplan,
Org.Coat.Appl.Poly,.Sci.Proc., (1982), 47, 212.

133. H. Yasuda, T. Hirotsu,
J.Polym.Sci.Polym.Chem.Ed., (1978), 16, 743.

134. A. Bell, p.49 in reference 131a.

135. A. Westwood,
Eur.Polym.J., (1971), 7, 363.

136. H. Yasuda,
J.Polym.Sci.Macromol.Rev., (1981), 16, 199.

137. D. Hutton,
Ph.D. Thesis, University of Durham (1983).

138. W. Brennan,
Ph.D. Thesis, University of Durham, (1984).

139. R. D'Agostino *et al*
J.Appl.Phys., (1983), 54, 1284.

140. H. Yasuda, M. Bumgarner, J. Hillman,
J.Appl.Polym.Sci., (1975), 19, 531.

141. H. Yasuda, p.37 in reference 130a.

142a. "Electrical Breakdown and Discharges in Gases",
NATO ASI Series B, No.89b,
Ed.: E. Kunhordt, L. Luessen,
Plenum Press, New York, (1983).

142b. A. Goldman, J. Amouroux, p.293 in reference 142a.

143. D. Clark, A. Dilks, D. Shuttleworth, Chapter 9 in
"Polymer Surfaces",
Ed.: D. Clark, W. Feast,
Wiley-Interscience, Chichester, (1978).

144. D. Clark, R. Wilson,
J.Polym.Sci.Polym.Chem.Ed., (1983), 21, 837.

145. M. Hudis, Chapter 3 in reference 98a.

146. C. Broganza *et al*, p.100 in
Int.Symp.Plasma Chem.4th,
Ed.: S. Veprek, J. Hertz,
Zurich, Switz., (1979).

147. E. Wirz, H. Oswald, S. Veprek,
*ibid*, p.492.

148. A. Gicquel, M. Bergougnan, J. Amouroux,
Proc. - Electrochem.Soc., (1983), 83(10), 169.

149. J. Osher, Chapter 12 in
"Plasma Diagnostic Techniques"
Ed.: R. Huddlestone, S. Leonard,
Academic Press, New York, (1965).

150. A. Dilks, E. Kay,
Macromolecules, (1981), 14, 855.

151. J. Coburn,
Rev.Sci.Inst., (1970), 41, 1219.

152. R. Gottscho, T. Miller,
Pur.Appl.Chem. (1984), 56, 189.

153. R. Waters, p.203 in reference 142a.

154. F. Bastien, p.267 in reference 142a.

155. D. Benenson, H. Kwoh,
Pur.Appl.Chem., (1982), 54, 1157.

156. W. Harshbarger, *et al*,
Appl.Spectrosc., (1977), 31, 201.

157. B. Soller, R. Shuman, R. Ross,
J.Electrochem.Soc., (1984), 131, 1353.

158. T. Venkatesan *et al*,
J.Vac.Sci.Technol., (1981), 19, 1379.

159. L. Ryabova, Chapter 5 in
"Current Topics in Materials Science, Vol.7",
Ed.: E. Kaldis,
North Holland, Amsterdam, (1981).

160. D. Carlson,
J.Electrochem.Soc., (1975), 122, 1334.

161. E. Kny *et al*,
Thin Solid Films, (1979), 64, 395.

162. E. Kny *et al*,
J.Phys.Chem., (1980), 84, 1635.

163. N. Inagaki, T. Yagi, K. Katsuura,
Eur.Polym.J., (1982), 18, 621.

164. N. Inagaki, M. Mitsuuchi,
J.Polym.Sci.Polym.Lett.Ed., (1984), 22, 301.

165. S. Morita *et al*, p.259 in
Int.Symp.Plasma Chem.5th
Ed.: B. Waldie, G. Farnell,
Heriot-Watt Univ., Edinburgh, U.K., (1981).

166. H. Munro, C. Till,
Thin Solid Films (in press).

167. N. Inagaki, M. Mitsuuchi,
J.Polym.Sci.Polym.Chem.Ed., (1983), 21, 2887.

168. N. Morosoff *et al*,
Thin Solid Films, (1984), 117, 33.

169. H. Munro, J. Eaves,
J.Polym.Sci.Polym.Chem.Ed. (in press).

170. E. Kay, A. Dilks, U. Hetzler,
J.Macromol.Sci.Chem., (1978), A12, 1393.

171. E. Kay, A. Dilks,
J.Vac.Sci.Technol., (1979), 16, 428.

172. E. Kay, A. Dilks, D. Seybold,
J.Appl.Phys., (1980), 51, 5678.

173. A. Dilks, E. Kay, p.195 in reference 130a.

174. E. Kay, M. Hecq,
J.Appl.Phys., (1984), 55, 370.

175. E. Kay, M. Hecq,
J.Vac.Sci.Technol., (1984), A2(2), 401.

176. D. Shuttleworth,
J.Phys.Chem., (1980), 84, 1629.

177. J. Blackborow, D. Young,
"Metal Vapour Synthesis in Organometallic Chemistry",
Springer-Verlag, Berlin, (1979).

178. P. Timms,
Adv.Inorg.Radiochem., (1972), 14, 121.

179. K. Klabunde,
Acc.Chem.Res., (1975), 8, 393.

180. H. Holzinger, K. Meyer, H. Tiller,
Z.Chem., (1973), 13, 32.

181. Y. Asano,
Thin Solid Films, (1983), 105, 1.

182. H. Munro, C. Till,
J.Polym.Sci.Polym.Chem.Ed. (in press).

183. H. Beale,
Ind.Res.Dev., (1981), 23, 135.

184. M. Yamada *et al*,
Jpn.J.Appl.Phys., (1982), 21, 768.

185. P. Timms,
J.Chem.Ed., (1972), 49, 782.

186. "Handbook of X-ray Photoelectron Spectroscopy",
Ed.: C. Wagner *et al*,
Perkin-Elmer, (1979).

187. T. Patterson *et al*,
J.Phys.Chem., (1976), 80, 1702.

188. K. Kim *et al*,
J.Electron Spectrosc.Relat.Phenom, (1974), 5, 351.

189. F. Cotton, G. Wilkinson, p.946 in
"Advanced Inorganic Chemistry",
Interscience, New York (3rd Edition, 1972).

190. O. Matsumoto, p.1379 in
Proc.Int.Ion.Eng.Congr., (1983),
Ed.: T. Takagi,
Kyoto, Japan.

191. M. Konuma, Y. Kanzaki, O. Matsumoto, p.174 in
Int.Symp.Plasma Chem., (4th),
Ed.: S. Veprek, J. Hertz,
Zurich, Switz. (1979).

192. R. Baumhardt-Neto *et al*,
J.Polym.Sci.Polym.Chem.Ed., (1981), 19, 819.

193. R. Chambers,
"Fluorine in Organic Chemistry",
Wiley, New York (1973).

194. R. Chambers, R. Middleton, R. Corbally,
J.Chem.Soc.Chem.Comm., (1975), 731.

195. R. Chambers, W. Musgrave, K. Srivastava,
J.Chem. Soc:Chem.Comm., (1971), 264.

196. R. Chambers, C. Sargent,
J.Chem.Soc.Chem.Comm., (1979), 446.

197. M. Dewar, W. Thiel,
J.Am.Chem.Soc., (1977), 99, 4899, 4907.

198. M. Dewar, H. Rzepa,
J.Am.Chem.Soc. (1978), 100, 58.

199a. R. Fletcher, M. Powell,
Comp.J. (1963), 6, 163.

199b. W. Davidson,
Comp.J. (1968), 10, 406.

200. "Tables of Interatomic Distances",
Chem.Soc.Special Publ.No.11 and (Supplement) No.18,
Ed.: L. Sutton,
Chem.Soc., London (1958, 1965).

201. W. Niessen, W. Kraemer, G. Diecksen,
Chem.Phys. (1979), 41, 113.

202. J. Almlöf *et al*,
J.Electron Spectrosc.Relat.Phenom. (1973), 2, 51.

203. R. Wagner, P. Hockman, M. El-Bayoumi,
J.Mol.Spectrosc. (1975), 54, 167.

204. R. Bingham, M. Dewar, D. Lo,
J.Am.Chem.Soc., (1975), 97, 1302.

205. J. Cox, G. Pilcher,
"Thermochemistry of Organic and Organometallic Compounds",
Academic Press, New York, (1970).

206. M. Cardillo, S. Bauer,
J.Am.Chem.Soc., (1970), 92, 2399.

207. B. Andersen, H. Seip, B. Beagley,
Acta Chem.Scand. (1969), 1837.

208. J. Oth,
Recl.Trav.Chim.Pays-Bas (1968), 87, 1185.

209. D. Lemal, L. Dunlap,
J.Am.Chem.Soc., (1972), 94, 6562.

210. M. Newton, J. Shulman, M. Manus
J.Am.Chem.Soc. (1974), 96, 17.

211. N. Baird, M. Dewar,
J.Am.Chem.Soc., (1969), 91. 352.

212. R. Bingham, M. Dewar, D. Lo,
J.Am.Chem.Soc., (1975), 97, 1294.

213. T. Koopmans,
Physica (1933), 1, 104.

214. R. Suffolk,
J.Electron Spectrosc.Relat.Phenom. (1974), 3, 53.

215. E. Heilbronner *et al*,
Helv.Chim.Acta (1971), 54, 783.

216. R. Chambers, J. MacBride, W. Musgrave,
Unpublished results.

217. S. Mason,
J.Chem.Soc., (1959), 1247.

218. K. Innes, J. Byrne, I. Ross,
J.Mol.Spectrosc., (1967), 22, 125.

219. R. Hochstrasser, C. Morzzacco,
J.Chem.Phys., (1968), 49, 971.

220a. General discussions of the rearrangement of these isomers are given in references 220b-223.

220b. D. Bryce-Smith, A. Gilbert,
Tetrahedron, (1976), 32, 1309.

221. J. Baltrop, J. Coyle,
"Excited States in Organic Chemistry",
Wiley, New York, (1975).

222. I. Haller,
J.Chem.Phys. (1967), 47, 1117.

223. L. Scott, M. Jones,
Chem.Rev., (1972), 72. 181.

224. K. Siegbahn *et al*,
"ESCA, Atomic, Molecular and Solid State Structure Studied by means of Electron Spectroscopy",
Almquist and Wiksells, Uppsala, (1967).

225. K. Siegbahn,
Rev.Mod.Phys., (1982), 54. 709.

226. K. Siegbahn,
Science, (1982), 217. 111.

227a. "Electron Emission Spectroscopy",
Ed.: W. Dekeyser,
D. Reidel, Dordrecht-Holland, (1973).

227b. D. Clark, p.373 in reference 227a.

228. D. Clark, Plenary lecture in
"Advances in Polymer Friction and Wear", Polymer Science and Technology, Vol.5A,
Ed.: L. Lee,
Plenum, New York, (1974).

229a. "Handbook of X-ray and Ultra-Violet Photoelectron Spectroscopy",
Ed.: D. Briggs,
Heyden, London, (1977).

229b. D. Clark, Chapter 6 in reference 229a.

230a. "Photon, Electron and Ion Probes of Polymer Structure and Properties",
Eds.: D. Dwight, T. Fabish, H. Thomas,
Am.Chem.Soc., Washington, (1981).

230b. D. Clark, Chapter 17 in reference 230a.

231. B. Henke,
Adv.X-ray Anal. (1969), 13, 1.

232. C. Wagner,
Farad.Disc.Chem.Soc., (1975), 60, 306.

233. A. Barrie, Chapter 2 in reference 229a.

234. Z. Horak,
Proc.Phys.Soc.London, (1961), 77, 980.

235. V. Demekhin, V. Sachenko,
Bull.Acad.Sci.USSR.Phys.Ser. (1967), 31, 913,921.

236. L. Parratt,
Rev.Mod.Phys. (1959), 31, 616.

237. E. Purcell,
Phys.Rev. (1938), 54, 818.

238a. "Practical Surface Analysis",
Ed.: D. Briggs, M. Seah,
J. Wiley, Chichester (1983).

238b. J. Rivière, Chapter 2 in reference 238a.

239. W. Heisenberg,
Zeitschr.f. Phys. (1927), 43, 172.

240. C. Fadley *et al*,
J.Chem.Phys. (1968), 48, 3779.

241a. "Electron Spectroscopy, Theory, Techniques and Applications", Vols. 1-4,
Eds.: C. Brundle, A. Baker,
Academic Press, London (1977, 1978, 1979, 1981).

241b. J. Fuggle, Chapter 2 in Vol.4 of reference 241a.

242. P. Sherwood, Appendix III in reference 238a.

243. G. Olah,
Acc.Chem.Res. (1976), 9, 41.

244. Kratos Ltd.,
Operators Handbook, ES200 Spectrometer.

245. Y. Cross, J. Castle,
J.Electron Spectrosc.Rel.Phenom, (1981), 22, 53.

246. C. Banwell,
"Fundamentals of Molecular Spectroscopy",
McGraw-Hill, London (1972).

247. P. Bagus,
Phys.Rev. (1965), 139A, 619.

248. M. Krause, A. Carlson, R. Dusmukes,
Phys.Rev. (1968), 170, 37.

249. R. Manne, T. Aberg,
Chem.Phys.Lett. (1970), 7, 282.

250. D. Shirley,
Adv.Chem.Phys. (1973), 23, 85.

251. A. Rosen, I. Lindgren,
Phys.Rev. (1968), 176, 114.

252. T. Carlson,
"Photoelectron and Auger Spectroscopy",
Plenum Press, New York (1975).

253. G. McGuire, P. Holloway, Chapter 1 in Vol.4 of reference 241a.

254. D. Urch, Chapter 1 in Vol.3 of reference 241a.

255. C. Nordling,
Arkiv.Physik (1959), 15, 397.

256. C. Kittel,
"Introduction to Solid State Physics", (4th Edn.),
Wiley, New York (1971).

257. W. Jolly, D. Hendrickson,
J.Am.Chem.Soc. (1970), 92, 1863.

258. D. Adams, D. Clark,
J.Electron Spectrosc.Rel.Phenom. (1973), 2, 201.

259. W. Jolly, Chapter 3 in Vol.1 of reference 241a.

260. U. Gelius, K. Siegbahn,
Farad.Disc.Chem.Soc. (1972), 54, 257.

261. O. Goscincki, B. Pickup, G. Purvis,
Chem.Phys.Lett. (1973), 22, 117.

262. J. Connolly *et al*,
J.Chem.Phys. (1973), 58, 4265.

263. M. Schwartz,
Chem.Phys.Lett. (1970), 6, 631.

264. D. Shirley,
Chem.Phys.Lett. (1972), 15, 325.

265. J. Murrell, B. Ralston,
J.Chem.Soc.Farad.Trans.II (1972), 68, 1393.

266. C. Fadley, Chapter 1 in Vol.2 of reference 241a.

267. L. Cederbaun, W. Domcke,
Adv.Chem.Phys. (1977), 36, 205.

268. C. Wagner, L. Gale, R. Raymond,
Anal.Chem.(1979), 51, 466.

269. C. Fadley *et al*,
Phys.Rev.Lett. (1969), 23, 1397.

270. D. Shirley, Chapter 4 in
"Photoemission in Solids I: General Principles",
Topics in Applied Physics, Vol.26,
Eds.: M. Cardona, L. Ley,
Springer-Verlag, Berlin (1978).

271. C. Fadley, p.151 in reference 227a.

272. J. Connor, Chapter 5 in reference 229a.

273. T. Novakov, J. Hollander,
Phys.Rev.Lett. (1968), 21, 1133.

274. T. Novakov, J. Hollander,
Bull.Am.Phys.Soc. (1969), 14, 524.

275. G. Bancroft *et al*,
Chem.Phys.Lett. (1975), 32, 173.

276. T. Carlson, G. McGuire,
J.Electron Spectrosc.Rel.Phenom. (1972), 1, 161.

277. C. Fadley *et al*,
J.Electron Spectrosc.Rel.Phenom. (1974), 4, 93.

278a. See for example references 278b and 279.

278b. D. Clark, H. Thomas,
J.Polym.Sci.Polym.Chem.Ed. (1977), 15, 2843.

279. A. Dilks, Chapter 18 in reference 230a.

280. D. Briggs, Chapter 22 in
"Molecular Spectroscopy",
Ed.: A. West,
Heyden, London (1977).

281. P. Swift,
Methodes Physiques d'Analyse (1972), 8, 43.